A CRITICAL APPROACH TO MODELLING OF DEPTH DISTRIBUTIONS AND TRANSPORT OF RADIONUCLIDES IN SOILS AND SEDIMENTS AND RELATED PROBLEMS

Roland Haas

Preface

This internet-publication centres around the vertical transport of radionuclides in soils and sediments. It’s approach can be summarized as follows: The basic data are taken from publications of many different authors. These authors treated their measured values in quite different ways, ranging from very simple to highly sophisticated methods. Time series analysis as a means to forecast the vertical transport of radionuclides in soils and sediments has been applied only in a few cases. In this publication, however, time series analysis, based on the time dependant Weibull-distribution, is generally applied. The results achieved are compared with the results from models widely published in the literature. Many tables and figures show that the new method is generally applicable. Such a broad presentation would have been impossible in a journal article, and last but not least an internet-publication allows an unbiased presentation of this new forecasting method.

Summary. The main goal of this publication is the development and application of an empirical method, which allows to forecast the transport of radionuclides in soils ad sediments. The calculations are based on data published in the literature. 10 case studies, comprising 30 time series, deal with the transport of ^{134}Cs, ^{137}Cs, ^{85}Sr, ^{90}Sr, and ^{106}Ru. Transport in undisturbed soils and experimental systems like lysimeters and columns in laboratories are dealt with. The soils involved cover a large range of soils, e. g. podsols, cambisols (FAO), and peaty soils. Different speciations are covered, namely ions, aerosols, and fuel particles. Time series analysis centres around the Weibull-distribution. All theoretical models failed to forecast the transport of radionuclides. It can be shown that the parameters D and v, the dispersion coefficient and the advection velocity, appearing in solutions of the advection-dispersion equation (ADE), have no real physical meaning. They are just fitting parameters. The calculation of primary photon fluence rates, caused by ^{137}Cs in the soil, stresses the unreliability of forecasts based on theoretical models.

Kurzfassung. Hauptgegenstand dieser Publikation ist die Entwicklung und Anwendung einer empirischen Methode, die es gestattet, den Transport von Radionukliden in Böden und Sedimenten vorherzusagen. Die Berechnungen stützen sich auf Daten, die in der Literatur bereits veröffentlicht waren. Im Rahmen von 10 Fallstudien, die 30 Zeitreihen umfassen, wird der Transport von ^{134}Cs, ^{137}Cs, ^{85}Sr, ^{90}Sr und ^{106}Ru untersucht. Die Untersuchungen behandeln den Transport in ungestörten Böden und experimentellen Systemen wie Lysimetern und Säulenanordnungen in Laboratorien. Die untersuchten Böden umfassen einen weiten Bereich, z. B. Podsole, Cambisole (FAO) und Torfböden. Weiterhin wird der Transport unterschiedlicher physiko-chemischer Formen wie Ionen, Aerosole und Brennstoffteilchen behandelt. Die Zeitreihenanalyse stützt sich im Kern auf die Weibullverteilung. Alle theoretischen Modelle waren nicht in der Lage, den Transport von Radionukliden vorherzusagen. Es kann nachgewiesen werden, dass die Parameter D und v, der Dispersionskoeffizient und die Advektionsgeschwindigkeit, die in den Lösungen der Advektions-Dispersions-Gleichung auftreten, keine reale physikalische Bedeutung haben. Sie sind nur Fitting-Parameter. Die Berechnung des primären Photonenflusses, welcher durch ^{137}Cs in Böden verursacht wird, unterstreicht die Unzuverlässigkeit der Vorhersagen, die sich auf theoretische Modelle stützen.

Keywords: ^{134}Cs / ^{137}Cs / ^{85}Sr / ^{90}Sr / ^{106}Ru / Soil / Advection-dispersion equation / Transfer function model / Time dependant Weibull-distribution / Transport / Time series analysis / Primary photon fluence rates

1. Introduction

Since the very beginning of the nuclear age artificial radionuclides were released to the atmosphere, and finally they have spread throughout the geosphere. This has caused an additional external and internal radiation exposure. It is therefore quite understandable that nuclear explosions in the atmosphere and especially the Chernobyl accident have led to intensive research in the field of radioecology. Special attention was paid to transport processes in the atmosphere, in soils and sediments, surface waters, fauna, and flora, since the transport of radionuclides finally determines the additional radiation exposure.

Finally, because of their half-lives, only cesium-137 (^{137}Cs) and strontium-90 (^{90}Sr) cause the additional radiation exposure. ^{137}Cs, a gamma emitter, has a half-life of 30.17 years, and ^{90}Sr, a beta emitter, has a half-life of 28.64 years. ^{137}Cs causes as a gamma emitter an external and internal radiation exposure, whereas ^{90}Sr only causes an internal radiation exposure. The internal radiation exposure is, amongst others, caused by the food chain. Since ^{137}Cs is, from the radioecological point of view, more important, it has attracted special attention.

Cesium and potassium are alkali metals, and therefore both of them behave similarly with respect to metabolism and transport in soils and sediments. This similar behaviour affects the internal and external radiation exposure caused by ^{137}Cs, since the depth distributions of ^{137}Cs influence its root uptake and the attenuation of its gamma radiation. Strontium and calcium are earth alkali metals, and therefore both of them behave similarly.

Because of the importance of depth distributions of radionuclides in soils and sediments and their time dependence, these problems have been approached by many workers in the field, both by theoretical and empirical models, but because of the problems involved essential questions remained unanswered. It is therefore justified to have a fresh look at the problems involved. All calculations were performed with Mathcad 2000 Professional.

2. Modelling of solute transport
2.1 Theoretical models
2.1.1 Advection-dispersion equation (ADE)

The basic differential equation describing the 1-dimensional transport of a radioactive solute in a porous, macroscopic homogeneous, and sorbing medium is based on the mass balance principle:

$$\frac{\partial C}{\partial t} = \frac{D}{R} \cdot \frac{\partial^2 C}{\partial x^2} - \frac{v}{R} \cdot \frac{\partial C}{\partial x} - \lambda \cdot C \quad \textbf{(2-1)}$$

where
$C = C(x,t)$
x is the depth coordinate in (cm).
t is the time in (a).
C is the concentration in (Bq cm^{-3}).
D is the dispersion coefficient in (cm^2 a^{-1}).
v is the advection velocity in (cm a^{-1}).
R is the retardation factor (–).
λ is the decay constant in (a^{-1}).

A few remarks should indicate that the properties of real soils and sediments differ from the assumptions on which Eq. (2-1) is based. Especially in the case of cesium the **L**ocal **E**quilibrium **A**ssumption (LEA), i. e. the instantaneous sorption equilibrium, is not applicable. R, D, and v are assumed to be constants. This has the advantage that in many cases analytical solutions of Eq. (2-1) can be derived, but the disadvantage is evident: The assumptions differ largely from reality, and this will of course have negative consequences. Haas [1] has treated these problems in detail.

For the complete definition of the transport problem the ADE has to be completed by the appropriate initial and boundary conditions. In the case of transport of radionuclides in soils it is usually assumed that for t < 0 there is no radionuclide in question, e. g. ^{137}Cs, in the soil. This assumption is of course mostly wrong, since ^{137}Cs was deposited over many years. But because of a lack of information about the initial condition, and also for other reasons, there is no other way out of this problem. Also the choice of the correct boundary condition for x = 0 causes problems. In principal there are two types of boundary conditions: the flux-type and the concentration-type boundary condition. A detailed discussion would show that both types are simplifications of the real deposition conditions. Since the concentration-type boundary condition leads to simpler solutions, it is preferred. In the case of a plane source the solution of Eq. (2-1) is [2]

$$C(x,t) = \frac{M_0 \exp(-\lambda t)}{\sqrt{\pi D t}} \cdot \exp\left[\frac{-(x - vt)^2}{4Dt}\right] - \frac{v}{2D} \cdot \exp\left(\frac{v}{D} x\right) \cdot \mathbf{erfc}\left[\frac{x + vt}{2\sqrt{Dt}}\right] \quad \textbf{(2-2)}$$

M_0 (Bq cm $^{-2}$) is the total specific inventory for t = 0. For practical reasons D/R and v/R in Eq. (2-1) are replaced by the apparent dispersion coefficient resp. the apparent advection velocity. For the sake of simplicity the symbols D and v are also used for the apparent quantities. erfc denotes the complementary error function. It can be shown that only the flux-type boundary condition leads under all circumstances to a correct mass balance, i. e. the mass conservation law is not violated.

There is an elegant way out of this problem. One can find a function C(x,t), which does not violate the mass conservation law in the case of a plane source, but C(x,t) is not a real solution of Eq. (2-1). This function

$$C(x,t) = \frac{M_0 \exp(-\lambda t)}{2\sqrt{\pi D t}} \cdot \left[\exp\left[\frac{-(x - vt)^2}{4Dt}\right] + \exp\left[\frac{-(x + vt)^2}{4Dt}\right]\right] \quad \textbf{(2-3)}$$

has been studied in detail by Haas [1] and is referred to as quasi-solution.

2.1.2 Transfer function model

Assuming convective-stochastic transport [3, 4], one gets

$$C(x,t) = \frac{M_0 \exp(-\lambda t)}{\sigma\sqrt{2\pi}} \cdot \frac{1}{x} \cdot \exp\left[\frac{\left(\ln\left(\frac{\tau}{t} \cdot x\right) - \mu\right)^2}{-2\sigma^2}\right] \quad \textbf{(2-4)}$$

The radionuclide was applied to the soil surface at t = 0, and after τ (a) soil samples were taken. σ (–) and μ (–) are the parameters of this lognormal distribution. They are determined by means of curve fitting. τ is the reference time, and τ/t is the scaling factor. If the underlying scaling law is correct, it is possible to calculate C(x,t) for each point of time.

2.2 Empirical models

2.2.1 Background

Since the early days of radioecology depth distributions of radionuclides were often approximated by simple exponential functions [5 - 7], but also after the development of highly sophisticated theoretical transport models certain workers in the field [8, 9] used the simple exponential function as a basis for time series analysis, i. e. as a basis to estimate the development of depth distributions of radionuclides in soils and sediments. It's evident that they did not want to rely on models, which are based on assumptions, which are rather questionable. Extensive tests after the Chernobyl accident have proved that D and v in Eq. (2-3) are not at all constants, in contrary, they varied over a period of 8 (a) dramatically, and because of fitting problems one even had to use a superposition of Eq. (2-3), i. e. one had to assume a slow and a fast ^{137}Cs component [10].

In some special cases it might be justified to use a simple exponential function to model depth distributions of radionuclides in soils and sediments, but in most cases a more general approach is needed. This more general approach is based on the Weibull-distribution.

2.2.2 Weibull-distribution

The Weibull-distribution, applied to depth distributions of radionuclides in soils and sediments [1], can be written as follows:

$$C(x) = M_0 \cdot \exp(-\lambda t) \cdot a \cdot n \cdot x^{n-1} \cdot \exp\left(-ax^n\right) \quad \textbf{(2-5)}$$

where

$$M_0 \cdot \exp(-\lambda t) = M_\infty \quad \textbf{(2-6)}$$

M_∞ is thus the total specific inventory for $t \geq 0$.
a (cm^{-n}) and n (–) are the Weibull-parameters.
a, n > 0
One can easily show that

$$\int_0^\infty C(x)dx = M_\infty \quad \textbf{(2-7)}$$

Eq. (2-5) is thus in line with the basic requirement: It does not violate the mass conservation law. For n = 1 Eq. (2-5) is the simple exponential function.

It's a general habit to use C(x,t) resp. C(x) as fitting equation for the estimation of the parameters involved. A better approach is the *integral method* used by Haas [1, 11]:

$$M(x,t) = \int_0^x C(y,t)dy \quad \textbf{(2-8)}$$

y is the integration variable. The integral method is adapted to the sampling method, i. e. to stacked samples. The use of M(x,t) resp. M(x) instead of C(x,t) resp. C(x) avoids using the difference quotient to approximate the differential quotient.

Taking into account Eq. (2-5) and (2-6), Eq. (2-8) leads to the cumulative Weibull-distribution

$$M(x) = M_\infty \cdot \left[1 - \exp\left(-ax^n\right)\right] \quad \textbf{(2-9)}$$

Normally only a and n are considered to be the fitting parameters, but sometimes it can be cumbersome and questionable to determine M_∞ experimentally. In such cases also M_∞ is considered to be a fitting parameter. Extensive tests have shown that Eq. (2-9) is an excellent fitting equation and extrapolation function [1].

The quality of a fit is characterized by the coefficient of determination r^2 [12]. r^2, in (%), is defined as

$$r^2 := \left[1 - \frac{\sum_{i=1}^{n}\left(F_i - M_i\right)^2}{\sum_{i=1}^{n}\left(M_i - \overline{M}\right)^2}\right] \cdot 100 \quad \textbf{(2-10)}$$

where F_i denotes the function's value, M_i the corresponding cumulative specific inventory, and $\overline{M}$ the arithmetical mean of the M_i. By definition is $0 \le r^2 \le 100$.

In [1] details about fits with Eq. (2-9) are given. For 46 fits the arithmetical mean of the coefficient of determination is 99.87 (%), and the standard deviation is only 0.21 (%). The corresponding figures for the fits with Eq. (2-3) are 86.20 (%) and 19.10 (%). A comparison of both sets of figures indicates the superiority of Eq. (2-9). For time series analysis it is of great importance that the standard deviation is very small, i. e. that the respective fitting equation is generally reliable.

For comparisons it is better to use the quantities $M(x)/M_\infty$ (–) and $C(x)/M_\infty$ (cm^{-1}) instead of M(x) ($Bq\ cm^{-2}$) and C(x) ($Bq\ cm^{-3}$). For the sake of simplicity the former symbols M(x) and C(x) are also used for the new quantities.

Haas [11] has demonstrated that it is possible to model the Weibull-parameters a and n in function of the time t, i. e. it is possible to arrive empirically at the time dependant Weibull-distributions

$$M(x,t) = 1 - \exp\left(-a(t) \cdot x^{n(t)}\right) \quad \textbf{(2-11)}$$

$$C(x,t) = a(t) \cdot n(t) \cdot x^{n(t)-1} \cdot \exp\left(-a(t) \cdot x^{n(t)}\right) \quad \textbf{(2-12)}$$

It is also possible to calculate further quantities depending on a(t) and n(t). An interesting distribution is the percentage distribution p(x,t), which results from Eq. (2-11).

$$p(x,t) = 100 \cdot \exp\left(-a(t) \cdot x^{n(t)}\right) \quad \textbf{(2-13)}$$

p denotes the percentage of the total specific inventory below x.

The nominal root depth of permanent pastures is 10 (cm). The retention of a radionuclide in the upper 10 (cm) in (%), R(10,t), is therefore an interesting quantity.

$$R(10,t) = 100 \cdot \left[1 - \exp\left(-a(t) \cdot 10^{n(t)}\right)\right] \quad \textbf{(2-14)}$$

A further interesting quantity is the penetration depth $P_p(t)$ (cm). It is the thickness of the top layer, which contains p (%) of the radionuclide.

$$P_p(t) = \left[-\frac{1}{a(t)} \cdot \ln\left(1 - \frac{p}{100}\right)\right]^{\frac{1}{n(t)}} \quad \textbf{(2-15)}$$

The treatment of 10 case studies, based on [7 - 9, 13 - 19], comprising 30 time series, exhibits that the following functions are extremely useful for the solution of different fitting problems involved in time series analysis:

$$f_1(t) = b \cdot \left[1 - \exp\left(-c \cdot t^m\right)\right] \quad \textbf{(2-16)}$$

$$f_2(t) = b \cdot \left[1 - \exp\left(-c \cdot t^m\right)\right] + d \quad \textbf{(2-17)}$$

$$f_3(t) = \frac{b}{t^k} \cdot \exp\left[-c \cdot \left[\sqrt{(\ln(t) - d)^2}\right]^m\right] \quad \textbf{(2-18)}$$

$$f_4(t) = \frac{b}{t^k} \cdot \exp\left[-c \cdot \left[\sqrt{(\ln(t) - d)^2}\right]^m\right] + f \quad \textbf{(2-19)}$$

$$f_5(t) = b \cdot \left[\exp\left[-c \cdot \left[\sqrt{(t-d)^2} \right]^m \right] + \exp\left[-c \cdot (t+d)^m \right] \right] \quad \textbf{(2-20)}$$

$$f_6(t) = b \cdot \left[\exp\left[-c \cdot \left[\sqrt{(t-d)^2} \right]^m \right] + \exp\left[-c \cdot (t+d)^m \right] \right] + f \quad \textbf{(2-21)}$$

b, c, d, f, k, and m are the fitting parameters. Eq. (2-16) and (2-17) are based on the cumulative Weibull-distribution, whereas Eq. (2-18) and (2-19) resp. (2-20) and (2-21) are based on the so-called loggamma distribution [1] resp. gamma-2-distribution [1].

For the purpose of prognoses the functions a(t) and n(t), resulting from the first fits, have to be adapted in a certain way. Extensive tests have shown that adaptation to $x_s(t)$, the fitting curve of the centres of gravity of the depth distributions, is the most appropriate adaptation method. The best fitting equation for $x_s(t)$ is Eq. (2-16). The centre of gravity of a depth distribution is

$$x_s = \int_0^\infty x \cdot C(x) dx \quad \textbf{(2-22)}$$

If C(x) represents the Weibull-distribution, one gets

$$x_s = \frac{\Gamma\left(\frac{1}{n}\right)}{n \cdot a^{\left(\frac{1}{n}\right)}} \quad \textbf{(2-23)}$$

where Γ denotes the gamma function. After the adaptation process the graph, represented by Eq. (2-24), should allow to match the graph of $x_s(t)$, represented by Eq. (2-16).

$$x_s(t) = \frac{\Gamma\left(\frac{1}{n(t)}\right)}{n(t) \cdot a(t)^{\left(\frac{1}{n(t)}\right)}} \quad \textbf{(2-24)}$$

The modified functions are based on the construction of a 2-dimensional nest of intervals for different points of time. The construction of such a 2-dimensional nest of intervals for a certain point of time t_p, for which a prognosis is wanted, can be described as follows:

$a(t_p)$, resulting from the first fit, is considered to be correct, and $n(t_p)$, resulting from the first fit, is adjusted by method of trial and error, until x_s (Eq. (2-23)) equals $x_s(t_p)$ (Eq. (2-16)). The result is called n_r.

$n(t_p)$, resulting from the first fit, is considered to be correct, and $a(t_p)$, resulting from the first fit,

is adjusted by method of trial and error, until x_s (Eq. (2-23)) equals $x_s(t_p)$ (Eq. (2-16)). The result is called a_r.
The arithmetical means

$$a_m = \frac{a(t_p) + a_r}{2} \quad \textbf{(2-25)}$$

$$n_m = \frac{n(t_p) + n_r}{2} \quad \textbf{(2-26)}$$

are first approximations of the correct a- and n-value. a_m and n_m are the basis for a second approximation. Higher order approximations can be calculated in the same way. The number of approximations required ranges from 2 to 4, depending on how much x_s (Eq. (2-23)) deviates from $x_s(t_p)$ (Eq. (2-16)). The result of this approximation procedure depends on the starting point ($a(t_p)$, $n(t_p)$) in the a, n-plane, but it's practical influence is limited to cases of an extreme relative deviation. The consequence of this fact is the following one: The fitting equations for the first fits a(t) and n(t) must be chosen in such a way that the relative deviations mentioned above are kept as small as possible.

The new sets of a- and n-values are fitted again. These second fits a(t) and n(t) are the basis for prognoses.

A prognosis should be complemented by an error estimation. The method applied is a simple, intuitive procedure. It can be described as follows: The x_s-fit is described by $x_s(t)$ (Eq. (2-16)). The data points, scattered around $x_s(t)$ (Eq. (2-16)), can be confined in a sector. The upper limit of this sector is $c_u x_s(t)$, and the lower limit of this sector is $c_l x_s(t)$. The constants c_u and c_l are determined by method of trial and error. It is assumed that this sector is also representative for the time interval (t_s, t_p). t_s is the point of time of the last sampling. This method will be referred to as *sector-method*.

3. Sampling

A critical study of the literature on depth distributions and transport of radionuclides in soils and sediments gives the impression that workers in the field are not always fully aware of the implications of sampling. Sampling should be seen from the scientific and economic point of view. First of all the aims of the research project must be clearly identified, and thereafter an adequate sampling strategy has to be elaborated, taking into account that besides sampling all subsequent work involved influences the overall economy of the research project. In other words, one has to minimize the costs for a maximum of high quality information.

Let's assume the aim of the research project is the following one: Estimation of the long term external radiation exposure caused by ^{137}Cs in the soil of a virtually flat permanent pasture. First of all, sampling should be representative. Representative sampling must take into account the area of the site and the variability of the relevant soil properties. Since it is impossible to base a prognosis of the development of a depth distribution on a single sampling, it is evident that one has to employ time series analysis [11]. This in turn necessitates that samples, taken at different points of time, must be representative for a narrow area. Then the question arises, how this can be achieved. Experience has shown that total specific inventories and depth distributions can change dramatically even within a narrow area [1]. In order to cope with these problems, a certain number of sampling points has to be chosen. Gamma spectrometric measurements, followed by a statistical analysis, will then show, whether the number of sampling points is sufficient or has to be increased. This strategy finally leads to representative sampling and representative data for a certain point of time. If it is also intended to study, whether the total specific inventories within a certain area belong to a single population or not, a statistical method, e. g. the Kruskal-Wallis-test [1, 12], has to be applied. In the case of the Kruskal-Wallis-test the number of sampling points within a sub-area must be at least 5.

Let's assume that sampling will be performed by means of frames and scrapers. Then it is possible to keep the errors involved within narrow limits, provided the right measures are taken [1]. In the case of ^{137}Cs it is mostly sufficient to sample to a depth of 20 (cm). For ^{90}Sr the sampling depth could be greater. It's in any way not necessary to catch M_∞ completely, since Eq. (2-9) is an excellent extrapolation function. Experience has shown that in the case of stacked samples the optimum number of layers is 5 [1]. Certain workers in the field have sampled 1 (cm) layers. This is not at all necessary, it's in fact a waste of time and money, i. e. not economic. The thickness of the layers has to be adapted to the depth distribution of the radionuclide in question, i. e. for greater depths the thickness of the layer can be increased. This measure has no negative effects.

Sampling of the top layer requires special attention. Because of the roots and the micro-relief it is advised to sample a layer with a nominal thickness of 3 (cm). The effective thicknesses mentioned in [1] range from 1.9 (cm) to 3.5 (cm). These figures also indicate that $x = 0$, i. e. the soil surface, is a mathematical idealization of the physical reality.

4. Application of models

It is not sufficient to establish a theory or method, but it must be complemented by extensive testing in order to find out its limitations. To the knowledge of the author of this paper Eq. (2-2), (2-3), and (2-4) were only used as fitting equations for depth profiles, but their predictive power was, until the work of Haas [11], an open question, i. e. the already existing experimental results were not used.

Haas [11] has extensively tested the predictive power of his empirical method, which is based on the time dependant Weibull-distribution. This paper deals with the transport of ^{134}Cs, ^{137}Cs, ^{85}Sr, ^{90}Sr, and ^{106}Ru. Transport in undisturbed soils and experimental systems like lysimeters and columns in laboratories are dealt with. The soils involved cover a large range of soils, e. g. podsols, cambisols (FAO), and peaty soils. Different speciations are covered, namely ions, aerosols, and fuel particles.

5. Calculation of primary photon fluence rates caused by gamma emitters in soils and sediments

The theory has been developed by Finck [20]. The geometry used for the calculation of primary photon fluence rates is based on 2 semi-infinite half-spaces of soil and air, which are separated by an infinite, plane soil surface. In this geometry a photon source element is contained in a volume element dV of soil at a vertical depth x below the soil surface. Suppose that the photon source distribution is represented by $C(x,r,\eta)$, where x denotes the depth below the soil surface, r the lateral distance, and η the azimuthal angle, then the photon emission from the volume element is C(x,r,η) dV. The primary photon fluence rate $d\Phi_p$ at the position of a hypothetical detector at height h above the ground and at the distance R from this volume element can be expressed as

$$d\Phi_p = \frac{C(x,r,\eta)\cdot dV \cdot \exp[-\mu_s \cdot (R - h\cdot \sec\theta) - \mu_a \cdot h \cdot \sec\theta]}{4\cdot\pi\cdot R^2} \quad \textbf{(5-1)}$$

where μ_s and μ_a are the linear attenuation coefficients in soil resp. air, and θ denotes the angle between the normal to the air-soil interface and the direction of the primary photons at the position of the detector. Since

$$dV = r\cdot R\cdot d\eta\cdot dR\cdot d\theta \quad \textbf{(5-2)}$$

and

$$\sin\theta = \frac{r}{R} \quad \textbf{(5-3)}$$

$$\Phi_p = \int_0^{\frac{\pi}{2}} \int_{h\sec\theta}^{\infty} \int_0^{2\pi} \frac{C(x,r,\eta)\cdot \sin\theta\cdot \exp[-\mu_s(R - h\sec\theta) - \mu_a h\sec\theta]}{4\pi} d\eta dR d\theta \quad \textbf{(5-4)}$$

If the photon source distribution does not depend on the azimuthal angle η

$$\Phi_p = \int_0^{\frac{\pi}{2}} \int_{h\sec\theta}^{\infty} \frac{C(x,r)\cdot \sin(\theta)\cdot \exp[-\mu_s(R - h\sec\theta) - \mu_a h\sec\theta]}{2} dR d\theta \quad \textbf{(5-5)}$$

If, in addition, the photon source distribution depends only on the depth x, one gets

$$\Phi_p = \int_0^{\frac{\pi}{2}} \int_{h\sec\theta}^{\infty} \frac{C(x)\cdot \sin(\theta)\cdot \exp[-\mu_s(R - h\sec\theta) - \mu_a h\sec\theta]}{2} dR d\theta \quad \textbf{(5-6)}$$

A general solution of the integral (5-6) for any C(x) is not possible, but also a numerical evaluation of this integral is impossible, since h secθ approaches ∞ if θ approaches π/2. But for h = 0 a numerical evaluation of the integral (5-6) is possible for any C(x). If h = 0

$$\Phi_p = \int_0^{\frac{\pi}{2}} \int_0^{\infty} \frac{C(x) \cdot \sin(\theta) \cdot \exp(-\mu_s R)}{2} dR d\theta \quad \textbf{(5-7)}$$

The argument of C(x) has to be expressed in terms of the variables R and θ:

$$x = R \cdot \cos\theta \quad \textbf{(5-8)}$$

Normally the position of the detector is 1 (m) above the ground. Model calculations for a uniform source distribution indicate that the difference between the primary photon fluence rates for h = 0 and h = 1 (m) is negligible.

For a decay energy of 661.6 (keV) (^{137}Cs) and a soil density of 1.6 (g cm^{-3}) the linear attenuation coefficient μ_s = 0.125152 (cm^{-1}). Finck [20] has based his calculations on the assumption that the composition of soil by weight is as follows: 55.8 (%) O, 31.5 (%) Si, 7.1 (%) Al, 3.2 (%) Fe, 1.3 (%) C, and 1.1 (%) H.

6. Case studies

6.1 Case study 1

Case study 1 is based on [13]. The experiments were carried out by means of open-air lysimeters, fabricated from polyethylene. They had a net cross section of about 1 (m^2) and a volume of about 0.5 (m^3). The walls were designed to minimize the influence of weather conditions. The soils involved are a podsol and a cambisol. ^{137}Cs was applied as chloride, and ^{90}Sr was applied as nitrate, in both cases 37 (MBq), carrier-free. The radionuclides were homogeneously distributed in the top layer with a thickness of 1 (cm). The surfaces were covered with grass. Stacked samples were taken in spring and autumn by means of a *Pürckhauer-Bohrstock*.

The data in Table 6.1-1 to 6.1-4 are based on Fig. 4 and 5 of [13]. They were gained with high precision by means of the digitizing program WinDig 2.5 (© D. Lovy, Geneva).These data are the basis of all further calculations. Fitting of the depth profiles in Table 6.1-1 to 6.1-4 with

$$M(x) = 1 - \exp\left(-ax^n\right) \quad \textbf{(6-1)}$$

leads to theWeibull-parameters a, n in Table 6.1-5 to 6.1-8.

Table 6.1-9 contains the Weibull-parameters a, n, which are based on 2-dimensional nests of intervals. Fig. 6.1-1 resp. 6.1-2 show the first and second fits of a resp. n for time series 1. Fig. 6.1-3 demonstrates the sector-method in the case of time series 1, and Table 6.1-10 contains the corresponding figures. Fig. 6.1-4 demonstrates the almost perfect matching of the centres of gravity and of the penetration depths in the case of time series 1. Table 6.1-11 and 6.1-12 contain the relevant fitting results for time series 1 to 4.

Fitting results can be sometimes improved, if the basic fitting equation, i. e. Eq. (2-16) to (2-21), is multiplied by

$$f_7(t) = \exp\left[\alpha \cdot (t - \beta)\right] \cdot t^{\gamma} \quad (6\text{-}2)$$

β and γ are mostly 0. Eq. (6-2) can be applied in different ways: α, β and γ are
– real fitting parameters.
– calculated by method of trial and error in the framework of the fitting procedure.
– calculated by method of trial and error after the fitting procedure, but this option should be restricted to very small adjustments.

Fig. 6.1-5 exhibits the relative concentrations and Fig. 6.1-6 the inventories below x (%), in both cases for different points of time for time series 1, and Fig. 6.1-7 demonstrates for time series 1 the relative concentrations after 50 (a), resulting from different models. It's obvious that theoretical models are unable to forecast the transport of ^{137}Cs in soils. Table 6.1-13 proves that D and v have no real physical meaning; they are just fitting parameters. The reason for the oscillations near x = 30 (cm) is unknown, but it is evident that they are physically meaningless. The integral over the concentration C (solution ADE, a-profile, $(0, \infty)$) equals 1.597. This violation of the mass conservation law is a consequence of the concentration-type boundary condition.

Table 6.1-14 contains the primary photon fluence rates for different models for time series 1, and Table 6.1-15 resp. 6.1-16 contain the fitting results concerning primary photon fluence rates resp. integrated primary photon fluence rates for different models for time series 1. Fig. 6.1-8 and 6.1-9 demonstrate clearly that theoretical models are completely unreliable.

Time series 2 is characterized by Fig. 6.1-10 to 6.1-13. Most comments concerning time series 1 are also applicable to time series 2, but p1(x) in Fig. 6.1-12 shows a very small disturbance, since it intersects p2(x) etc. The integral over the concentration C (solution ADE, a-profile, $(0, \infty)$) equals this time 2, i. e., the mass conservation law is again violated.

Time series 3 causes some difficulties. This is due to the steep decrease of a(t), but by means of special adaptations the problems are solvable. Fig. 6.1-14 proves this. Fig. 6.1-14, 6.1-15, and 6.1-16 demonstrate the different behaviour of ^{90}Sr. The integral over the concentration C (solution ADE, l-profile, $(0, \infty)$) equals again 2. Fig. 6.1-17 shows that the mass conservation law is again violated. Fig. 6.1-18 and 6.1-19 demonstrate the regular decrease of the relative concentration maxima.

Fig. 6.1-20 to 6.1-23 indicate the similarities between time series 3 and 4. The comments concerning the oscillations, this time near x = 100 (cm), are the same as in the case of time series 1. The mass conservation law is again violated. The integral over the concentration C (solution ADE, l-profile, $(0, \infty)$) equals this time 1.133.

Fig. 6.1-24 demonstrates by means of the retention in the upper 10 (cm) the quite different behaviour of ^{137}Cs and ^{90}Sr.

6.2 Case study 2

Case study 2 is based on [14]. The experiments concerned are column experiments with field soils. Undisturbed soil columns were obtained by slowly pressing 100 (cm) long polyvinyl chloride (PVC) tubes with a diameter of 30 (cm), having sharp edges on the front, into the soil. Case study 2 deals with a podsol, taken near Gorleben, a small town in northwest Germany. In the laboratory 5 (cm) of the soil at the bottom of the column was replaced by a filter of coarse, purified sand (1 (mm) diameter) for better drainage. The column was mounted on a PVC plate, having a small hole in the middle for the effluent. A rain simulator allowed even irrigation of the soil surface. The composition and amount of rainwater supplied corresponded to that determined at the site of sampling. About 300 (μCi) ^{85}Sr (carrier-free) and about 50 (μCi) ^{137}Cs (3 (μg Cs)/100 (μCi)) were added with one portion of rainwater to the soil surface. The distribution of the radionuclides in the soil was measured from the outside after various time intervals, using a gamma-scanner technique. Because of the gamma-scanner technique ^{85}Sr was used to simulate the beta-emitter ^{90}Sr.

The data in Table 6.2-1 and 6.2-2 are based on Fig. 3 of [14]. They were gained with high precision by means of the digitizing program WinDig 2.5 (© D. Lovy, Geneva).These data are the basis of all further calculations. Fitting of the depth profiles in Table 6.2-1 and 6.2-2 with Eq. (6-1) leads to theWeibull-parameters a, n in Table 6.2-3 and 6.2-4.

Table 6.2-5 contains the Weibull-parameters a, n, which are based on 2-dimensional nests of intervals, and Table 6.2-6 contains the figures concerning the sector-method. They indicate a very small scattering of the x_s-values around the x_s-fit. Fig. 6.2-1 demonstrates the almost perfect matching of the centres of gravity and of the penetration depths in the case of time series 1. Table 6.2-7 contains the relevant fitting results for time series 1 and 2. Fig. 6.2-2 exhibits the relative concentrations and Fig. 6.2-3 the inventories below x (%), in both cases for different points of time for time series 1, and Fig. 6.2-4 demonstrates for time series 1 the relative concentrations after 10 (a), resulting from different models. It's again obvious that theoretical models are unable to forecast the transport of ^{137}Cs in soils. Table 6.2-8 proves that D and v have no real physical meaning; they are just fitting parameters.

Time series 2 is characterized by Fig. 6.2-5 to 6.2-8. The comments concerning time series 1 are also applicable to time series 2.

Fig. 6.2-9 demonstrates by means of the retention in the upper 10 (cm) the different behaviour of ^{137}Cs and ^{85}Sr.

6.3 Case study 3

Case study 3 is based on [15]. This paper deals with the transport of Chernobyl ^{137}Cs in 2 grassland sites. The near-field site of the Chernobyl nuclear power plant (ChNPP) is located at a distance of 3 (km) from the former village Chistogalovka, about 6 (km) west-south-west of ChNPP. The mean annual precipitation is 590 (mm), and the mean annual temperature is 6.5 (˚C). The sampling location in Germany is situated 40 (km) north-west of Munich, 545 (m) above sea level. The mean annual precipitation is 800 (mm), and the mean annual temperature is 7.3 (˚C). All samples were taken on a flat area to exclude precipitation run-off. The soil, undisturbed by agricultural processes for at least 40 (a), is classified as *Parabrown earth soil, paraverglyt*. In the US-system this corresponds to a slightly wet Alfisol (Aqualf). The soil at the near-field site of the ChNPP is a soddy-podzolic loamy sand on sandy fluvioglacial deposits. The soil was ploughed formerly (more than 10 (a) ago), and the genetic profile of this soil has been formed under the influence of cultivation, resulting in the formation of an organo-mineral horizon up to 20 (cm) thick. The soil samples were mostly taken annually since 1987. At the ChNPP-site soil cores (4 replicates) were extracted to a depth of 10 (cm) with a stainless steel sampler (diameter 100 (mm) and subsequently cut into slices of 1 (cm) thickness. It is not mentioned, whether mixed samples were used for the gamma spectrometry. At the German site the soil samples were taken with a frame (50 (cm) x 50 (cm)). The sampling depth was 40 (cm). Sample preparation was performed in the usual way. ^{134}Cs and ^{137}Cs were determined by direct gamma spectrometry, using a high purity germanium detector and a multichannel analyser. The Chernobyl ^{137}Cs was, for the German site, determined by means of the $^{134}Cs/^{137}Cs$-ratio. At the ChNPP-site the contribution of ^{137}Cs from the global fallout is negligible to Chernobyl-derived ^{137}Cs, and therefore no corrections are required. It should be stressed that the speciation of the fallout influences its transport in the soil. At the near-field site the fallout is dominated by fuel particles, and at greater distances aerosols prevail.

The data in Table 6.3-1 and 6.3-2 are based on Fig. 1 of [15]. They were gained with high precision by means of the digitizing program WinDig 2.5 (© D. Lovy, Geneva).These data are the basis of all further calculations. Fitting of the depth profiles in Table 6.3-1 and 6.3-2 with Eq. (6-1) leads to theWeibull-parameters a, n in Table 6.3-3 and 6.3-4.

Table 6.3-5 contains the Weibull-parameters a, n, which are based on 2-dimensional nests of intervals, and Table 6.3-6 contains the figures concerning the sector-method. Fig. 6.3-1 demonstrates the matching of the centres of gravity and of the penetration depths in the case of time series 1 (German site). Fig. 6.3-2 and 6.3-3 show irregularities (relative concentrations and inventories below x (%) for different points of time), but they are relatively unimportant compared to the results achieved by theoretical models (Fig. 6.3-4, relative concentrations after 20 (a)). It's again obvious that theoretical models are unable to forecast the transport of ^{137}Cs in soils. Table 6.3-7 contains the relevant fitting results for time series 1 (German site) and time series 2 (ChNPP-site). Table 6.3-8 proves that D and v have no real physical meaning; they are just fitting parameters.

Time series 2 is characterized by Fig. 6.3-5 to 6.3-8. There are no irregularities. The matching of the centres of gravity and of the penetration depths (Fig. 6.3-5) is almost perfect, and the sequence of the relative concentration maxima for different points of time in Fig. 6.3-6 is excellent. Fig. 6.3-8 proves again that theoretical models are unable to forecast the transport of ^{137}Cs in soils.

A comparison of the results achieved for time series 1 and 2 reveals the different behaviour of different speciations in soils.

6.4 Case study 4

Case study 4 is based on [9]. This paper deals with the transport of Chernobyl ^{137}Cs. 3 sampling areas were selected in the mountainous area of the Friuli-Venezia Giulia region, where the ^{137}Cs deposition following the Chernobyl accident ranged from 20 to 40 (kBq m^{-2}). Areas 1 and 2 are natural grassland, and on area 3 medicinal herbs are grown. Table 6.4-1 (Table 1 of [9]) characterizes the soils of the 3 sampling areas. Sampling of soils was carried out with seasonal frequency from July 1987 to July 1992. The samples were taken at distances of at least 1 (m) to avoid interferences. A soil monolith with a surface of 30 (cm) x 30 (cm) was isolated by digging a trench. Samples were taken to a depth of 20 (cm), and the monolith was subsequently cut into layers with a thickness of 5 (cm). The error associated with this sampling method is in homogeneous soils, according to the authors of [9], about 20 (%), but it is unclear what this really means. All soil samples were air-dried and sieved through a 2 (mm) mesh. The samples were analysed by gamma spectrometry, using HPGe detectors. The total measured ^{137}Cs was separated into its weapons fallout and Chernobyl contribution, using the $^{137}Cs/^{134}Cs$ ratio of 2, measured in rainfall samples of May 1986.

The data in Table 6.4-2 to 6.4-4 are based on Fig. 1 of [9]. They were gained with high precision by means of the digitizing program WinDig 2.5 (© D. Lovy, Geneva).These data are the basis of all further calculations. Fitting of the depth profiles in Table 6.4-2 to 6.4-4 with Eq.

(6-1) leads to the Weibull-parameters a, n in Table 6.4-5 to 6.4-7.

Table 6.4-8 contains the Weibull-parameters a, n, which are based on 2-dimensional nests of intervals, and Table 6.4-9 contains the figures concerning the sector-method. Fig. 6.4-1 demonstrates the very good matching of the centres of gravity and of the penetration depths for time series 1 (area 1). Table 6.4-10 and 6.4-11 contain the relevant fitting results for time series 1 to 3. Fig. 6.4-2 exhibits the relative concentrations and Fig. 6.4-3 the inventories below x (%), in both cases for different points of time for time series 1, and Fig. 6.4-4 demonstrates for time series 1 the relative concentrations after 40 (a), resulting from different models. Fig. 6.4-4 indicates as well that the exponential model C(x), used in [9], approximates C7(x) much better than all the theoretical models tested. The Weibull-parameter n(40) = 1.21835 (–). The more or less acceptable approximation is of course a consequence of the fact that n deviates not too much from 1. Table 6.4-13, based on Table 2 of [9], contains the parameter values of the exponential model for time series 1 to 3 (area 1 to 3). It's again obvious that theoretical models are unable to forecast the transport of ^{137}Cs in soils. Table 6.4-12 proves that D and v have no real physical meaning, they are just fitting parameters.

Time series 2 (area 2) is characterized by Fig. 6.4-5 to 6.4-8. Fig. 6.4-5 demonstrates the almost perfect matching of the centres of gravity and of the penetration depths for time series 2. Fig. 6.4-6 exhibits the relative concentrations and Fig. 6.4-7 the inventories below x (%), in both cases for different points of time for time series 2, and Fig. 6.4-8 demonstrates for time series 2 the relative concentrations after 20 (a), resulting from different models. The exponential model C(x), used in [9], approximates C7(x) this time very good, since n(20) = 1.066 (–). Further comments concerning time series 1 are also applicable to time series 2.

Time series 3 (area 3) is characterized by Fig. 6.4-9 to 6.4-12. Fig. 6.4-9 demonstrates a good matching of the centres of gravity and of the penetration depths for time series 3. Fig. 6.4-10 exhibits the relative concentrations and Fig. 6.4-11, this time a little disturbed, the inventories below x (%), in both cases for different points of time for time series 3, and Fig. 6.4-12 demonstrates for time series 3 the relative concentrations after 30 (a), resulting from different models. The exponential model C(x), used in [9], approximates C7(x) this time very poor, since n(30) = 1.46 (–). Further comments concerning time series 1 and 2 are also applicable to time series 3.

6.5 Case study 5

Case study 5 is based on [8]. This paper deals with the transport of ^{137}Cs, originating from bomb fallout (global fallout) and Chernobyl fallout. 2 sampling areas were selected in the mountainous area of the Friuli-Venezia Giulia region, where the ^{137}Cs deposition following the Chernobyl accident ranged from 20 to 40 (kBq m^{-2}). Area 1 is a natural grassland in a region, where soils originate from ancient alluvium. Area 2 is situated in a beech wood on deep soils, originating from calcareous rocks. Table 6.5-1 (Table 1 and 2 of [8]) characterizes the soils of the 2 sampling areas. Sampling of soils was carried out with seasonal frequency from July 1987 to October 1989. The samples were taken at distances of at least 1 (m) to avoid interferences. A soil monolith with a surface of 30 (cm) x 30 (cm) was isolated by digging a trench. Samples were taken to a depth of 20 to 30 (cm), and the monolith was subsequently cut into layers with a thickness of 1 to 5 (cm). In the wood, each horizon (i. e., leaves in various stages of decomposition and humus) was sampled separately. In the natural grassland, soil layers with a thickness of 5 (cm) were sampled. The error associated with this sampling method is in homogeneous soils, according to the authors of [8], about 20 (%), but it is unclear what this really means. All soil samples were air-dried and sieved through a 2 (mm) mesh, and the litter samples were oven-dried at 100 (˚C) and then ground. The samples were analysed by gamma spectrometry, using HPGe detectors. The total measured ^{137}Cs was separated into its weapons fallout and Chernobyl contribution, using the $^{137}Cs/^{134}Cs$ ratio of 2, measured in rainfall samples of May 1986. Table 3 and 4 of [8] contain the activities in (Bq kg^{-1}). Multiplication of these activities in (Bq kg^{-1}) with the thicknesses of the samples and the corresponding densities yields the inventories of the layers in (Bq cm^{-2}). The mean soil density of area 1 is 1.4E-3 (kg cm^{-3}). The densities of area 2 range from 1E-3 (kg cm^{-3}) (organic horizons) to 1.5E-3 (kg cm^{-3}) (mineral soils). The depth profiles were fitted with Eq. (2-9), and M_∞ was treated as an additional fitting parameter, since the sampling depths were not sufficient.

A simultaneous use of the Weibull-parameters a, n, based on Eq. (2-9), concerning the bomb fallout (global fallout) and Chernobyl fallout, contained in Table 6.5-2 and 6.5-3, eases a long-term prognosis of the transport of ^{137}Cs in the soils of the 2 areas. This approach is justified, since the Chernobyl fallout consists, far away from the Chernobyl nuclear power plant (ChNPP), mainly of aerosols, i. e., it has the same speciation as the bomb fallout. Model calculations revealed that it is justified to treat the bomb fallout as a single deposition 30 (a) before the first sampling after the Chernobyl accident.

Table 6.5-4 contains the Weibull-parameters a, n, which are based on 2-dimensional nests of intervals, and Table 6.5-5 contains the figures concerning the sector-method. Fig. 6.5-1 demonstrates the matching of the centres of gravity and of the penetration depths for time series 1 (area 1,). Table 6.5-6 contains the relevant fitting results for time series 1 and 2. Fig. 6.5-2 exhibits the relative concentrations and Fig. 6.5-3 the inventories below x (%), in both cases for different points of time for time series 1, and Fig. 6.5-4 demonstrates for time series 1 the relative concentrations after 20 (a), resulting from different models. It indicates as well that the exponential model C(x), used in [8], approximates C20(x) rather poor. The Weibull-parameter n(20) = 1.4391 (–). Table 6.5-8, based on Table 5 of [8], contains the parameter values of the exponential model for time series 1 and 2 (area 1and 2). It's again obvious that theoretical models are unable to forecast the transport of ^{137}Cs in soils. Table 6.5-7 proves that D and v have no real physical meaning, they are just fitting parameters.

Time series 2 (area 2) is characterized by Fig. 6.5-5 to 6.5-8. Fig. 6.5-5 demonstrates the good matching of the centres of gravity and of the penetration depths for time series 2. Fig. 6.5-6 exhibits the relative concentrations and Fig. 6.5-7 the inventories below x (%), in both cases for different points of time for time series 2, and Fig. 6.5-8 demonstrates for time series 2 the relative concentrations after 20 (a), resulting from different models. The exponential model C(x), used in [8], approximates C20(x) rather poor. The Weibull-parameter n(20) = 1.35075 (–). Further comments concerning time series 1 are also applicable to time series 2.

6.6 Case study 6

Case study 6 is based on [7]. This paper deals with the transport of ^{134}Cs and ^{106}Ru, originating from Chernobyl fallout. 2 localities were selected, Ivrea and Castagneto Po, situated in the Piemonte region in northern Italy. Sampling was performed in unused parts of residential gardens over a period of about 3 (a). Table 6.6-1 (Table 1 of [7]) characterizes the soils of the 2 sampling areas. Nothing is said in [7] about the vegetation. The soils were only sampled to a depth of 4 (cm) and cut into layers of 1 (cm). Samples were prepared in the usual way, and the spectrometry was performed by means of a HPGe detector and an 8000-channel pulse-height analyser.

The data in Table 6.6-2 to 6.6-5 are based on Table 3 of [7]. These data are the basis of all further calculations. Fitting of the depth profiles in Table 6.6-2 to 6.6-5 with Eq. (2-9) leads to theWeibull-parameters a, n in Table 6.6-6 to 6.6-9.

Table 6.6-10 contains the Weibull-parameters a, n, which are based on 2-dimensional nests of intervals, and Table 6.6-11 contains the figures concerning the sector-method. The fitting results for time series 1 to 4 are presented in Table 6.6-12 and 6.6-13. Table 6.6-14 proves that D and v have no real physical meaning, they are just fitting parameters.

Time series 1 to 4 are characterized by Fig. 6.6-1 to 6.6-16. Fig. 6.6-1, 6.6-5, 6.6-9, and 6.6-13 demonstrate the perfect resp. almost perfect matching of the centres of gravity and of the penetration depths. Fig. 6.6-4, 6.6-8, 6.6-12, and 6.6-16 demonstrate clearly that theoretical models are unable to forecast the transport of radionuclides in soils.

Fig. 6.6-17 shows the somewhat different behaviour of ^{134}Cs and ^{106}Ru in the 2 soils concerned.

6.7 Case study 7

Case study 7 is based on [16]. This paper deals with the transport of ^{137}Cs in different soils. Table 6.7-1 (Table 1 of [16]) characterizes the 4 soils concerned. The soils were placed in concrete cylinders, 0.9 (m) dia. and 0.9 (m) deep. These concrete cylinders were sited along a bank and buried in soil to within 5 (cm) of their rims to minimize temperature changes. A 5 (cm) layer of gravel was placed at the bottom of each cylinder and covered with a 2.5 (cm) layer of sand. The cylinders were filled with soil which had been screened through a 2.5 (cm) sieve. During the following 9 month extra soil was added as necessary to maintain the soil surface 10 (cm) below the rims of the cylinders. In June 1958, the surface was uniformly contaminated with a solution of carrier-free ^{137}Cs at a rate equivalent to 3.7 (mCi m $^{-2}$). The surfaces were left bare and maintained free of weeds. Soil cores, 2 (cm) dia., were withdrawn annually, mostly duplicate cores, and divided into 2.5 (cm) fractions. These were counted directly with a well-type gamma-scintillation counter.

The data in Table 6.7-2 to 6.7-5 are based on Table 2 of [16]. These data are the basis of all further calculations. Fitting of the depth profiles in Table 6.7-2 to 6.7-5 with Eq. (2-9) leads to theWeibull-parameters a, n in Table 6.7-6 to 6.7-9.

Table 6.7-10 contains the Weibull-parameters a, n, which are based on 2-dimensional nests of intervals, and Table 6.7-11 contains the figures concerning the sector-method. The fitting results for time series 1 to 4 are presented in Table 6.7-12 and 6.7-13. Table 6.7-14 proves that D and v have no real physical meaning, they are just fitting parameters.

Time series 1 to 4 are characterized by Fig. 6.7-1 to 6.7-16 and by Fig. 6.7-9a. Fig. 6.7-1, 6.7-5, 6.7-9, and 6.7-13 demonstrate the matching of the centres of gravity and of the penetration depths. The quality of the approximations ranges from still acceptable to almost perfect. Fig. 6.7-9a demonstrates that fitting of n(t) in 2 pieces leads to an excellent approximation. Fig. 6.7-4, 6.7-8, 6.7-12, and 6.7-16 demonstrate clearly that theoretical models are unable to forecast the transport of ^{137}Cs in soils.

6.8 Case study 8

Case study 8 is based on [17]. This paper deals with the transport of ^{90}Sr in the soils characterized in Table 6.7-1 (Table 1 of [16]). Besides a solution of carrier-free ^{137}Cs at a rate equivalent to 3.7 (mCi m^{-2}), carrier-free ^{90}Sr was homogeneously applied to the soil surface at a rate equivalent to 0.4 (mCi m^{-2}).

The data in Table 6.8-1 to 6.8-4 are based on Table 2 of [17]. These data are the basis of all further calculations. Fitting of the depth profiles in Table 6.8-1 to 6.8-4 with Eq. (2-9) leads to theWeibull-parameters a, n in Table 6.8-5 to 6.8-8.

Table 6.8-9 contains the Weibull-parameters a, n, which are based on 2-dimensional nests of intervals, and Table 6.8-10 contains the figures concerning the sector-method. The fitting results for time series 1 to 4 are presented in Table 6.8-11 and 6.8-12. Table 6.8-13 proves that D and v have no real physical meaning, they are just fitting parameters.

Time series 1 to 4 are characterized by Fig. 6.8-1 to 6.8-16. Fig. 6.8-1, 6.8-5, 6.8-9, and 6.8-13 demonstrate the matching of the centres of gravity and of the penetration depths. The quality of the approximations ranges from acceptable to almost perfect. Fig. 6.8-7 shows a small disturbance. Fig. 6.8-4, 6.8-8, 6.8-12, and 6.8-16 demonstrate clearly that theoretical models are unable to forecast the transport of ^{90}Sr in soils.

Fig. 6.8-17 to 6.8-20 show the different behaviour of ^{137}Cs and ^{90}Sr in the 4 soils concerned.

6.9 Case study 9

Case study 9 is based on [18]. This paper deals with the transport of Chernobyl ^{137}Cs in several soils of the 30-km restriction zone of the Chernobyl nuclear power plant (ChNPP). Table 6.9-1 (extract from Table 1 of [18]) contains information about the 4 experimental sites concerned and the fallout, and Table 6.9-2 (extract from Table 2 of [18]) characterizes 3 of the 4 soils concerned. Soil cores with 5 or 10 (cm) dia. were sampled to a maximum depth of 40 (cm) and sectioned horizontally at different intervals. The soil samples were air-dried, ground and passed through a 2-mm sieve before radiometric analysis. ^{137}Cs in the soil samples was determined directly by gamma spectrometry, using a HPGe detector, coupled to a multichannel analyser.

The data in Table 6.9-3 to 6.9-6 are based on Table 3 of [18]. These data are the basis of all further calculations. Fitting of the depth profiles in Table 6.9-3 to 6.9-6 with Eq. (2-9) leads to theWeibull-parameters a, n in Table 6.9-7 to 6.9-10.

Table 6.9-11 contains the Weibull-parameters a, n, which are based on 2-dimensional nests of intervals, and Table 6.9-12 contains the figures concerning the sector-method. The fitting results for time series 1 to 4 are presented in Table 6.9-13 and 6.9-14. Table 6.9-15 proves that D and v have no real physical meaning, they are just fitting parameters.

Time series 1 to 4 are characterized by Fig. 6.9-1 to 6.9-16. Fig. 6.9-1, 6.9-5, 6.9-9, and 6.9-13 demonstrate the matching of the centres of gravity and of the penetration depths. The quality of the approximations ranges from excellent to perfect. The excellent approximations in the case of Fig. 6.9-5 are achieved by fitting n(t) in 2 pieces. The fitting equation for the second part of n(t) is

$$f_8(t) = b \cdot (t + c)^{\frac{1}{m}} + d \quad (6\text{-}3)$$

Fig. 6.9-2 (C1(x)) and 6.9-7 (p1(x)) show disturbances. Fig. 6.9-4, 6.9-8, 6.9-12, and 6.9-16 demonstrate clearly that theoretical models are unable to forecast the transport of Chernobyl ^{137}Cs in soils.

6.10 Case study 10

Case study 10 is based on [19]. This paper deals with the transport of Chernobyl ^{137}Cs in an undisturbed soil of the university farm of Thessaloniki (northern Greece). Table 6.10-1 (Table

1 of [19]) characterizes the soil concerned. The total deposition of ^{137}Cs at the site was 20 (kBq m^{-2}). The contribution of weapons fallout was found to be negligible. Soil samples were periodically collected from 1987 to 1994 from a 10 (m) x 10 (m) area. Slices of soil with a cross section of 50 (cm^2) and a height of 5 (cm) were collected to a depth of 30 (cm). The soil samples were air-dried, ground, and passed through a 2-mm sieve. ^{137}Cs in the soil samples was determined directly by gamma spectrometry, using a HPGe detector, coupled to a multichannel analyser.

The data in Table 6.10-2 are based on Fig. 1 of [19]. They were gained with high precision by means of the digitizing program WinDig 2.5 (© D. Lovy, Geneva).These data are the basis of all further calculations. Fitting of the depth profiles in Table 6.10-2 with Eq. (2-9) leads to theWeibull-parameters a, n in Table 6.10-3.

Table 6.10-4 contains the Weibull-parameters a, n, which are based on 2-dimensional nests of intervals, and Table 6.10-5 contains the figures concerning the sector-method. They indicate a comparatively small scattering of the x_s-values around the x_s-fit. The fitting results for time series 1 are presented in Table 6.10-6. Table 6.10-7 proves that D and v have no real physical meaning, they are just fitting parameters.

Time series 1 is characterized by Fig. 6.10-1 to 6.10-4. Fig. 6.10-1 demonstrates the matching of the centres of gravity and of the penetration depths. The quality of the approximations was improved by fitting n(t) in 2 pieces. Fig. 6.10-3 shows minor disturbances. Fig. 6.10-4 demonstrates once again that theoretical models are unable to forecast the transport of ^{137}Cs in soils.

7. Conclusions

All theoretical models treated failed to forecast the transport of radionuclides in soils. The solution of the ADE, Eq. (2-2), even violates for certain data sets of D, v, and t the mass conservation law. By means of the *integral method* excellent fitting results are achieved for the modelling of depth distributions. It can be argued that the fitting results D and v have no real physical meaning, they are just fitting parameters which depend often heavily on the starting-vector. It is thus unfortunately not sufficient to achieve excellent fitting results. Because of the complexity of the transport of radionuclides in soils and sediments one can argue that any theoretical model is unable to forecast the transport of radionuclides in soils and sediments. This cognition has probably inspired certain workers in the field to employ an empirical approach, but their choice, to employ the simple exponential function for time series analysis, is no general solution of the problem. An empirical approach, based on time series analysis by means of the time dependant Weibull-distribution, is, on the contrary, able to solve the transport problem in question generally.

A critical study of the relevant literature revealed that workers in the field are often not fully aware of the importance of sampling, but a problem oriented sampling strategy improves the reliability of a prognosis.

References

1. Haas, R.: Vertikale und laterale Verteilung von Cäsium-137 an Hängen unter Dauergrünland in Luxemburg – Entwicklung, Anwendung und Bewertung alternativer Modellierungsmethoden. Trierer Geologische Arbeiten, **3**, Herausg. J.-F. Wagner. 1. Aufl., Mainz, Aachen, orig. Doctoral Thesis, University of Trier (2001).
2. Schuller, P., Ellies, A., Kirchner, G.: Vertical migration of fallout ^{137}Cs in agricultural soils from Southern Chile. The Sci. of the Tot. Environ. **193**, 197 (1997).
3. Jury, W. A., Roth, K.: Transfer functions and solute movement through soil - Theory and applications. Birkhäuser, Basel (1990).
4. Kirchner, G.: Modeling the migration of fallout radionuclides in soil using a transfer function model. Health Physics **74**, 78 (1998).
5. Beck, H. L.: Environmental gamma radiation from deposited fisson products, 1960-1964. Health Physics **12**, 313 (1966).
6. Blagoeva, R., Zikovsky, L.: Geographic and vertical distribution of Cs-137 in soils in Canada. J. Environ. Radioact. **27**, 269 (1995).
7. Bonazzola, G. C., Ropolo, R., Facchinelli, A.: Profiles and downward migration of ^{134}Cs and ^{106}Ru deposited on Italian soils after the Chernobyl accident. Health Physics **64**, 479 (1993).
8. Velasco, R. H., Belli, M., Sansone, U., Menegon, S.: Vertical transport of radiocesium in surface soils: Model implementation and dose-rate computation. Health Physics **64,** 37 (1993).
9. Velasco, R. H., Toso, J. P., Belli, M., Sansone, U.: Radiocesium in the Northeastern part of Italy after the Chernobyl accident: Vertical soil transport and soil-to-plant transfer. J. Environ. Radioact. **37**, 73 (1997).
10. European Commission - Belarus, The Russian Federation, Ukraine (Edit.): Behaviour of radionuclides in natural and semi-natural environments. Experimental collaboration project No 5. Final report EUR 16531 EN, Office for Offical Publications of the European Communities, Luxembourg (1996).
11. Haas, R.: Modellierung des vertikalen Transportes von Radionukliden in Böden - Ein Vergleich alternativer Methoden mit herkömmlichen Verfahren. Trierer Bodenkundliche Schriften, **5**, Abt. Bodenkunde, Universität Trier (Hrsg.), orig. Doctoral Thesis, University of Trier (2003).
12. Hartung, J., Elpelt, B., Klösener, K.-H.: Statistik: Lehr- und Handbuch der angewandten Statistik. 10. Aufl., Oldenbourg, München (1995).
13. Steffens, W., Führ, F., Mittelstaedt, W., Klaes, J., Förstel, H.: Untersuchung des Transfers von ^{90}Sr, ^{137}Cs, ^{60}Co und ^{54}Mn vom Boden in die Pflanze und der wichtigsten, den Transfer beeinflussenden Bodenparameter. Institut f. Radioagronomie, Kernforschungsanlage Jülich GmbH, Abschlußbericht, Forschungsvorhaben St. Sch. 702 a (1988).
14. Bachhuber, H., Bunzl, K., Schimmack, W., Gans, I.: The migration of ^{137}Cs and ^{90}Sr in multilayered soils: Results from batch, column, and fallout investigations. Nucl. Technol. **59**, 291 (1982).
15. Bunzl, K., Schimmack, W., Krouglov, S. V., Alexakhin, R. M.: Changes with time in the migration of radiocesium in the soil, as observed near Chernobyl and in Germany, 1986-1994. Sci. Tot. Environ. **175**, 49 (1995).
16. Squire, H. M., Middleton, L. J.: Behaviour of Cs-137 in soils and pastures: A long term experiment. Rad. Botany **6**, 413 (1966).
17. Squire, H. M.: Long-term studies of Strontium-90 in soils and pastures. Rad. Botany **6**, 49

(1966).
18. Ivanov, Y. A., Lewyckyji, N., Levchuk, S. E., Prister, B. S., Firsakova, S. K., Arkhipov, N. P., Arkhipov, A. N., Kruglov, S. V., Alexakhin, R. M., Sandalls, J., Askbrant, S.: Migration of ^{137}Cs and ^{90}Sr from Chernobyl fallout in Ukrainian, Belarussian, and Russian soils. J. Environ. Radioact. **35**, 1 (1997).
19. Antonopoulos-Domis, M., Clouvas, A., Hiladakis, A., Kadi, S.: Radiocesium distribution in undisturbed soil: Measurements and diffusion-advection model. Health Physics **69**, 949 (1995).
20. Finck, R. R.: High resolution field gamma spectrometry and its application to problems in environmental radiology. Doctoral thesis, Departments of Radiation Physics, Malmö and Lund, Lund University (1992).

Tables

Table 6.1-1. Relative cumulated ^{137}Cs inventories in a podsol; time series 1.

	Profile	a	b	c	d	e	f	g	h	i	j	k	l
	Time (a)	0.33	0.83	1.34	1.83	2.42	2.83	3.42	3.84	4.75	5.76	6.67	7.59
Depth (cm)	1	0.87	0.71	0.62	0.59	0.56	0.52	0.49	0.47	0.45	0.40	0.30	0.26
	5	0.99	0.98	0.97	0.99	0.98	0.97	0.97	0.96	0.98	0.95	0.92	0.87
	15	1.00	1.00	0.99	1.00	0.99	1.00	0.99	0.99	1.00	1.00	0.97	0.96
	40	1.00	1.00	1.00	1.00	1.00	1.00	1.00	1.00	1.00	1.00	1.00	1.00

Table 6.1-2. Relative cumulated ^{137}Cs inventories in a cambisol; time series 2.

	Profile	a	b	c	d	e	f	g	h	i	j	k	l
	Time (a)	0.33	0.83	1.34	1.83	2.42	2.83	3.42	3.84	4.75	5.76	6.67	7.59
Depth (cm)	1	0.90	0.76	0.63	0.60	0.60	0.56	0.50	0.45	0.46	0.42	0.38	0.31
	5	0.98	0.99	0.98	0.95	0.97	0.93	0.97	0.95	0.94	0.94	0.91	0.88
	15	1.00	1.00	0.99	0.99	0.99	0.99	0.99	0.99	1.00	0.99	0.98	0.99
	40	1.00	1.00	1.00	1.00	1.00	1.00	1.00	1.00	1.00	1.00	1.00	1.00

Table 6.1-3. Relative cumulated ^{90}Sr inventories in a podsol; time series 3.

	Profile	a	b	c	d	e	f	g	h	i	j	k	l
	Time (a)	0.24	0.74	1.24	1.74	2.33	2.73	3.24	3.74	4.64	5.63	6.72	7.67
Depth (cm)	1	0.37	0.18	0.07	0.07	0.03	0.04	0.02	0.03	0.02	0.02	0.01	0.01
	5	0.96	0.76	0.24	0.25	0.09	0.11	0.05	0.05	0.03	0.03	0.03	0.03
	15	1.00	0.99	0.95	0.98	0.91	0.91	0.69	0.64	0.27	0.24	0.16	0.07
	40	1.00	1.00	1.00	1.00	1.00	1.00	1.00	1.00	1.00	1.00	1.00	1.00

Table 6.1-4. Relative cumulated ^{90}Sr inventories in a cambisol; time series 4.

	Profile	a	b	c	d	e	f	g	h	i	j	k	l
	Time (a)	0.24	0.74	1.24	1.74	2.33	2.73	3.24	3.74	4.64	5.63	6.72	7.67
Depth (cm)	1	0.50	0.18	0.09	0.07	0.05	0.05	0.05	0.04	0.02	0.02	0.02	0.02
	5	0.97	0.81	0.59	0.55	0.39	0.29	0.22	0.19	0.12	0.07	0.06	0.07
	15	1.00	0.99	0.97	0.97	0.96	0.90	0.91	0.91	0.86	0.69	0.63	0.54
	40	1.00	1.00	1.00	1.00	1.00	1.00	1.00	1.00	1.00	1.00	1.00	1.00

Table 6.1-5. Fitting results, based on Eq. (6-1), and related figures; time series 1.

Profile	a (cm^{-n})	n (–)	r^2 (%)	x_s (cm)
a	2.010	0.590	99.748	0.471
b	1.238	0.737	99.988	0.904
c	0.968	0.784	99.929	1.199
d	0.892	0.966	99.980	1.143
e	0.821	0.960	99.945	1.251
f	0.734	0.990	99.976	1.373
g	0.673	1.017	99.966	1.466
h	0.631	1.016	99.918	1.563
i	0.593	1.151	99.993	1.498
j	0.517	1.108	99.995	1.746
k	0.357	1.216	99.747	2.187
l	0.303	1.185	99.651	2.585

Table 6.1-6. Fitting results, based on Eq. (6-1), and related figures; time series 2.

Profile	a (cm^{-n})	n (–)	r^2 (%)	x_s (cm)
a	2.270	0.330	99.747	0.520
b	1.417	0.740	99.995	0.752
c	0.988	0.824	99.941	1.126
d	0.917	0.728	99.950	1.376
e	0.921	0.840	99.938	1.209
f	0.820	0.720	99.982	1.625
g	0.687	0.995	99.928	1.461
h	0.598	1.009	99.971	1.658
i	0.616	0.962	99.997	1.683
j	0.550	1.007	99.940	1.805
k	0.473	1.000	99.908	2.114
l	0.368	1.085	99.985	2.436

Table 6.1-7. Fitting results, based on Eq. (6-1), and related figures; time series 3.

Profile	a (cm^{-n})	n (–)	r^2 (%)	x_s (cm)
a	4.620E-1	1.206	99.997	1.782
b	1.935E-1	1.231	100	3.523
c	9.846E-3	2.096	99.435	8.030
d	7.481E-3	2.293	99.384	7.491
e	8.592E-4	2.933	99.866	9.902
f	1.333E-3	2.762	99.773	9.781
g	4.799E-4	2.881	99.922	12.650
h	8.272E-4	2.627	99.897	13.243
i	1.815E-4	2.752	99.919	20.359
j	9.273E-5	2.957	99.899	20.624
k	1.368E-5	3.495	99.863	22.170
l	3.284E-7	4.545	99.855	24.381

Table 6.1-8. Fitting results, based on Eq. (6-1), and related figures; time series 4.

Profile	a (cm^{-n})	n (–)	r^2 (%)	x_s (cm)
a	6.931E-1	1.030	99.991	1.410
b	2.015E-1	1.314	99.971	3.119
c	1.029E-1	1.339	99.974	5.018
d	8.135E-2	1.419	99.984	5.330
e	3.561E-2	1.640	99.936	6.837
f	2.260E-2	1.701	99.898	8.281
g	9.766E-3	2.036	99.812	8.606
h	6.247E-3	2.195	99.824	8.943
i	2.323E-3	2.487	99.944	10.164
j	1.169E-3	2.549	99.940	12.549
k	1.158E-3	2.490	99.942	13.404
l	2.347E-3	2.142	99.927	14.956

Table 6.1-9. Weibull-parameters, based on 2-dimensional nests of intervals.

Time series									
1; 2	1		2		3; 4	3		4	
t (a)	a (cm^{-n})	n (–)	a (cm^{-n})	n (–)	t (a)	a (cm^{-n})	n (–)	a (cm^{-n})	n (–)
0.332	1.971	0.553	2.194	0.341	0.244	0.525	1.362	0.692	0.898
1.343	1.059	0.925	1.11	0.758	1.238	0.02179	2.003	0.103	1.413
3.836	0.591	1.05	0.633	0.954	3.735	9.891E-4	2.464	7.533E-3	2.079
7.588	0.367	1.163	0.427	1.036	7.666	1.35435E-4	2.675	6.77E-4	2.595
15	0.226	1.233	0.288	1.088	15	1.41875E-5	2.98883	4.94E-5	3.063
30	0.14	1.272	0.193	1.122	30	6.695E-7	3.52965	2.415E-6	3.522
50	0.099	1.287	0.145	1.137	50	9.0266E-8	3.91116	2.48E-7	3.811

Table 6.1-10. Upper and lower sector limits.

Time series	c_u (–)	p_u (%)	c_l (–)	p_l (%)
1	1.236	23.6	0.833	16.7
2	1.161	16.1	0.899	10.1
3	1.175	17.5	0.852	14.8
4	1.090	9.0	0.888	11.2

Table 6.1-11. Fitting results.

Time series	Quantity	Basic type of function	Parameter						r^2 (%)
			b	c	d	k	m	α	
1	a(t); 1. fit	(2-18)	1.49466	0.25362	0.98357	0.54766	0.30264		98.88156
	a(t); 2. fit	(2-18)	39.37004	20.97288	-7.12412	0.9445	-0.91789	5E-4	99.99026
	n(t); 1. fit	(2-17)	1.16444	0.57203	0.26505		0.51578		96.3267
	n(t); 2. fit	(2-17)	9.52015	2.94663	-8.18076		0.14885	6E-5	99.62186
	$x_s(t)$	(2-16)	3.21588E3	2.6287E-4			0.4826		90.17745
	$P_{90}(t)$	(2-16)	1.36062E6	1.51031E-6			0.42065	1.595E-3	99.99655
2	a(t); 1. fit	(2-18)	2.05554	0.47502	0.88624	0.53541	0.0263		99.00165
	a(t); 2. fit	(2-18)	2.70142	6.94986	-6.53822	0.64445	-1.19528	3E-4	99.99929
	n(t); 1. fit	(2-17)	5.25691	2.29902	-4.05371		0.20109		85.175
	n(t); 2. fit	(2-17)	9.01066	2.95248	-7.85446		0.18688		99.9997
	$x_s(t)$	(2-16)	8.82437E5	1.02172E-6			0.4493		93.54613
	$P_{90}(t)$	(2-16)	1.39752E6	1.55129E-6			0.42093	2E-4	99.90344

Table 6.1-12. Fitting results.

Time series	Quantity	Basic type of function	Parameter								r^2 (%)
			b	c	d	f	k	m	α	β	
3	a(t); 1. fit	(2-21)	0.56993	4.8003	0.3857	2.03438E-4		1.71115			99.9998
	a(t); 2. fit	(2-20)	127.791	9.187	0.362			0.234	0.02365		100
	n(t); 1. fit	(2-17)	2.17621E3	9.42618E-4	-0.16927			0.17293			96.40328
	n(t); 2. fit	(2-17)	2.14513E3	9.26445E-4	-0.13194			0.17904	2.19E-4		99.34955
	$x_s(t)$	(2-16)	61.14196	0.08523				0.88886			96.78527
	$P_{90}(t)$	(2-16)	3.57751E6	3.98851E-6				0.4538			96.92773
4	a(t); 1. fit	(2-18)	0.31802	1.19833	0.66968		2.32501	1.00407			99.97203
	a(t); 2. fit	(2-18)	3.91581	12.91427	-3.30237		3.11815	-1.16843	-0.07	0.4	99.99995
	n(t); 1. fit	(2-16)	31.07249	0.04533				0.30689			84.82402
	n(t); 2. fit	(2-16)	4.64983	0.35095				0.40844	1.2E-4		99.84915
	$x_s(t)$	(2-16)	822.51863	4.83203E-3				0.64945			99.20938
	$P_{90}(t)$	(2-16)	2.57268E6	2.85774E-6				0.56462			99.9563

Table 6.1-13. Parameter values concerning theoretical models, based on the *integral method*.

Time series	Profile	Model					
		Solution ADE		Quasi solution		Transf. function mod.	
		D ($cm^2 a^{-1}$)	v ($cm a^{-1}$)	D ($cm^2 a^{-1}$)	v ($cm a^{-1}$)	σ (–)	μ (–)
1	a	0.449	0.644	0.547	0.807	1.335	-1.504
	1	0.894	-0.101	0.678	-0.027	0.928	0.592
2	a	0.261	1.042	0.499	0.493	1.975	-2.529
	1	167.838	-66.592	0.595	-5.358E-4	0.963	0.478
3	a	16.498	-4.118	9.145	0.834	0.773	0.256
	1	2.835	3.06	2.337	3.104	0.185	2.982
4	a	70.136	-48.342	4.517	0.059	0.855	7.519E-6
	1	3.783	1.607	2.71	1.873	0.589	2.629

Table 6.1-14. Primary photon fluence rates (time series 1, ^{137}Cs).

Time t (a)	Model						
	Weibull	Solution ADE		Quasi solution		Transf. function mod.	
		Profile					
		a	l	a	l	a	l
	Φ (Bq cm^{-2})						
0.332	1.9	1.24	1.243	1.296	1.29	1.522	2.011
1.343	1.116	0.776	0.924	0.848	0.952	0.885	1.309
3.836	0.806	0.409	0.691	0.44	0.696	0.482	0.802
7.588	0.582	0.203	0.539	0.197	0.527	0.279	0.506
15	0.39	0.065	0.386	0.051	0.358	0.135	0.264
30	0.215	9.278E-3	0.233	5.063E-3	0.199	0.048	0.1
50	0.112	1.13E-3	0.133	3.22E-4	0.103	0.017	0.035

Table 6.1-15. Fitting results concerning primary photon fluence rates (time series 1, ^{137}Cs).

Parameter (function (2-20))	Model						
	Weibull	Solution ADE		Quasi solution		Transf. function mod.	
		Profile					
		a	l	a	l	a	l
	r^2 (%)						
	99.92846	99.98982	99.97166	99.99732	99.97958	99.99916	99.99751
b	1.22824	0.74048	0.72372	0.76296	0.75019	1.31284	1.31538
c	0.70085	0.53258	0.39896	0.48135	0.40043	0.96933	0.61191
d	0.332	0.332	0.332	0.33203	0.332	0.23796	0.31403
m	0.36157	0.6556	0.4491	0.71391	0.47669	0.41489	0.49112

Table 6.1-16. Fitting results concerning integrated primary photon fluence rates (time series 1, ^{137}Cs).

Parameter (function (2-17))	Model						
	Weibull	Solution ADE		Quasi solution		Transf. function mod.	
		Profile					
		a	l	a	l	a	l
	r^2 (%)						
	99.99959	99.99965	99.99959	99.9998	99.9995	99.99941	99.99923
b	26.33108	5.53798	24.95865	5.55206	21.07707	8.95475	15.17278
c	0.07605	0.28216	0.05712	0.29253	0.07168	0.23587	0.16841
m	0.70618	0.78328	0.77546	0.81911	0.77048	0.64201	0.71356
d	-1.01619	-0.69147	-0.70078	-0.68695	-0.74569	-1.09409	-1.27599

Table 6.2-1. Relative cumulated ^{137}Cs inventories in a podsol; time series 1.

	Profile	a	b	c	d
	Time (a)	0.685	1.068	1.468	1.756
Depth (cm)	1	0.16	0.13	0.13	0.12
	2	0.41	0.35	0.30	0.30
	3	0.59	0.54	0.49	0.46
	4	0.72	0.69	0.65	0.61
	5	0.82	0.82	0.80	0.78
	6	0.88	0.89	0.88	0.87
	7	0.93	0.93	0.93	0.93
	8	0.97	0.97	0.97	0.97
	15	1.00	1.00	1.00	1.00

Table 6.2-2. Relative cumulated ^{85}Sr inventories in a podsol; time series 2.

	Profile	a	b	c	d
	Time (a)	0.534	0,838	1.203	1.586
Depth (cm)	1	0.35	0.24	0.19	0.20
	2	0.67	0.57	0.47	0.44
	3	0.90	0.81	0.72	0.65
	4	0.96	0.94	0.83	0.81
	5	0.98	0.99	0.90	0.86
	6	0.99	1.00	0.94	0.90
	7	1.00	1.00	0.97	0.94
	8	1.00	1.00	0.98	0.98
	15	1.00	1.00	1.00	1.00

Table 6.2-3. Fitting results, based on Eq. (6-1), and related figures; time series 1.

Profile	a (cm^{-n})	n (–)	r^2 (%)	x_s (cm)
a	0.196	1.357	99.92054	3.045
b	0.144	1.529	99.97556	3.199
c	0.118	1.607	99.93765	3.388
d	0.106	1.634	99.82236	3.534

Table 6.2-4. Fitting results, based on Eq. (6-1), and related figures; time series 2.

Profile	a (cm^{-n})	n (–)	r^2 (%)	x_s (cm)
a	0.419	1.475	99.91441	1.632
b	0.267	1.677	99.98346	1.963
c	0.234	1.460	99.80365	2.450
d	0.236	1.337	99.79093	2.705

Table 6.2-5. Weibull-parameters, based on 2-dimensional nests of intervals.

Time series					
1			2		
t (a)	a (cm^{-n})	n (–)	t (a)	a (cm^{-n})	n (–)
685	195	1369	534	421	1482
1068	145	151	838	262	1655
1468	118	16	1203	238	1476
1756	105	16505	1586	235	1332
4	62	18507	4	88	15637
7	43	19755	7	62	15278
10	34	20497	10	53	14783

Table 6.2-6. Upper and lower sector limits.

Time series	c_u (–)	p_u (%)	c_l (–)	p_l (%)
1	1.009	0.9	0.99	1
2	1.023	2.3	0.975	2.5

Table 6.2-7. Fitting results.

Time series	Quantity	Basic type of function	Parameter						r^2 (%)
			b	c	d	k	m	α	
1	a(t); 1. fit	(2-18)	0.53997	1.25806	-1.08359	0.41898	0.20311		100
	a(t); 2. fit	(2-18)	1.13795	26.16817	-58.63619	0.67336	-0.62995		99.99434
	n(t); 1. fit	(2-17)	551.11419	0.20739	-101.73784		3.208E-3		97.3374
	n(t); 2. fit	(2-17)	13.6438	2.51426	-11.05171		0.10749	2.5E-4	99.98784
	$x_s(t)$	(2-16)	2.01933E4	1.58725E-4			0.15803		97.46282
	$P_{90}(t)$	(2-16)	2.36442E6	2.62357E-6			0.09749		99.30727
2	a(t); 1. fit	(2-18)	332.485	7.387	0.442	1.031	0.016	0.1	99.32365
	a(t); 2. fit	(2-18)	5.9159E3	43.90082	-16.9561	0.99024	-0.52248	1E-3	96.69832
	n(t); 1. fit	(2-17)	276.62	0.456	-99.789		-3.003E-4		4.7556
	n(t); 2. fit	(2-17)	13.56556	2.65485	-11.10786		-9.08813E-4	-1.365E-3	0.0677
	$x_s(t)$	(2-16)	1.66764E4	1.31214E-4			0.47932		99.06614
	$P_{90}(t)$	(2-16)	1.86896E6	2.07409E-6			0.52093		99.72244

Table 6.2-8. Parameter values concerning theoretical models, based on the *integral method*.

Time series	Profile	Model					
		Solution ADE		Quasi solution		Transf. function mod.	
		D ($cm^2 a^{-1}$)	v ($cm a^{-1}$)	D ($cm^2 a^{-1}$)	v ($cm a^{-1}$)	σ (–)	μ (–)
1	a	9.0626	0.52277	9.7072	-1.34872	0.79501	0.87607
	d	2.41059	1.11756	1.69088	-1.84309	0.67989	1.09802
2	a	2.40375	1.09848	1.65796	-2.58728	0.69146	0.30167
	d	3.20193	0.14015	3.82446	5.19625E-5	0.78698	0.7582

Table 6.3-1. Relative cumulated ^{137}Cs inventories in a *parabrown earth soil* in Bavaria; time series 1.

	Profile	a	b	c	d	e	f	g
	Time (a)	0.1	2.1	3.1	4.2	5.1	6.2	8.1
Depth (cm)	2	0.85	0.41	0.38	0.24	0.25	0.21	0.22
	4	0.97	0.78	0.74	0.66	0.70	0.70	0.68
	7	0.99	0.91	0.91	0.86	0.90	0.90	0.88
	10	1.00	1.00	1.00	1.00	1.00	1.00	1.00

Table 6.3-2. Relative cumulated ^{137}Cs inventories in a podsol near Chernobyl; time series 2.

	Profile	a	b	c	d	e	f
	Time (a)	1.1	2.0	4.2	5.1	6.0	7.0
Depth (cm)	1	0.93	0.78	0.46	0.55	0.27	0.26
	2	0.98	0.92	0.80	0.78	0.50	0.44
	3	1.00	0.94	0.93	0.90	0.71	0.65
	4	1.00	0.95	0.98	0.96	0.82	0.80
	15	1.00	1.00	1.00	1.00	1.00	1.00

Table 6.3-3. Fitting results, based on Eq. (6-1), and related figures; time series 1.

Profile	a (cm^{-n})	n (–)	r^2 (%)	x_s (cm)
a	1.04	0.87	99.66	1.025
b	0.22	1.34	98.78	2.842
c	0.19	1.37	99.44	3.074
d	0.10	1.61	98.46	3.745
e	0.09	1.77	98.77	3.469
f	0.07	2.04	98.38	3.262
g	0.09	1.77	98.24	3.469

Table 6.3-4. Fitting results, based on Eq. (6-1), and related figures; time series 2.

Profile	a (cm^{-n})	n (–)	r^2 (%)	x_s (cm)
a	2.652	0.632	99.99498	0.301
b	1.546	0.569	99.89260	0.753
c	0.620	1.351	99.99131	1.306
d	0.791	0.971	99.98112	1.290
e	0.304	1.252	99.94121	2.410
f	0.266	1.258	99.70294	2.665

Table 6.3-5. Weibull-parameters, based on 2-dimensional nests of intervals.

Time series					
1			2		
t (a)	a (cm^{-n})	n (–)	t (a)	a (cm^{-n})	n (–)
1.1	0.292	1.233	1.1	2.873	0.460
2.1	0.173	1.475	2.0	1.854	0.811
4.2	0.101	1.738	4.2	0.694	1.099
6.2	0.077	1.885	6.0	0.393	1.148
8.1	0.063	2.002	7.0	0.300	1.180
12	0.049	2.160	12	0.105	1.293
20	0.036	2.370	20	0.036	1.376

Table 6.3-6. Upper and lower sector limits.

Time series	c_u (–)	p_u (%)	c_l (–)	p_l (%)
1	1.126	12.6	0.941	5.9
2	1.452	45.2	0.740	26.0

Table 6.3-7. Fitting results.

Time series	Quantity	Basic type of function	Parameter						r^2 (%)
			b	c	d	k	m	α	
1	a(t); 1. fit	(2-18)	1.068	0.673	-1.292	0.284	0.966		99.68339
	a(t); 2. fit	(2-18)	0.817	24.269	65.096	0.756	-0.773	7E-3	99.89189
	n(t); 1. fit	(2-17)	589.871	0.099	-54.053		4.365E-3		80.5677
	n(t); 2. fit	(2-17)	45.21256	1.08076	-28.68617		0.0237	2.8E-4	99.93393
	$x_s(t)$	(2-16)	3.621	1.143			0.551		94.96028
	$P_{90}(t)$	(2-16)	2.248E6	2.496E-6			0.025		34.16643
2	a(t); 1. fit	(2-18)	2.215E-4	-6.029	-1.907	4.153	0.697		97.77885
	a(t); 2. fit	(2-18)	3.21	0.496	0.337	0.662	1.649	-1E-3	99.99972
	n(t); 1. fit	(2-17)	2.141	0.242	0.075		0.645		72.37804
	n(t); 2. fit	(2-17)	36.008	3.55	-34.564		0.177	6.9E-4	99.59216
	$x_s(t)$	(2-16)	5.162E3	4.01E-5			1.305		92.12794
	$P_{90}(t)$	(2-16)	6.801E5	7.54E-7			1.231		99.99491

Table 6.3-8. Parameter values concerning theoretical models, based on the *integral method*.

Time series	Profile	Model					
		Solution ADE		Quasi solution		Transf. function mod.	
		D ($cm^2\ a^{-1}$)	v ($cm\ a^{-1}$)	D ($cm^2\ a^{-1}$)	v ($cm\ a^{-1}$)	σ (–)	μ (–)
1	b	152.695	-50.132	3.521	-2.484E-4	0.722	0.853
	g	288.026	-71.704	0.249	0.408	0.594	1.136
2	a	71.692	-188.5	0.258	-2.598E-5	1.022	-1.504
	f	152.698	-51.762	0.418	-0.277	0.935	0.716

Table 6.4-1. Soil Characteristics (Table 1, Soil Characteristics, [9]).

Area	Soil layers (cm)	Sand (%)	Silt (%)	Clay (%)	pH (KCl)	Cation exchange capacity (meq g^{-1})	Organic matter (%)
Area 1	0 – 5	28	54	18	5.9	0.45	10.0
	5 – 10	35	46	19	5.9	0.41	7.5
	10 – 15	33	48	19	6.6	0.38	6.0
	15 – 20	37	42	21	6.8	0.33	4.6
Area 2	0 – 5	21	63	16	7.1	0.55	14.0
	5 – 10	25	61	14	7.2	0.48	11.0
	10 – 15	25	60	15	7.2	0.48	9.7
	15 – 20	25	60	15	7.2	0.48	9.2
Area 3	0 – 5	30	49	21	6.9	0.24	2.3
	5 – 10	28	51	21	6.9	0.25	2.3
	10 – 15	29	50	21	6.9	0.25	2.2
	15 – 20	28	50	22	6.9	0.26	2.3

Table 6.4-2. Relative cumulated ^{137}Cs inventories, area 1; time series 1.

	Profile	a	b	c	d	e	f	g	h	i	j	k	l
	Time (a)	1.2	1.4	2.1	2.3	2.5	2.8	3.0	3.3	3.4	3.8	4.1	4.3
Depth (cm)	5	0.88	0.79	0.77	0.80	0.75	0.75	0.75	0.71	0.64	0.65	0.64	0.70
	10	0.94	0.93	0.91	0.94	0.92	0.92	0.92	0.91	0.87	0.89	0.86	0.90
	15	0.98	0.98	0.97	0.98	0.98	0.97	0.97	0.97	0.98	0.97	0.94	0.97
	20	1.00	1.00	1.00	1.00	1.00	1.00	1.00	1.00	1.00	1.00	1.00	1.00

	Profile	m	n	o	p	q	r	s
	Time (a)	4.5	4.9	5.3	5.5	5.8	6.0	6.2
Depth (cm)	5	0.67	0.64	0.60	0.60	0.60	0.59	0.60
	10	0.91	0.89	0.85	0.85	0.86	0.84	0.86
	15	0.97	0.97	0.92	0.94	0.95	0.93	0.94
	20	1.00	1.00	1.00	1.00	1.00	1.00	1.00

Table 6.4-3. Relative cumulated ^{137}Cs inventories, area 2; time series 2.

	Profile	a	b	c	d	e	f	g	h	i	j	k	l	m	n
	Time (a)	1.2	1.5	2.0	2.3	2.5	2.8	3.0	3.3	3.4	3.8	4.0	4.3	5.3	5.5
Depth (cm)	5	0.85	0.89	0.75	0.70	0.73	0.73	0.71	0.73	0.68	0.64	0.56	0.71	0.61	0.62
	10	0.96	0.98	0.93	0.91	0.92	0.94	0.93	0.91	0.90	0.88	0.85	0.88	0.85	0.89
	15	0.99	0.99	0.98	0.98	0.98	0.98	0.99	0.98	0.97	0.96	0.96	0.92	0.96	0.97
	20	1.00	1.00	1.00	1.00	1.00	1.00	1.00	1.00	1.00	1.00	1.00	1.00	1.00	1.00

Table 6.4-4. Relative cumulated ^{137}Cs inventories, area 3; time series 3.

	Profile	a	b	c	d	e	f	g	h	i	j	k	l
	Time (a)	1.2	1.5	2.0	2.3	2.5	2.8	3.0	3.3	3.4	4.0	4.3	4.5
Depth (cm)	5	0.72	0.81	0.76	0.67	0.65	0.60	0.65	0.61	0.63	0.56	0.72	0.51
	10	0.88	0.92	0.90	0.88	0.89	0.82	0.88	0.81	0.87	0.84	0.90	0.81
	15	0.95	0.97	0.96	0.97	0.96	0.92	0.94	0.93	0.96	0.95	0.96	0.95
	20	1.00	1.00	1.00	1.00	1.00	1.00	1.00	1.00	1.00	1.00	1.00	1.00

Table 6.4-5. Fitting results, based on Eq. (6-1), and related figures; time series 1.

Profile	a (cm^{-n})	n (–)	r^2 (%)	x_s (cm)
a	0.872	0.545	95.518	2.220
b	0.411	0.827	99.518	3.245
c	0.417	0.779	99.416	3.551
d	0.403	0.859	99.775	3.114
e	0.321	0.908	99.928	3.660
f	0.339	0.874	99.749	3.688
g	0.340	0.873	99.929	3.684
h	0.263	0.962	99.881	4.078
i	0.172	1.099	99.401	4.789
j	0.182	1.087	99.840	4.644
k	0.215	0.964	99.305	5.007
l	0.252	0.968	99.686	4.213
m	0.197	1.075	99.899	4.407
n	0.172	1.107	99.965	4.722
o	0.177	1.017	98.991	5.450
p	0.163	1.072	99.709	5.287
q	0.151	1.117	99.715	5.216
r	0.163	1.051	99.550	5.508
s	0.166	1.066	99.654	5.258

Table 6.4-6. Fitting results, based on Eq. (6-1), and related figures; time series 2.

Profile	a (cm^{-n})	n (–)	r^2 (%)	x_s (cm)
a	0.547	0.783	99.908	2.487
b	0.682	0.738	99.942	2.027
c	0.294	0.957	99.888	3.665
d	0.226	1.037	99.912	4.135
e	0.254	1.010	99.916	3.868
f	0.243	1.052	99.972	3.761
g	0.215	1.093	99.967	3.946
h	0.285	0.939	99.698	3.918
i	0.222	1.021	99.857	4.330
j	0.189	1.049	99.753	4.803
k	0.115	1.222	99.875	5.497
l	0.342	0.794	97.565	4.400
m	0.158	1.097	99.615	5.192
n	0.142	1.198	99.958	4.800

Table 6.4-7. Fitting results, based on Eq. (6-1), and related figures; time series 3.

Profile	a (cm^{-n})	n (–)	r^2 (%)	x_s (cm)
a	0.339	0.813	98.727	4.238
b	0.535	0.698	98.800	3.110
c	0.412	0.762	98.777	3.763
d	0.229	0.980	99.557	4.540
e	0.191	1.057	99.795	4.685
f	0.188	0.972	98.584	5.651
g	0.221	0.968	99.080	4.825
h	0.197	0.961	98.348	5.519
i	0.176	1.071	99.689	4.931
j	0.123	1.182	99.787	5.561
k	0.301	0.889	99.482	4.089
l	0.091	1.272	99.740	6.107

Table 6.4-8. Weibull-parameters, based on 2-dimensional nests of intervals.

Time series								
1			2			3		
t (a)	a (cm^{-n})	n (–)	t (a)	a (cm^{-n})	n (–)	t (a)	a (cm^{-n})	n (–)
1.2	0.643	0.671	1.2	0.588	0.796	1.2	0.413	0.785
2.5	0.323	0.906	2.0	0.323	0.957	2.0	0.288	0.886
4.3	0.208	1.015	3.4	0.209	1.040	2.5	0.236	0.951
6.2	0.160	1.066	5.5	0.177	1.058	3.0	0.205	0.995
15	0.095	1.14475	8	0.169	1.065	4.5	0.155	1.082
25	0.073	1.1866	12	0.168	1.066	10	0.098	1.23805
40	0.060	1.21835	20	0.1675	1.066	30	0.059	1.460

Table 6.4-9. Upper and lower sector limits.

Time series	c_u (–)	p_u (%)	c_l (–)	p_l (%)
1	1.179	17.9	0.862	13.8
2	1.173	17.3	0.764	23.6
3	1.190	19.0	0.757	24.3

Table 6.4-10. Fitting results.

Time series	Quantity	Basic type of function	Parameter							r^2 (%)
			b	c	d	f	k	m	α	
1	a(t); 1. fit	(2-18)	2.585	1.473	0.182		0.694	0.012		93.82195
	a(t); 2. fit	(2-19)	0.71669	-0.18494	-0.53437	0.01341	1.29248	1.66705		99.99934
	n(t); 1. fit	(2-17)	1.355	0.881	-0.234			0.766		80.11387
	n(t); 2. fit	(2-17)	21.61494	3.54751	-20.38535			0.17738	2.525E-4	99.76622
	$x_s(t)$	(2-16)	10.78352	0.24252				0.58228		88.12233
	$P_{90}(t)$	(2-16)	2.48082E6	2.77673E-6				0.29817		98.8274
2	a(t); 1. fit	(2-18)	4.724E3	10.593	0.305		-0.421	0.07		87.68887
	a(t); 2. fit	(2-19)	0.57988	0.24724	-0.33351	0.1674	1.51622	2.58439		99.99958
	n(t); 1. fit	(2-17)	44.623	4.53	-43.498			0.273		46.81695
	n(t); 2. fit	(2-17)	6.28188	2.86528	-5.21539			0.5073		99.95971
	$x_s(t)$	(2-16)	5.21309	0.44606				1.18149		81.25022
	$P_{90}(t)$	(2-17)	10.46308	0.43159	1.21166			1.19576		99.99821

Table 6.4-11. Fitting results.

Time series	Quantity	Basic type of function	Parameter							r^2 (%)
			b	c	d	f	k	m	α	
3	a(t); 1. fit	(2-18)	5.69353E3	10.03742	0.3743		0.24084	0.02633		73.6234
	a(t); 2. fit	(2-19)	0.4722	0.01002	-0.69105	0.04324	0.96319	-14.24109	-1E-3	99.96023
	n(t); 1. fit	(2-17)	46.67533	2.40497	-41.79698			0.03092		56.05171
	n(t); 2. fit	(2-17)	7.15072	1.42495	-4.69073			0.09461	2E-5	99.91224
	$x_s(t)$	(2-16)	6.30565	0.73037				0.66699		45.71125
	$P_{90}(t)$	(2-17)	7.74601	0.63623	4.80197			1.00608		98.665

Table 6.4-12. Parameter values concerning theoretical models, based on the *integral method*.

Time series	Profile	Model					
		Solution ADE		Quasi solution		Transf. function mod.	
		D ($cm^2 a^{-1}$)	v ($cm a^{-1}$)	D ($cm^2 a^{-1}$)	v ($cm a^{-1}$)	σ (–)	μ (–)
1	a	242.54552	-98.16738	4.372	0.162	1.334	0.06194
	s	295.18403	-55.95342	3.243	-0.024	0.80152	1.41123
2	a	259.71972	-96.71611	5.102	0.11	0.911	0.6674
	n	318.46027	-65.43851	3.114	0.135	0.71885	1.39275
3	a	630.37944	-150.76437	10.345	-0.076	1.00773	1.03493
	l	743.01067	-120.13376	6.177	-0.027	0.72211	1.60319

Table 6.4-13. Parameter values concerning the exponential model (Table 2, [9]).

Area	α_0 (cm^{-1})	α_1 (a^{-1})	α_2 (cm^{-1})
Area 1, time series 1	0.29	0.219	0.10
Area 2, time series 2	0.61	0.913	0.20
Area 3, time series 3	0.24	0.190	0.07

Table 6.5-1. Soil Characteristics (Table 1 and 2, Soil Characteristics, [8]).

Area	Soil layers (cm)	Sand (%)	Silt (%)	Clay (%)	pH (KCl)	Cation exchange capacity (meq g^{-1})	Organic matter (%)
Area 1	0 – 5	28	54	18	5.9	0.45	10.0
	5 – 10	35	46	19	5.9	0.41	7.5
	10 – 15	33	48	19	6.6	0.38	6.0
	15 – 20	37	42	21	6.8	0.33	4.6
Area 2	0 – 1 (L)						100
	1 – 2 (F)						100
	2 – 5 (H)				4.1	0.67	68
	5 – 10	44	40	16	5.5	0.66	26
	10 – 15	48	38	14	6.4	0.55	21
	15 – 20	48	38	14	7.0	0.47	10

L: litter horizon; F: fermentation horizon; H: humus horizon

Table 6.5-2. Fitting results, based on Eq. (2-9), and related figures; time series 1.

Profile	Bomb-^{137}Cs				Chernobyl-^{137}Cs			
	a (cm^{-n})	n (–)	r^2 (%)	x_s (cm)	a (cm^{-n})	n (–)	r^2 (%)	x_s (cm)
a	3.109E-3	2.393	99.85647	9.896	0.842	0.494	99.93400	2.897
b	4.700E-2	1.426	99.99316	7.757	0.470	0.688	99.99864	3.857
c	2.700E-2	1.469	99.95894	7.993	0.453	0.661	99.99996	4.445
d	3.100E-2	1.592	99.99227	7.951	0.445	0.762	99.99909	3.401
e	3.100E-2	1.591	99.97991	7.962	0.340	0.845	99.99843	3.915
f	6.300E-2	1.449	99.99997	6.111	0.373	0.777	99.99418	4.119
g	4.200E-2	1.472	99.96497	7.796	0.356	0.814	99.99810	3.981
h	3.600E-2	1.500	99.94830	8.280	0.277	0.887	99.99901	4.510
i	2.400E-2	1.623	99.96884	8.914	0.202	0.962	99.99021	5.365

Table 6.5-3. Fitting results, based on Eq. (2-9), and related figures; time series 2.

Profile	Bomb-^{137}Cs				Chernobyl-^{137}Cs			
	a (cm^{-n})	n (–)	r^2 (%)	x_s (cm)	a (cm^{-n})	n (–)	r^2 (%)	x_s (cm)
a	27.500E-2	0.972	99.96367	3.821	0.816	0.638	99.99802	1.919
b	2.700E-2	1.930	99.32565	5.763	0.640	0.775	99.99736	2.063
c	1.900E-2	1.660	99.52592	9.730	0.360	1.653	98.77989	1.659
d	2.400E-2	1.840	99.12489	6.744	0.734	0.786	99.96173	1.701
e	9.000E-2	1.332	99.47862	5.604	0.422	0.999	99.08049	2.373
f	7.551E-3	2.487	99.77112	6.328	0.033	2.680	99.84575	3.175
g	2.300E-2	1.507	99.34264	11.026	0.684	0.450	99.90333	5.764
h	14.000E-2	1.049	99.47545	6.393	0.430	1.080	97.60400	2.121

Table 6.5-4. Weibull-parameters, based on 2-dimensional nests of intervals.

Time series					
1			2		
t (a)	a (cm^{-n})	n (–)	t (a)	a (cm^{-n})	n (–)
0.30	1.533	0.335	1.00	0.805	0.651
1.17	0.727	0.546	1.67	0.487	0.908
2.42	0.363	0.788	2.42	0.359	1.036
3.42	0.255	0.909	3.42	0.275	1.126
33.42	0.035	1.522	33.42	0.062	1.364
50	0.029	1.587	50	0.049	1.378
100	0.022	1.689	100	0.032	1.403

Table 6.5-5. Upper and lower sector limits.

Time series	c_u (–)	p_u (%)	c_l (–)	p_l (%)
1	1.230	23.0	0.757	24.3
2	1.572	57.2	0.556	44.4

Table 6.5-6. Fitting results.

Time series	Quantity	Basic type of function	Parameter							r^2 (%)
			b	c	d	k	m	α	γ	
1	a(t); 1. fit	(2-18)	1.245	0.57	0.157	0.781	0.03			97.24101
	a(t); 2. fit	(2-20)	1.032E3	7.968	0.507		0.097	0.01		99.97457
	n(t); 1. fit	(2-17)	1.17	0.137	0.363		1.199			82.90924
	n(t); 2. fit	(2-17)	1.769	0.415	-0.049		0.477	7E-5		99.81899
	$x_s(t)$	(2-16)	8.706	0.402			0.539			88.18123
	$P_{90}(t)$	(2-17)	4.372E6	4.874E-6	-13.544		0.229	-1.482E-3	-0.21	99.98302
2	a(t); 1. fit	(2-18)	1.278	0.528	0.157	0.593	0.03			68.06377
	a(t); 2. fit	(2-18)	1.954	1.191	-0.468	0.404	0.389			99.99983
	n(t); 1. fit	(2-17)	892.531	6.823	-890.934		0.147			17.44002
	n(t); 2. fit	(2-17)	27.41	3.619	-26.019		0.206	1E-4		99.89898
	$x_s(t)$	(2-16)	1.561E4	1.223E-4			0.372			62.46614
	$P_{90}(t)$	(2-16)	2.025E6	2.244E-6			0.33			99.78913

Table 6.5-7. Parameter values concerning theoretical models, based on the *integral method*.

Time series	Profile	Model					
		Solution ADE		Quasi solution		Transf. function mod.	
		D ($cm^2\ a^{-1}$)	v ($cm\ a^{-1}$)	D ($cm^2\ a^{-1}$)	v ($cm\ a^{-1}$)	σ (–)	μ (–)
1	a	444.202	-155.689	5.38	0.074	1.507	0.08
	i	559.33	-104.549	5.952	-4.437E-3	0.901	1.358
2	a	276.878	-186.565	4.512	-3.111E-4	1.292	-0.096
	h	310.813	-163.857	1.058	4.361E-5	1.03	0.258

Table 6.5-8. Parameter values concerning the exponential model (Table 5, [8]).

Area	α_0 (cm^{-1})	α_1 (a^{-1})	α_2 (cm^{-1})
Area 1, time series 1	0.30	0.329	0.14
Area 2, time series 2	0.75	0.219	0.11

Table 6.6-1. Soil Characteristics (Table 1, Average values for 0 – 4 cm depth, [7]).

Site	Textural classes	Cation exchange capacity (meq/100 g)	pH	Organic matter (%)	Clay (%) (≤ 2 μm)	Clay and silt (%) (≤ 20 μm)
Castagneto Po	Sandy loam	33	Neutral	8	8	38
Ivrea	Loamy sand	16	Slightly acid	6	3	22

Table 6.6-2. Cumulated inventories of Chernobyl-^{134}Cs in (%), Ivrea; time series 1.

	Profile	a	b	c	d	e	f
	Time (a)	0.583	1.000	1.583	2.083	2.583	3.083
Depth (cm)	1	74.5	70.5	70.2	68.3	48.2	47.8
	2	90.7	93.3	91.1	90.2	75.8	74.3
	3	94.4	96.7	96.2	95.8	87.9	87.2
	4	96.7	98.5	98.6	98.4	95.4	94.1

Table 6.6-3. Cumulated inventories of Chernobyl-^{106}Ru in (%), Ivrea; time series 2.

	Profile	a	b	c	d	e	f
	Time (a)	0.583	1.000	1.583	2.083	2.583	3.083
Depth (cm)	1	58.1	54.6	50.9	50.8	31.2	27.7
	2	77.8	79.1	75.6	77.6	59.4	52.0
	3	87.0	87.9	86.7	88.4	77.7	68.5
	4	93.8	94.0	93.3	94.7	89.2	80.0

Table 6.6-4. Cumulated inventories of Chernobyl-^{134}Cs in (%), Castagneto Po; time series 3.

	Profile	a	b	c	d	e	f
	Time (a)	0.333	0.917	1.417	2.083	2.500	3.083
Depth (cm)	1	73.6	68.7	66.8	59.9	49.5	42.3
	2	90.7	87.3	83.1	82.2	76.8	67.0
	3	96.2	92.6	91.4	91.1	86.3	84.9
	4	98.0	96.2	95.7	95.5	93.1	92.5

Table 6.6-5. Cumulated inventories of Chernobyl-^{106}Ru in (%), Castagneto Po; time series 4.

	Profile	a	b	c	d	e	f
	Time (a)	0.333	0.917	1.417	2.083	2.500	3.083
Depth (cm)	1	61.8	56.7	51.9	46.2	34.3	25.4
	2	81.9	78.9	73.8	68.5	61.5	50.1
	3	89.5	86.3	85.2	83.4	78.4	68.7
	4	93.7	92.2	91.4	93.1	90.8	81.6

Table 6.6-6. Fitting results concerning Chernobyl-^{134}Cs, based on Eq. (2-9), and related figures; time series 1.

Profile	x_{opt} (cm)	M_∞ (%)	a (cm^{-n})	n (–)	r^2 (%)	x_s (cm)
a	10	100	1.381	0.706	99.96500	0.795
b	5	100	1.229	1.055	99.94816	0.805
c	7	100	1.216	0.950	99.98734	0.833
d	7	100	1.155	0.966	99.98588	0.875
e	9	100	0.660	1.087	99.98585	1.420
f	10	100	0.651	1.055	99.99862	1.471

Table 6.6-7. Fitting results concerning Chernobyl-^{106}Ru, based on Eq. (2-9), and related figures; time series 2.

Profile	x_{opt} (cm)	M_∞ (%)	a (cm^{-n})	n (–)	r^2 (%)	x_s (cm)
a	13	100	0.866	0.805	99.97954	1.349
b	11	100	0.799	0.916	99.96439	1.332
c	11	100	0.715	0.959	99.99313	1.446
d	9	100	0.716	1.026	99.98197	1.370
e	10	100	0.372	1.278	99.99598	2.009
f	14	100	0.327	1.151	99.99717	2.513

Table 6.6-8. Fitting results concerning Chernobyl-^{134}Cs, based on Eq. (2-9), and related figures; time series 3.

Profile	x_{opt} (cm)	M_∞ (%)	a (cm^{-n})	n (–)	r^2 (%)	x_s (cm)
a	8	100	1.335	0.816	99.99698	0.784
b	10	100	1.172	0.761	99.97540	0.995
c	12	100	1.095	0.732	99.98785	1.074
d	10	100	0.918	0.891	99.99561	1.165
e	10	100	0.698	0.990	99.92512	1.444
f	10	100	0.536	1.119	99.93169	1.675

Table 6.6-9. Fitting results concerning Chernobyl-^{106}Ru, based on Eq. (2-9), and related figures; time series 4.

Profile	x_{opt} (cm)	M_∞ (%)	a (cm^{-n})	n (–)	r^2 (%)	x_s (cm)
a	13	100	0.971	0.777	99.98327	1.202
b	14	100	0.850	0.805	99.94581	1.380
c	13	100	0.732	0.783	99.99999	1.530
d	11	100	0.602	1.008	99.89223	1.649
e	10	100	0.413	1.222	99.95437	1.931
f	12	100	0.290	1.266	99.99777	2.469

Table 6.6-10. Weibull-parameters, based on 2-dimensional nests of intervals.

Time series									
1; 3	1		3		2; 4	2		4	
t (a)	a (cm^{-n})	n (–)	a (cm^{-n})	n (–)	t (a)	a (cm^{-n})	n (–)	a (cm^{-n})	n (–)
0.583	1.607	0.947	1.221	0.971	0.583	0.987	0.912	0.827	0.989
1.583	1.008	0.993	0.893	0.896	1.000	0.729	1.042	0.681	1.003
2.583	0.819	0.956	0.765	0.886	1.583	0.596	1.039	0.577	1.011
3.083	0.760	0.948	0.723	0.883	2.083	0.529	1.038	0.523	1.014
8	0.509	0.922	0.536	0.872	3.083	0.445	1.037	0.454	1.018
12	0.429	0.917	0.472	0.869	5	0.360	1.036	0.381	1.022
20	0.347	0.910	0.402	0.866	8	0.294	1.034	0.321	1.025

Table 6.6-11. Upper and lower sector limits.

Time series	c_u (–)	p_u (%)	c_l (–)	p_l (%)
1	1.300	30.0	0.770	23.0
2	1.277	27.7	0.753	24.7
3	1.164	16.4	0.876	12.4
4	1.196	19.6	0.872	12.8

Table 6.6-12. Fitting results.

Time series	Quantity	Basic type of function	Parameter						r^2 (%)
			b	c	d	k	m	α	
1	a(t); 1. fit	(2-18)	10.629	0.302	-152.829	0.351	0.393		67.51579
	a(t); 2. fit	(2-18)	1.33841	7.56262	152.25872	0.44114	-0.95453	1.7E-3	99.92505
	n(t); 1. fit	(2-16)	1.023	13.81			4.571		85.01664
	n(t); 2. fit	(2-16)	0.96807	5.43592			-0.23475	4E-4	66.47913
	$x_s(t)$	(2-16)	1.03479E4	7.7245E-5			0.47809		68.51792
	$P_{90}(t)$	(2-16)	1.29489E6	1.43788E-6			0.48698		99.99341
2	a(t); 1. fit	(2-18)	11.381	0.322	-196.324	0.417	0.405		68.34221
	a(t); 2. fit	(2-18)	1.17104	17.82977	-295.39385	0.43859	-0.63765	1E-4	99.9994
	n(t); 1. fit	(2-16)	1.066	11.454			3.888		39.29165
	n(t); 2. fit	(2-16)	1.08453	3.21764			-0.0236		95.13781
	$x_s(t)$	(2-16)	1.35313E4	9.85647E-5			0.42498		62.08877
	$P_{90}(t)$	(2-16)	1.64876E6	1.8307E-6			0.42617		99.99962

Table 6.6-13. Fitting results.

Time series	Quantity	Basic type of function	Parameter						r^2 (%)
			b	c	d	k	m	α	
3	a(t); 1. fit	(2-18)	23.438	0.327	-244.004	0.289	0.411		76.75408
	a(t); 2. fit	(2-18)	1.31371	10.68599	77.89207	0.31156	-0.86916	1E-5	99.99979
	n(t); 1. fit	(2-16)	0.899	138.349			3.692		5.19887
	n(t); 2. fit	(2-16)	3.86407	0.27435			-0.03307	9E-4	75.1162
	$x_s(t)$	(2-16)	1.16947E4	8.62923E-5			0.37327		87.74981
	$P_{90}(t)$	(2-16)	1.47343E6	1.63672E-6			0.37954		99.98897
4	a(t); 1. fit	(2-18)	23.736	0.337	-282.481	0.361	0.416		76.98712
	a(t); 2. fit	(2-18)	1.15264	18.43768	-278.50671	0.3619	-0.63172	-1E-4	99.99959
	n(t); 1. fit	(2-16)	1.035	98.614			3.876		24.7707
	n(t); 2. fit	(2-16)	1.02727	3.71929			0.22224	1E-4	99.82795
	$x_s(t)$	(2-16)	1.42022E4	1.03245E-4			0.3435		79.09368
	$P_{90}(t)$	(2-16)	1.74119E6	1.93331E-6			0.34004		99.99603

Table 6.6-14. Parameter values concerning theoretical models, based on the *integral method*.

Time series	Profile	Model					
		Solution ADE		Quasi solution		Transf. function mod.	
		D ($cm^2\ a^{-1}$)	v ($cm\ a^{-1}$)	D ($cm^2\ a^{-1}$)	v ($cm\ a^{-1}$)	σ (–)	μ (–)
1	a	185.871	-240.058	0.729	-0.02	1.126	-0.748
	f	236.424	-159.103	0.502	3.709E-4	0.91	0.062
2	a	219.043	-170.945	1.958	4.73E-3	1.134	-0.217
	f	286.615	-107.362	1.406	0.109	0.969	0.61
3	a	165.482	-211.937	1.324	-0.05	0.979	-0.617
	f	212.268	-123.516	0.666	-1.362E-3	0.901	0.208
4	a	205.733	-180.637	2.656	0.096	1.135	-0.34
	f	268.455	-99.226	1.424	0.13	0.891	0.642

Table 6.7-1. Soil Characteristics (Table 1, Description of soils, [16]).

Soil no./Soil	Site of collection	pH	Exchangeable cations Total	Exchangeable cations Ca	Exchangeable cations K	Org. mat.	Clay cont.
			(meq/100 g)			(%)	(%)
1/Acid clay	Watlington, Oxon	4.6	16.3	3.2	0.20	4.2	19.5
3/Sand	Wigginton. Oxon	6.6	6.8	5.6	0.14	2.0	3.2
6/Lower greensand	Nuneham Courtney. Berks	6.0	13.2	8.5	0.28	2.1	11.0
8/Calcareous loam	Compton. Berks	7.6	26.0	28.5	0.95	5.5	16.8

Table 6.7-2. Cumulated ^{137}Cs inventories in (%), Soil no. 1; time series 1.

	Profile	a	b	c	d	e
	Time (a)	0.500	1.750	2.833	3.833	6.083
Depth (cm)	2.5	95.545	96.700	92.993	90.390	86.500
	5.0	97.426	98.100	97.197	96.196	94.900
	7.5	99.604	99.000	97.998	97.689	97.900
	10.0		99.500	98.699	98.498	98.800
	15.0				99.700	99.500
	19.0	100				
	20.0					99.900
	26.0		100		100	
	27.0			100		
	30.0					100

Table 6.7-3. Cumulated ^{137}Cs inventories in (%), Soil no. 3; time series 2.

	Profile	a	b	c	d	e
	Time (a)	0.500	1.750	2.833	3.833	6.083
Depth (cm)	2.5	96.596	91.792	86.900	77.200	58.058
	5.0	99.499	97.097	97.800	95.700	86.687
	7.5	99.900	99.199	99.400	99.200	95.095
	10.0	100	99.800	99.800	99.800	98.398
	15.0		100	100		99.900
	20.0				100	100

Table 6.7-4. Cumulated ^{137}Cs inventories in (%), Soil no. 6; time series 3.

	Profile	a	b	c	d	e
	Time (a)	0.500	1.750	2.833	3.833	6.083
Depth (cm)	2.5	95.904	85.185	75.776	74.675	47.100
	5.0	98.302	97.497	90.691	90.991	76.400
	7.5	99.400	99.299	96.997	96.897	90.000
	10.0		99.700	99.399	98.899	95.100
	15.0	100	100		99.800	98.200
	18.0			100		
	20.0				100	99.200
	30.0					100

Table 6.7-5. Cumulated ^{137}Cs inventories in (%), Soil no. 8; time series 4.

	Profile	a	b	c	d	e
	Time (a)	0.500	1.750	2.833	3.833	6.083
Depth (cm)	2.5	75.876	60.320	53.700	57.000	45.800
	5.0	95.395	81.663	83.800	83.400	71.800
	7.5	99.499	93.286	94.400	93.100	85.700
	10.0	100	98.497	99.000	96.300	92.200
	15.0			100	99.500	97.200
	20.0		100		100	99.300
	30.0					100

Table 6.7-6. Fitting results concerning ^{137}Cs, based on Eq. (2-9), and related figures; time series 1.

Profile	x_{opt} (cm)	M_∞ (%)	a (cm^{-n})	n (–)	r^2 (%)	x_s (cm)
a	19	100	2.142	0.394	99.98492	0.502
b	26	100	2.583	0.293	99.99711	0.405
c	27	100	1.865	0.389	99.99418	0.724
d	26	100	1.549	0.453	99.99675	0.929
e	30	100	1.177	0.579	99.99924	1.191

Table 6.7-7. Fitting results concerning ^{137}Cs, based on Eq. (2-9), and related figures; time series 2.

Profile	x_{opt} (cm)	M_∞ (%)	a (cm^{-n})	n (–)	r^2 (%)	x_s (cm)
a	10	100	1.863	0.650	99.99999	0.525
b	15	100	1.498	0.555	99.99692	0.811
c	15	100	0.896	0.894	99.99942	1.194
d	20	100	0.546	1.087	99.99991	1.690
e	20	100	0.299	1.171	99.98718	2.655

Table 6.7-8. Fitting results concerning ^{137}Cs, based on Eq. (2-9), and related figures; time series 3.

Profile	x_{opt} (cm)	M_∞ (%)	a (cm^{-n})	n (–)	r^2 (%)	x_s (cm)
a	15	100	2.171	0.417	99.99746	0.464
b	15	100	0.815	0.930	99.99875	1.289
c	18	100	0.675	0.803	99.98177	1.844
d	20	100	0.640	0.831	99.99798	1.889
e	30	100	0.225	1.148	99.96970	3.492

Table 6.7-9. Fitting results concerning ^{137}Cs, based on Eq. (2-9), and related figures; time series 4.

Profile	x_{opt} (cm)	M_∞ (%)	a (cm^{-n})	n (–)	r^2 (%)	x_s (cm)
a	10	100	0.506	1.127	99.99882	1.752
b	20	100	0.373	0.973	99.92539	2.789
c	15	100	0.250	1.229	99.99351	2.889
d	20	100	0.327	1.044	99.97977	2.868
e	30	100	0.240	1.031	99.98856	3.942

Table 6.7-10. Weibull-parameters, based on 2-dimensional nests of intervals.

Time series								
1 - 4	1		2		3		4	
t (a)	a (cm^{-n})	n (–)	a (cm^{-n})	n (–)	a (cm^{-n})	n (–)	a (cm^{-n})	n (–)
0.500	2.569	0.432	2.810	0.633	2.219	0.582	0.509	1.117
1.750	1.921	0.438	1.419	0.593	0.956	0.838	0.351	1.081
3.833	1.553	0.465	0.630	0.921	0.4644	0.962	0.2792	1.0636
6.083	1.339	0.491	0.333	1.109	0.2601	1.0863	0.2447	1.0546
15	0.928	0.570	0.058	1.5238	0.0514	1.4318	0.1895	1.0395
30	0.626	0.671	7.843E-3	1.934	7.7928E-3	1.8083	0.1566	1.0278
50	0.420	0.785	1.126E-3	2.289	1.1346E-3	2.1712	0.1359	1.021

Table 6.7-11. Upper and lower sector limits.

Time series	c_u (–)	p_u (%)	c_l (–)	p_l (%)
1	1.630	63.0	0.680	32.0
2	1.024	2.4	0.912	8.8
3	1.140	14.0	0.830	17.0
4	1.087	8.7	0.885	11.5

Table 6.7-12. Fitting results.

Time series	Quantity	Basic type of function	Parameter							r^2 (%)
			b	c	d	f	k	m	α	
1	a(t); 1. fit	(2-18)	57.096	0.322	-299.441		0.173	0.408	-0.019	43.26691
	a(t); 2. fit	(2-19)	3.92086	-4.49195	-48.82209	-7.78068	0.04317	-0.40362	1E-4	99.99677
	n(t); 1. fit	(2-16)	868.547	4.062E-4				0.2		42.65339
	n(t); 2. fit	(2-17)	157.47828	0.47113	-58.82637			2.18178E-3		91.96332
	$x_s(t)$	(2-16)	7.91183E3	5.58491E-5				0.52678		80.73437
	$P_{90}(t)$	(2-16)	1.03243E6	1.16752E-6				0.51007		99.8708
2	a(t); 1. fit	(2-20)	2.43	0.986	1.075			0.6	0.0386187	99.84984
	a(t); 2. fit	(2-21)	2.99676	1.13125	0.66461	4.38792E-4		0.52293	4.22E-3	99.99999
	n(t); 1. fit	(2-16)	9.605E3	6.709E-5				0.324		74.05389
	n(t); 2. fit	(2-17)	166.11307	0.44881	-59.81219			0.01036	7.3E-4	99.09922
	$x_s(t)$	(2-16)	9.53311E3	5.38227E-5				0.89804		97.13307
	$P_{90}(t)$	(2-16)	1.13249E6	1.28019E-6				0.75592		99.99378

Table 6.7-13. Fitting results.

Time series	Quantity	Basic type of function	Parameter							r^2 (%)
			b	c	d	f	k	m	α	
3	a(t); 1. fit	(2-20)	1.535	0.925	0.5			0.504	-0.0252	98.17767
	a(t); 2. fit	(2-21)	1.76774	0.99818	0.5179	1.36118E-4		0.53418		100
	n(t); 1. fit	(2-16)	9.365E3	6.554E-5				0.323		77.92772
	n(t); 2. fit	(2-17)	166.23746	0.44727	-59.47676			8.31192E-3	1.0395E-3	95.12705
	n(t); 2. fit/1	(2-17)	166.39129	0.44758	-59.40433			5.8203E-3		95.51162
	n(t); 2. fit/2	(2-17)	165.63573	0.44514	-59.7194			0.01263		99.32772
	$x_s(t)$	(2-16)	1.12876E4	6.36972E-5				0.85192		96.16567
	$P_{90}(t)$	(2-16)	1.34005E6	1.51585E-6				0.71594		99.99026
4	a(t); 1. fit	(2-18)	21.97495	0.34094	-345.40288		0.28346	0.41997		87.67956
	a(t); 2. fit	(2-19)	3.22742	-3.68043	-14.64579	-8.65567	-0.02003	-0.47319	2.4E-4	99.98747
	n(t); 1. fit	(2-17)	166.83356	0.45027	-59.38653			-4.42618E-4		4.14626
	n(t); 2. fit	(2-17)	166.83186	0.45026	-59.38711			-4.2542E-4	9.7E-5	98.03671
	$x_s(t)$	(2-16)	1.98113E4	1.09217E-4				0.30023		89.84967
	$P_{90}(t)$	(2-16)	2.06032E6	2.33114E-6				0.30752		99.99935

Table 6.7-14. Parameter values concerning theoretical models, based on the *integral method*.

Time series	Profile	Model					
		Solution ADE		Quasi solution		Transf. function mod.	
		D ($cm^2\ a^{-1}$)	v ($cm\ a^{-1}$)	D ($cm^2\ a^{-1}$)	v ($cm\ a^{-1}$)	σ (−)	μ (−)
1	a	365.13988	-447.27092	1.51897	0.3578	1.73889	-2.01418
	e	433.72666	-335.05224	0.32179	-1.44351E-5	1.22857	-0.43539
2	a	321.37763	-433.52862	0.77728	1.78097	0.90814	-0.74043
	e	552.43919	-205.75576	0.85396	2.1838E-3	0.75257	0.76462
3	a	275.8361	-349.04603	1.48172	-0.2479	1.48544	-1.65804
	e	513.51572	-143.74317	1.476	-2.4912E-6	0.82714	0.98404
4	a	346.70536	-200.6288	4.68064	-0.13745	0.68134	0.43858
	e	445.83003	-112.28199	1.79854	-4.2053E-3	0.92475	1.03156

Table 6.8-1. Cumulated ^{90}Sr inventories in (%), Soil no. 1; time series 1.

	Profile	a	b	c	d	e
	Time (a)	0.500	1.750	2.833	3.833	6.083
Depth (cm)	2.5	63.200	48.649	52.953	51.300	44.945
	5.0	80.000	68.669	72.472	66.800	61.061
	7.5	95.200	80.380	82.082	77.100	71.571
	10.0		90.290	91.692	84.600	79.479
	15.0				95.800	89.690
	20.0					95.696
	33.0	100				
	40.0		100	100		
	60.0				100	
	70.0					100

Table 6.8-2. Cumulated ^{90}Sr inventories in (%), Soil no. 3; time series 2.

	Profile	a	b	c	d	e
	Time (a)	0.500	1.750	2.833	3.833	6.083
Depth (cm)	2.5	96.400	63.600	54.900	50.500	47.600
	5.0	99.400	91.200	90.700	87.400	79.700
	7.5		98.800	98.900	98.000	95.700
	10.0	100		99.900	99.700	99.100
	12.0		100			
	15.0			100		99.900
	17.0				100	
	20.0					100

Table 6.8-3. Cumulated ^{90}Sr inventories in (%), Soil no. 6; time series 3.

	Profile	a	b	c	d	e
	Time (a)	0.500	1.750	2.833	3.833	6.083
Depth (cm)	2.5	87.000	68.332	43.900	50.700	35.200
	5.0	97.500	92.308	82.300	78.100	65.600
	7.5		98.401	95.500	90.500	85.000
	10.0	100	99.900	98.700	95.300	93.400
	15.0		100	100	99.800	98.000
	20.0				100	99.800
	22.0					100

Table 6.8-4. Cumulated ^{90}Sr inventories in (%), Soil no. 8; time series 4.

	Profile	a	b	c	d	e
	Time (a)	0.500	1.750	2.833	3.833	6.083
Depth (cm)	2.5	63.100	35.664	33.467	29.200	23.924
	5.0	85.300	57.243	59.241	53.300	48.649
	7.5	94.400	76.424	79.720	71.700	67.768
	10.0		9.110	93.606	81.700	79.880
	15.0				98.500	92.693
	20.0					97.898
	23.0	100				
	26.0			100		
	32.0		100			
	35.0				100	
	36.0					100

Table 6.8-5. Fitting results concerning ^{90}Sr, based on Eq. (2-9), and related figures; time series 1.

Profile	x_{opt} (cm)	M_∞ (%)	a (cm^{-n})	n (–)	r^2 (%)	x_s (cm)
a	33	100	0.437	0.875	99.68546	2.754
b	40	100	0.296	0.864	99.91419	4.408
c	40	100	0.354	0.809	99.90515	4.058
d	60	100	0.349	0.739	99.73155	5.009
e	70	100	0.285	0.755	99.86341	6.244

Table 6.8-6. Fitting results concerning ^{90}Sr, based on Eq. (2-9), and related figures; time series 2.

Profile	x_{opt} (cm)	M_∞ (%)	a (cm^{-n})	n (–)	r^2 (%)	x_s (cm)
a	10	100	1.834	0.649	99.99979	0.538
b	12	100	0.311	1.284	99.99642	2.299
c	15	100	0.188	1.577	100	2.591
d	17	100	0.169	1.559	99.99992	2.812
e	20	100	0.181	1.375	99.96309	3.169

Table 6.8-7. Fitting results concerning ^{90}Sr, based on Eq. (2-9), and related figures; time series 3.

Profile	x_{opt} (cm)	M_∞ (%)	a (cm^{-n})	n (–)	r^2 (%)	x_s (cm)
a	10	100	0.902	0.890	99.99667	1.189
b	15	100	0.396	1.162	99.99934	2.106
c	15	100	0.140	1.555	99.98977	3.184
d	20	100	0.262	1.087	99.99086	3.322
e	22	100	0.128	1.327	99.98053	4.330

Table 6.8-8. Fitting results concerning ^{90}Sr, based on Eq. (2-9), and related figures; time series 4.

Profile	x_{opt} (cm)	M_∞ (%)	a (cm^{-n})	n (–)	r^2 (%)	x_s (cm)
a	23	100	0.415	0.956	99.99867	2.560
b	32	100	0.140	1.170	99.70033	5.084
c	26	100	0.113	1.325	99.77810	4.770
d	35	100	0.107	1.227	99.77980	5.782
e	36	100	0.087	1.268	99.99348	6.369

Table 6.8-9. Weibull-parameters, based on 2-dimensional nests of intervals.

Time series								
1 - 4	1		2		3		4	
t (a)	a (cm^{-n})	n (–)	a (cm^{-n})	n (–)	a (cm^{-n})	n (–)	a (cm^{-n})	n (–)
0.500	0.4293	0.9020	1.3265	0.5304	0.8826	0.9330	0.3733	0.9374
1.750	0.3514	0.8183	0.3992	1.2747	0.3578	1.174	0.1684	1.1631
3.833	0.3148	0.7759	0.1654	1.6040	0.1897	1.2742	0.09894	1.2817
6.083	0.2969	0.7529	0.0924	1.7707	0.1268	1.3289	0.07085	1.3494
15	0.2679	0.7113	0.02475	2.0861	0.05404	1.4323	0.035702	1.4732
30	0.2504	0.6816	7.6925E-3	2.3208	0.02675	1.50525	0.02019	1.56748
50	0.2398	0.6605	3.0073E-3	2.4862	0.01564	1.55382	0.013257	1.62793

Table 6.8-10. Upper and lower sector limits.

Time series	c_u (–)	p_u (%)	c_l (–)	p_l (%)
1	1.101	10.1	0.871	12.9
2	1.200	20.0	0.926	7.4
3	1.092	9.2	0.924	7.6
4	1.154	15.4	0.874	12.6

Table 6.8-11. Fitting results.

Time series	Quantity	Basic type of function	Parameter							r^2 (%)
			b	c	d	f	k	m	α	
1	a(t); 1. fit	(2-18)	21.066	0.349	-324.677		0.137	0.422		63.68169
	a(t); 2. fit	(2-19)	3.60854	-1.19904	-9.46838	-4.52217	-7.27437E-3	-0.60615		99.99997
	n(t); 1. fit	(2-17)	166.6096	0.4495	-59.46782			-1.17007E-3		75.05795
	n(t); 2. fit	(2-17)	166.60803	0.4495	-59.4675			-1.07851E-3	2.55E-4	99.00677
	$x_s(t)$	(2-16)	2.37002E4	1.41299E-4				0.31901		90.22008
	$P_{90}(t)$	(2-16)	2.70022E6	3.05736E-6				0.33627		99.99584
2	a(t); 1. fit	(2-18)	24.898	0.334	-287.966		1.276	0.415		99.25148
	a(t); 2. fit	(2-19)	0.43634	-0.55305	1.16041	-4.91612E-3	1.15728	-0.06348	3.7E-6	99.97819
	n(t); 1. fit	(2-16)	1.208E4	8.518E-5				0.254		67.26796
	n(t); 2. fit	(2-17)	205.7484	3.98439	-200.88033			0.02866	3.2E-5	99.98351
	$x_s(t)$	(2-16)	1.45248E4	1.00937E-4				0.46869		87.33206
	$P_{90}(t)$	(2-16)	1.66642E6	1.87731E-6				0.38827		99.73151

Table 6.8-12. Fitting results.

Time series	Quantity	Basic type of function	Parameter							r^2 (%)
			b	c	d	f	k	m	α	
3	a(t); 1. fit	(2-18)	22.962	0.341	-307.529		0.751	0.419		95.69295
	a(t); 2. fit	(2-19)	0.36706	-0.38289	0.24228	-0.01376	0.73267	-0.08718		99.99035
	n(t); 1. fit	(2-16)	1.23E4	8.683E-5				0.14		39.98472
	n(t); 2. fit	(2-17)	204.45306	5.112	-202.12391			0.0222	1E-5	99.99751
	$x_s(t)$	(2-16)	1.58652E4	1.0686E-4				0.52187		98.16952
	$P_{90}(t)$	(2-16)	1.81328E6	2.03853E-6				0.48642		99.99055
4	a(t); 1. fit	(2-18)	18.876	0.358	-338.926		0.72	0.428		98.32327
	a(t); 2. fit	(2-19)	0.21423	-0.14523	0.23118	-8.76482E-3	0.62384	-0.08518	1.194E-3	99.99806
	n(t); 1. fit	(2-16)	1.238E4	8.737E-5				0.112		77.22317
	n(t); 2. fit	(2-17)	204.77303	4.6904	-201.81883			0.0184	1.53E-5	99.99457
	$x_s(t)$	(2-16)	2.29684E4	1.59935E-4				0.31802		90.5662
	$P_{90}(t)$	(2-16)	2.69042E6	3.02084E-6				0.27287		99.95425

Table 6.8-13. Parameter values concerning theoretical models, based on the *integral method*.

Time series	Profile	Model					
		Solution ADE		Quasi solution		Transf. function mod.	
		D (cm^2 a^{-1})	v (cm a^{-1})	D (cm^2 a^{-1})	v (cm a^{-1})	σ (−)	μ (−)
1	a	431.10658	-159.84427	10.51774	4.61567E-3	1.03627	0.59138
	e	574.91812	-104.11086	3.92075	7.58892E-5	1.31155	1.16753
2	a	324.80076	-430.66486	3.92075	-5.68504E-5	0.9138	-0.72712
	e	592.41467	-182.76739	1.48917	1.97668E-5	0.68933	0.97018
3	a	342.85449	-277.8264	2.75273	-1.12603E-5	0.77782	0.04125
	e	451.38697	-99.35981	2.30555	0.08576	0.77063	1.23832
4	a	465.79987	-182.70206	9.26377	-0.04676	0.92111	0.61233
	e	577.5445	-84.60115	4.99888	1.94487E-4	0.84397	1.59162

Table 6.9-1. Experimetal Sites and Fallout (extract from Table 1, [18]).

Sites	Locality	Dist./ChNPP	Soil type	Character. of site
UIP 16	Kopachy	6 (km) S	Loamy sand	Tillage before fallout
UIP 17	Chistogalovka	3–4 (km) W	Soddy podsolic sand	Natural meadow with rare sod
UIP 20		12 (km) W	Soddy podsolic, sandy loam	Tillage before fallout
UIP 25		6 (km) NE	Peaty podsolic, gley loamy sand	Humus layer, 20–30 (cm)

UIP: Ukraine
Type of fallout: fuel and condensed 1:1 (UIP 16, 17, 20); fuel and condensed 1:2 (UIP 25)

Table 6.9-2. Properties of Experimental Soils (extract from Table 2, [18]).

Site	Depth (cm)	Sand[a] (%)	Clay[b] (%)	Organ. (%)	pH (KCl)	Ca (Cmol kg^{-1})	Mg (Cmol kg^{-1})	K (g kg^{-1})
UIP 16	0 – 20	80.4	2.0	0.7	4.0	1.0	0.3	3.0
	20 – 30	83.3	0.0	0.0	4.5	0.9	0.2	2.1
UIP 17	0 – 20	85.3	0.0	0.8	4.0	0.8	0.1	0.8
	20 – 30	89.5	1.2	0.4	4.1	0.8	0.2	1.1
	>30	88.7	1.3	0.7	4.0	0.9	0.1	1.0
UIP 25	0 – 20	62.5	5.5	3.5	4.3	6.1	0.7	3.4
	20 – 30	85.1	3.4	0.6	5.1	3.9	0.5	1.1

[a]Sand fraction > 0.025 – 0.05(mm)
[b]Clay fraction < 0.005 – 0.001 (mm)

Table 6.9-3. Cumulated inventories of Chernobyl-^{137}Cs in (%), Site UIP 16; time series 1.

	Profile	a	b	c	d	e
	Time (a)	1	4	6	7	8
Depth (cm)	1	65.400				
	2	95.400	88.611	84.900	72.900	75.350
	3	99.300				
	4				95.500	92.785
	5	100	99.001	98.600		
	6					97.795
	7				98.100	
	10		99.600	99.500	98.900	98.098
	15		99.800	99.640	99.200	99.298
	20		100	99.760	99.300	99.499
	25			99.860	99.800	99.599
	30			99.910	99.900	99.899
	35			99.960		
	40			100	100	100

Table 6.9-4. Cumulated inventories of Chernobyl-^{137}Cs in (%), Site UIP 17; time series 2.

	Profile	a	b	c	d	e
	Time (a)	2	4	5	6	7
Depth (cm)	2	93.800	90.500	78.277	83.900	76.700
	4					95.000
	5	98.300	99.300	98.071	98.000	
	7					98.800
	10	98.900	99.600	99.170	98.800	99.200
	15	99.800	99.800	99.670	99.200	99.500
	20		100	99.870	99.700	99.700
	25			99.970	99.800	99.800
	29	100				
	30			99.980	99.900	99.900
	35			99.990		
	40			100	100	100

Table 6.9-5. Cumulated inventories of Chernobyl-^{137}Cs in (%), Site UIP 20; time series 3.

	Profile	a	b	c	d	e
	Time (a)	1	4	5	6	7
Depth (cm)	1	80.120				
	2		89.400	96.500	83.400	88.000
	4					97.600
	5	97.103	98.500	97.500	98.400	
	7					99.200
	10	98.601	99.400	98.400	99.100	99.400
	15	99.400	99.800	98.900	99.400	99.700
	20		100	99.200	99.600	99.850
	25			99.400	99.700	99.880
	27	100				
	30			99.700	99.800	99.920
	35			99.900	99.900	
	40			100	100	100

Table 6.9-6. Cumulated inventories of Chernobyl-^{137}Cs in (%), Site UIP 25; time series 4.

	Profile	a	b	c	d	e
	Time (a)	1	4	6	7	8
Depth (cm)	1	71.000				
	2	87.500	78.000	62.800	58.500	62.257
	3	95.600				
	4	98.000			85.400	90.691
	5		99.200	95.200		
	6					96.398
	7				94.300	
	10		99.700	97.100	95.700	97.772
	11	100				
	15		99.800	97.800	97.400	98.724
	20		100	100	98.400	99.569
	25				98.800	99.781
	30				99.100	99.886
	40				100	100

Table 6.9-7. Fitting results concerning Chernobyl-^{137}Cs, based on Eq. (2-9), and related figures; time series 1.

Profile	x_{opt} (cm)	M_∞ (%)	a (cm^{-n})	n (–)	r^2 (%)	x_s (cm)
a	5	100	1.062	1.528	99.99827	0.866
b	20	100	1.238	0.811	99.99781	0.862
c	40	100	1.027	0.881	99.99516	1.033
d	40	100	0.564	1.213	99.94172	1.504
e	40	100	0.757	0.890	99.95898	1.448

Table 6.9-8. Fitting results concerning Chernobyl-^{137}Cs, based on Eq. (2-9), and related figures; time series 2.

Profile	x_{opt} (cm)	M_∞ (%)	a (cm^{-n})	n (–)	r^2 (%)	x_s (cm)
a	29	100	2.158	0.370	99.99609	0.523
b	20	100	1.348	0.804	99.99769	0.779
c	40	100	0.748	1.030	99.99143	1.310
d	40	100	1.049	0.802	99.97782	1.065
e	40	100	0.723	1.013	99.98389	1.370

Table 6.9-9. Fitting results concerning Chernobyl-^{137}Cs, based on Eq. (2-9), and related figures; time series 3.

Profile	x_{opt} (cm)	M_∞ (%)	a (cm^{-n})	n (–)	r^2 (%)	x_s (cm)
a	27	100	1.617	0.467	99.99394	0.817
b	20	100	1.419	0.662	99.99683	0.789
c	40	100	2.933	0.167	99.99459	1.120
d	40	100	0.965	0.896	99.98427	1.098
e	40	100	1.240	0.776	99.99241	0.878

Table 6.9-10. Fitting results concerning Chernobyl-^{137}Cs, based on Eq. (2-9), and related figures; time series 4.

Profile	x_{opt} (cm)	M_{∞} (%)	a (cm^{-n})	n (–)	r^2 (%)	x_s (cm)
a	11	100	1.230	0.807	99.98176	0.871
b	20	100	0.630	1.265	99.99837	1.338
c	20	100	0.340	1.170	98.31500	2.381
d	40	100	0.335	1.030	97.76800	2.857
e	40	100	0.410	1.090	99.30000	2.193

Table 6.9-11. Weibull-parameters, based on 2-dimensional nests of intervals.

Time series										
1; 4	1		4		2	2		3	3	
t (a)	a (cm^{-n})	n (–)	a (cm^{-n})	n (–)	t (a)	a (cm^{-n})	n (–)	t (a)	a (cm^{-n})	n (–)
1	1.406	1.5805	1.2940	1.1498	2	2.1175	0.3822	1	1.7297	0.4131
4	0.905	1.0195	0.5455	1.0700	4	1.0705	1.1680	4	1.4665	0.4941
6	0.850	0.9260	0.4123	1.0913	5	0.8415	1.2950	5	1.4261	0.5087
8	0.8213	0.8685	0.3355	1.1086	7	0.5548	1.4545	7	1.3643	0.5317
15	0.7864	0.7563	0.20857	1.14835	15	0.1734	1.7629	15	1.2272	0.5889
30	0.7949	0.6378	0.11924	1.1932	30	0.04374	2.0617	30	1.1046	0.6485
50	0.8456	0.54723	0.077249	1.22505	50	5.3845E-3	2.7557	50	1.0156	0.6970

Table 6.9-12. Upper and lower sector limits.

Time series	c_u (–)	p_u (%)	c_l (–)	p_l (%)
1	1.197	19.7	0.786	21.4
2	1.240	24.0	0.866	13.4
3	1.160	16.0	0.837	16.3
4	1.197	19.7	0.780	22.0

Table 6.9-13. Fitting results.

Time series	Quantity	Basic type of function	Parameter							r^2 (%)
			b	c	d	f	k	m	α	
1	a(t); 1. fit	(2-18)	29.73526	0.32256	-276.47739		0.14513	0.41119		24.31489
	a(t); 2. fit	(2-19)	3.29968	-2.15229	-4.25955	-6.94062	-0.05675	-0.58049	1.35E-4	99.94379
	n(t); 1. fit	(2-17)	163.3525	0.43782	-56.47346			-5.73142E-3		54.49821
	n(t); 2. fit	(2-19)	3.81949	-0.21042	-0.14357	-3.42613	0.03455	-0.12968	-1.199E-4	99.99183
	$x_s(t)$	(2-16)	1.08972E4	6.64339E-5				0.29897		56.54747
	$P_{90}(t)$	(2-16)	1.15332E6	1.30874E-6				0.36619		99.77108
2	a(t); 1. fit	(2-19)	1.64229	-2.4416	-18.40011	-0.11151	0.89226	-0.33916		98.38527
	a(t); 2. fit	(2-19)	2.43893	-2.24576	-62.04012	0.08483	0.79222	-0.34897	-0.0782905	99.99631
	n(t); 1. fit	(2-17)	205.07548	3.82035	-201.05192			0.07491		97.07092
	n(t); 2. fit/1	(2-17)	204.5207	4.30724	-202.60634			0.18552	1.555E-3	99.75045
	n(t); 2. fit/2	(6-3)	0.019	173.026	-3.307			0.936	-5.045E-4	97.99821
	$x_s(t)$	(2-16)	7.13248E3	4.43492E-5				0.74912		80.70833
	$P_{90}(t)$	(2-16)	8.49481E5	9.68017E-7				0.6148		99.90341

Table 6.9-14. Fitting results.

Time series	Quantity	Basic type of function	Parameter							r^2 (%)
			b	c	d	f	k	m	α	
3	a(t); 1. fit	(2-18)	29.545	0.31	-229.289		0.035	0.408		0.50978
	a(t); 2. fit	(2-19)	4.31044	-1.60087	-58.45633	-4.17032	0.03068	-0.40045	-9.8E-5	99.9999
	n(t); 1. fit	(2-16)	1.367E4	2.967E-5				0.269		13.02182
	n(t); 2. fit	(2-17)	166.19535	0.4481	-59.6146			1.30255E-3	1.3615E-3	99.90892
	$x_s(t)$	(2-16)	1.20997E4	6.68382E-5				0.10992		23.86232
	$P_{90}(t)$	(2-16)	1.34189E6	1.52304E-6				0.14163	-1.89E-3	99.65687
4	a(t); 1. fit	(2-18)	27.068	0.319	-243.33		0.591	0.413		96.38765
	a(t); 2. fit	(2-19)	2.91559	0.98858	-63.20341	-0.02903	0.65493	-0.07968	-1.1633E-3	99.99534
	n(t); 1. fit	(2-16)	2.02E4	4.4E-5				0.128		43.0341
	n(t); 2. fit	(2-17)	166.72398	0.44991	-59.42244			1.26113E-3	7.65E-5	99.94766
	$x_s(t)$	(2-16)	1.21721E4	6.25006E-5				0.58732		78.14859
	$P_{90}(t)$	(2-16)	1.23998E6	1.40752E-6				0.56607		99.99307

Table 6.9-15. Parameter values concerning theoretical models, based on the *integral method*.

Time series	Profile	Model					
		Solution ADE		Quasi solution		Transf. function mod.	
		D ($cm^2\ a^{-1}$)	v ($cm\ a^{-1}$)	D ($cm^2\ a^{-1}$)	v ($cm\ a^{-1}$)	σ (–)	μ (–)
1	a	130.12153	-153.1345	0.968	-9.535E-4	0.53672	-0.21258
	e	158.4354	-109.0931	0.203	-9.986E-4	0.89934	0.07515
2	a	107.69208	-149.18233	0.223	0.257	1.72014	-1.95602
	e	128.36649	-93.80051	0.213	1.421E-3	0.77611	0.12632
3	a	94.88204	-153.17048	0.192	0.455	1.57743	-1.33519
	e	110.89176	-116.48397	0.132	-3.202E-5	0.91041	-0.37823
4	a	105.24728	-122.46252	0.523	-7.485E-3	1.02185	-0.55553
	e	142.73077	-74.23926	0.523	1.226E-3	0.71655	0.46655

Table 6.10-1. Soil Characteristics (Table 1, [19]).

pH	Clay (%)	Silt (%)	Sand (%)	Org. matter (%)	Exch. K (meq/100 g)	Total K (mg/100 g)	CEC (meq/100 g)	$CaCO_3$ (%)
8	22	37	41	1.28	0.48	800	22.28	1.8

Table 6.10-2. Cumulated inventories of Chernobyl-^{137}Cs in (%); time series 1.

	Profile	a	b	c	d
	Time (a)	1.2	3.4	5.8	7.0
Depth (cm)	5	66	66	60	47
	10	78	78	79	71
	15	87	85	86	83
	20	93	91	92	90
	25	97	96	96	97
	30	100	100	100	100

Table 6.10-3. Fitting results concerning Chernobyl-^{137}Cs, based on Eq. (2-9), and related figures; time series 1.

Profile	x_{opt} (cm)	M_∞ (%)	a (cm^{-n})	n (–)	r^2 (%)	x_s (cm)
a	30	100	0.350	0.680	99.63700	6.099
b	30	100	0.370	0.640	99.55800	6.574
c	30	100	0.265	0.765	99.83477	6.649
d	30	100	0.129	0.990	99.80900	7.948

Table 6.10-4. Weibull-parameters, based on 2-dimensional nests of intervals.

Time series 1		
t (a)	a (cm^{-n})	n (–)
1.2	0.40504	0.62994
3.4	0.27799	0.7418
5.8	0.21914	0.81499
7	0.19927	0.84486
15	0.12641	0.99129
30	0.07103	1.1847
50	0.038605	1.39728

Table 6.10-5. Upper and lower sector limits.

Time series	c_u (–)	p_u (%)	c_l (–)	p_l (%)
1	1.078	7.8	0.9227	7.73

Table 6.10-6. Fitting results.

Time series	Quantity	Basic type of function	Parameter							r^2 (%)
			b	c	d	f	k	m	α	
	a(t); 1. fit	(2-17)	166.19619	0.44808	-59.61083			-1.85292E-3	-0.017	54.22056
	a(t); 2. fit	(2-19)	2.24594	1.30532	0.18232	-0.16751	0.22943	-2.43511E-4	-0.0147576	99.99818
	n(t); 1. fit	(2-16)	776.987	7.604E-4				0.199		49.35078
1	n(t); 2. fit/1	(2-17)	166.37524	0.44869	-59.54558			1.99407E-3	9.288E-3	99.9851
	n(t); 2. fit/2	(6-3)	0.01	234.808	-1.821			0.979		99.69307
	$x_s(t)$	(2-16)	3.126E4	1.86051E-4				0.12173		63.04316
	$P_{90}(t)$	(2-16)	3.74701E6	4.26996E-6				0.06334	-1.62E-3	95.32666

Table 6.10-7. Parameter values concerning theoretical models, based on the *integral method*.

Time series	Profile	Model					
		Solution ADE		Quasi solution		Transf. function mod.	
		D ($cm^2\ a^{-1}$)	v ($cm\ a^{-1}$)	D ($cm^2\ a^{-1}$)	v ($cm\ a^{-1}$)	σ (–)	μ (–)
1	a	1.61963E3	-281.03153	18.416	-0.012	1.27932	1.14686
	d	1.88566E3	-233.34415	7.092	8.778E-6	0.95941	1.71628

Figures

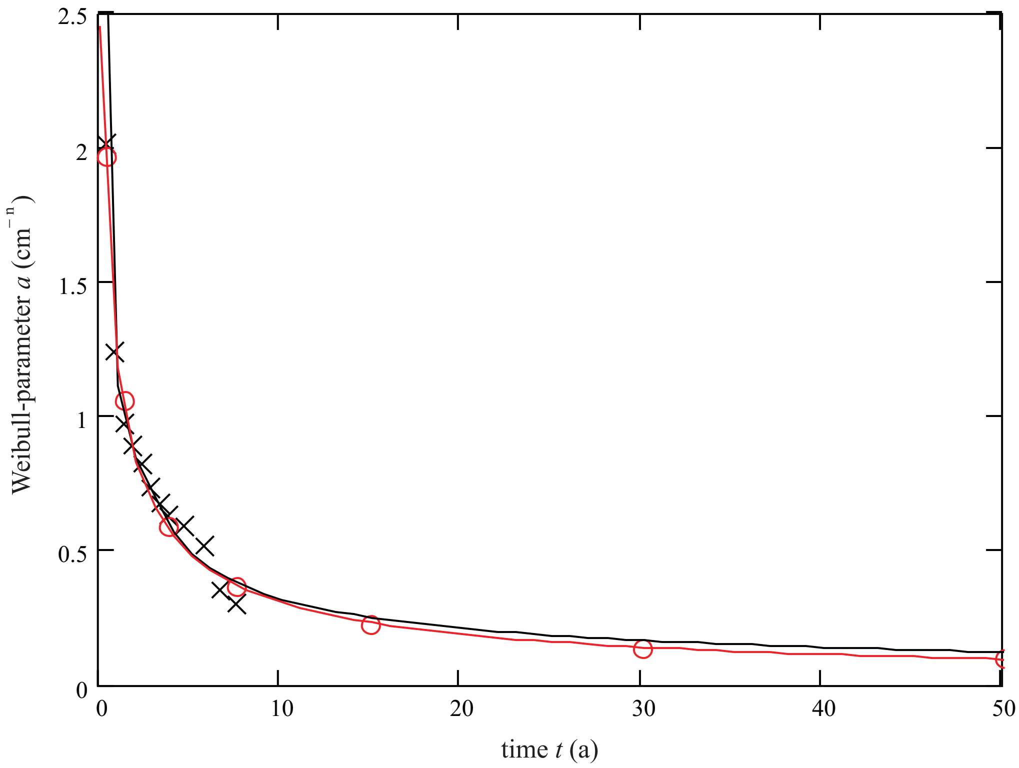

Fig. 6.1-1: Comparison of the first and the second fit (time series 1, Cs-137)
legend:
black: first fit
red : second fit

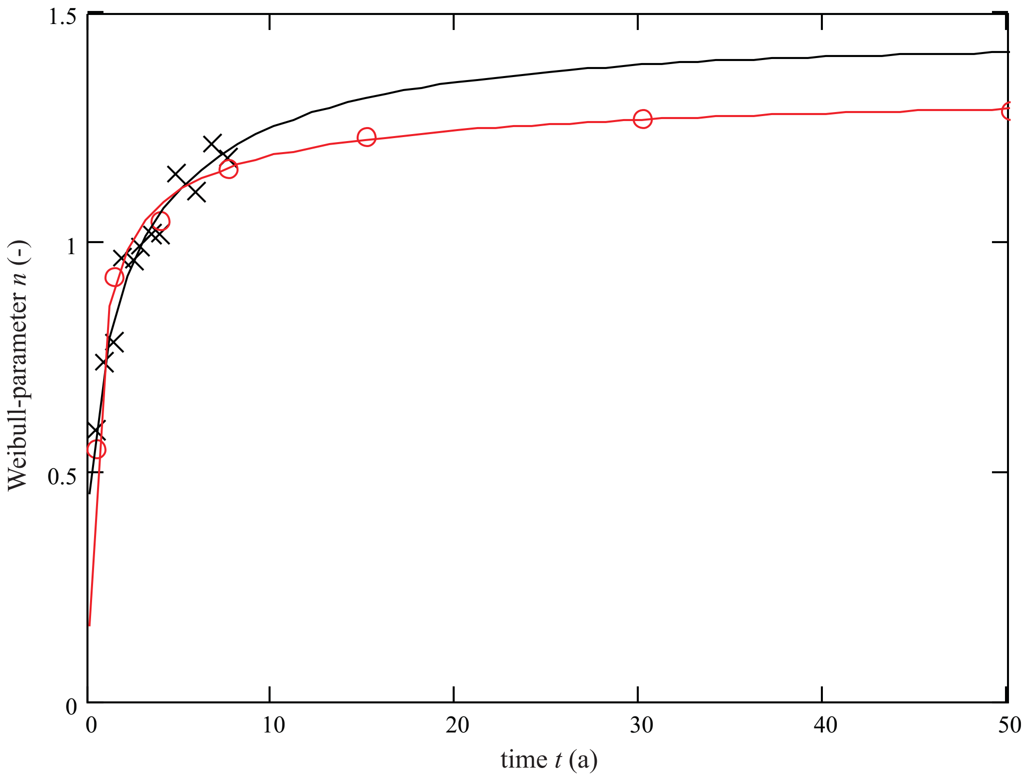

Fig. 6.1-2: Comparison of the first and the second fit (time series 1, Cs-137)

legend:
black: first fit
red : second fit

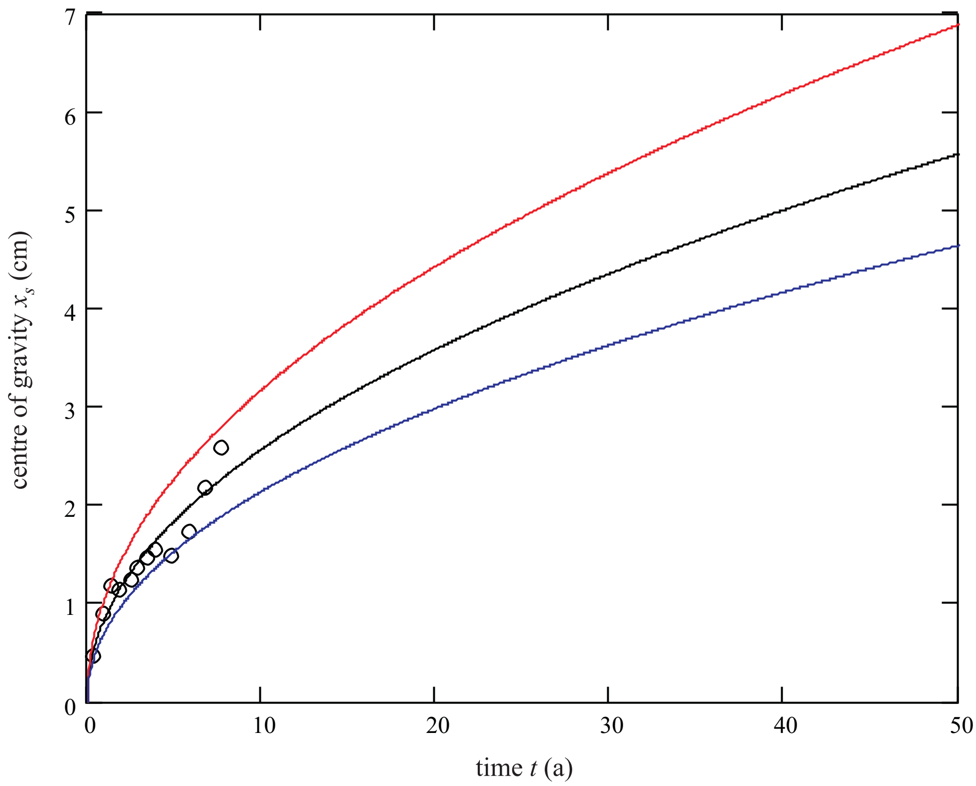

Fig. 6.1-3: Demonstration of the sector-method (time series 1, Cs-137)
legend:
black: fitting of the centres of gravity
red : upper limit
blue : lower limit

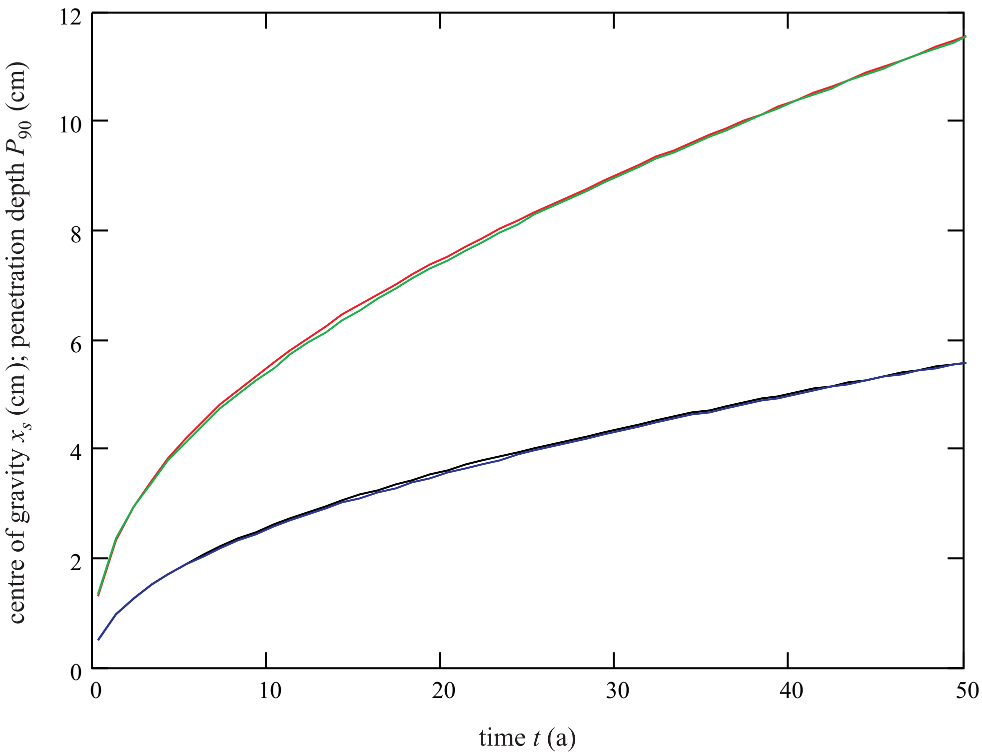

Fig. 6.1-4: Matching of the centres of gravity and of the penetration depths (time series 1, Cs-137)

legend:

black: x_s-fit

blue : matching of the x_s-fit, based on Eq. (2-24)

red : P_{90}-fit

green: matching of the P_{90}-fit; (a(t), n(t) from second fits)

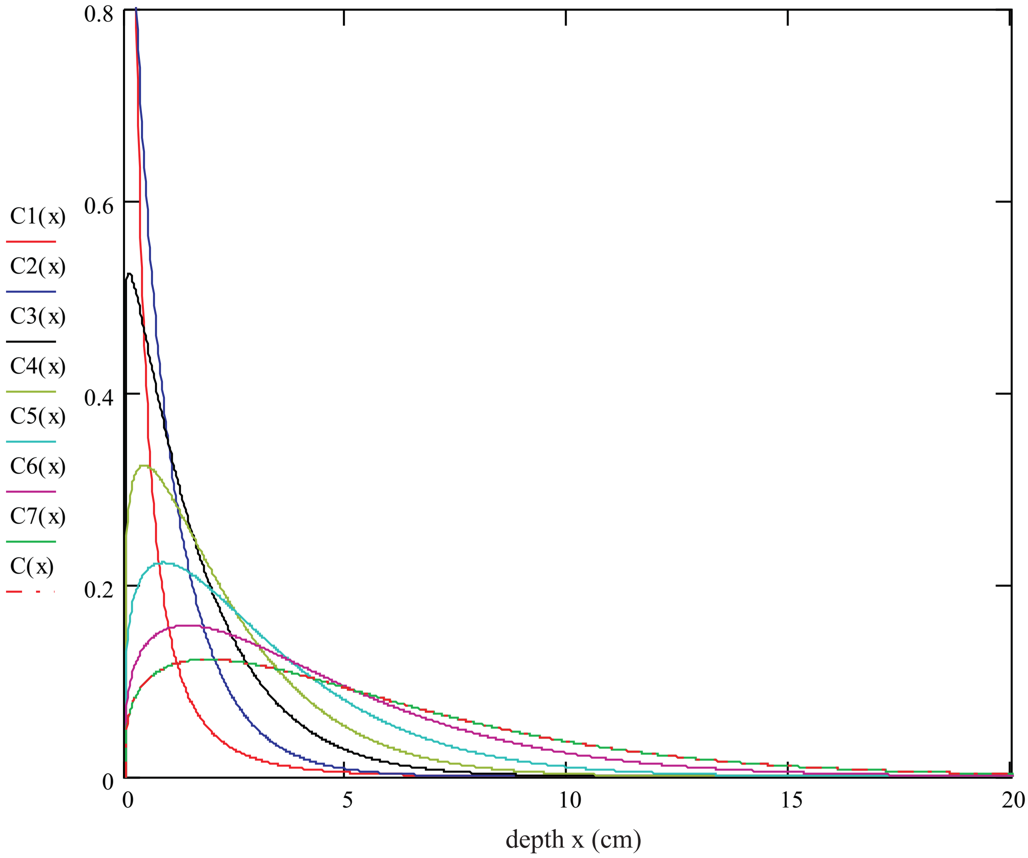

Fig. 6.1-5: Relative concentrations for different points of time (time series 1, Cs-137)
legend:
ordinate axis: relative concentration (cm^{-1})

$\left.\begin{array}{l}\text{C1(x): relative concentration after 0.332 (a)}\\ \text{C2(x): relative concentration after 1.343 (a)}\\ \text{C3(x): relative concentration after 3.836 (a)}\\ \text{C4(x): relative concentration after 7.588 (a)}\\ \text{C5(x): relative concentration after 15 (a)}\\ \text{C6(x): relative concentration after 30 (a)}\\ \text{C7(x): relative concentration after 50 (a)}\end{array}\right\}$ based on 2-dimensional nest of intervals

C(x) : relative concentration after 50 (a), based on second fits of a(t) and n(t)

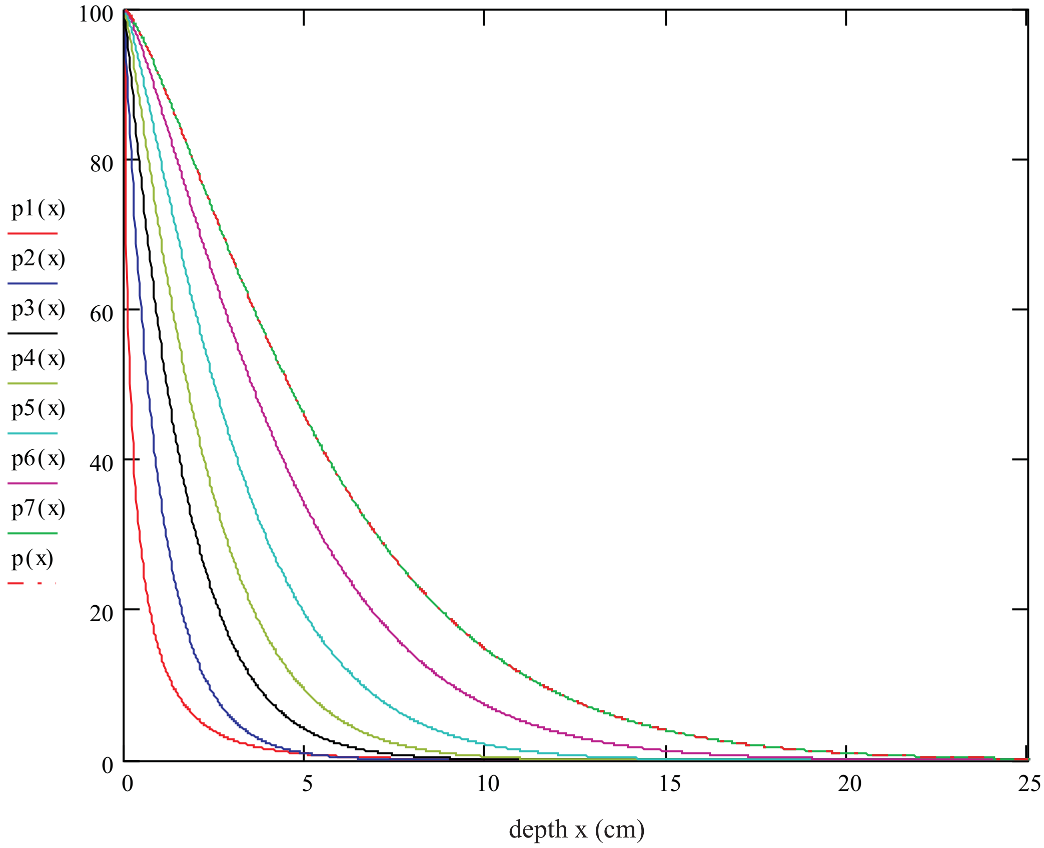

Fig. 6.1-6: Inventories below x in (%) for different points of time (time series 1, Cs-137)
legend:
ordinate axis: inventories below x (%)
p1(x): inventory below x in (%) after 0.332 (a)
p2(x): inventory below x in (%) after 1.343 (a)
p3(x): inventory below x in (%) after 3.836 (a)
p4(x): inventory below x in (%) after 7.588 (a) } based on 2-dimensional nest of intervals
p5(x): inventory below x in (%) after 15 (a)
p6(x): inventory below x in (%) after 30 (a)
p7(x): inventory below x in (%) after 50 (a)
p(x) : inventory below x in (%) after 50 (a), based on second fits of a(t) and n(t)

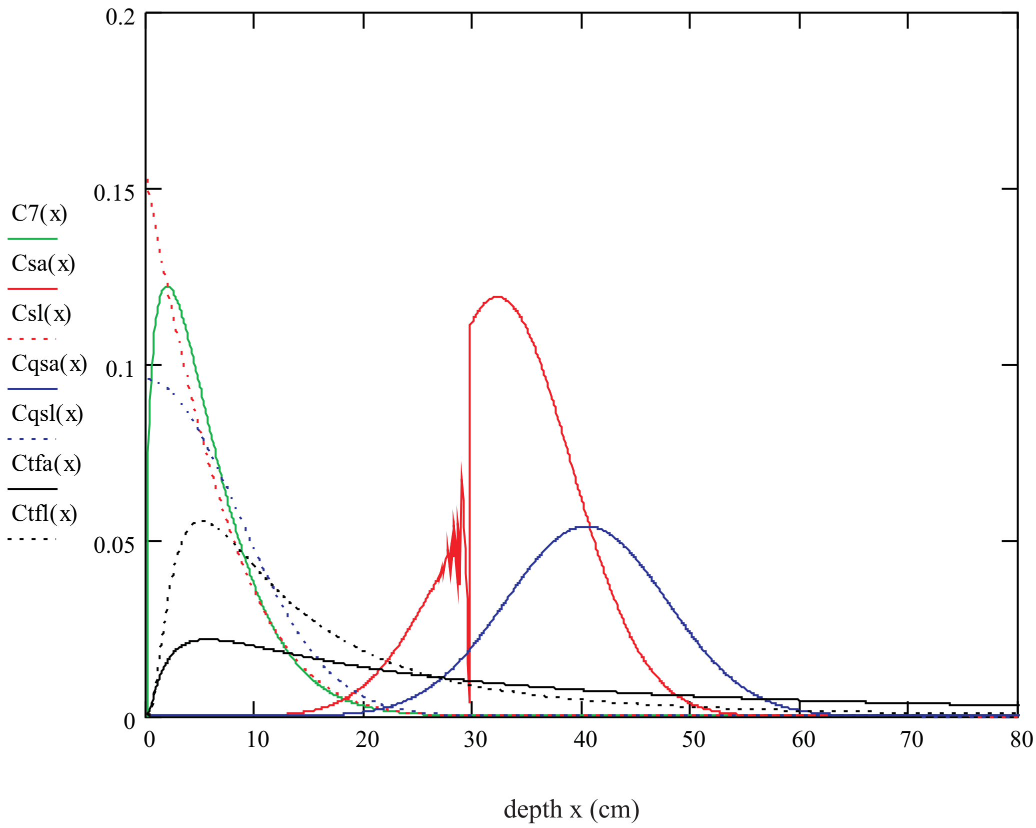

Fig. 6.1-7: Relative concentrations after 50 (a), resulting from different models (time series 1, Cs-137)

legend:

ordinate axis: relative concentration (cm^{-1})

C7(x) : relative concentration after 50 (a), based on 2-dimensional nest of intervals
Csa(x) : relative concentration after 50 (a), based on Eq. (2-2), a-profile
Csl(x) : relative concentration after 50 (a), based on Eq. (2-2), l-profile
Cqsa(x): relative concentration after 50 (a), based on Eq. (2-3), a-profile
Cqsl(x) : relative concentration after 50 (a), based on Eq. (2-3), l-profile
Ctfa(x) : relative concentration after 50 (a), based on Eq. (2-4), a-profile
Ctfl(x) : relative concentration after 50 (a), based on Eq. (2-4), l-profile

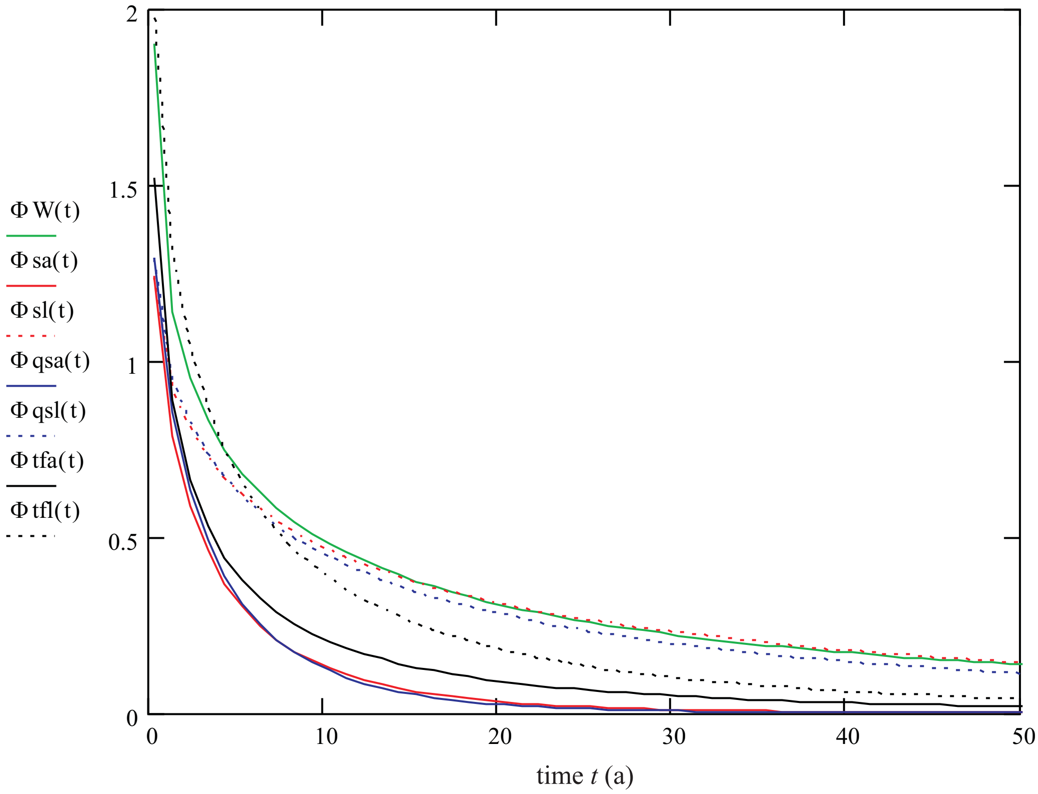

Fig. 6.1-8: Primary photon fluence rates, resulting from different models (time series 1, Cs-137)

legend:

ordinate axis: primary photon fluence rate ($cm^{-2}s^{-1}$)

ΦW(t) : primary photon fluence rate; concentration based on Eq. (2-5)

Φsa(t) : primary photon fluence rate; concentration based on Eq. (2-2), a-profile

Φsl(t) : primary photon fluence rate; concentration based on Eq. (2-2), l-profile

Φqsa(t): primary photon fluence rate; concentration based on Eq. (2-3), a-profile

Φqsl(t) : primary photon fluence rate; concentration based on Eq. (2-3), l-profile

Φtfa(t) : primary photon fluence rate; concentration based on Eq. (2-4), a-profile

Φtfl(t) : primary photon fluence rate; concentration based on Eq. (2-4), l-profile

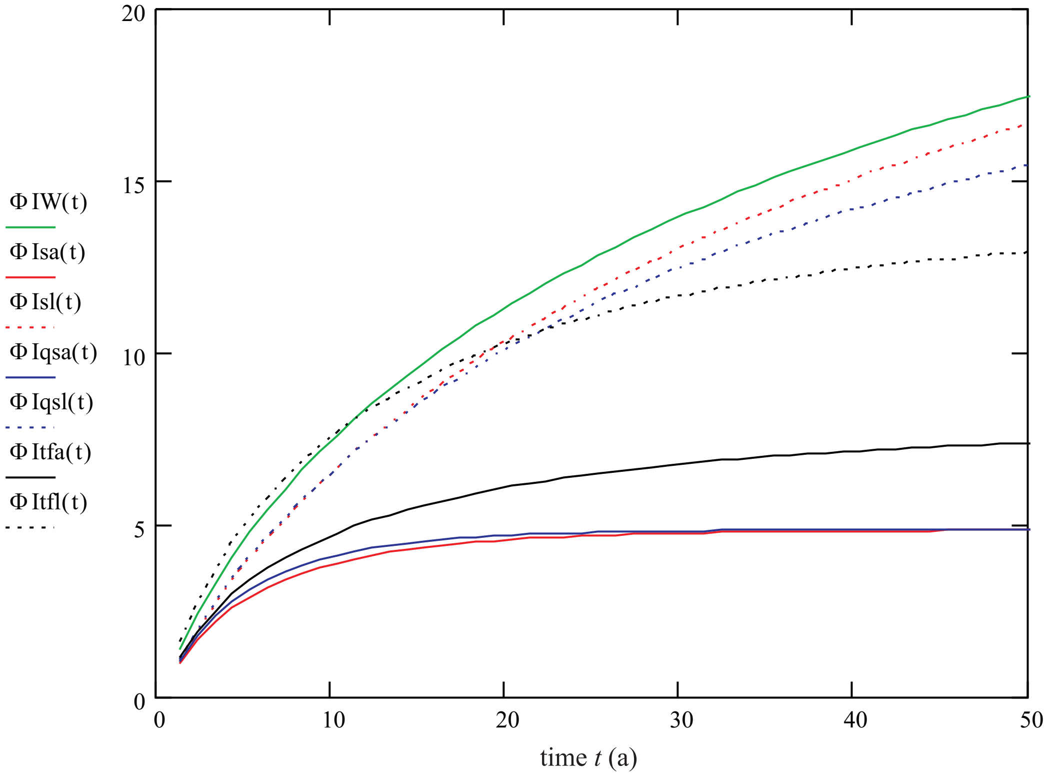

Fig. 6.1-9: Integrated primary photon fluence rates, resulting from different models (time series 1, Cs-137)

legend:

ordinate axis: integrated primary photon fluence rate ($cm^{-2}s^{-1}a$)

ΦIW(t) : integrated primary photon fluence rate; concentration based on Eq. (2-5)

ΦIsa(t) : integrated primary photon fluence rate; concentration based on Eq. (2-2), a-profile

ΦIsl(t) : integrated primary photon fluence rate; concentration based on Eq. (2-2), l-profile

ΦIqsa(t): integrated primary photon fluence rate; concentration based on Eq. (2-3), a-profile

ΦIqsl(t) : integrated primary photon fluence rate; concentration based on Eq. (2-3), l-profile

ΦItfa(t) : integrated primary photon fluence rate; concentration based on Eq. (2-4), a-profile

ΦItfl(t) : integrated primary photon fluence rate; concentration based on Eq. (2-4), l-profile

Remark: The primary photon fluence rates are, for practical reasons, integrated over the time t in (a). If the time t is expressed in (s), the integrated primary photon fluence rates have to be multiplied by the factor 31 536 000. The **real dimension** of the integrated primary photon fluence rate is of course **(cm^{-2})**.

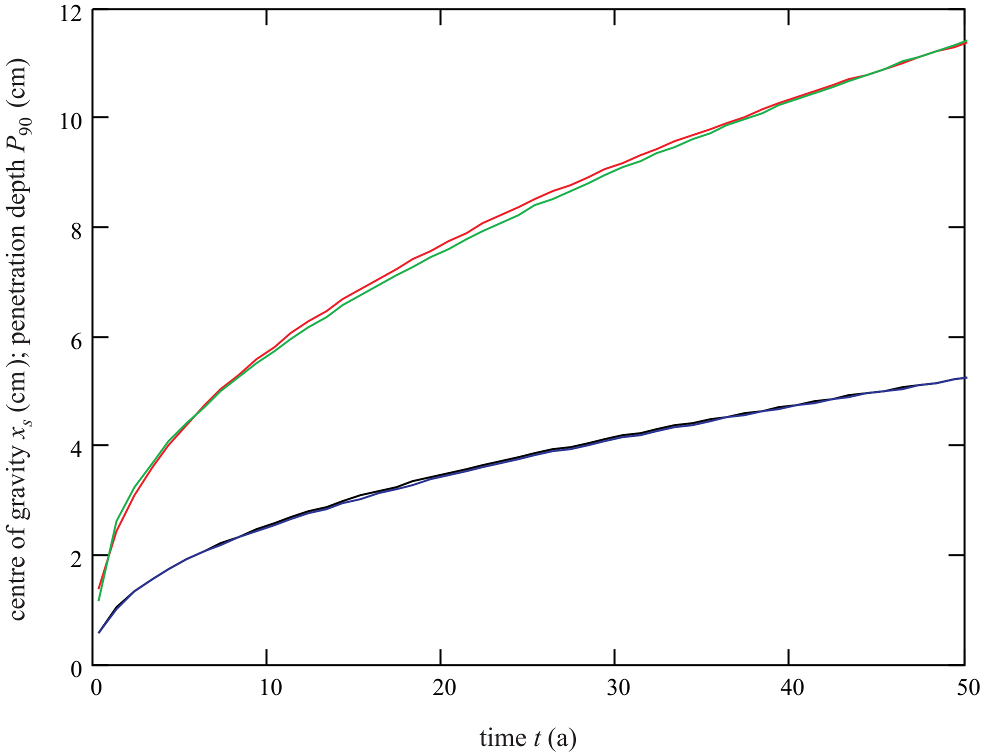

Fig. 6.1-10: Matching of the centres of gravity and of the penetration depths (time series 2, Cs-137)

legend:

black: x_s-fit

blue : matching of the x_s-fit, based on Eq. (2-24)

red : P_{90}-fit

green: matching of the P_{90}-fit; (a(t), n(t) from second fits)

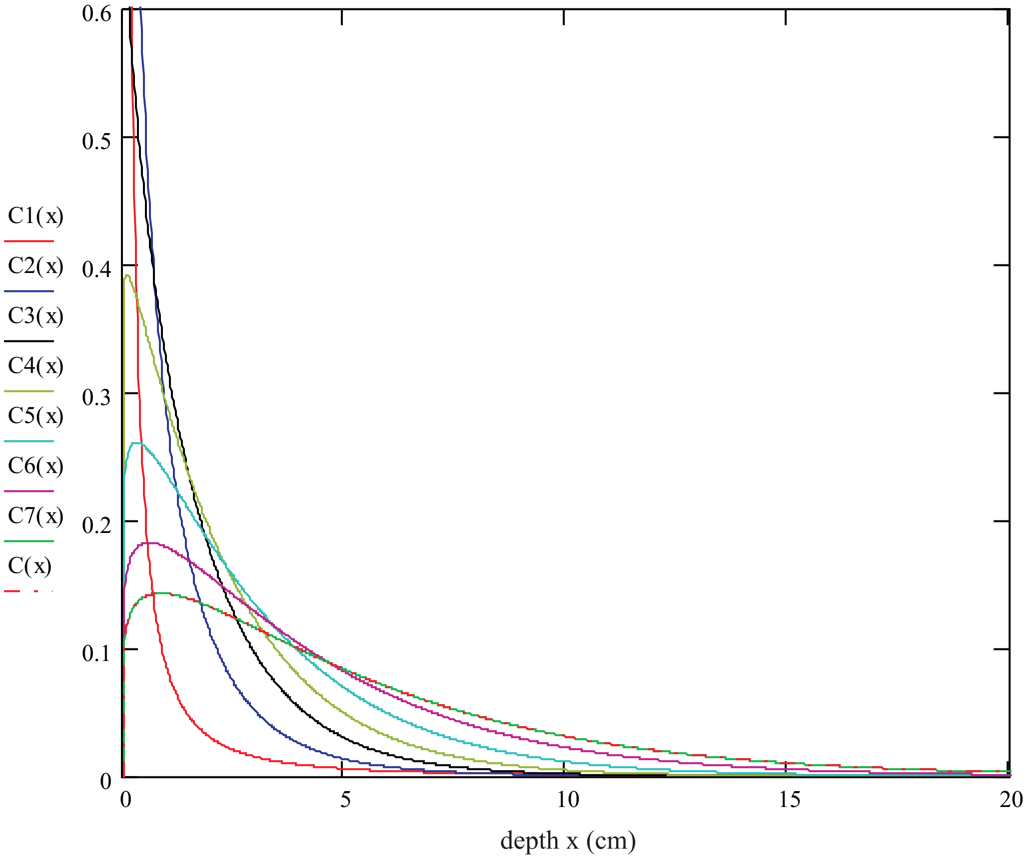

Fig. 6.1-11: Relative concentrations for different points of time (time series 2, Cs-137)
legend:

ordinate axis: relative concentration (cm^{-1})

C1(x): relative concentration after 0.332 (a)
C2(x): relative concentration after 1.343 (a)
C3(x): relative concentration after 3.836 (a)
C4(x): relative concentration after 7.588 (a) } based on 2-dimensional nest of intervals
C5(x): relative concentration after 15 (a)
C6(x): relative concentration after 30 (a)
C7(x): relative concentration after 50 (a)
C(x) : relative concentration after 50 (a), based on second fits of a(t) and n(t)

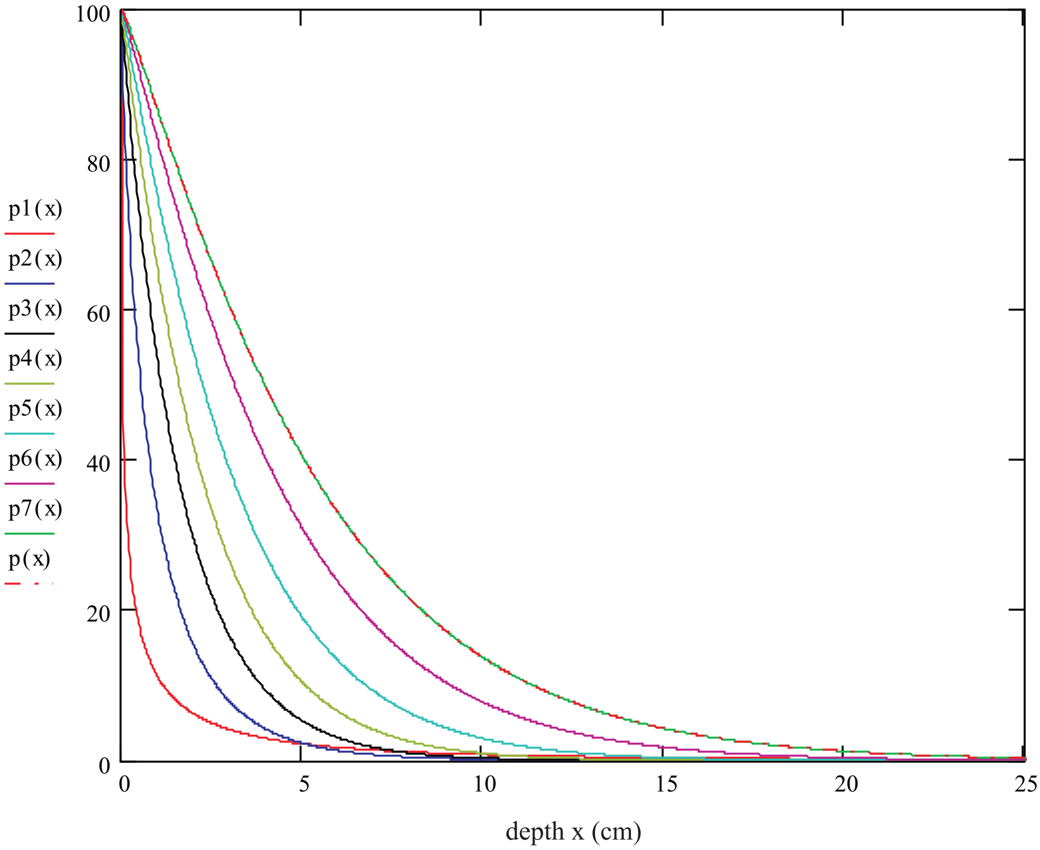

Fig. 6.1-12: Inventories below x in (%) for different points of time (time series 2, Cs-137)
legend:
ordinate axis: inventories below x (%)

p1(x): inventory below x in (%) after 0.332 (a)
p2(x): inventory below x in (%) after 1.343 (a)
p3(x): inventory below x in (%) after 3.836 (a)
p4(x): inventory below x in (%) after 7.588 (a) — based on 2-dimensional nest of intervals
p5(x): inventory below x in (%) after 15 (a)
p6(x): inventory below x in (%) after 30 (a)
p7(x): inventory below x in (%) after 50 (a)
p(x) : inventory below x in (%) after 50 (a), based on second fits of a(t) and n(t)

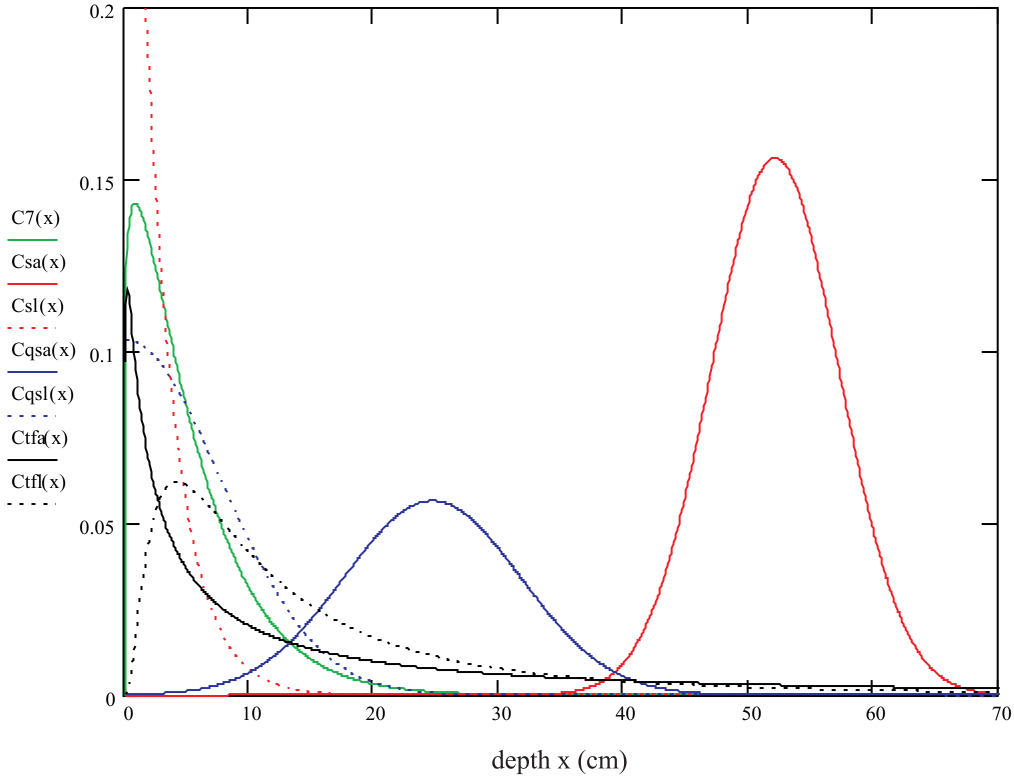

Fig. 6.1-13: Relative concentrations after 50 (a), resulting from different models (time series 2, Cs-137)

legend:

ordinate axis: relative concentration (cm^{-1})

C7(x) : relative concentration after 50 (a), based on 2-dimensional nest of intervals
Csa(x) : relative concentration after 50 (a), based on Eq. (2-2), a-profile
Csl(x) : relative concentration after 50 (a), based on Eq. (2-2), l-profile
Cqsa(x): relative concentration after 50 (a), based on Eq. (2-3), a-profile
Cqsl(x) : relative concentration after 50 (a), based on Eq. (2-3), l-profile
Ctfa(x) : relative concentration after 50 (a), based on Eq. (2-4), a-profile
Ctfl(x) : relative concentration after 50 (a), based on Eq. (2-4), l-profile

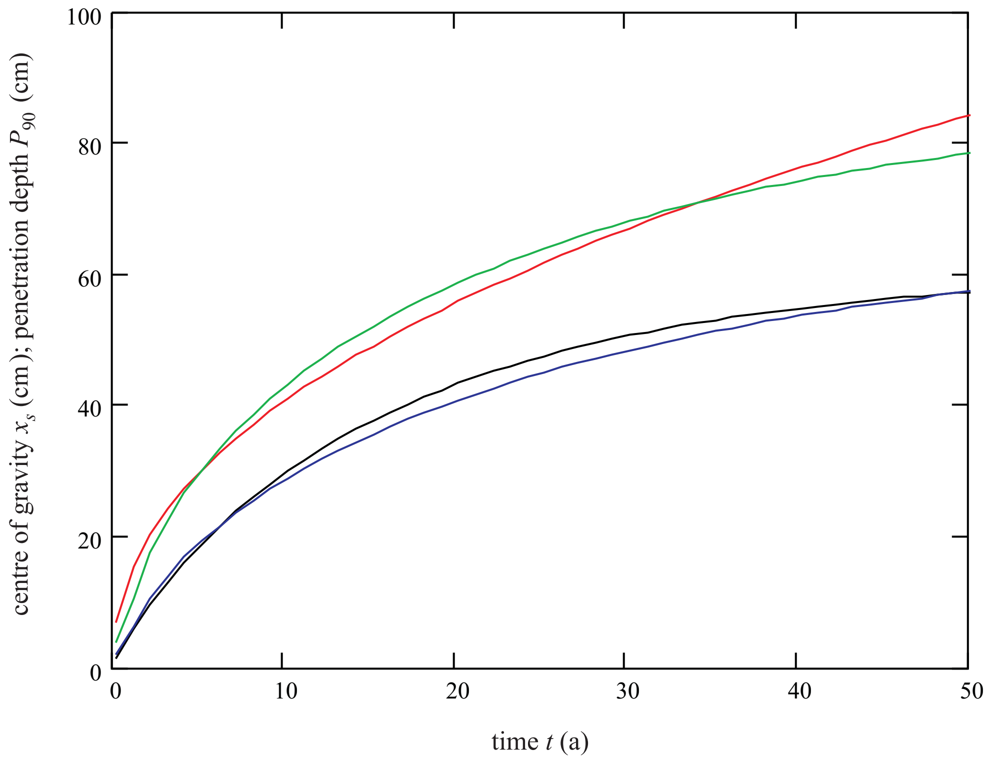

Fig. 6.1-14: Matching of the centres of gravity and of the penetration depths (time series 3, Sr-90)

legend:

black: x_s-fit

blue : matching of the x_s-fit, based on Eq. (2-24)

red : P_{90}-fit

green: matching of the P_{90}-fit; (a(t), n(t) from second fits)

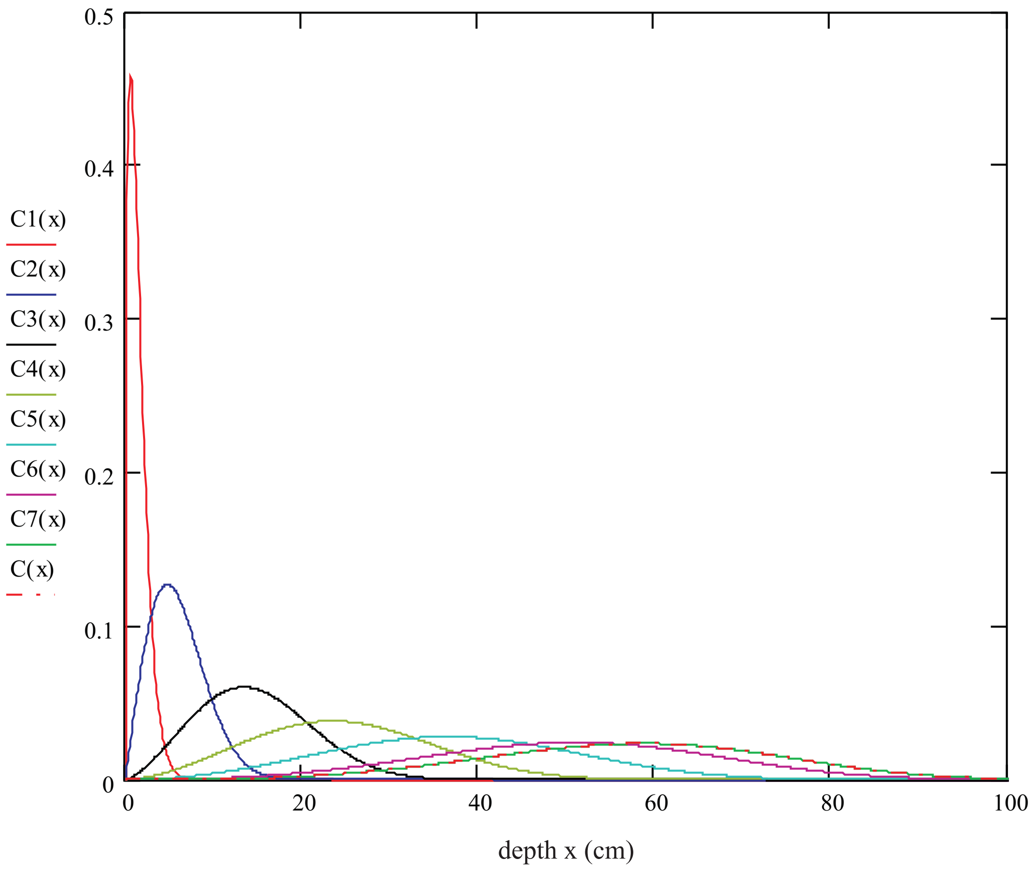

Fig. 6.1-15: Relative concentrations for different points of time (time series 3, Sr-90)
legend:
ordinate axis: relative concentration (cm^{-1})

$\left.\begin{array}{l}\text{C1(x): relative concentration after 0.244 (a)}\\ \text{C2(x): relative concentration after 1.238 (a)}\\ \text{C3(x): relative concentration after 3.735 (a)}\\ \text{C4(x): relative concentration after 7.666 (a)}\\ \text{C5(x): relative concentration after 15 (a)}\\ \text{C6(x): relative concentration after 30 (a)}\\ \text{C7(x): relative concentration after 50 (a)}\end{array}\right\}$ based on 2-dimensional nest of intervals

C(x) : relative concentration after 50 (a), based on second fits of a(t) and n(t)

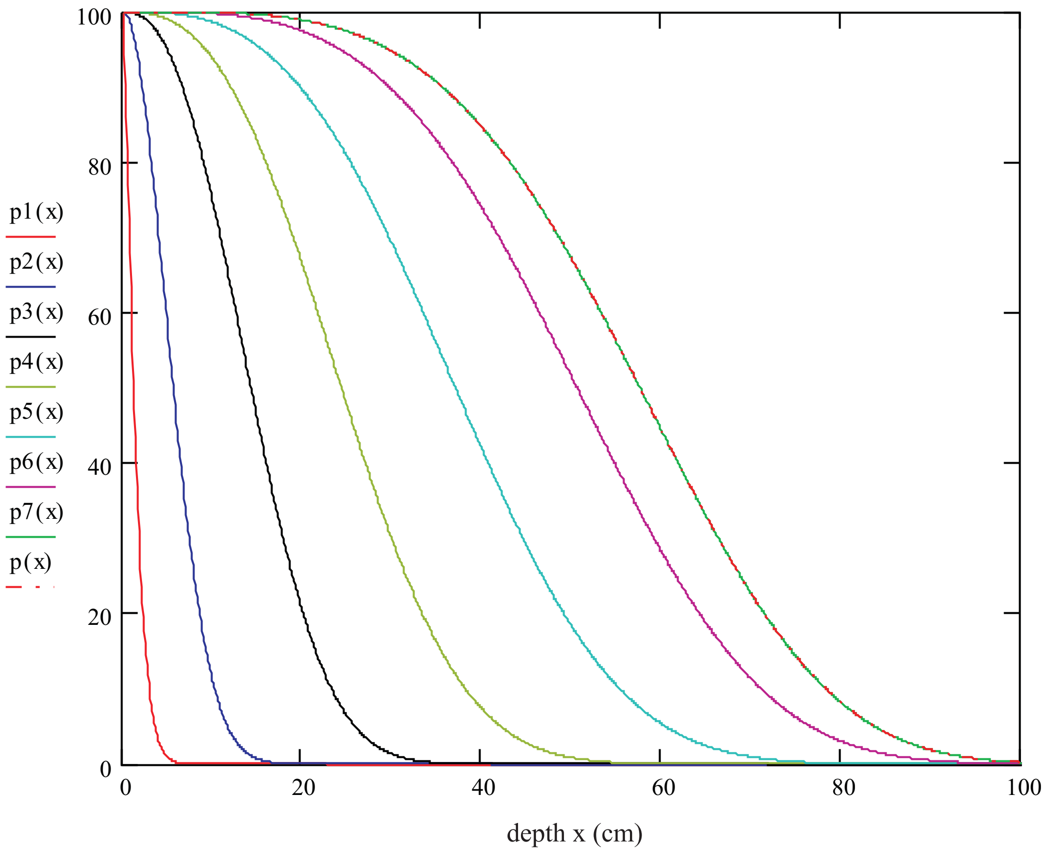

Fig. 6.1-16: Inventories below x in (%) for different points of time (time series 3, Sr-90)
legend:
ordinate axis: inventories below x (%)
p1(x): inventory below x in (%) after 0.244 (a)
p2(x): inventory below x in (%) after 1.238 (a)
p3(x): inventory below x in (%) after 3.735 (a)
p4(x): inventory below x in (%) after 7.666 (a) based on 2-dimensional nest of intervals
p5(x): inventory below x in (%) after 15 (a)
p6(x): inventory below x in (%) after 30 (a)
p7(x): inventory below x in (%) after 50 (a)
p(x) : inventory below x in (%) after 50 (a), based on second fits of a(t) and n(t)

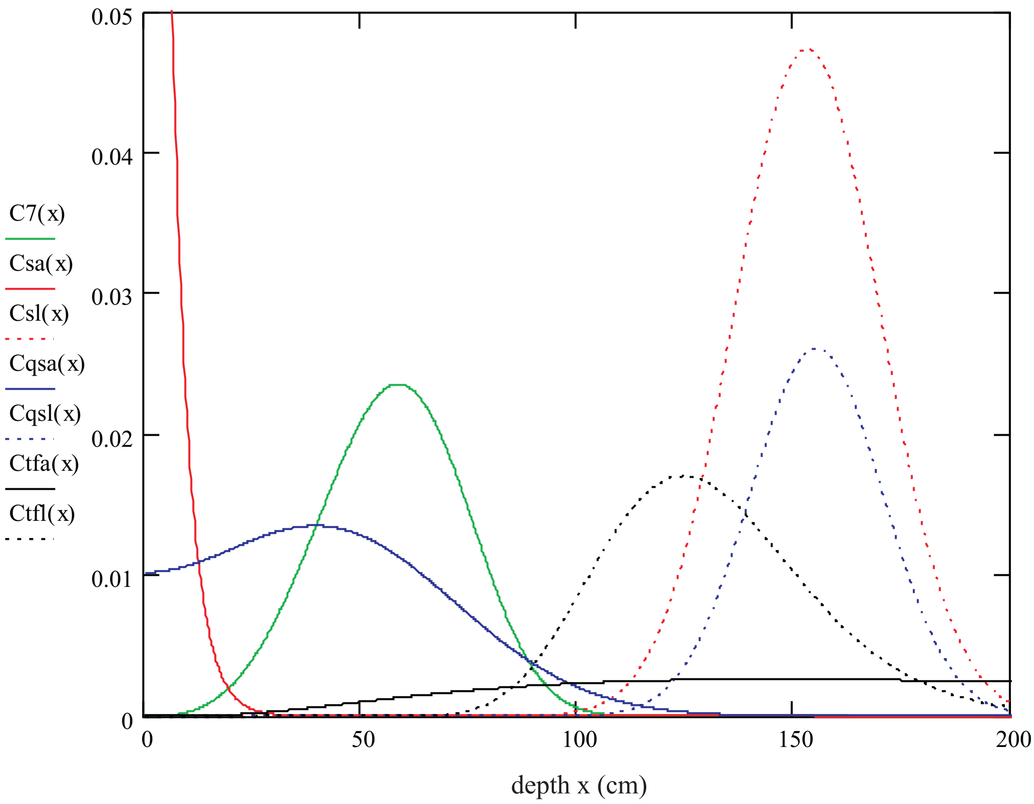

Fig. 6.1-17: Relative concentrations after 50 (a), resulting from different models (time series 3, Sr-90)

legend:

ordinate axis: relative concentration (cm^{-1})

C7(x) : relative concentration after 50 (a), based on 2-dimensional nest of intervals

Csa(x) : relative concentration after 50 (a), based on Eq. (2-2), a-profile

Csl(x) : relative concentration after 50 (a), based on Eq. (2-2), l-profile

Cqsa(x): relative concentration after 50 (a), based on Eq. (2-3), a-profile

Cqsl(x) : relative concentration after 50 (a), based on Eq. (2-3), l-profile

Ctfa(x) : relative concentration after 50 (a), based on Eq. (2-4), a-profile

Ctfl(x) : relative concentration after 50 (a), based on Eq. (2-4), l-profile

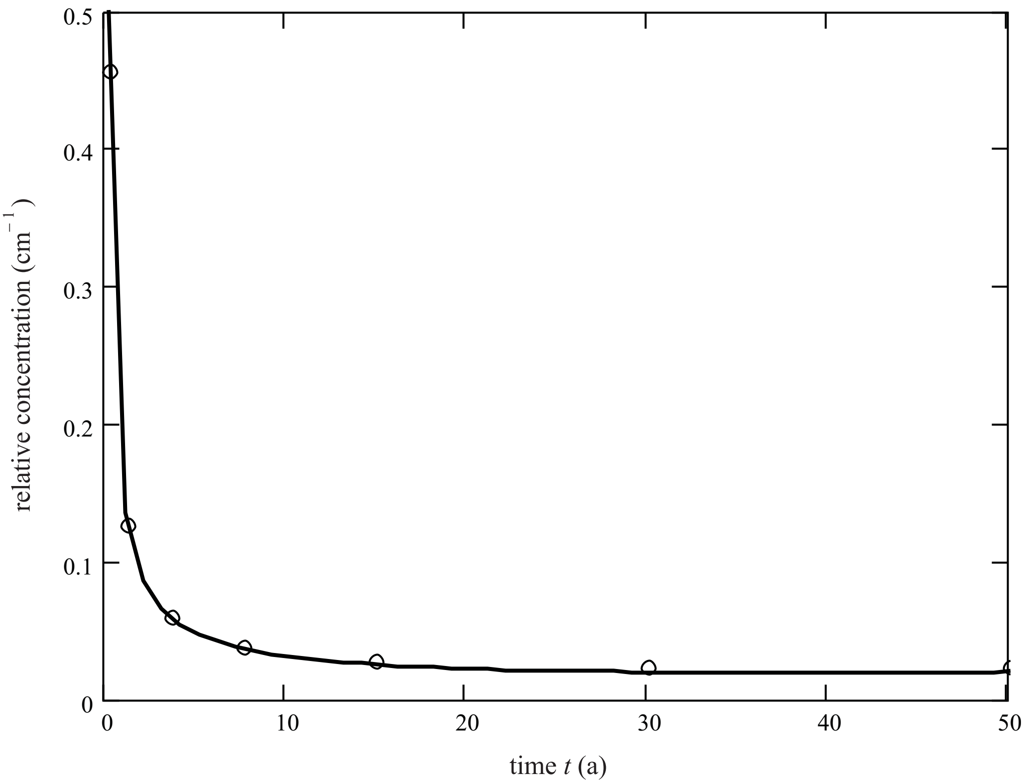

Fig. 6.1-18: Fitting of the relative concentration maxima (time series 3, Sr-90)

Remark: concentration maxima are taken from Fig. 6.1-15

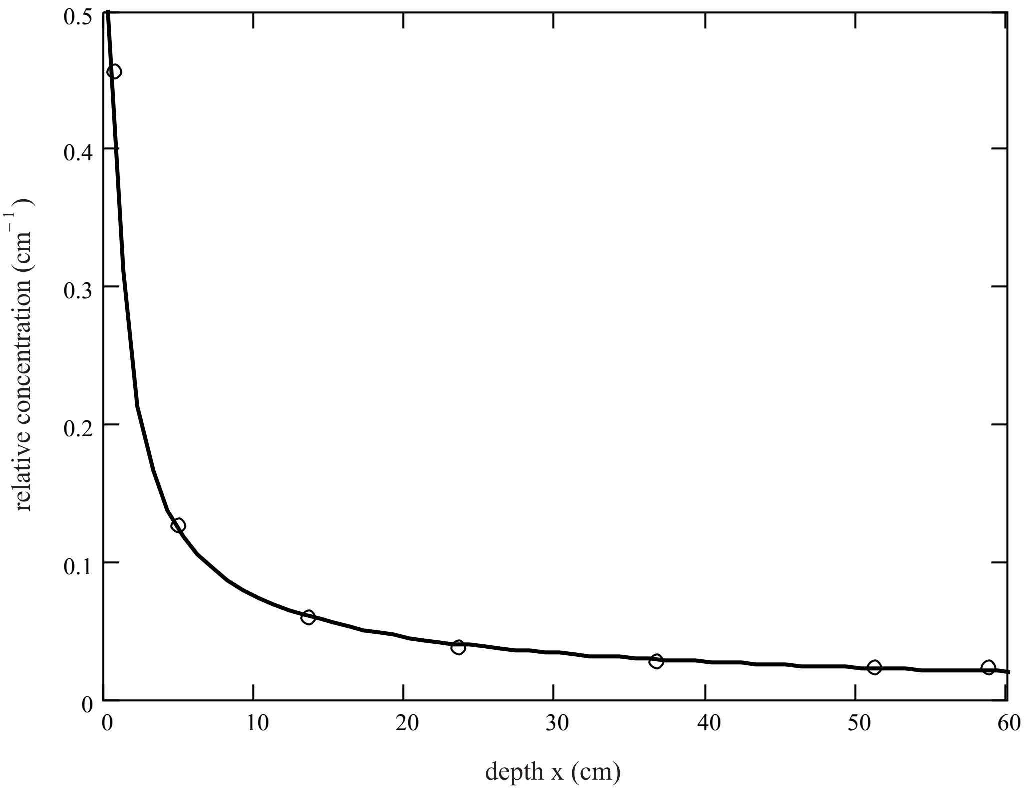

Fig. 6.1-19: Fitting of the relative concentration maxima (time series 3, Sr-90)

Remark: coordinates of the concentration maxima are taken from Fig. 6.1-15

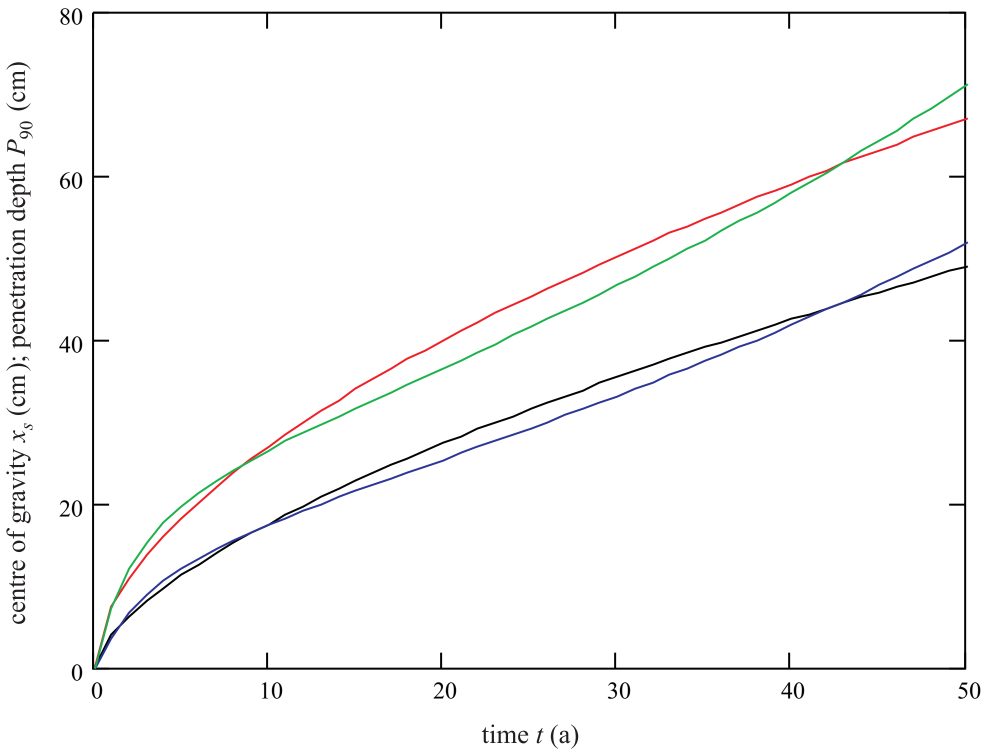

Fig. 6.1-20: Matching of the centres of gravity and of the penetration depths (time series 4, Sr-90)

legend:

black: x_s-fit

blue : matching of the x_s-fit, based on Eq. (2-24)

red : P_{90}-fit

green: matching of the P_{90}-fit; (a(t), n(t) from second fits)

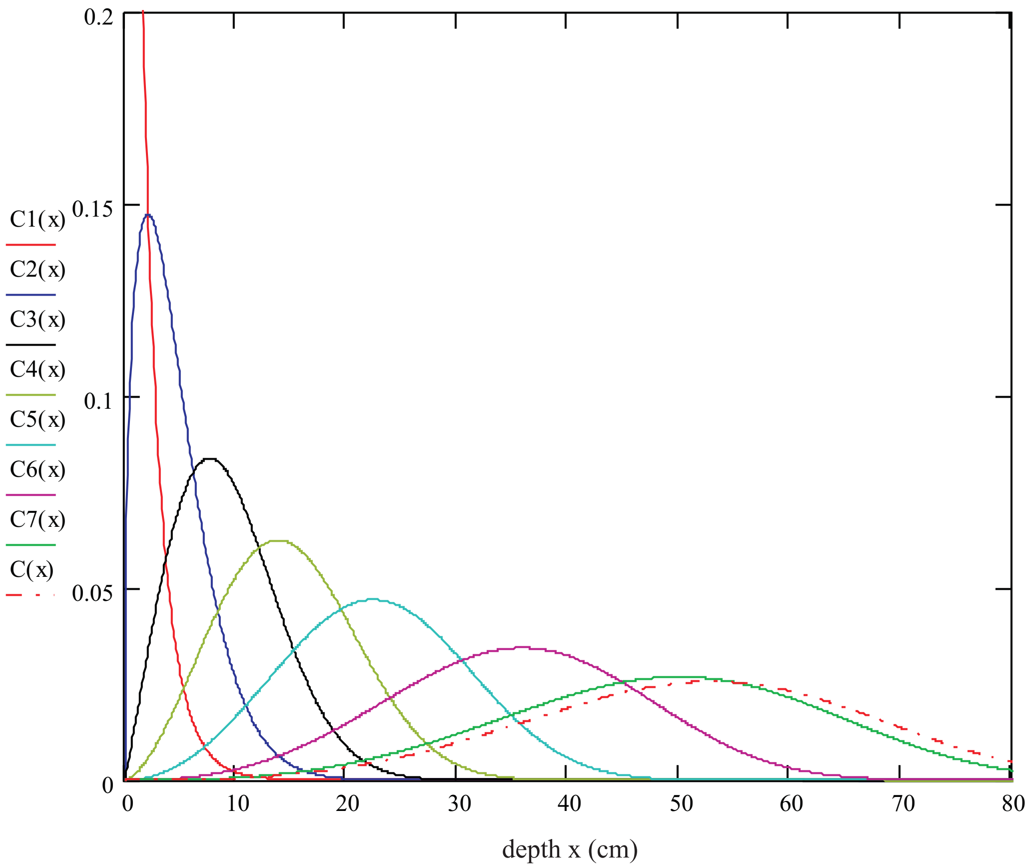

Fig. 6.1-21: Relative concentrations for different points of time (time series 4, Sr-90)
legend:
ordinate axis: relative concentration (cm^{-1})

C1(x): relative concentration after 0.244 (a)
C2(x): relative concentration after 1.238 (a)
C3(x): relative concentration after 3.735 (a)
C4(x): relative concentration after 7.666 (a)
C5(x): relative concentration after 15 (a)
C6(x): relative concentration after 30 (a)
C7(x): relative concentration after 50 (a)
} based on 2-dimensional nest of intervals

C(x) : relative concentration after 50 (a), based on second fits of a(t) and n(t)

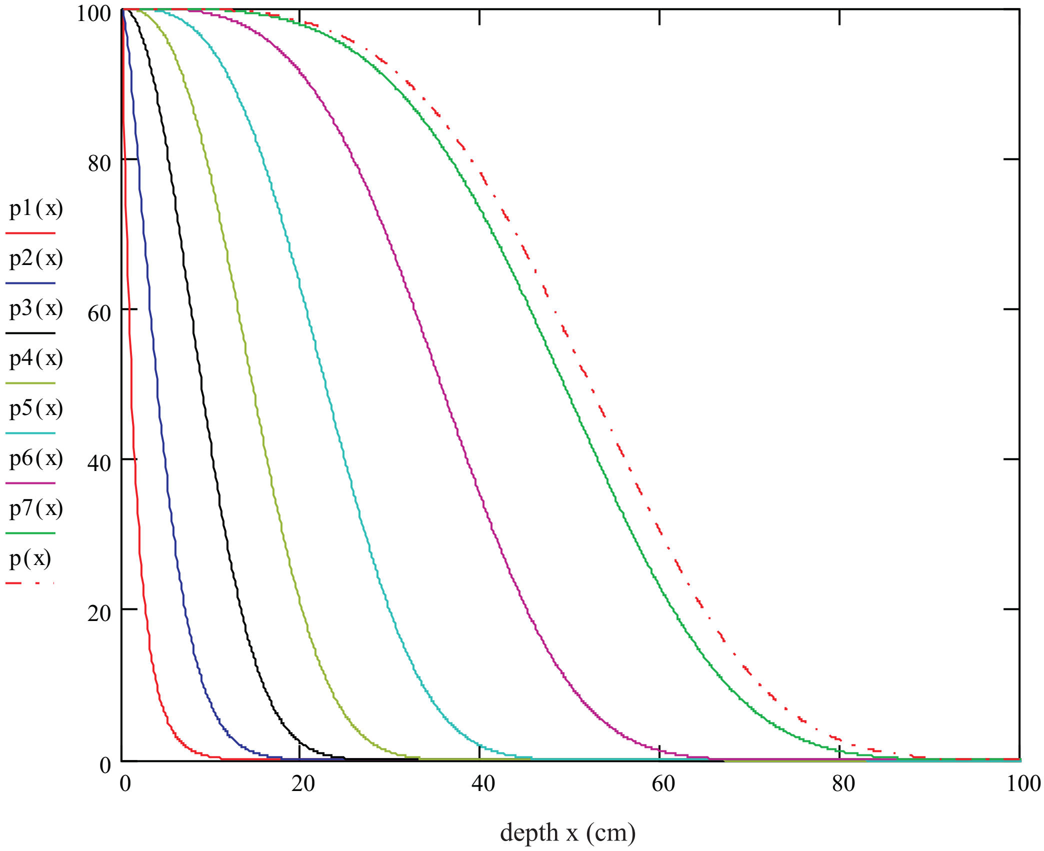

Fig. 6.1-22: Inventories below x in (%) for different points of time (time series 4, Sr-90)
legend:
ordinate axis: inventories below x (%)
p1(x): inventory below x in (%) after 0.244 (a)
p2(x): inventory below x in (%) after 1.238 (a)
p3(x): inventory below x in (%) after 3.735 (a)
p4(x): inventory below x in (%) after 7.666 (a) based on 2-dimensional nest of intervals
p5(x): inventory below x in (%) after 15 (a)
p6(x): inventory below x in (%) after 30 (a)
p7(x): inventory below x in (%) after 50 (a)
p(x) : inventory below x in (%) after 50 (a), based on second fits of a(t) and n(t)

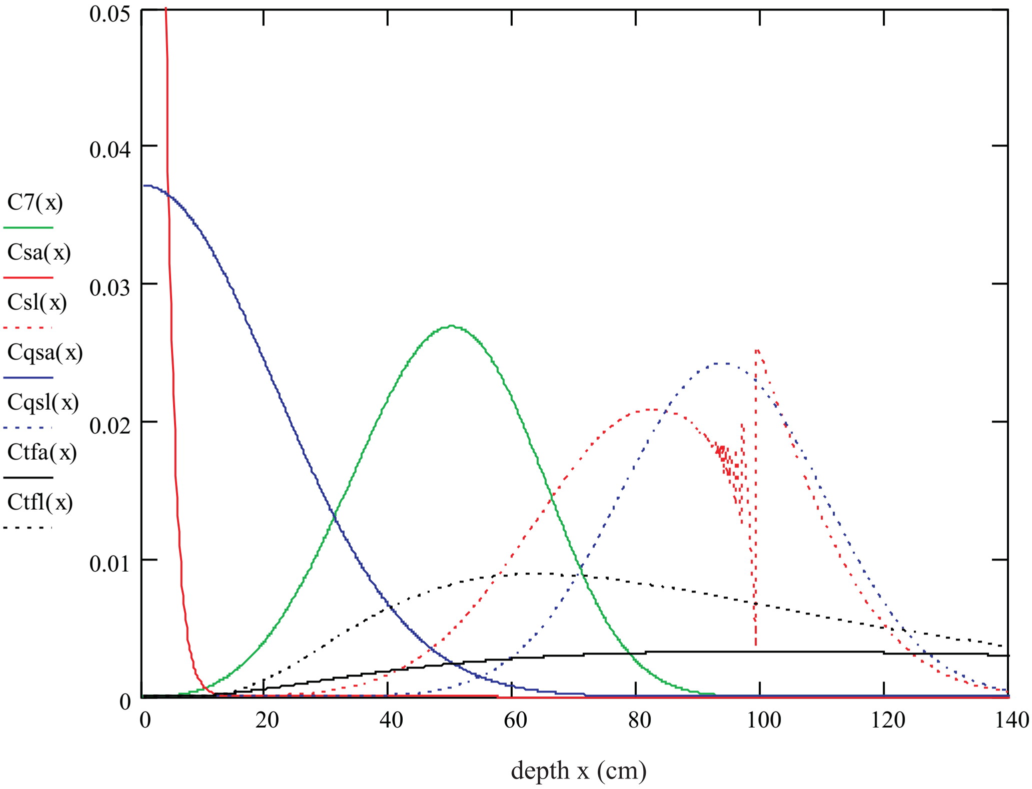

Fig. 6.1-23: Relative concentrations after 50 (a), resulting from different models (time series 4, Sr-90)

legend:

ordinate axis: relative concentration (cm^{-1})

C7(x) : relative concentration after 50 (a), based on 2-dimensional nest of intervals
Csa(x) : relative concentration after 50 (a), based on Eq. (2-2), a-profile
Csl(x) : relative concentration after 50 (a), based on Eq. (2-2), l-profile
Cqsa(x): relative concentration after 50 (a), based on Eq. (2-3), a-profile
Cqsl(x) : relative concentration after 50 (a), based on Eq. (2-3), l-profile
Ctfa(x) : relative concentration after 50 (a), based on Eq. (2-4), a-profile
Ctfl(x) : relative concentration after 50 (a), based on Eq. (2-4), l-profile

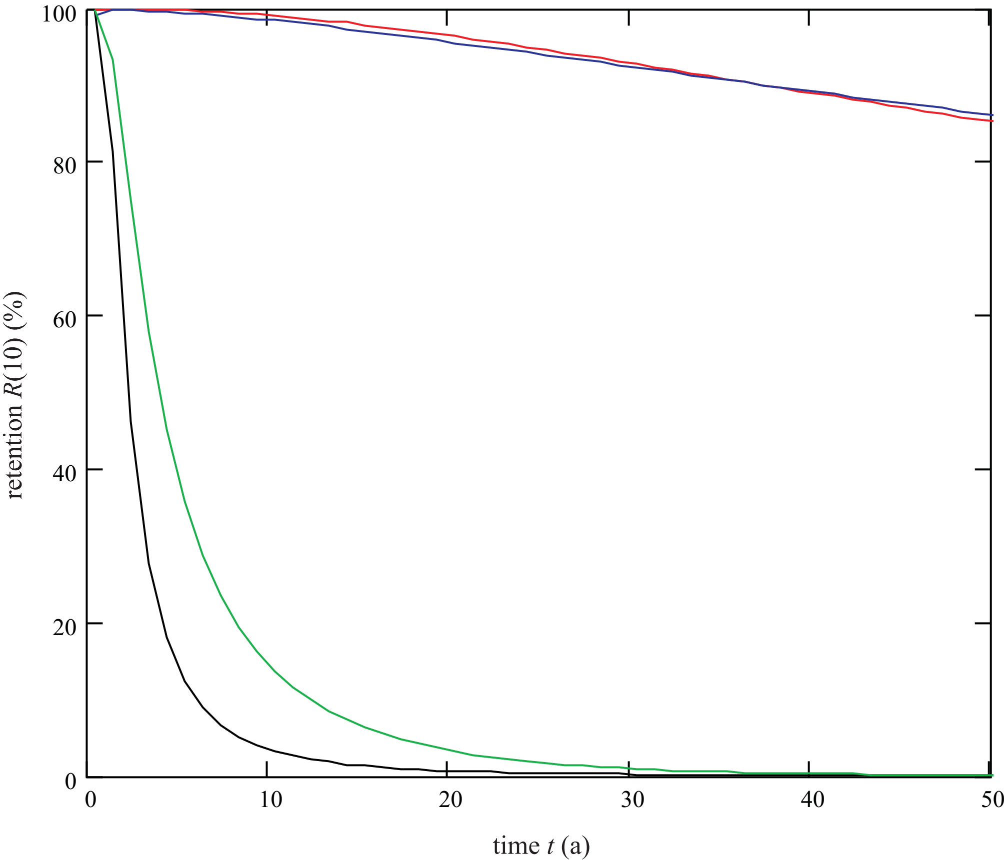

Fig. 6.1-24: Retention in the upper 10 (cm)

legend:
red : time series 1, Cs-137, podsol
blue : time series 2, Cs-137, cambisol
black: time series 3, Sr-90, podsol
green: time series 4, Sr-90, cambisol

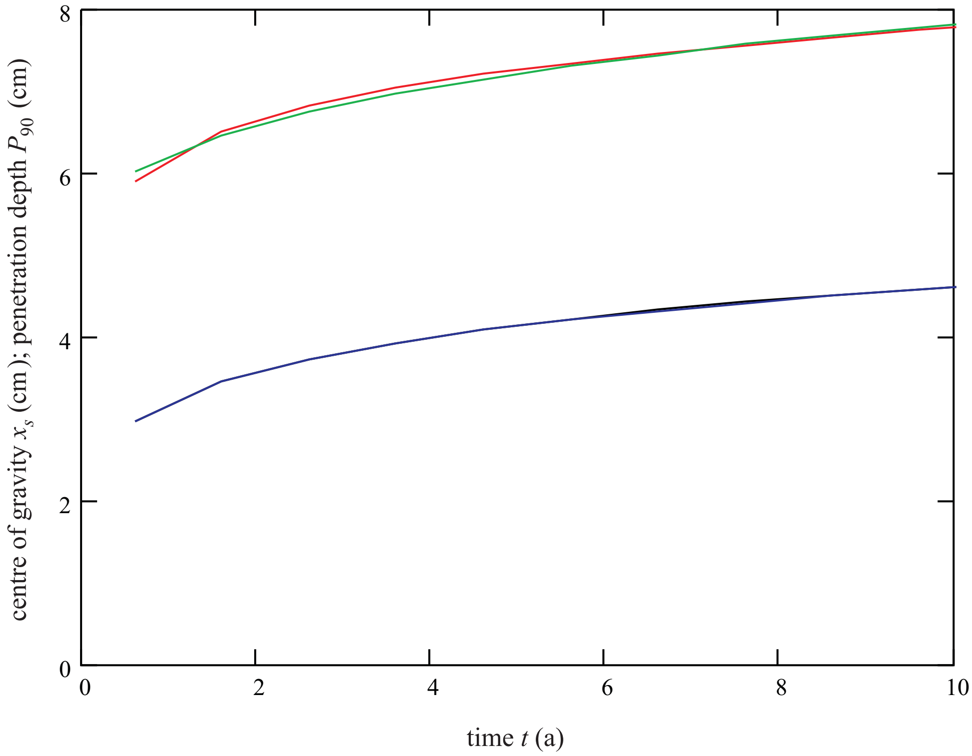

Fig. 6.2-1: Matching of the centres of gravity and of the penetration depths (time series 1, Cs-137)

legend:

black: x_s-fit

blue : matching of the x_s-fit, based on Eq. (2-24)

red : P_{90}-fit

green: matching of the P_{90}-fit; (a(t), n(t) from second fits)

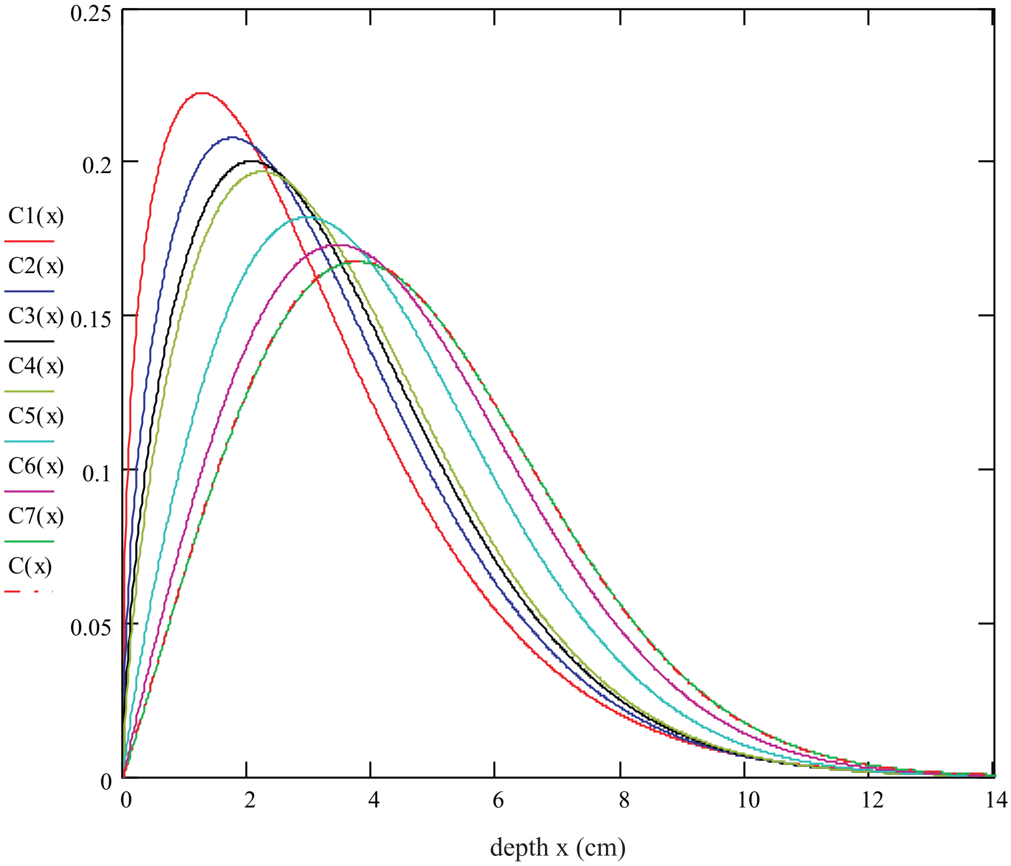

Fig. 6.2-2: Relative concentrations for different points of time (time series 1, Cs-137)
legend:
ordinate axis: relative concentration (cm^{-1})

C1(x): relative concentration after 0.685 (a)
C2(x): relative concentration after 1.068 (a)
C3(x): relative concentration after 1.468 (a)
C4(x): relative concentration after 1.756 (a)
C5(x): relative concentration after 4 (a)
C6(x): relative concentration after 7 (a)
C7(x): relative concentration after 10 (a)

based on 2-dimensional nest of intervals

C(x) : relative concentration after 10 (a), based on second fits of a(t) and n(t)

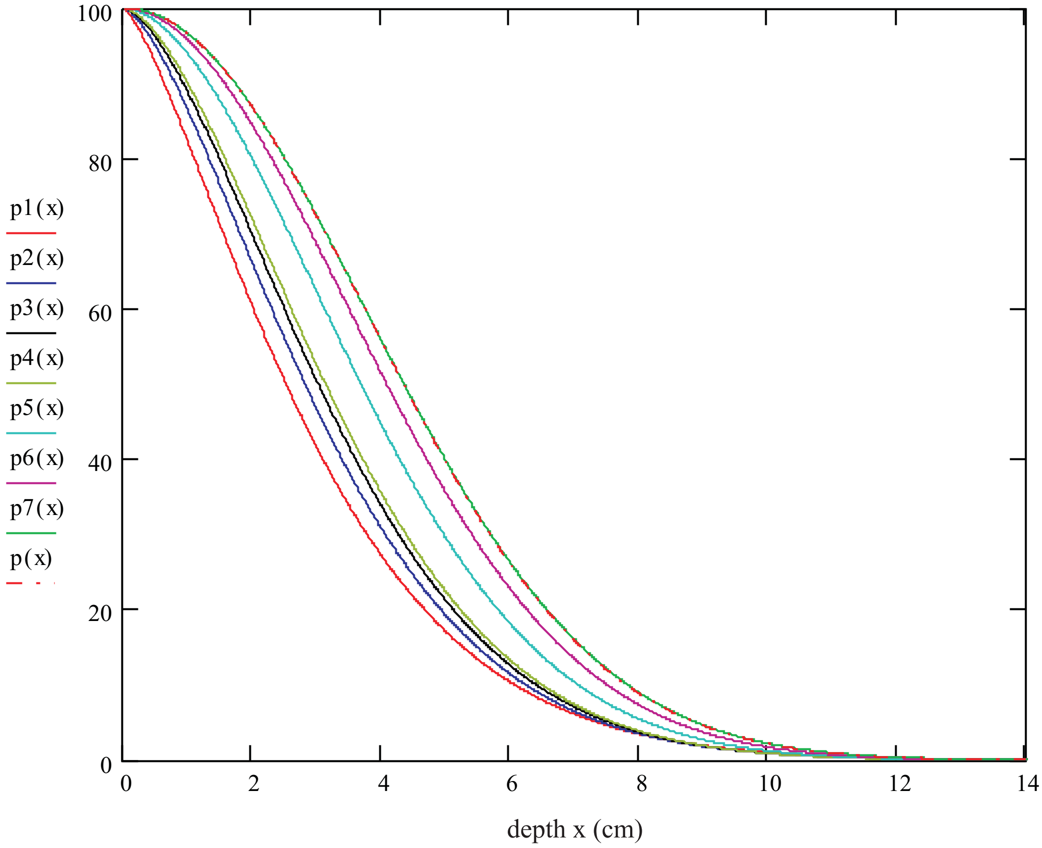

Fig. 6.2-3: Inventories below x in (%) for different points of time (time series 1, Cs-137)
legend:
ordinate axis: inventories below x (%)

$$\left.\begin{array}{l}\text{p1(x): inventory below x in (\%) after 0.685 (a)}\\ \text{p2(x): inventory below x in (\%) after 1.068 (a)}\\ \text{p3(x): inventory below x in (\%) after 1.468 (a)}\\ \text{p4(x): inventory below x in (\%) after 1.756 (a)}\\ \text{p5(x): inventory below x in (\%) after 4 (a)}\\ \text{p6(x): inventory below x in (\%) after 7 (a)}\\ \text{p7(x): inventory below x in (\%) after 10 (a)}\end{array}\right\}\text{ based on 2-dimensional nest of intervals}$$

p(x) : inventory below x in (%) after 10 (a), based on second fits of a(t) and n(t)

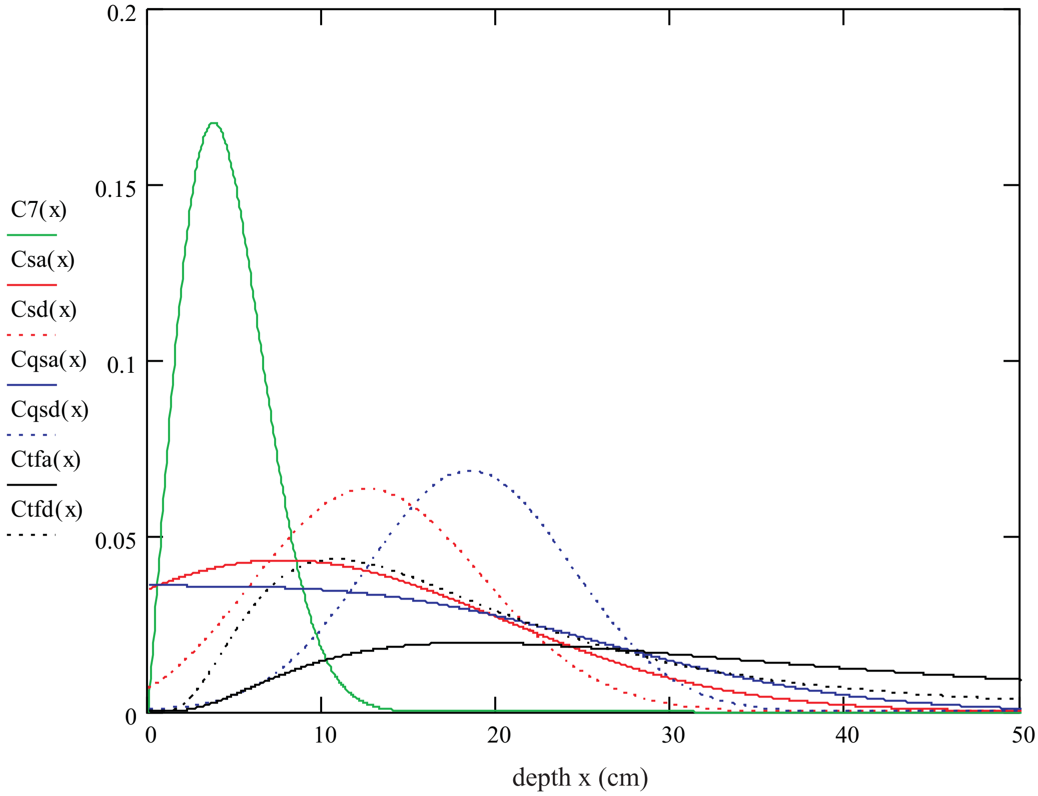

Fig. 6.2-4: Relative concentrations after 10 (a), resulting from different models (time series 1, Cs-137)

legend:

ordinate axis: relative concentration (cm^{-1})

C7(x) : relative concentration after 10 (a), based on 2-dimensional nest of intervals

Csa(x) : relative concentration after 10 (a), based on Eq. (2-2), a-profile

Csd(x) : relative concentration after 10 (a), based on Eq. (2-2), d-profile

Cqsa(x): relative concentration after 10 (a), based on Eq. (2-3), a-profile

Cqsd(x): relative concentration after 10 (a), based on Eq. (2-3), d-profile

Ctfa(x) : relative concentration after 10 (a), based on Eq. (2-4), a-profile

Ctfd(x) : relative concentration after 10 (a), based on Eq. (2-4), d-profile

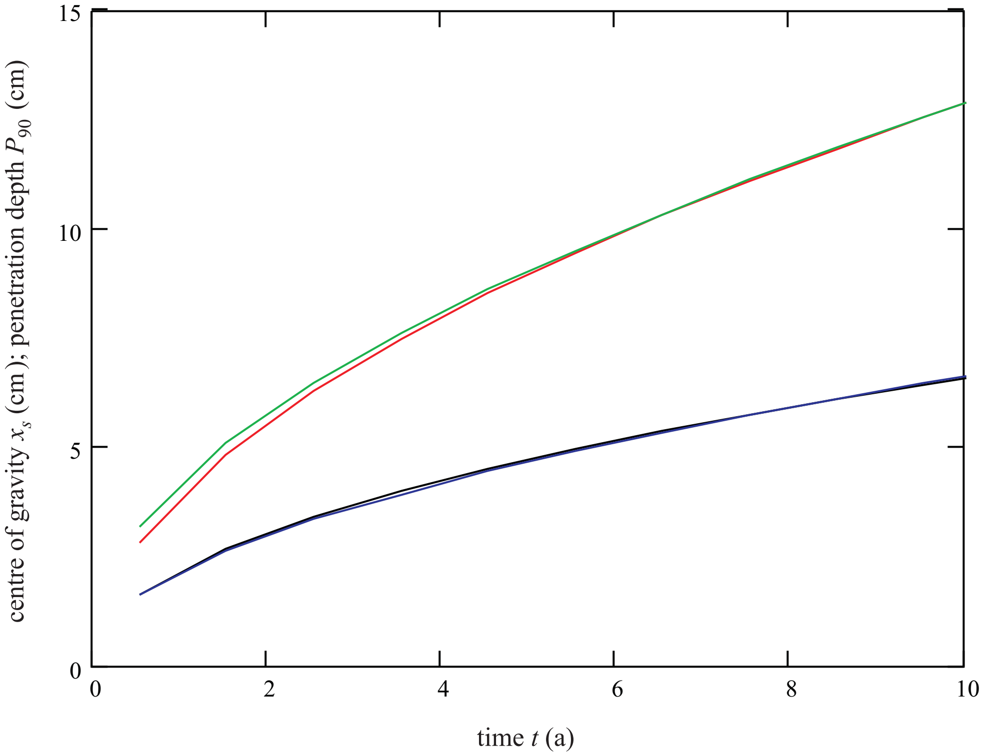

Fig. 6.2-5: Matching of the centres of gravity and of the penetration depths (time series 2, Sr-85)

legend:

black: x_s-fit

blue : matching of the x_s-fit, based on Eq. (2-24)

red : P_{90}-fit

green: matching of the P_{90}-fit; (a(t), n(t) from second fits)

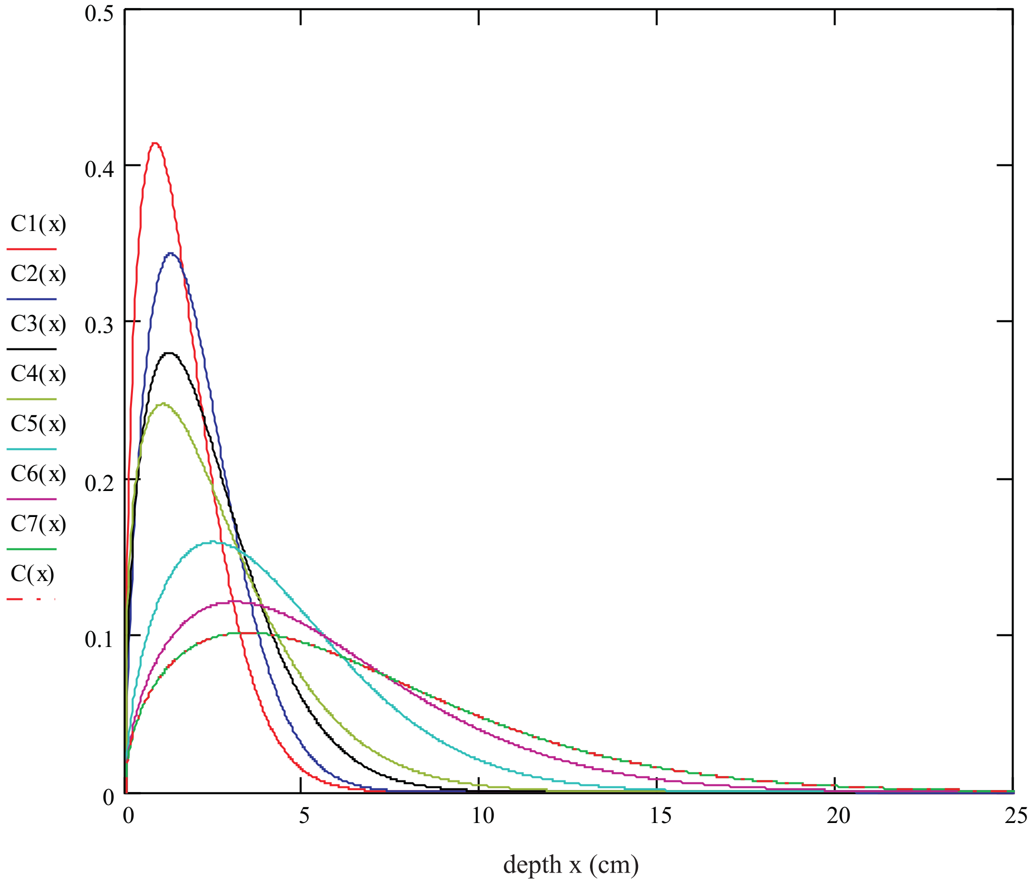

Fig. 6.2-6: Relative concentrations for different points of time (time series 2, Sr-85)
legend:
ordinate axis: relative concentration (cm^{-1})

C1(x): relative concentration after 0.534 (a)
C2(x): relative concentration after 0.838 (a)
C3(x): relative concentration after 1.203 (a)
C4(x): relative concentration after 1.586 (a)
C5(x): relative concentration after 4 (a)
C6(x): relative concentration after 7 (a)
C7(x): relative concentration after 10 (a)

based on 2-dimensional nest of intervals

C(x) : relative concentration after 10 (a), based on second fits of a(t) and n(t)

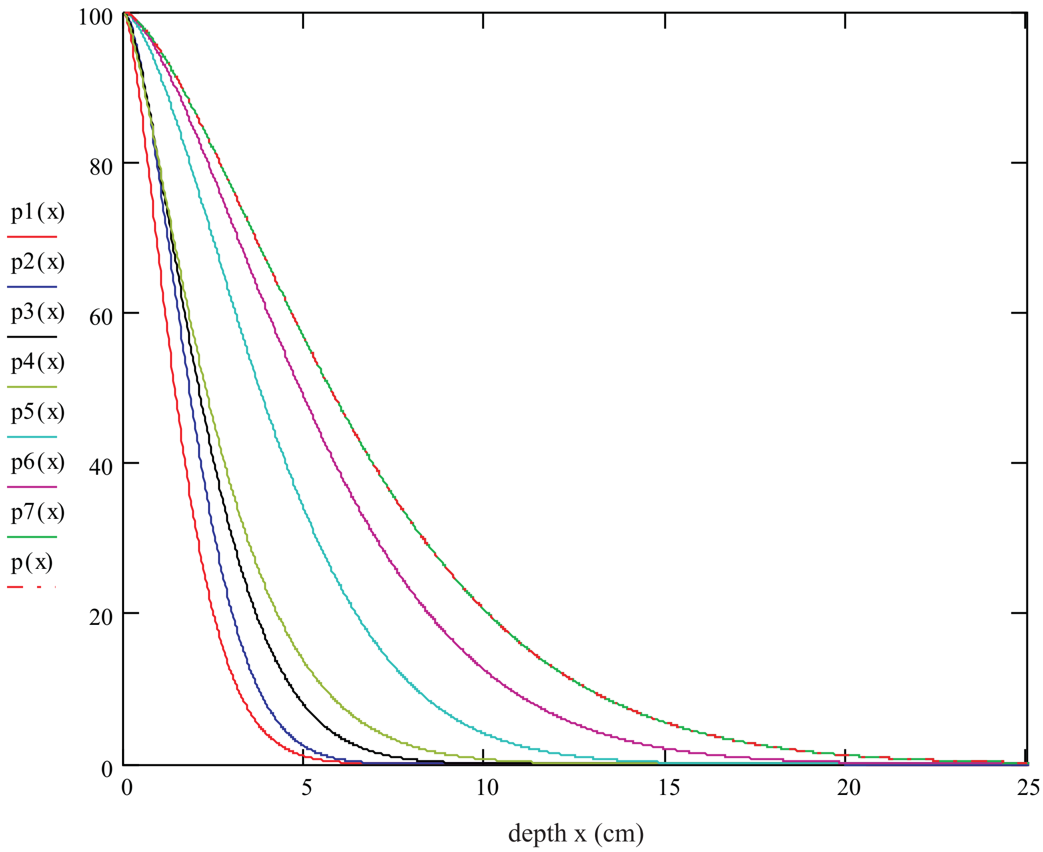

Fig. 6.2-7: Inventories below x in (%) for different points of time (time series 2, Sr-85)
legend:
ordinate axis: inventories below x (%)
p1(x): inventory below x in (%) after 0.534 (a)
p2(x): inventory below x in (%) after 0.838 (a)
p3(x): inventory below x in (%) after 1.203 (a)
p4(x): inventory below x in (%) after 1.586 (a)
p5(x): inventory below x in (%) after 4 (a)
p6(x): inventory below x in (%) after 7 (a)
p7(x): inventory below x in (%) after 10 (a)

(p1(x)–p7(x): based on 2-dimensional nest of intervals)

p(x) : inventory below x in (%) after 10 (a), based on second fits of a(t) and n(t)

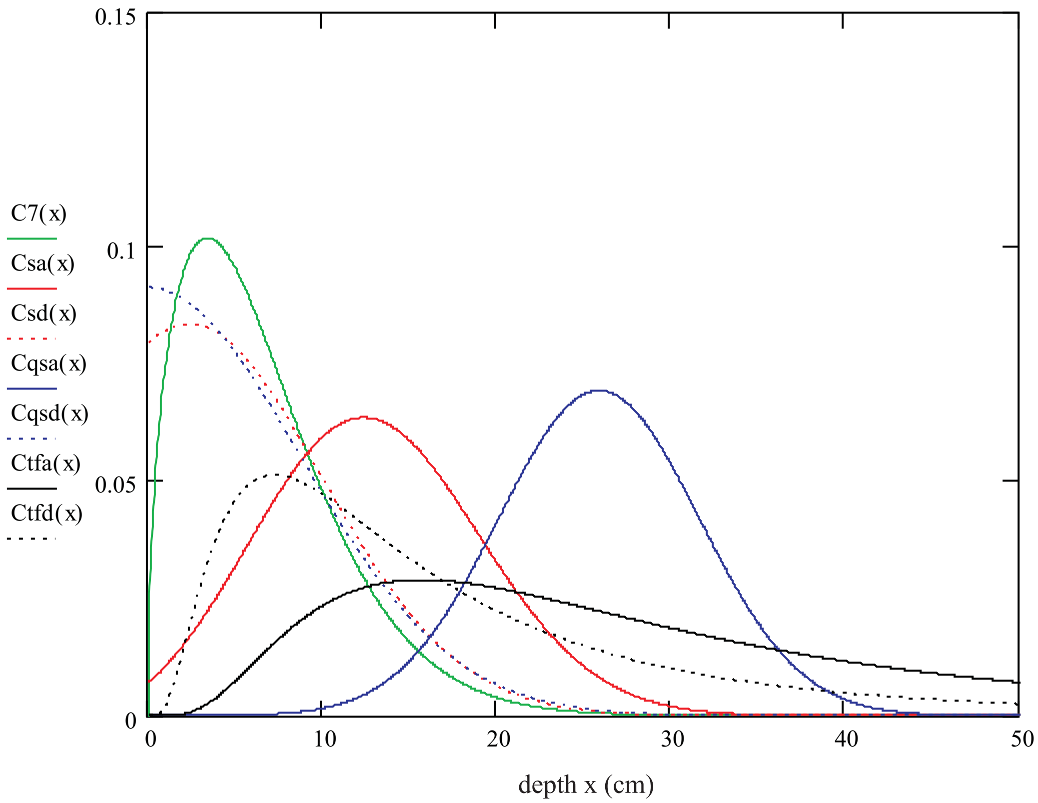

Fig. 6.2-8: Relative concentrations after 10 (a), resulting from different models (time series 2, Sr-85)

legend:

ordinate axis: relative concentration (cm^{-1})

C7(x) : relative concentration after 10 (a), based on 2-dimensional nest of intervals
Csa(x) : relative concentration after 10 (a), based on Eq. (2-2), a-profile
Csd(x) : relative concentration after 10 (a), based on Eq. (2-2), d-profile
Cqsa(x): relative concentration after 10 (a), based on Eq. (2-3), a-profile
Cqsd(x) : relative concentration after 10 (a), based on Eq. (2-3), d-profile
Ctfa(x) : relative concentration after 10 (a), based on Eq. (2-4), a-profile
Ctfd(x) : relative concentration after 10 (a), based on Eq. (2-4), d-profile

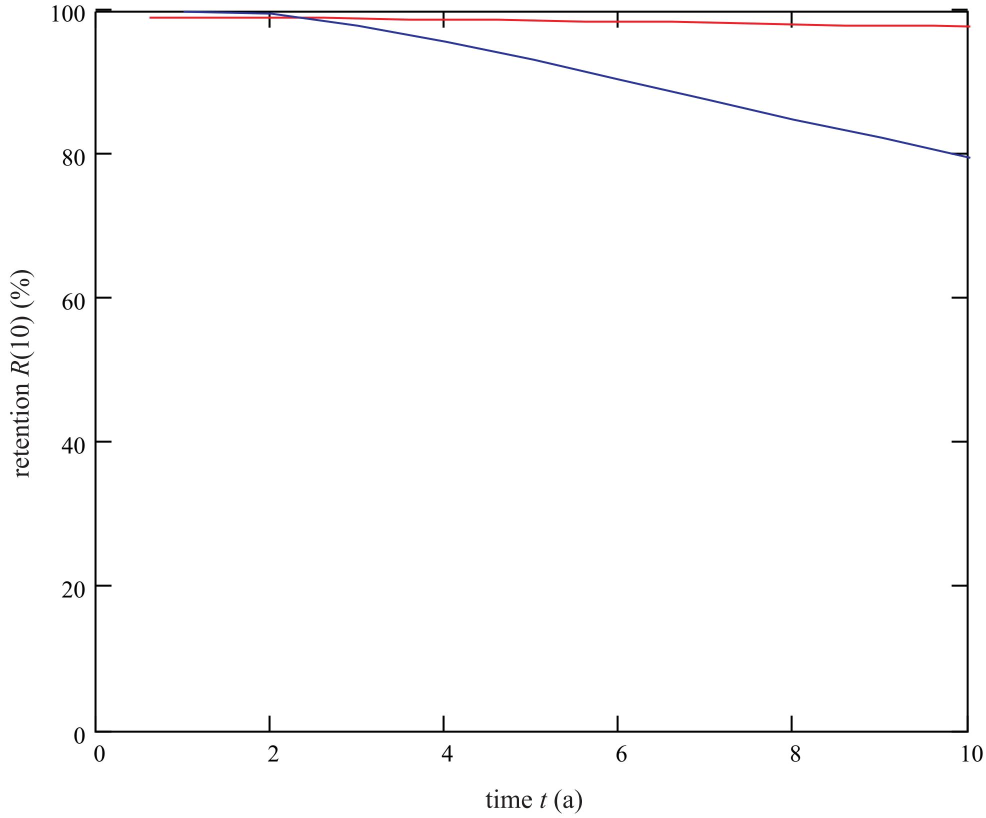

Fig. 6.2-9: Retention in the upper 10 (cm)

legend:

red : time series 1, Cs-137, podsol

blue : time series 2, Sr-85, podsol

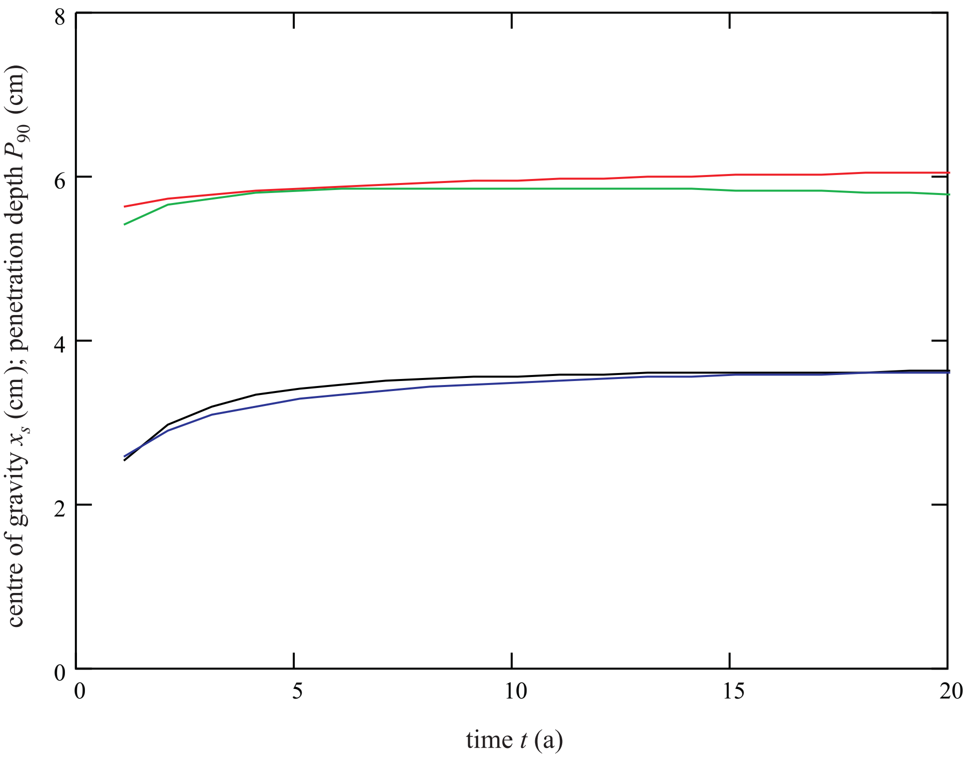

Fig. 6.3-1: Matching of the centres of gravity and of the penetration depths (time series 1, Chernobyl-Cs-137)
legend:
black: x_s-fit
blue : matching of the x_s-fit, based on Eq. (2-24)
red : P_{90}-fit
green: matching of the P_{90}-fit; (a(t), n(t) from second fits)

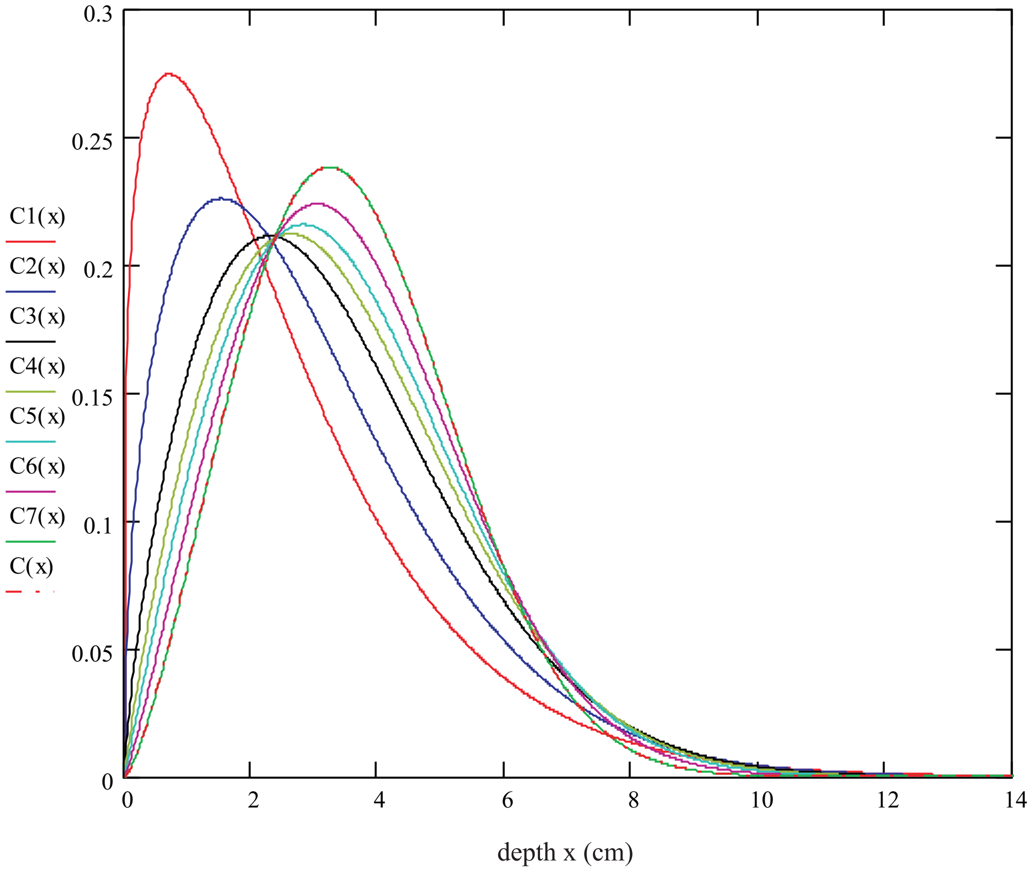

Fig. 6.3-2: Relative concentrations for different points of time (time series 1, Chernobyl-Cs-137)

legend:

ordinate axis: relative concentration (cm^{-1})

C1(x): relative concentration after 1.1 (a)
C2(x): relative concentration after 2.1 (a)
C3(x): relative concentration after 4.2 (a)
C4(x): relative concentration after 6.2 (a)
C5(x): relative concentration after 8.1 (a)
C6(x): relative concentration after 12 (a)
C7(x): relative concentration after 20 (a)

} based on 2-dimensional nest of intervals

C(x) : relative concentration after 20 (a), based on second fits of a(t) and n(t)

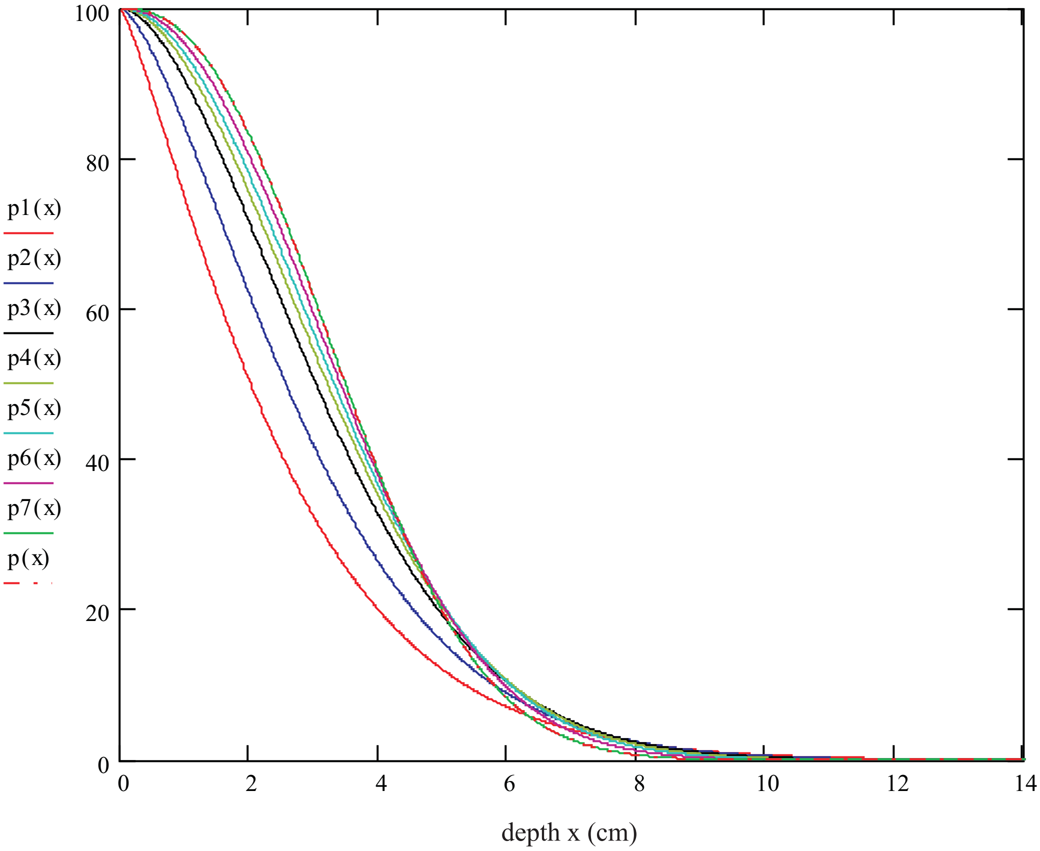

Fig. 6.3-3: Inventories below x in (%) for different points of time (time series 1, Chernobyl-Cs-137)

legend:

ordinate axis: inventories below x (%)

p1(x): inventory below x in (%) after 1.1 (a)
p2(x): inventory below x in (%) after 2.1 (a)
p3(x): inventory below x in (%) after 4.2 (a)
p4(x): inventory below x in (%) after 6.2 (a)
p5(x): inventory below x in (%) after 8.1 (a)
p6(x): inventory below x in (%) after 12 (a)
p7(x): inventory below x in (%) after 20 (a)

based on 2-dimensional nest of intervals

p(x) : inventory below x in (%) after 20 (a), based on second fits of a(t) and n(t)

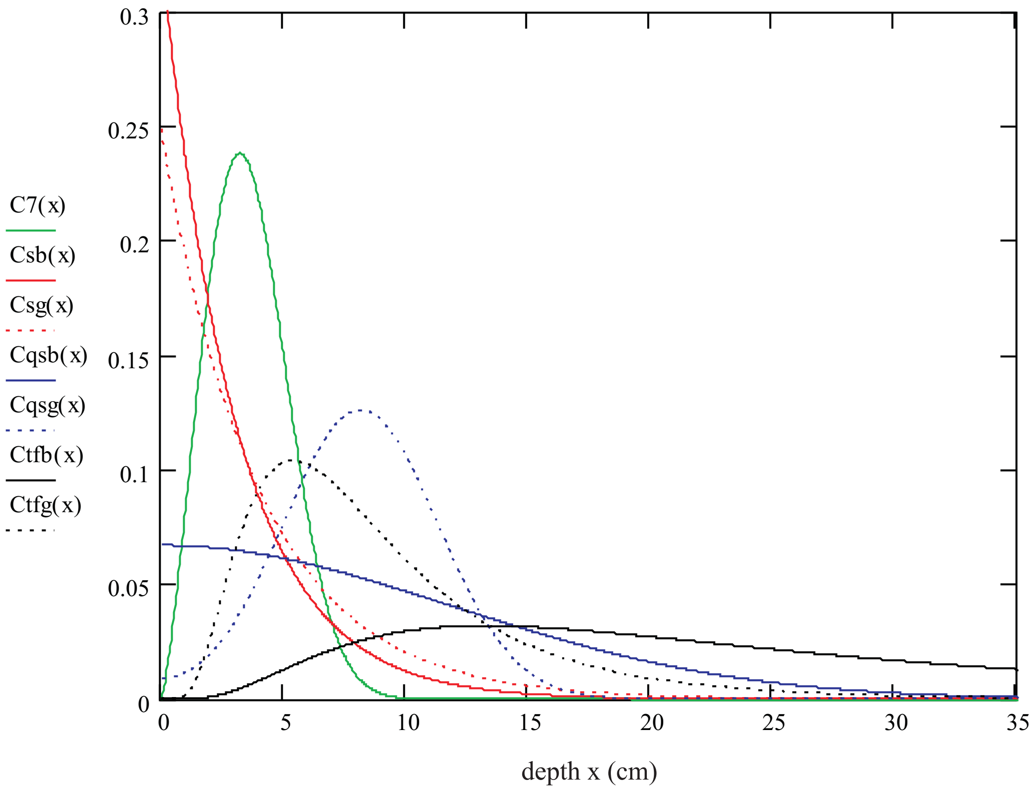

Fig. 6.3-4: Relative concentrations after 20 (a), resulting from different models (time series 1, Chernobyl-Cs-137)

legend:

ordinate axis: relative concentration (cm^{-1})

C7(x) : relative concentration after 20 (a), based on 2-dimensional nest of intervals

Csb(x) : relative concentration after 20 (a), based on Eq. (2-2), b-profile

Csg(x) : relative concentration after 20 (a), based on Eq. (2-2), g-profile

Cqsb(x): relative concentration after 20 (a), based on Eq. (2-3), b-profile

Cqsg(x) : relative concentration after 20 (a), based on Eq. (2-3), g-profile

Ctfb(x) : relative concentration after 20 (a), based on Eq. (2-4), b-profile

Ctfg(x) : relative concentration after 20 (a), based on Eq. (2-4), g-profile

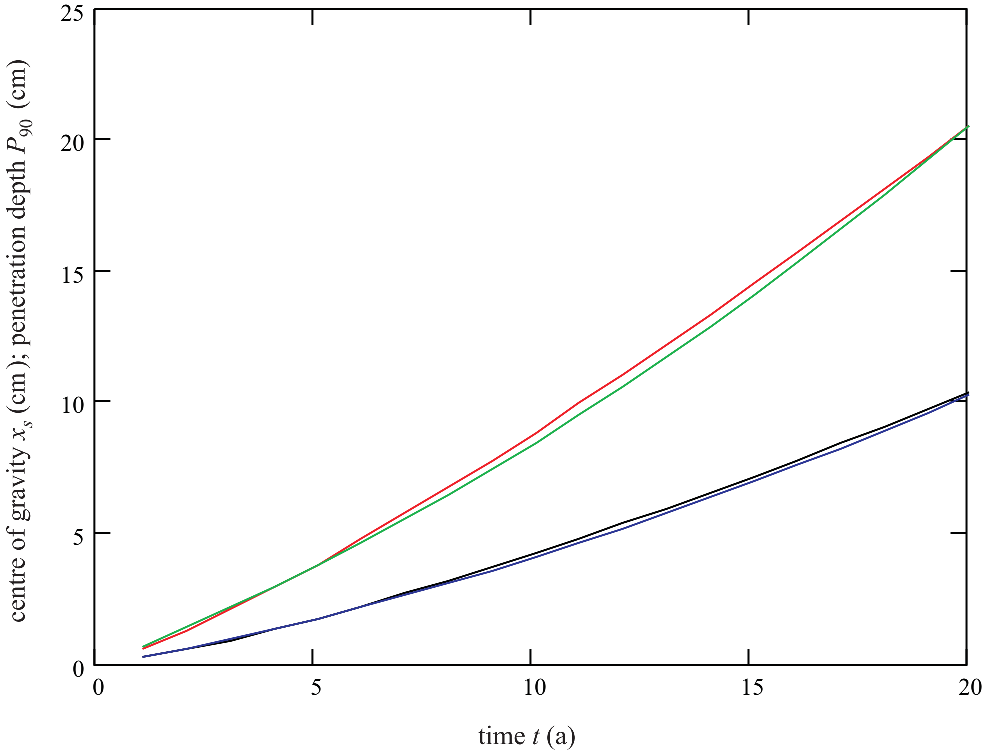

Fig. 6.3-5: Matching of the centres of gravity and of the penetration depths (time series 2, Chernobyl-Cs-137, mainly fuel particles)
legend:
black: x_s-fit
blue : matching of the x_s-fit, based on Eq. (2-24)
red : P_{90}-fit
green: matching of the P_{90}-fit; (a(t), n(t) from second fits)

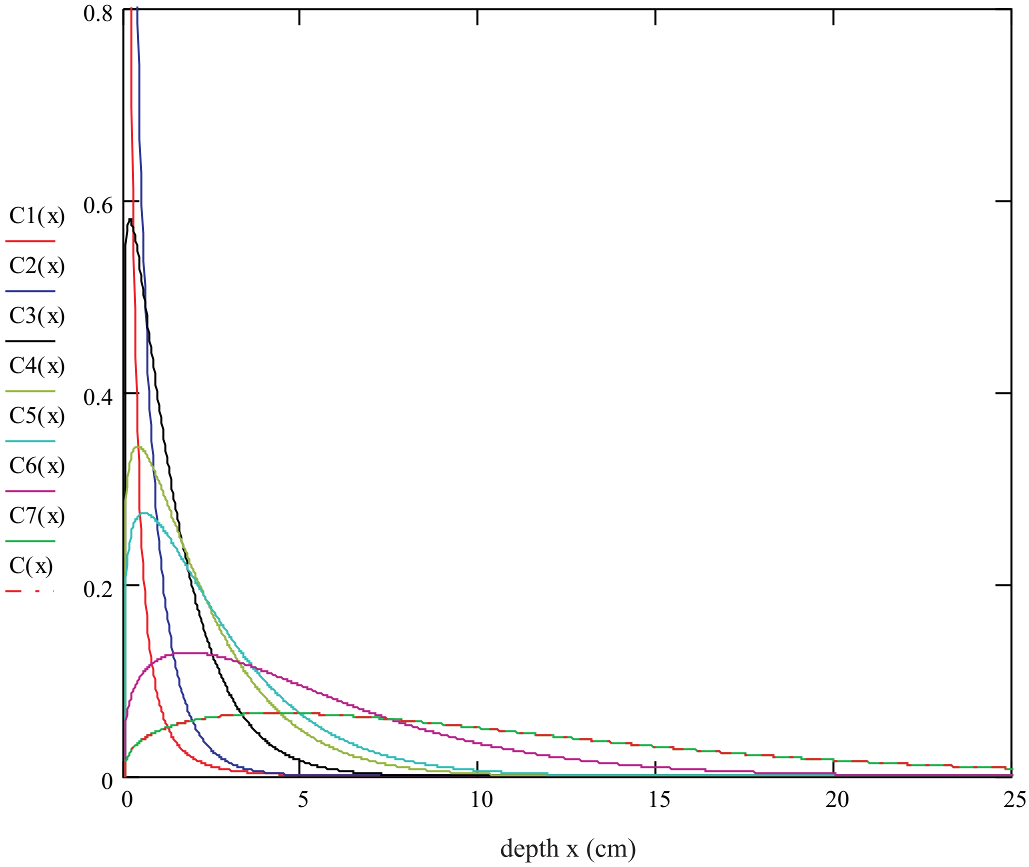

Fig. 6.3-6: Relative concentrations for different points of time (time series 2, Chernobyl-Cs-137, mainly fuel particles)

legend:

ordinate axis: relative concentration (cm^{-1})

$$\left.\begin{array}{l}\text{C1(x): relative concentration after 1.1 (a)}\\ \text{C2(x): relative concentration after 2.0 (a)}\\ \text{C3(x): relative concentration after 4.2 (a)}\\ \text{C4(x): relative concentration after 6.0 (a)}\\ \text{C5(x): relative concentration after 7.0 (a)}\\ \text{C6(x): relative concentration after 12 (a)}\\ \text{C7(x): relative concentration after 20 (a)}\end{array}\right\}\text{based on 2-dimensional nest of intervals}$$

C(x) : relative concentration after 20 (a), based on second fits of a(t) and n(t)

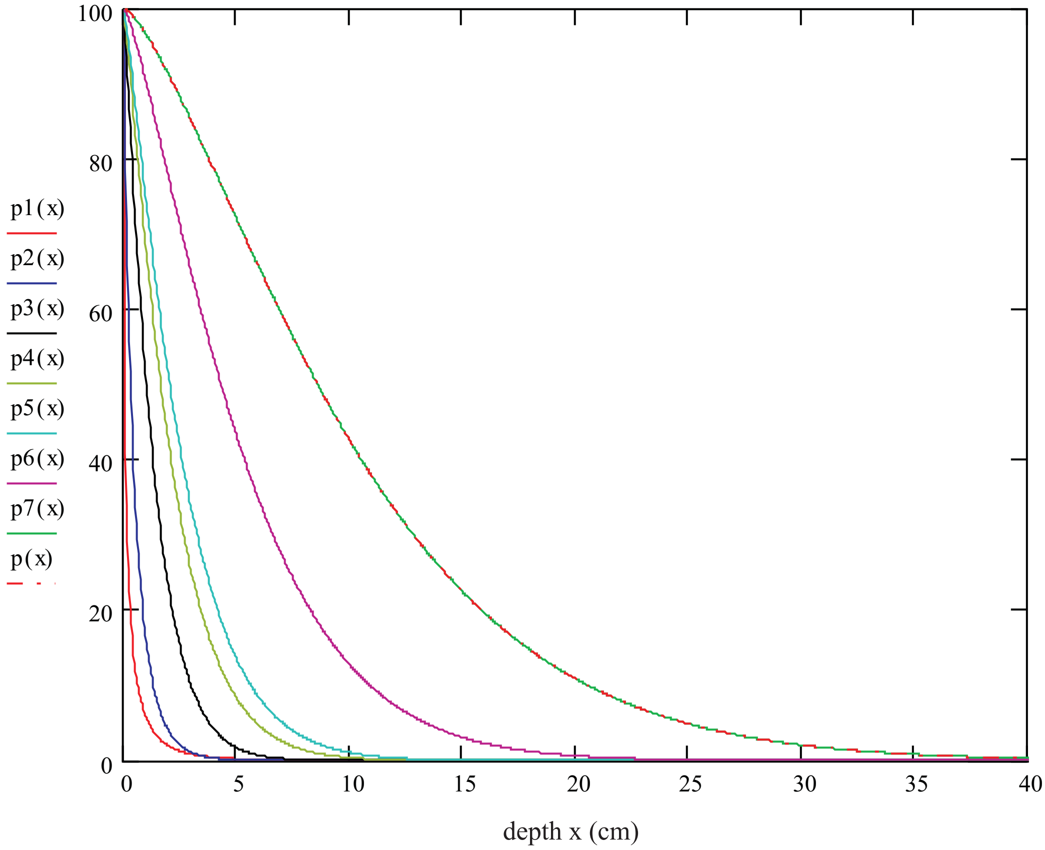

Fig. 6.3-7: Inventories below x in (%) for different points of time (time series 2, Chernobyl-Cs-137, mainly fuel particles)

legend:

ordinate axis: inventories below x (%)

p1(x): inventory below x in (%) after 1.1 (a)
p2(x): inventory below x in (%) after 2.0 (a)
p3(x): inventory below x in (%) after 4.2 (a)
p4(x): inventory below x in (%) after 6.0 (a)
p5(x): inventory below x in (%) after 7.0 (a)
p6(x): inventory below x in (%) after 12 (a)
p7(x): inventory below x in (%) after 20 (a)

$\Big\}$ based on 2-dimensional nest of intervals

p(x) : inventory below x in (%) after 20 (a), based on second fits of a(t) and n(t)

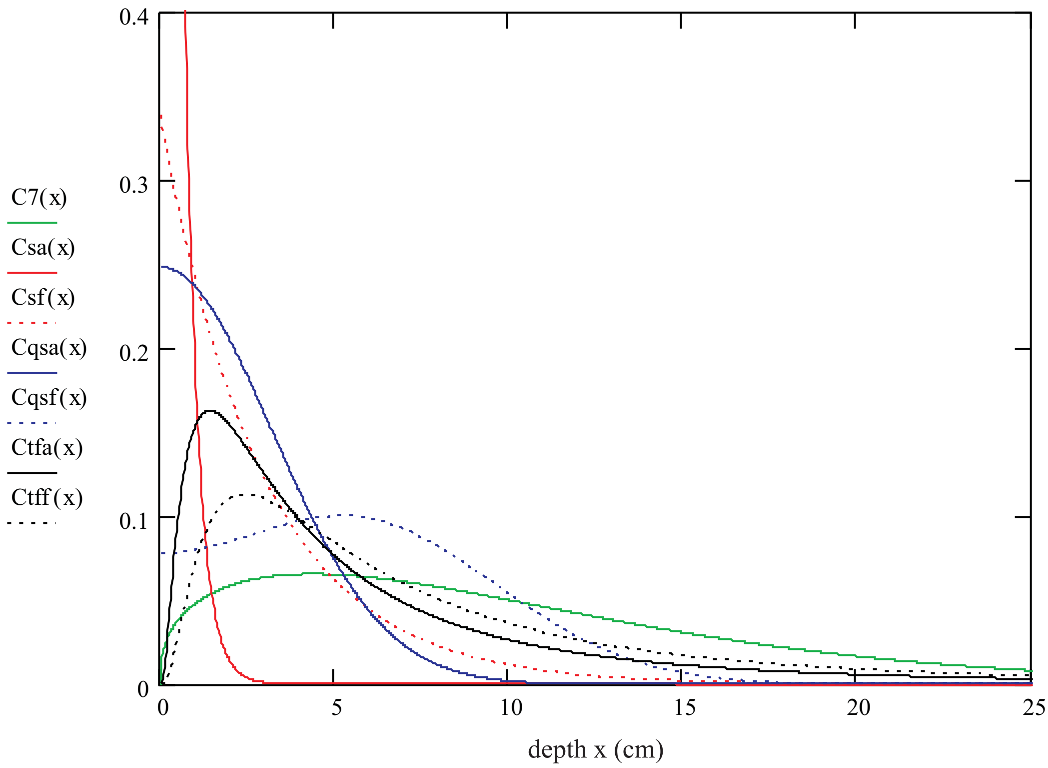

Fig. 6.3-8: Relative concentrations after 20 (a), resulting from different models (time series 2, Chernobyl-Cs-137, mainly fuel particles)

legend:

ordinate axis: relative concentration (cm^{-1})

C7(x) : relative concentration after 20 (a), based on 2-dimensional nest of intervals

Csa(x) : relative concentration after 20 (a), based on Eq. (2-2), a-profile

Csf(x) : relative concentration after 20 (a), based on Eq. (2-2), f-profile

Cqsa(x): relative concentration after 20 (a), based on Eq. (2-3), a-profile

Cqsf(x) : relative concentration after 20 (a), based on Eq. (2-3), f-profile

Ctfa(x) : relative concentration after 20 (a), based on Eq. (2-4), a-profile

Ctff(x) : relative concentration after 20 (a), based on Eq. (2-4), f-profile

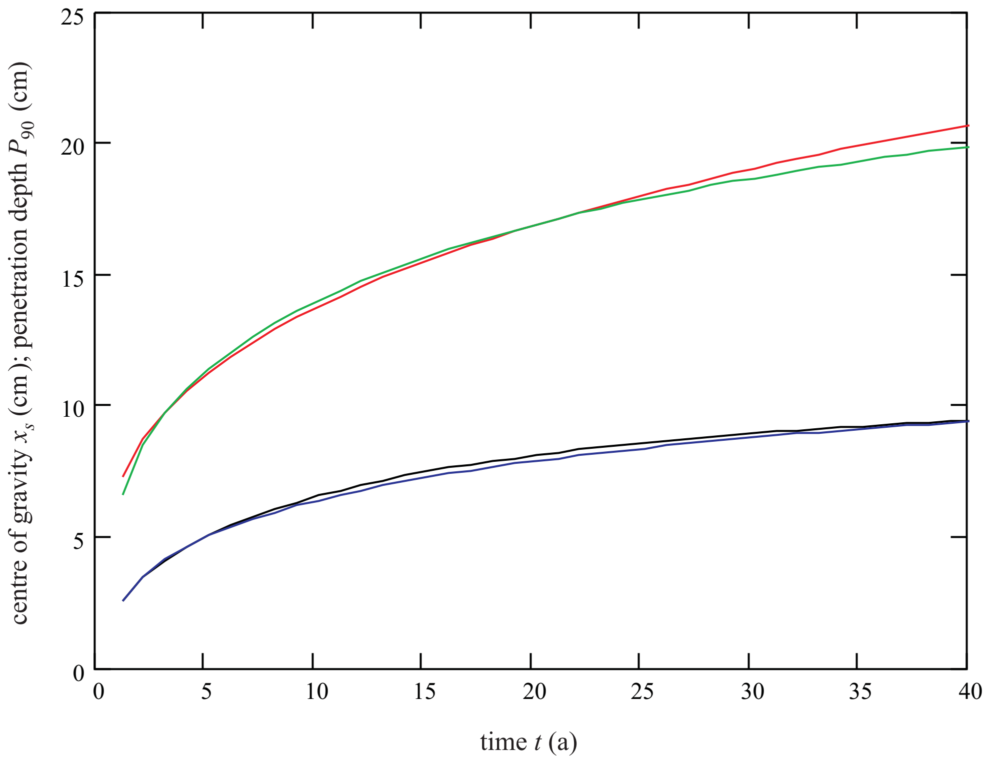

Fig. 6.4-1: Matching of the centres of gravity and of the penetration depths (time series 1, Cs-137)

legend:

black: x_s-fit

blue : matching of the x_s-fit, based on Eq. (2-24)

red : P_{90}-fit

green: matching of the P_{90}-fit; (a(t), n(t) from second fits)

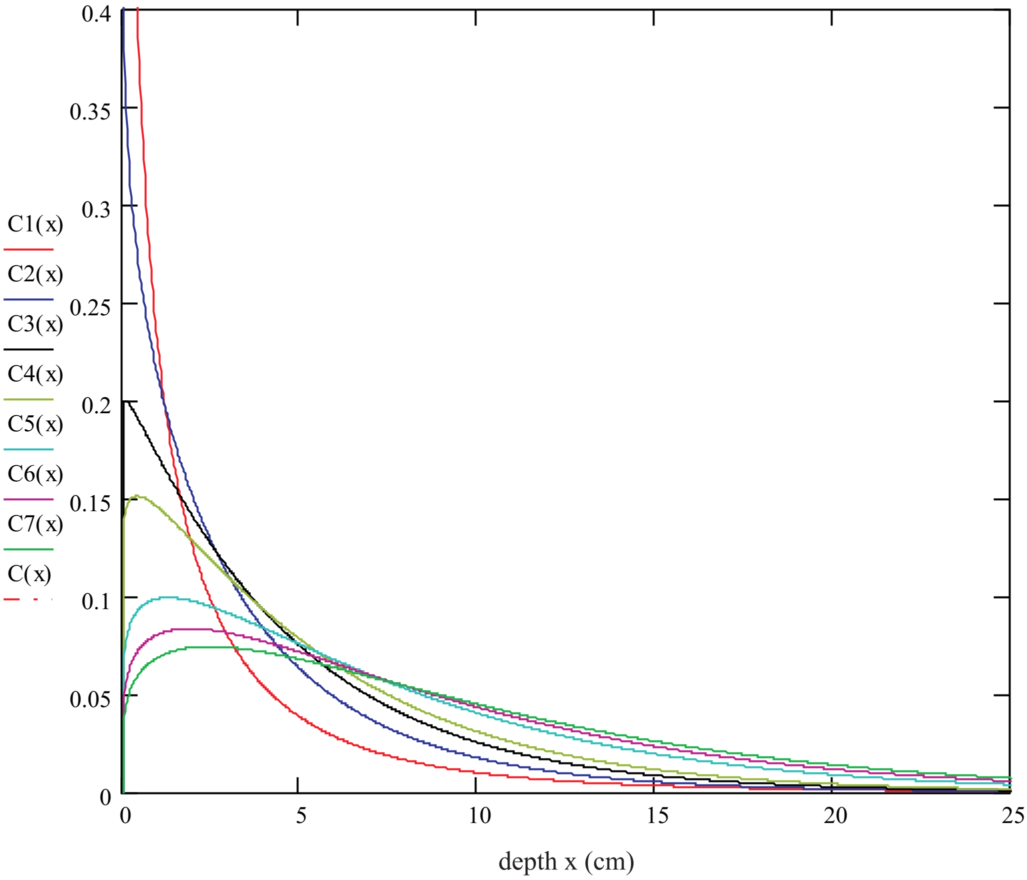

Fig. 6.4-2: Relative concentrations for different points of time (time series 1, Cs-137)

legend:

ordinate axis: relative concentration (cm^{-1})

C1(x): relative concentration after 1.2 (a)
C2(x): relative concentration after 2.5 (a)
C3(x): relative concentration after 4.3 (a)
C4(x): relative concentration after 6.2 (a)
C5(x): relative concentration after 15 (a)
C6(x): relative concentration after 25 (a)
C7(x): relative concentration after 40 (a)

$\Big\}$ based on 2-dimensional nest of intervals (C1(x) to C7(x))

C(x) : relative concentration after 40 (a), based on second fits of a(t) and n(t)

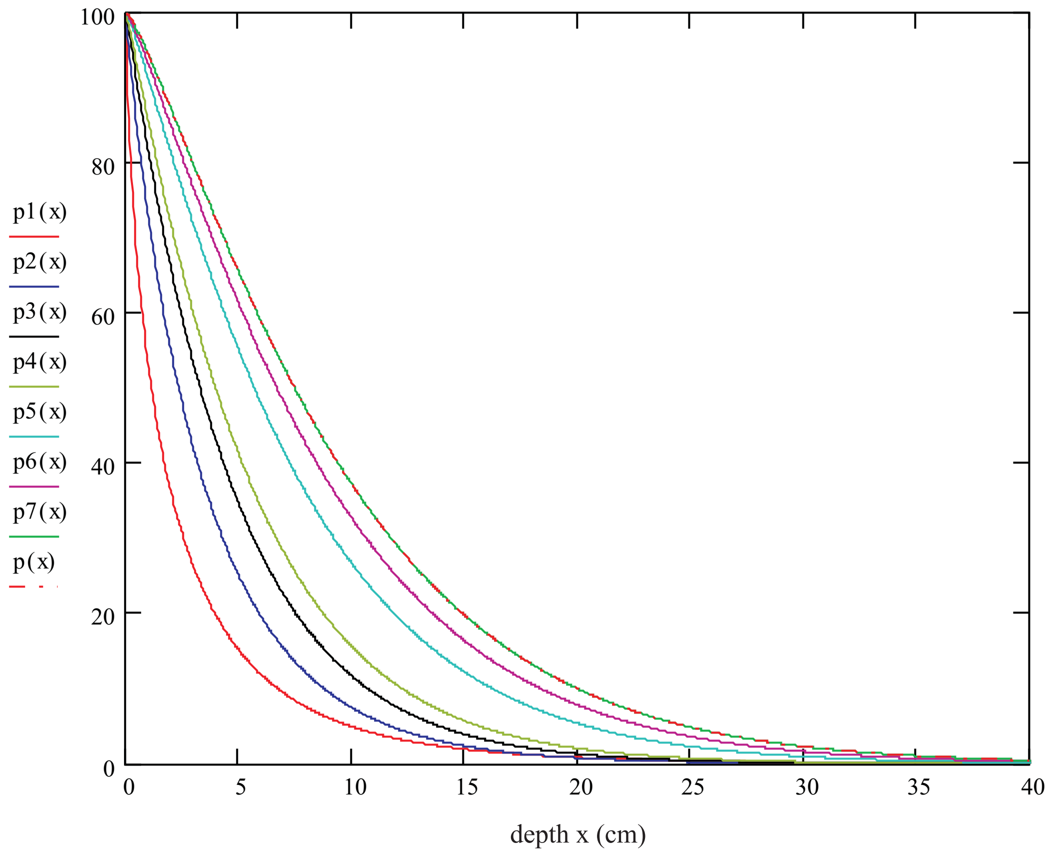

Fig. 6.4-3: Inventories below x in (%) for different points of time (time series 1, Cs-137)

legend:

ordinate axis: inventories below x (%)

p1(x): inventory below x in (%) after 1.2 (a)
p2(x): inventory below x in (%) after 2.5 (a)
p3(x): inventory below x in (%) after 4.3 (a)
p4(x): inventory below x in (%) after 6.2 (a) } based on 2-dimensional nest of intervals
p5(x): inventory below x in (%) after 15 (a)
p6(x): inventory below x in (%) after 25 (a)
p7(x): inventory below x in (%) after 40 (a)
p(x) : inventory below x in (%) after 40 (a), based on second fits of a(t) and n(t)

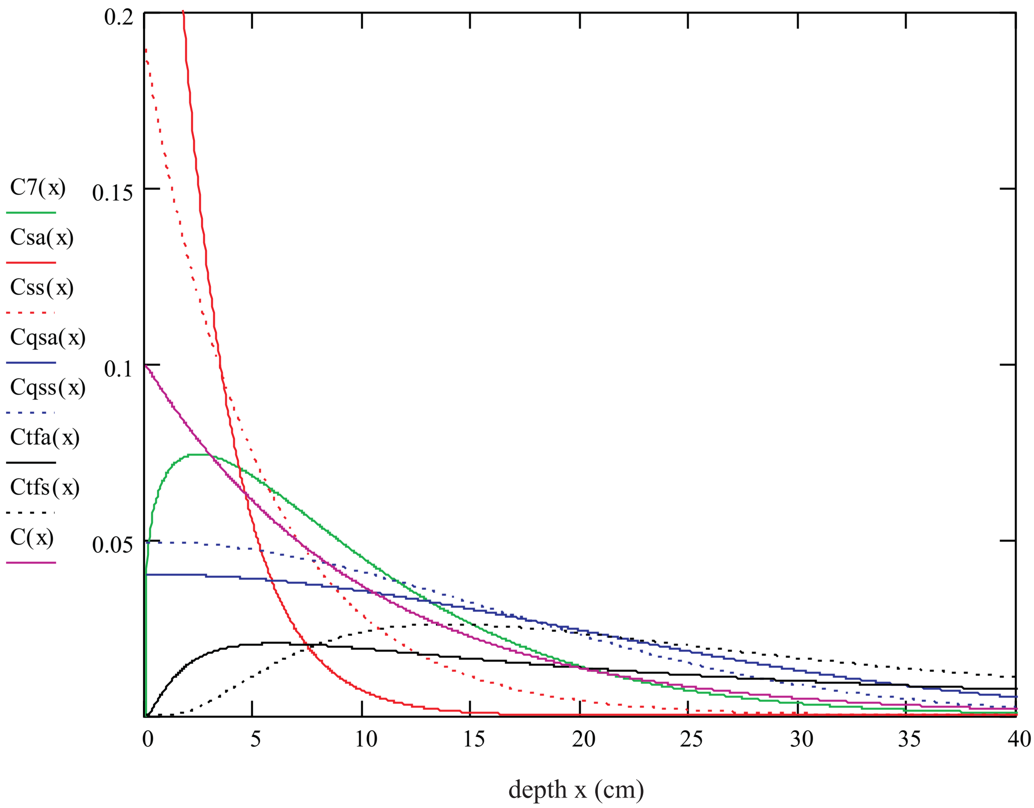

Fig. 6.4-4: Relative concentrations after 40 (a), resulting from different models (time series 1, Cs-137)

legend:

ordinate axis: relative concentration (cm^{-1})

C7(x) : relative concentration after 40 (a), based on 2-dimensional nest of intervals
Csa(x) : relative concentration after 40 (a), based on Eq. (2-2), a-profile
Css(x) : relative concentration after 40 (a), based on Eq. (2-2), s-profile
Cqsa(x) : relative concentration after 40 (a), based on Eq. (2-3), a-profile
Cqss(x) : relative concentration after 40 (a), based on Eq. (2-3), s-profile
Ctfa(x) : relative concentration after 40 (a), based on Eq. (2-4), a-profile
Ctfs(x) : relative concentration after 40 (a), based on Eq. (2-4), s-profile
C(x) : relative concentration after 40 (a), based on a simple exponential function

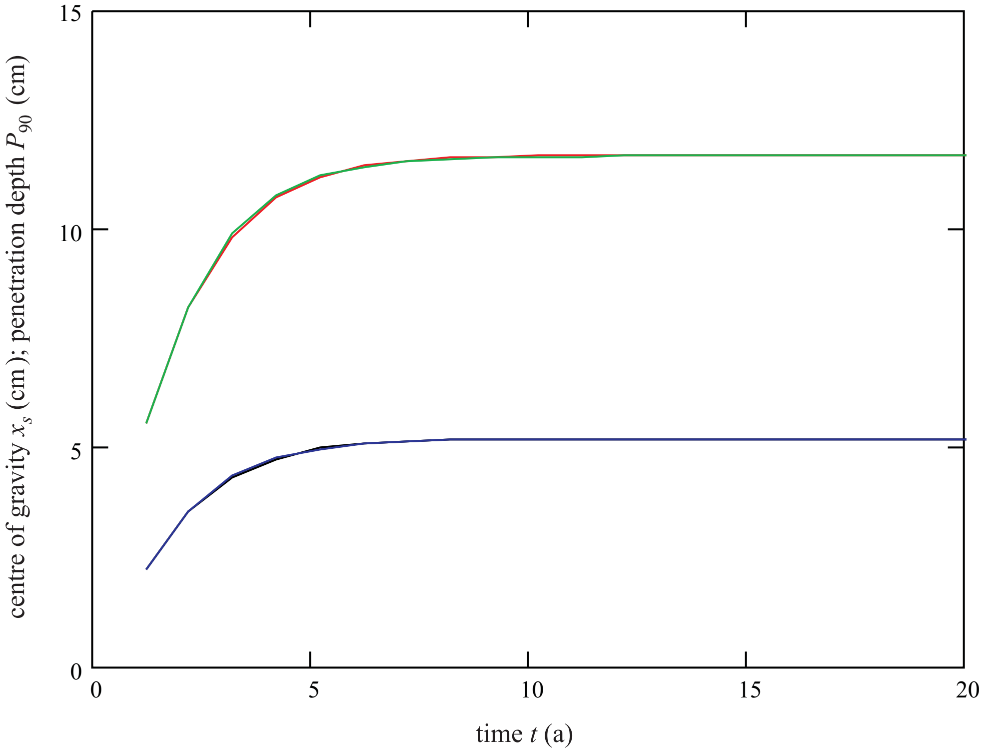

Fig. 6.4-5: Matching of the centres of gravity and of the penetration depths (time series 2, Cs-137)

legend:

black: x_s-fit

blue : matching of the x_s-fit, based on Eq. (2-24)

red : P_{90}-fit

green: matching of the P_{90}-fit; (a(t), n(t) from second fits)

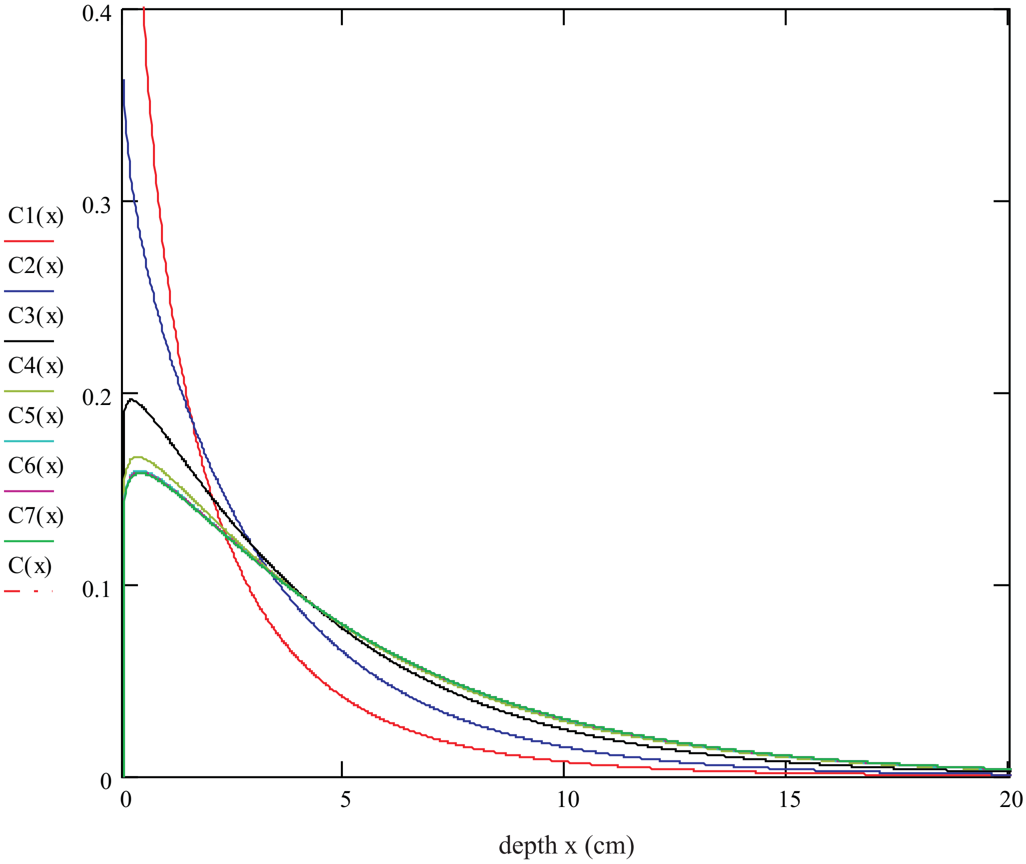

Fig. 6.4-6: Relative concentrations for different points of time (time series 2, Cs-137)
legend:
ordinate axis: relative concentration (cm^{-1})
C1(x): relative concentration after 1.2 (a)
C2(x): relative concentration after 2.0 (a)
C3(x): relative concentration after 3.4 (a)
C4(x): relative concentration after 5.5 (a)
C5(x): relative concentration after 8 (a)
C6(x): relative concentration after 12 (a)
C7(x): relative concentration after 20 (a)
based on 2-dimensional nest of intervals
C(x) : relative concentration after 20 (a), based on second fits of a(t) and n(t)

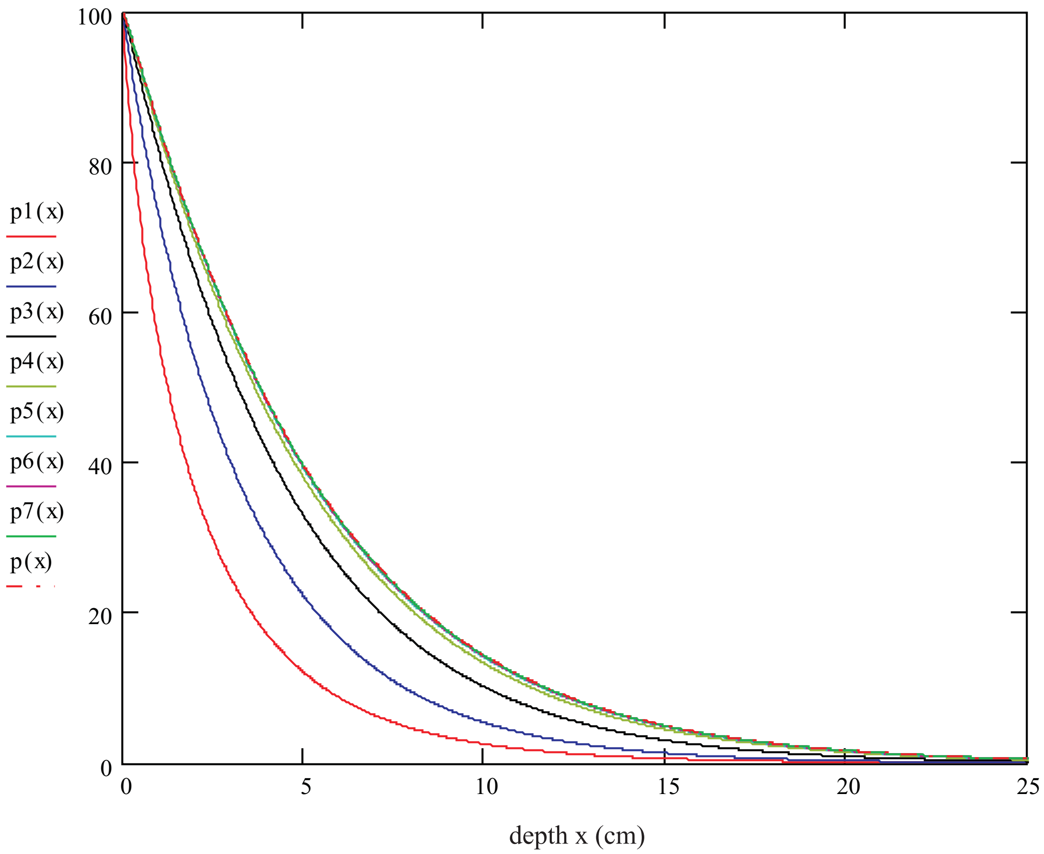

Fig. 6.4-7: Inventories below x in (%) for different points of time (time series 2, Cs-137)
legend:
ordinate axis: inventories below x (%)
p1(x): inventory below x in (%) after 1.2 (a)
p2(x): inventory below x in (%) after 2.0 (a)
p3(x): inventory below x in (%) after 3.4 (a)
p4(x): inventory below x in (%) after 5.5 (a)
p5(x): inventory below x in (%) after 8 (a)
p6(x): inventory below x in (%) after 12 (a)
p7(x): inventory below x in (%) after 20 (a)

based on 2-dimensional nest of intervals

p(x) : inventory below x in (%) after 20 (a), based on second fits of a(t) and n(t)

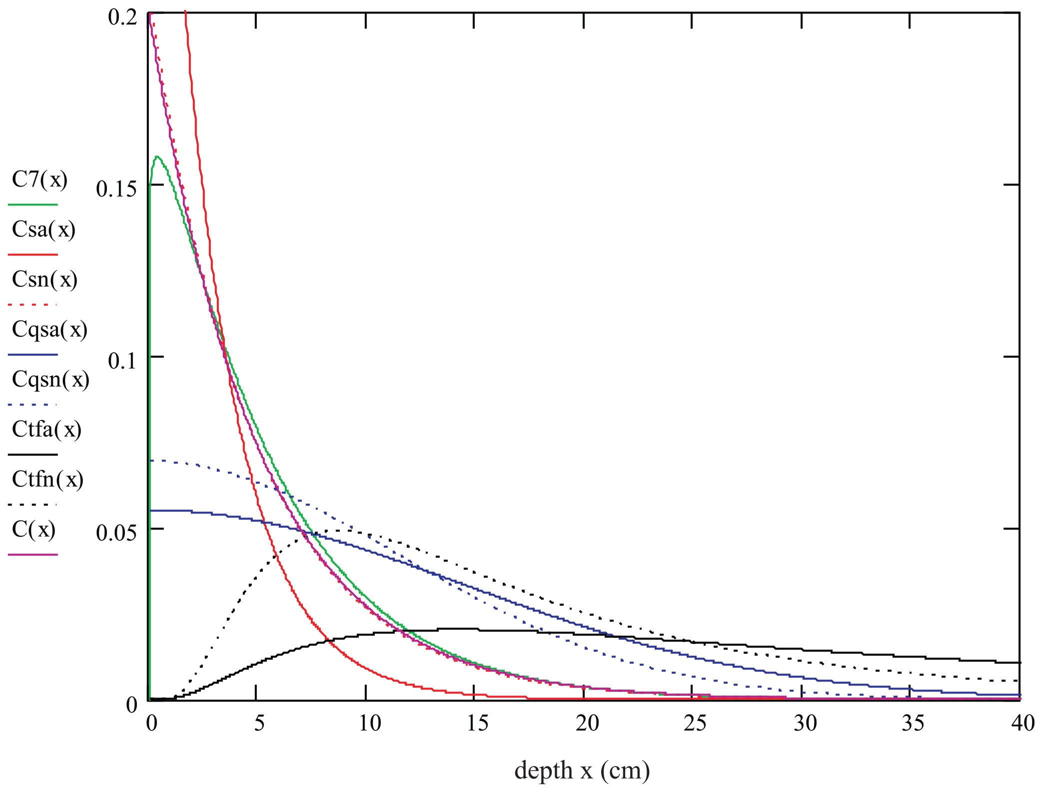

Fig. 6.4-8: Relative concentrations after 20 (a), resulting from different models (time series 2, Cs-137)

legend:

ordinate axis: relative concentration (cm^{-1})

C7(x) : relative concentration after 20 (a), based on 2-dimensional nest of intervals
Csa(x) : relative concentration after 20 (a), based on Eq. (2-2), a-profile
Csn(x) : relative concentration after 20 (a), based on Eq. (2-2), n-profile
Cqsa(x) : relative concentration after 20 (a), based on Eq. (2-3), a-profile
Cqsn(x) : relative concentration after 20 (a), based on Eq. (2-3), n-profile
Ctfa(x) : relative concentration after 20 (a), based on Eq. (2-4), a-profile
Ctfn(x) : relative concentration after 20 (a), based on Eq. (2-4), n-profile
C(x) : relative concentration after 20 (a), based on a simple exponential function

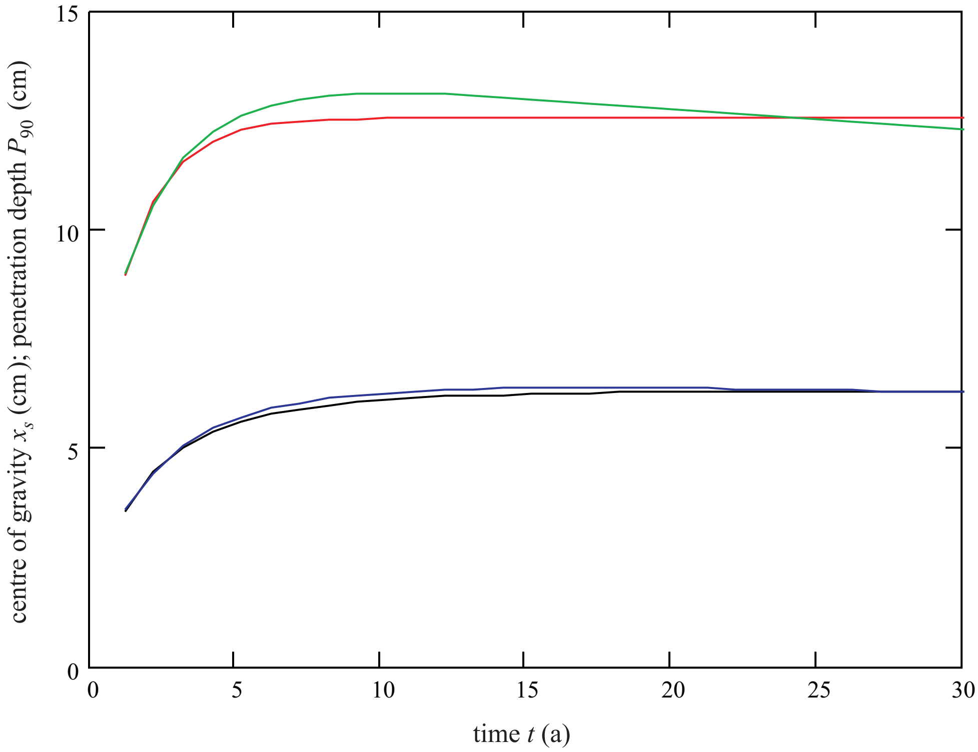

Fig. 6.4-9: Matching of the centres of gravity and of the penetration depths (time series 3, Cs-137)

legend:

black: x_s-fit

blue : matching of the x_s-fit, based on Eq. (2-24)

red : P_{90}-fit

green: matching of the P_{90}-fit; (a(t), n(t) from second fits)

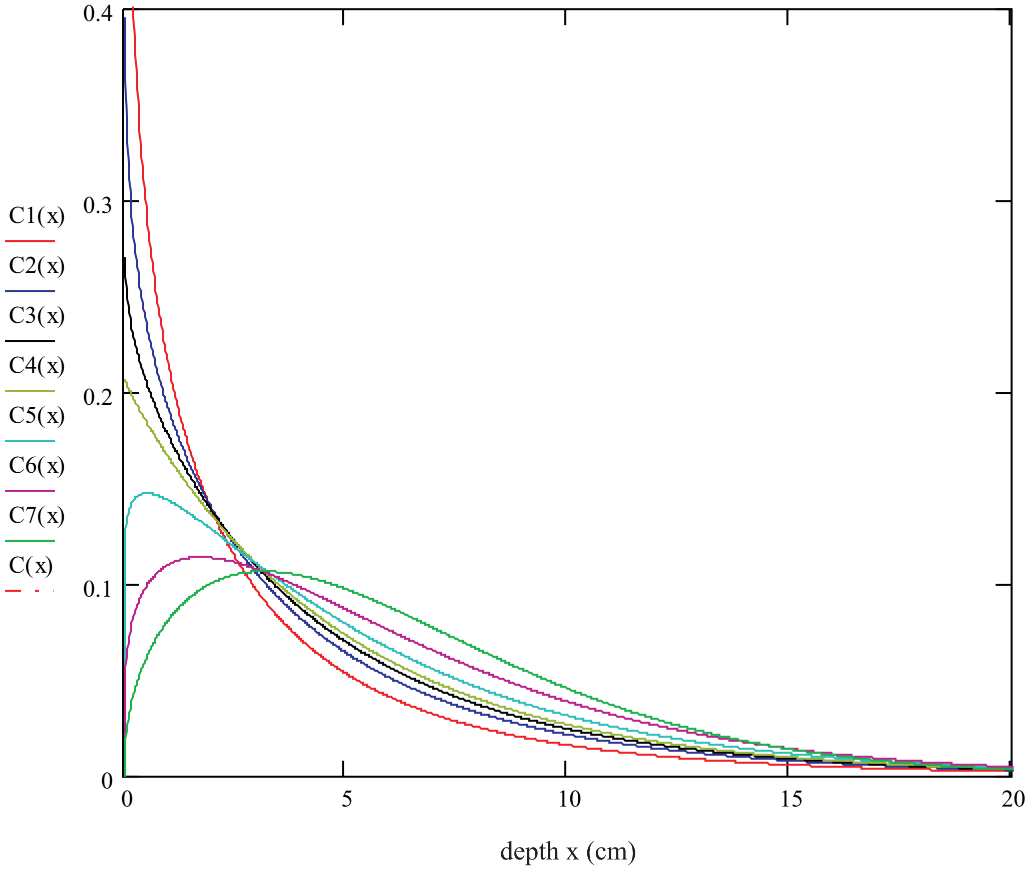

Fig. 6.4-10: Relative concentrations for different points of time (time series 3, Cs-137)
legend:
ordinate axis: relative concentration (cm^{-1})
C1(x): relative concentration after 1.2 (a)
C2(x): relative concentration after 2.0 (a)
C3(x): relative concentration after 2.5 (a)
C4(x): relative concentration after 3.0 (a) } based on 2-dimensional nest of intervals
C5(x): relative concentration after 4.5 (a)
C6(x): relative concentration after 10 (a)
C7(x): relative concentration after 30 (a)
C(x) : relative concentration after 30 (a), based on second fits of a(t) and n(t)

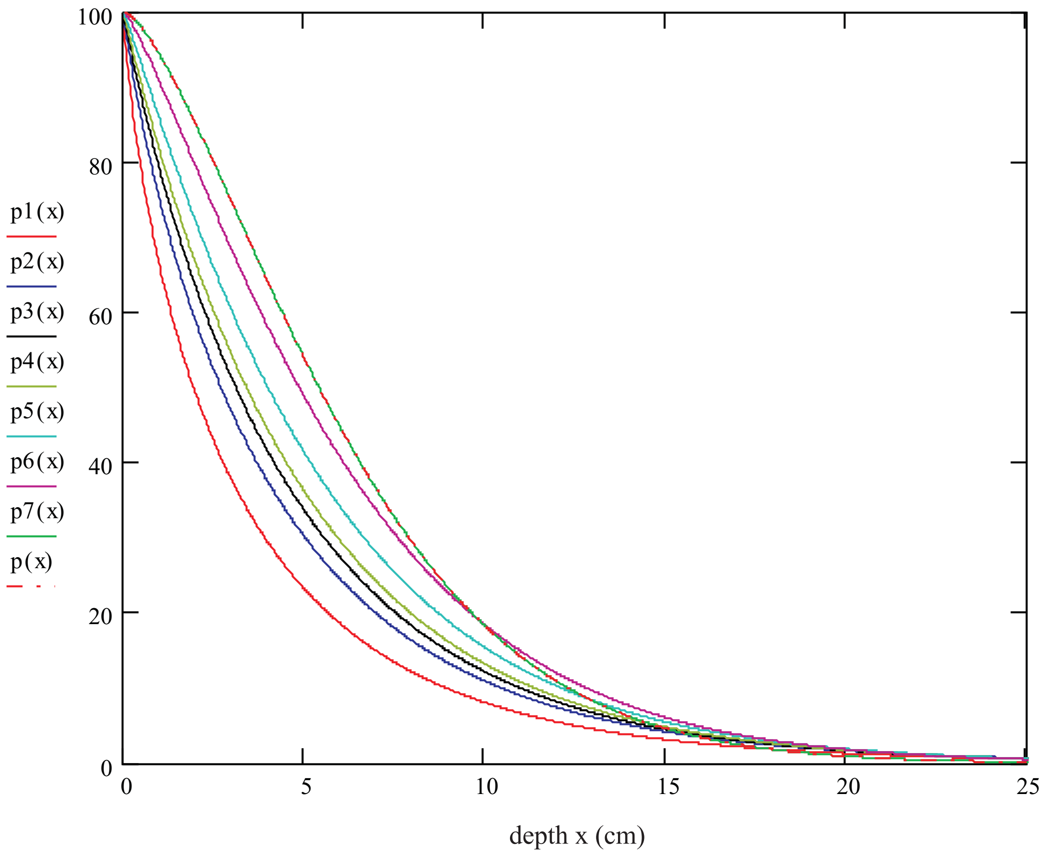

Fig. 6.4-11: Inventories below x in (%) for different points of time (time series 3, Cs-137)
legend:
ordinate axis: inventories below x (%)
p1(x): inventory below x in (%) after 1.2 (a)
p2(x): inventory below x in (%) after 2.0 (a)
p3(x): inventory below x in (%) after 2.5 (a)
p4(x): inventory below x in (%) after 3.0 (a)
p5(x): inventory below x in (%) after 4.5 (a)
p6(x): inventory below x in (%) after 10 (a)
p7(x): inventory below x in (%) after 30 (a)

based on 2-dimensional nest of intervals

p(x) : inventory below x in (%) after 30 (a), based on second fits of a(t) and n(t)

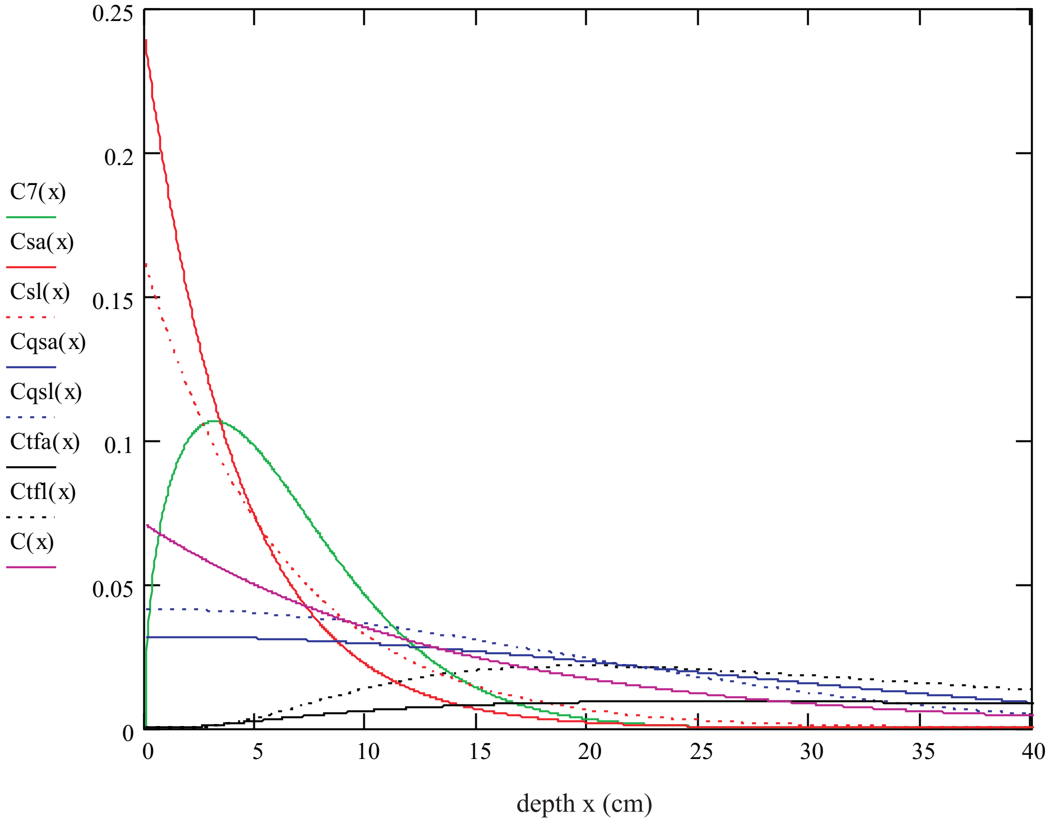

Fig. 6.4-12: Relative concentrations after 30 (a), resulting from different models (time series 3, Cs-137)

legend:

ordinate axis: relative concentration (cm^{-1})

C7(x) : relative concentration after 30 (a), based on 2-dimensional nest of intervals

Csa(x) : relative concentration after 30 (a), based on Eq. (2-2), a-profile

Csl(x) : relative concentration after 30 (a), based on Eq. (2-2), l-profile

Cqsa(x): relative concentration after 30 (a), based on Eq. (2-3), a-profile

Cqsl(x) : relative concentration after 30 (a), based on Eq. (2-3), l-profile

Ctfa(x) : relative concentration after 30 (a), based on Eq. (2-4), a-profile

Ctfl(x) : relative concentration after 30 (a), based on Eq. (2-4), l-profile

C(x) : relative concentration after 30 (a), based on a simple exponential function

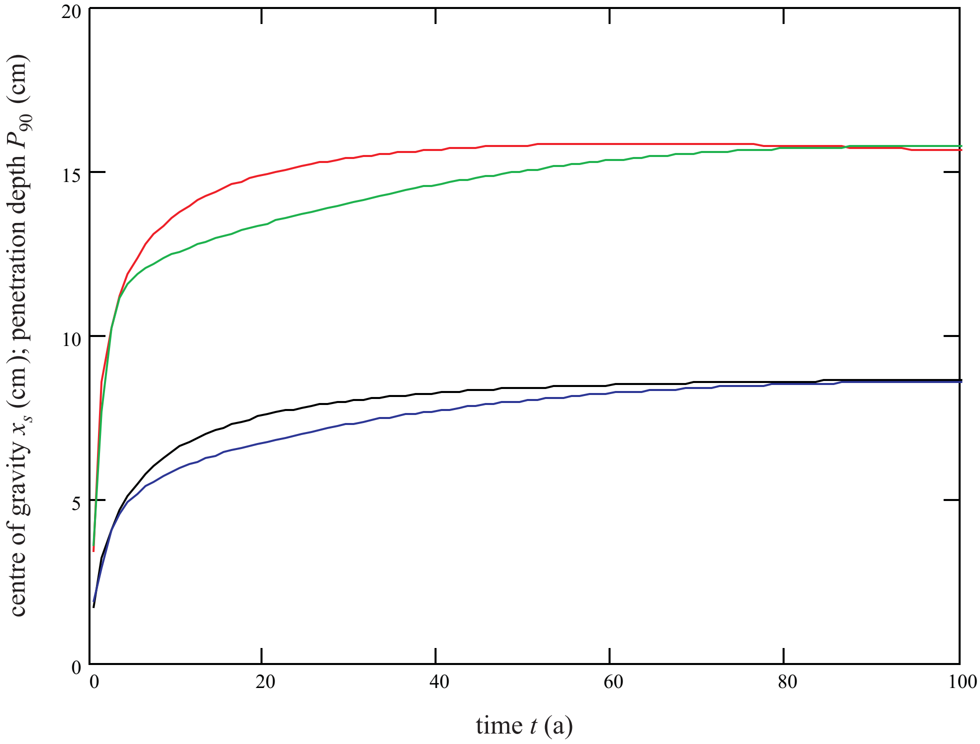

Fig. 6.5-1: Matching of the centres of gravity and of the penetration depths (time series 1, Cs-137)

legend:

black: x_s-fit

blue : matching of the x_s-fit, based on Eq. (2-24)

red : P_{90}-fit

green: matching of the P_{90}-fit; (a(t), n(t) from second fits)

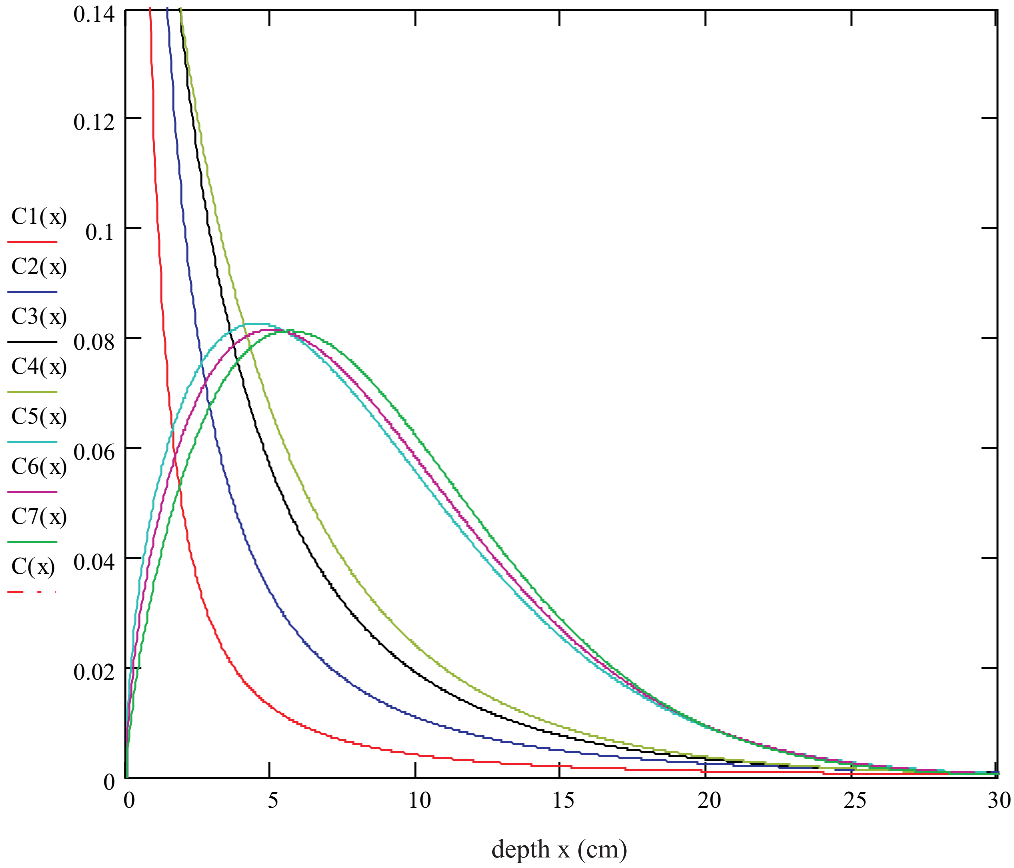

Fig. 6.5-2: Relative concentrations for different points of time (time series 1, Cs-137)
legend:
ordinate axis: relative concentration (cm^{-1})
C1(x): relative concentration after 0.3 (a)
C2(x): relative concentration after 1.17 (a)
C3(x): relative concentration after 2.42 (a)
C4(x): relative concentration after 3.42 (a)
C5(x): relative concentration after 33.42 (a)
C6(x): relative concentration after 50 (a)
C7(x): relative concentration after 100 (a)
} based on 2-dimensional nest of intervals
C(x) : relative concentration after 100 (a), based on second fits of a(t) and n(t)

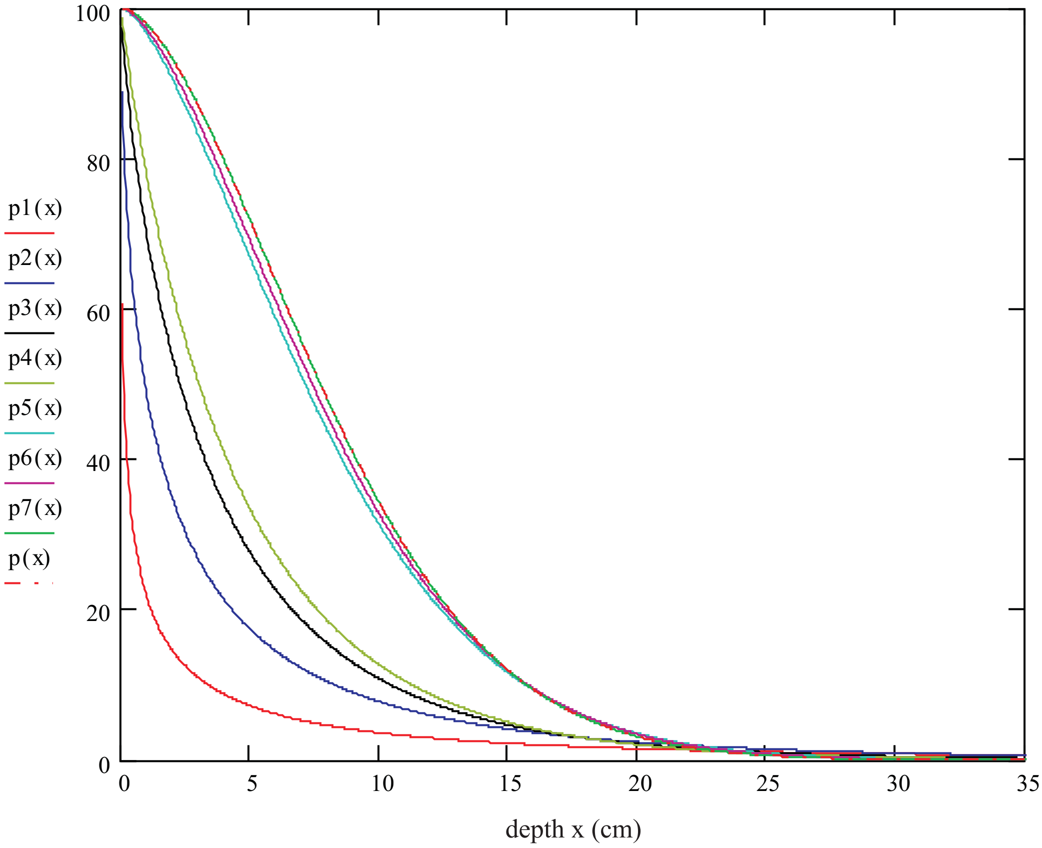

Fig. 6.5-3: Inventories below x in (%) for different points of time (time series 1, Cs-137)
legend:
ordinate axis: inventories below x (%)

p1(x): inventory below x in (%) after 0.3 (a)
p2(x): inventory below x in (%) after 1.17 (a)
p3(x): inventory below x in (%) after 2.42 (a)
p4(x): inventory below x in (%) after 3.42 (a)
p5(x): inventory below x in (%) after 33.42 (a)
p6(x): inventory below x in (%) after 50 (a)
p7(x): inventory below x in (%) after 100 (a)

based on 2-dimensional nest of intervals

p(x) : inventory below x in (%) after 100 (a), based on second fits of a(t) and n(t)

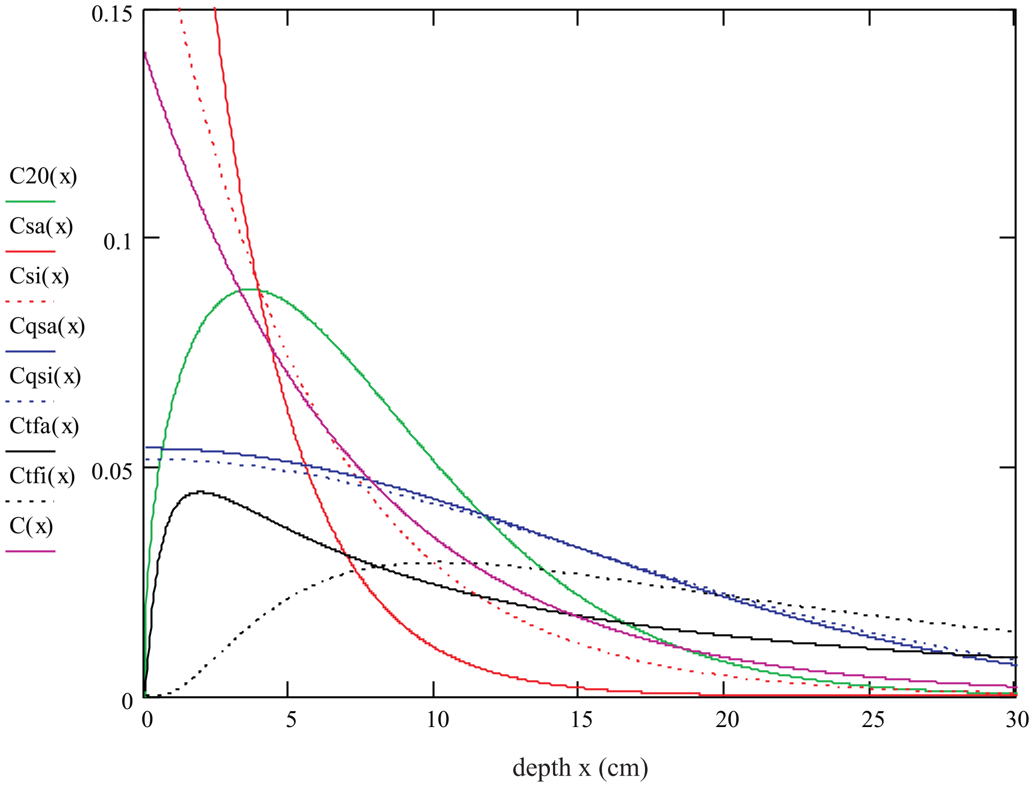

Fig. 6.5-4: Relative concentrations after 20 (a), resulting from different models (time series 1, Cs-137)

legend:

ordinate axis: relative concentration (cm^{-1})

C20(x) : relative concentration after 20 (a), based on 2-dimensional nest of intervals
Csa(x) : relative concentration after 20 (a), based on Eq. (2-2), a-profile
Csi(x) : relative concentration after 20 (a), based on Eq. (2-2), i-profile
Cqsa(x): relative concentration after 20 (a), based on Eq. (2-3), a-profile
Cqsi(x) : relative concentration after 20 (a), based on Eq. (2-3), i-profile
Ctfa(x) : relative concentration after 20 (a), based on Eq. (2-4), a-profile
Ctfi(x) : relative concentration after 20 (a), based on Eq. (2-4), i-profile
C(x) : relative concentration after 20 (a), based on a simple exponential function

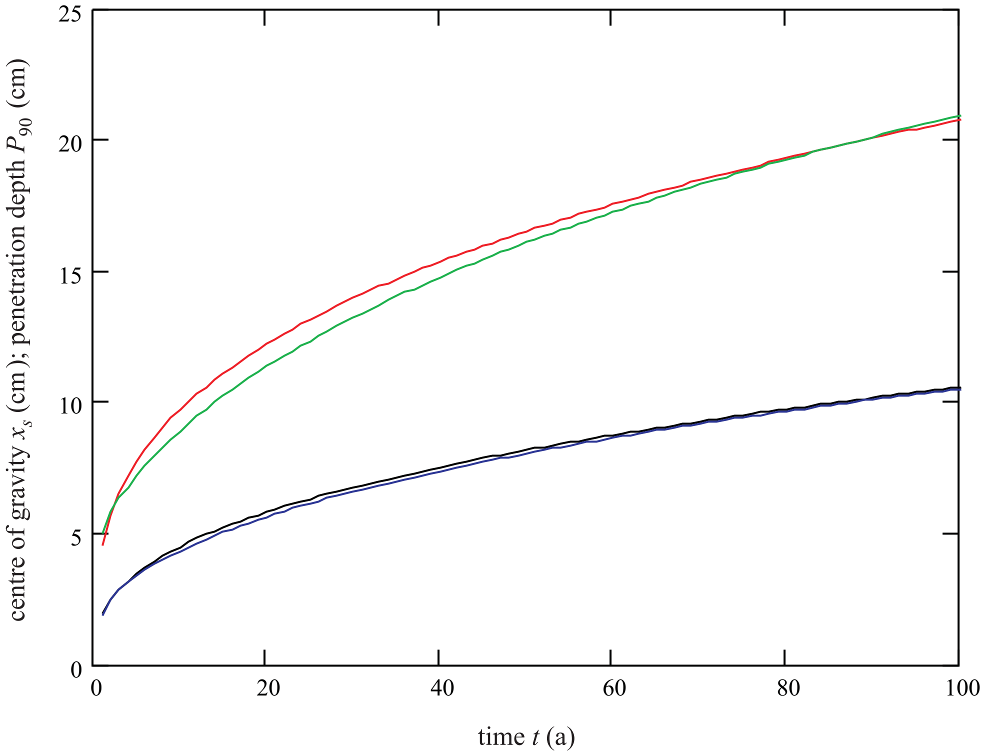

Fig. 6.5-5: Matching of the centres of gravity and of the penetration depths (time series 2, Cs-137)

legend:

black: x_s-fit

blue : matching of the x_s-fit, based on Eq. (2-24)

red : P_{90}-fit

green: matching of the P_{90}-fit; (a(t), n(t) from second fits)

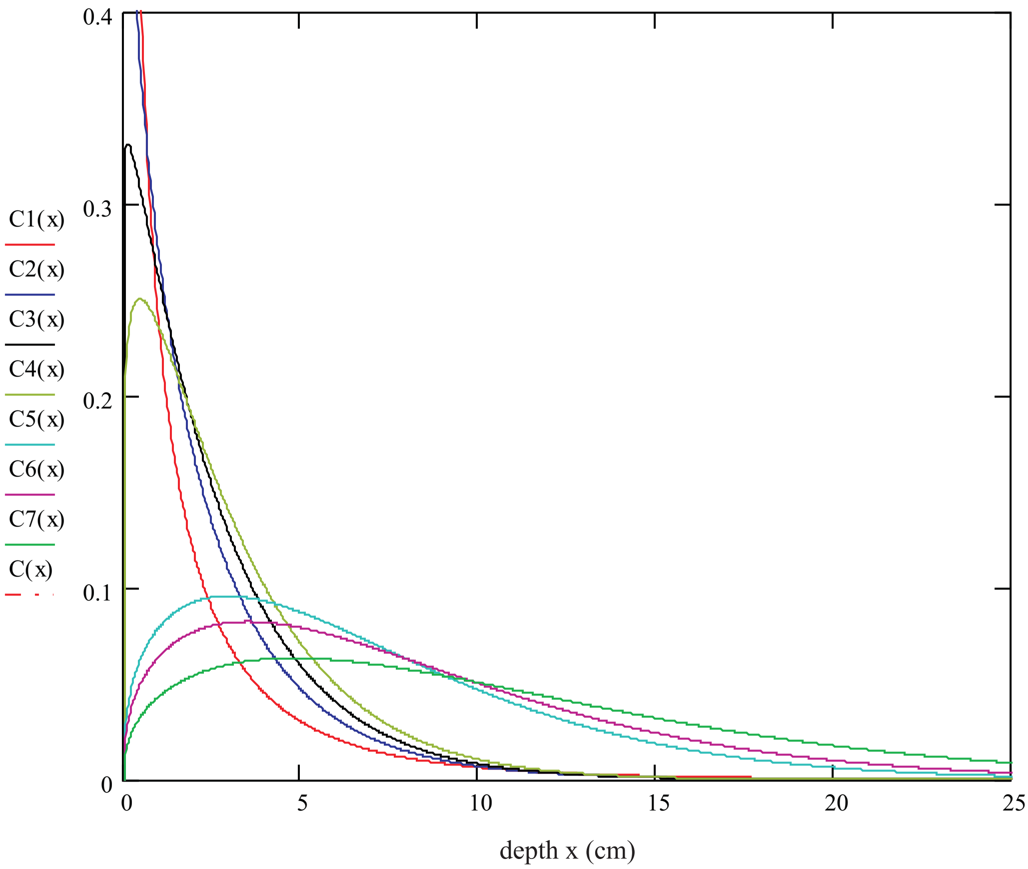

Fig. 6.5-6: Relative concentrations for different points of time (time series 2, Cs-137)
legend:
ordinate axis: relative concentration (cm^{-1})
C1(x): relative concentration after 1.0 (a)
C2(x): relative concentration after 1.67 (a)
C3(x): relative concentration after 2.42 (a)
C4(x): relative concentration after 3.42 (a) } based on 2-dimensional nest of intervals
C5(x): relative concentration after 33.42 (a)
C6(x): relative concentration after 50 (a)
C7(x): relative concentration after 100 (a)
C(x) : relative concentration after 100 (a), based on second fits of a(t) and n(t)

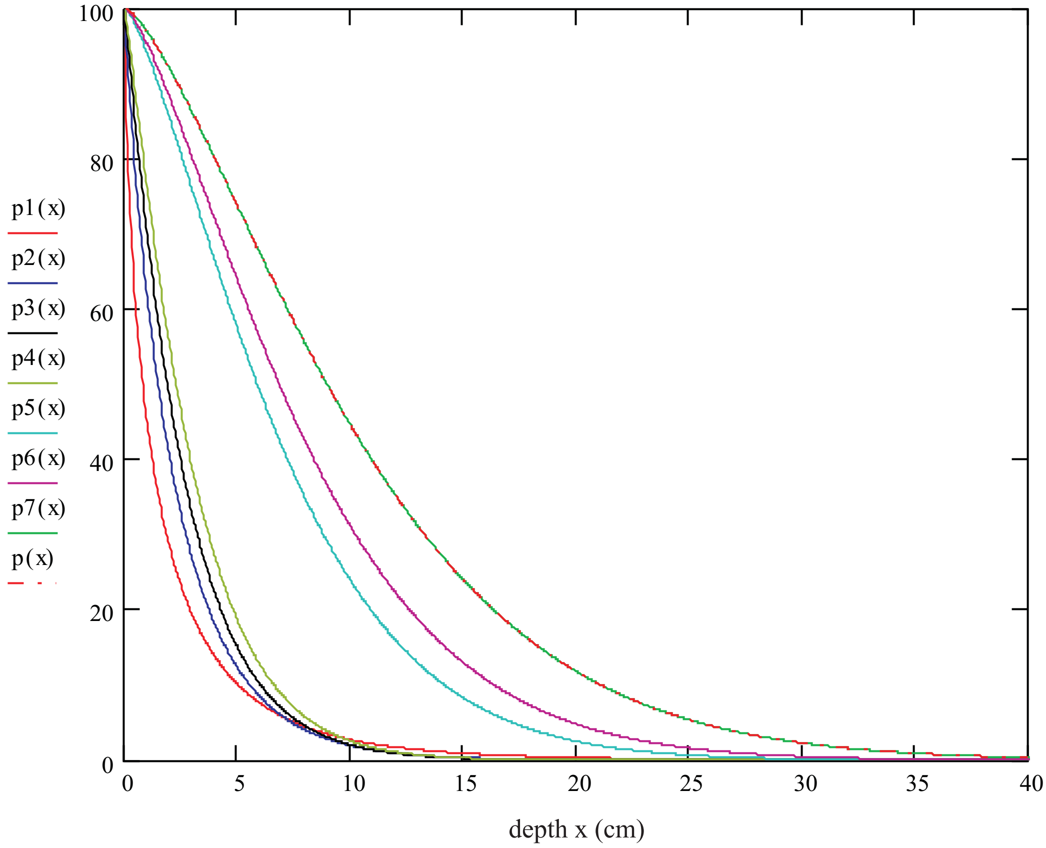

Fig. 6.5-7: Inventories below x in (%) for different points of time (time series 2, Cs-137)
legend:
ordinate axis: inventories below x (%)

$$\left.\begin{array}{l}\text{p1(x): inventory below x in (\%) after 1.0 (a)}\\ \text{p2(x): inventory below x in (\%) after 1.67 (a)}\\ \text{p3(x): inventory below x in (\%) after 2.42 (a)}\\ \text{p4(x): inventory below x in (\%) after 3.42 (a)}\\ \text{p5(x): inventory below x in (\%) after 33.42 (a)}\\ \text{p6(x): inventory below x in (\%) after 50 (a)}\\ \text{p7(x): inventory below x in (\%) after 100 (a)}\end{array}\right\}\text{based on 2-dimensional nest of intervals}$$

p(x) : inventory below x in (%) after 100 (a), based on second fits of a(t) and n(t)

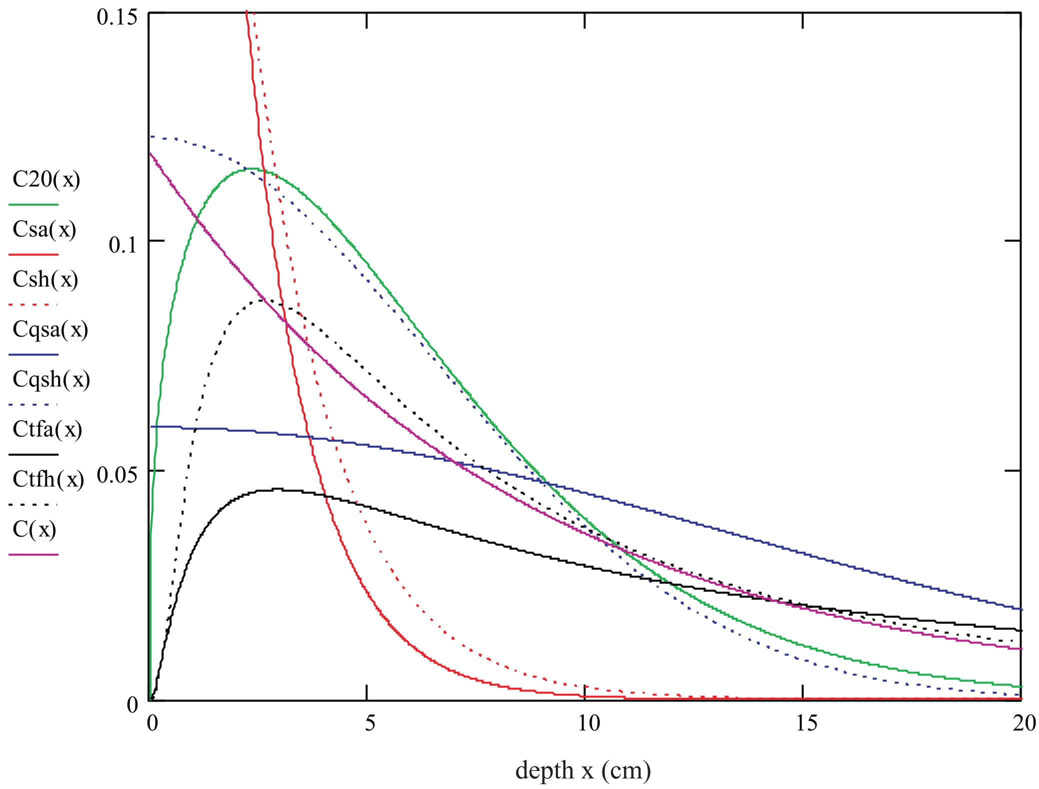

Fig. 6.5-8: Relative concentrations after 20 (a), resulting from different models (time series 2, Cs-137)

legend:

ordinate axis: relative concentration (cm^{-1})

C20(x) : relative concentration after 20 (a), based on 2-dimensional nest of intervals
Csa(x) : relative concentration after 20 (a), based on Eq. (2-2), a-profile
Csh(x) : relative concentration after 20 (a), based on Eq. (2-2), h-profile
Cqsa(x): relative concentration after 20 (a), based on Eq. (2-3), a-profile
Cqsh(x): relative concentration after 20 (a), based on Eq. (2-3), h-profile
Ctfa(x) : relative concentration after 20 (a), based on Eq. (2-4), a-profile
Ctfh(x) : relative concentration after 20 (a), based on Eq. (2-4), h-profile
C(x) : relative concentration after 20 (a), based on a simple exponential function

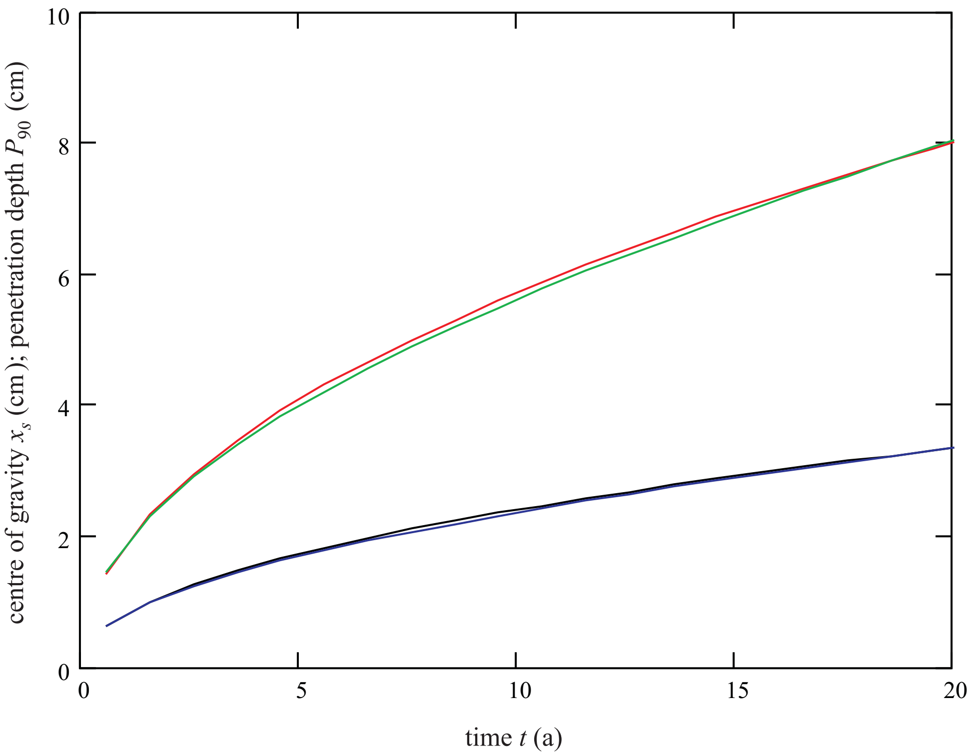

Fig. 6.6-1: Matching of the centres of gravity and of the penetration depths (time series 1, Cs-134)
legend:
black: x_s-fit
blue : matching of the x_s-fit, based on Eq. (2-24)
red : P_{90}-fit
green: matching of the P_{90}-fit; (a(t), n(t) from second fits)

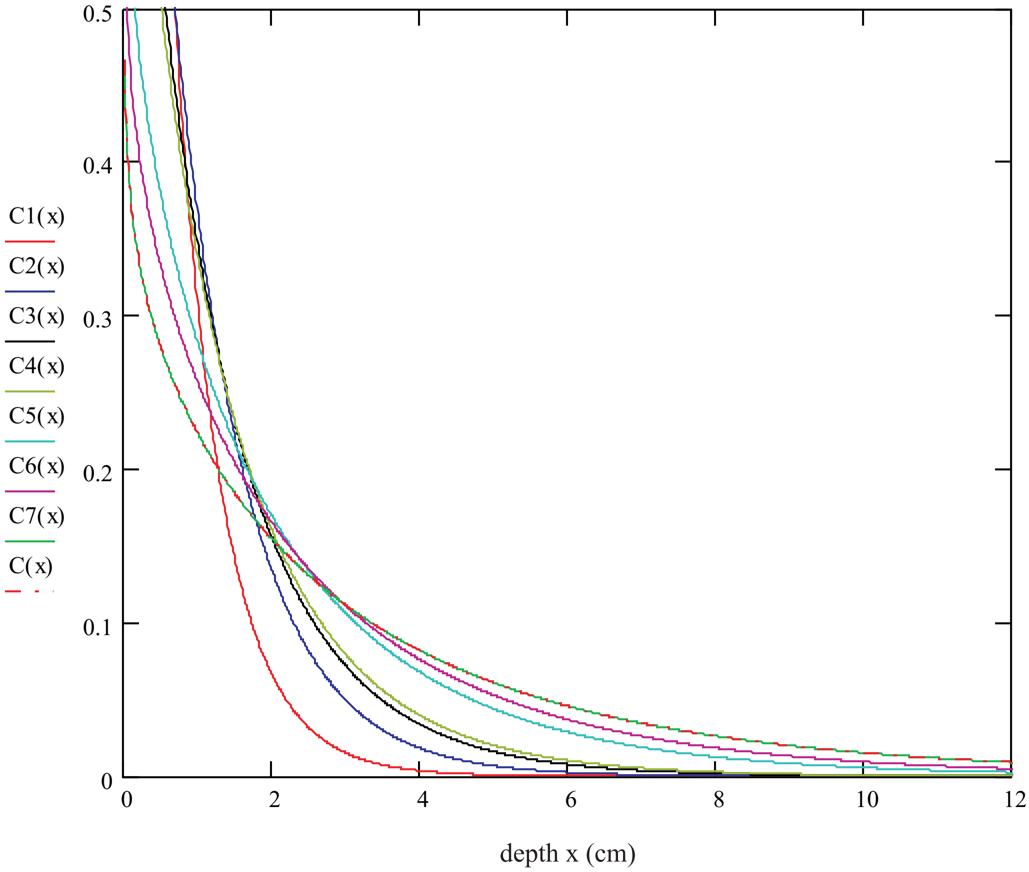

Fig. 6.6-2: Relative concentrations for different points of time (time series 1, Cs-134)

legend:

ordinate axis: relative concentration (cm^{-1})

$$\left.\begin{array}{l}\text{C1(x): relative concentration after 0.583 (a)}\\ \text{C2(x): relative concentration after 1.583 (a)}\\ \text{C3(x): relative concentration after 2.583 (a)}\\ \text{C4(x): relative concentration after 3.083 (a)}\\ \text{C5(x): relative concentration after 8 (a)}\\ \text{C6(x): relative concentration after 12 (a)}\\ \text{C7(x): relative concentration after 20 (a)}\end{array}\right\}\text{ based on 2-dimensional nest of intervals}$$

C(x) : relative concentration after 20 (a), based on second fits of a(t) and n(t)

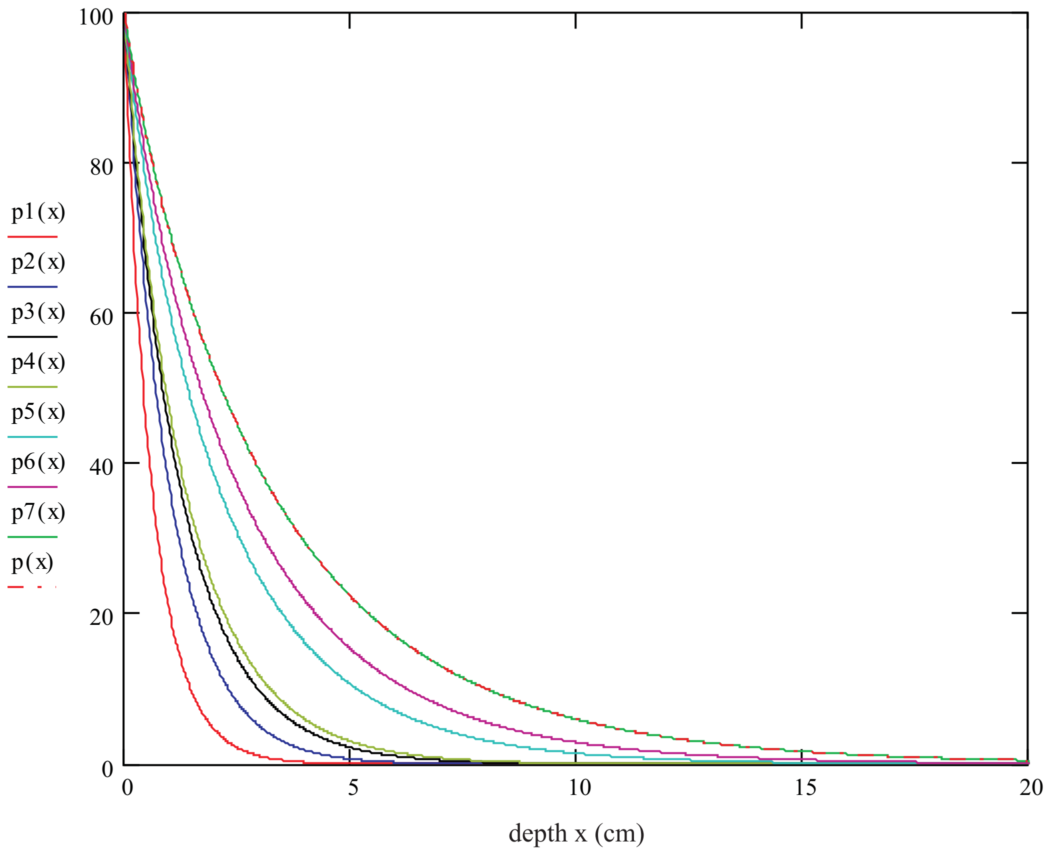

Fig. 6.6-3: Inventories below x in (%) for different points of time (time series 1, Cs-134)

legend:

ordinate axis: inventories below x (%)

p1(x): inventory below x in (%) after 0.583 (a)
p2(x): inventory below x in (%) after 1.583 (a)
p3(x): inventory below x in (%) after 2.583 (a)
p4(x): inventory below x in (%) after 3.083 (a)
p5(x): inventory below x in (%) after 8 (a)
p6(x): inventory below x in (%) after 12 (a)
p7(x): inventory below x in (%) after 20 (a)

based on 2-dimensional nest of intervals

p(x) : inventory below x in (%) after 20 (a), based on second fits of a(t) and n(t)

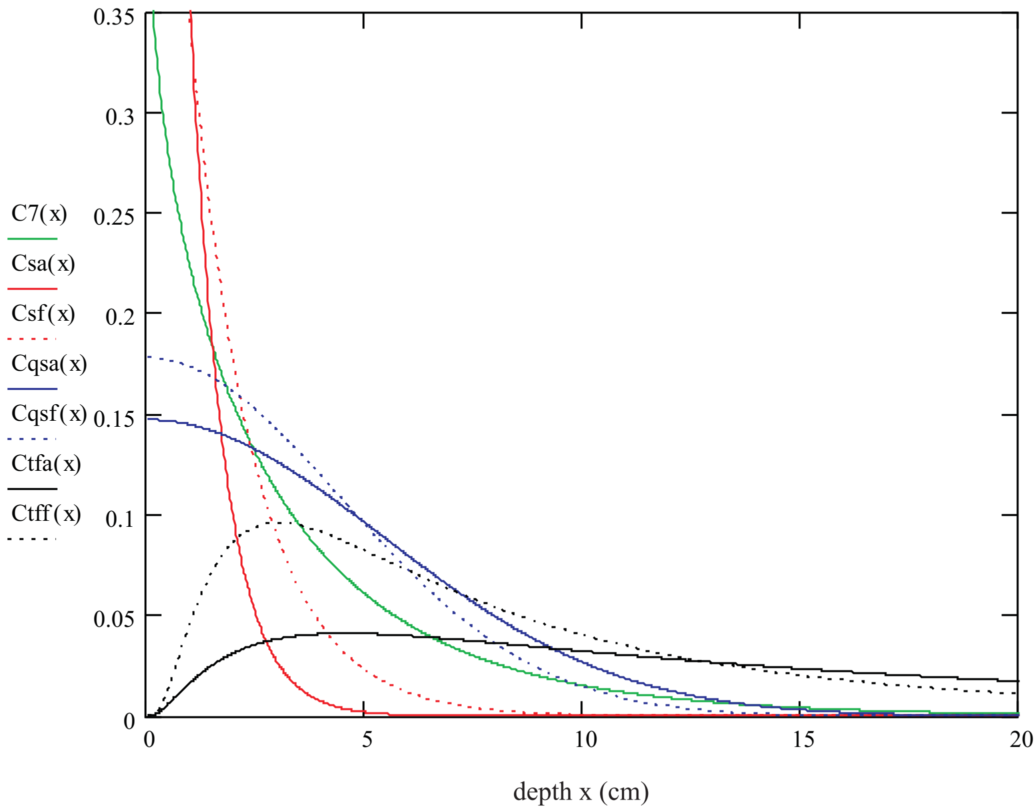

Fig. 6.6-4: Relative concentrations after 20 (a), resulting from different models (time series 1, Cs-134)

legend:

ordinate axis: relative concentration (cm^{-1})

C7(x) : relative concentration after 20 (a), based on 2-dimensional nest of intervals
Csa(x) : relative concentration after 20 (a), based on Eq. (2-2), a-profile
Csf(x) : relative concentration after 20 (a), based on Eq. (2-2), f-profile
Cqsa(x): relative concentration after 20 (a), based on Eq. (2-3), a-profile
Cqsf(x): relative concentration after 20 (a), based on Eq. (2-3), f-profile
Ctfa(x) : relative concentration after 20 (a), based on Eq. (2-4), a-profile
Ctff(x) : relative concentration after 20 (a), based on Eq. (2-4), f-profile

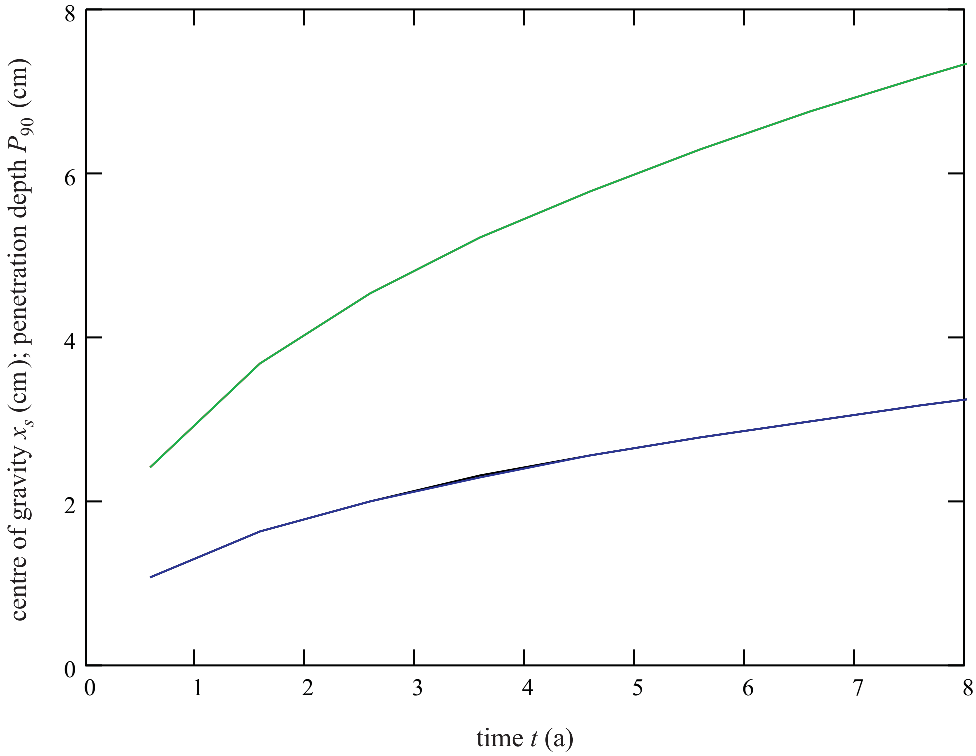

Fig. 6.6-5: Matching of the centres of gravity and of the penetration depths (time series 2, Ru-106)

legend:

black: x_s-fit

blue : matching of the x_s-fit, based on Eq. (2-24)

red : P_{90}-fit

green: matching of the P_{90}-fit; (a(t), n(t) from second fits)

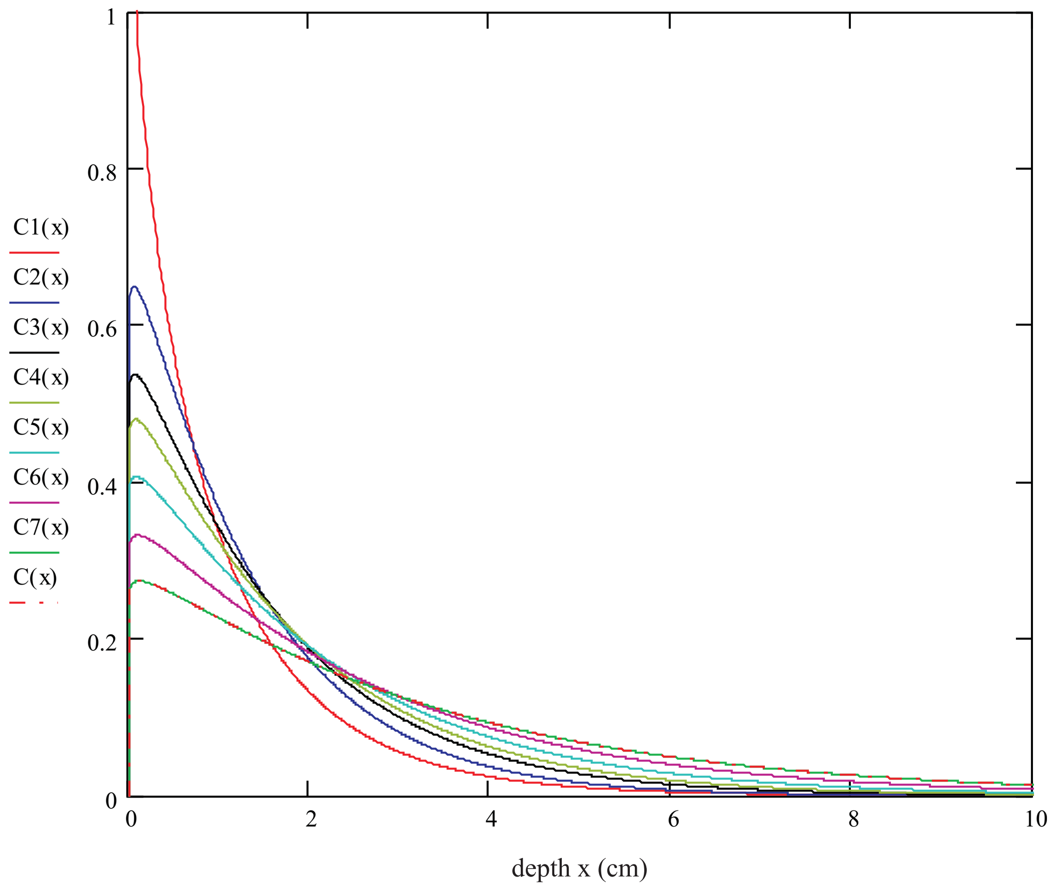

Fig. 6.6-6: Relative concentrations for different points of time (time series 2, Ru-106)
legend:
ordinate axis: relative concentration (cm^{-1})

$$\left.\begin{array}{l}\text{C1(x): relative concentration after 0.583 (a)}\\ \text{C2(x): relative concentration after 1.0 (a)}\\ \text{C3(x): relative concentration after 1.583 (a)}\\ \text{C4(x): relative concentration after 2.083 (a)}\\ \text{C5(x): relative concentration after 3.083 (a)}\\ \text{C6(x): relative concentration after 5 (a)}\\ \text{C7(x): relative concentration after 8 (a)}\end{array}\right\}\text{ based on 2-dimensional nest of intervals}$$

C(x) : relative concentration after 8 (a), based on second fits of a(t) and n(t)

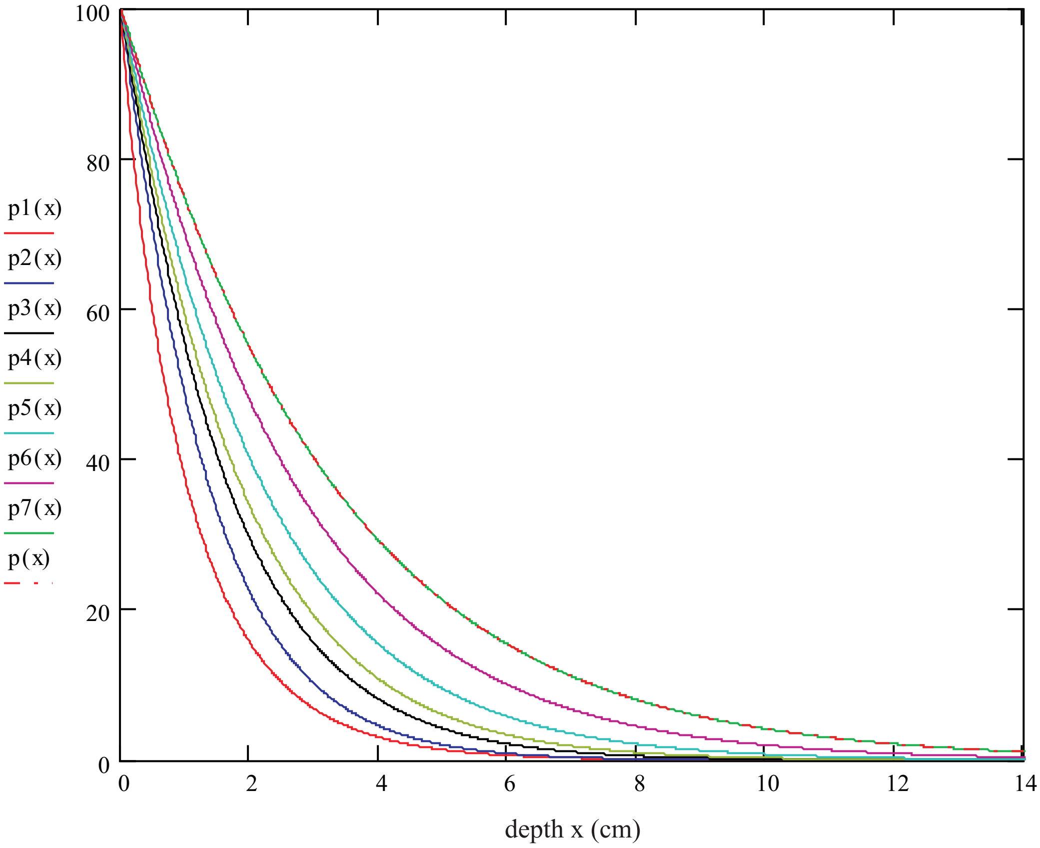

Fig. 6.6-7: Inventories below x in (%) for different points of time (time series 2, Ru-106)
legend:
ordinate axis: inventories below x (%)
p1(x): inventory below x in (%) after 0.583 (a)
p2(x): inventory below x in (%) after 1.0 (a)
p3(x): inventory below x in (%) after 1.583 (a)
p4(x): inventory below x in (%) after 2.083 (a)
p5(x): inventory below x in (%) after 3.083 (a)
p6(x): inventory below x in (%) after 5 (a)
p7(x): inventory below x in (%) after 8 (a)
based on 2-dimensional nest of intervals
p(x) : inventory below x in (%) after 8 (a), based on second fits of a(t) and n(t)

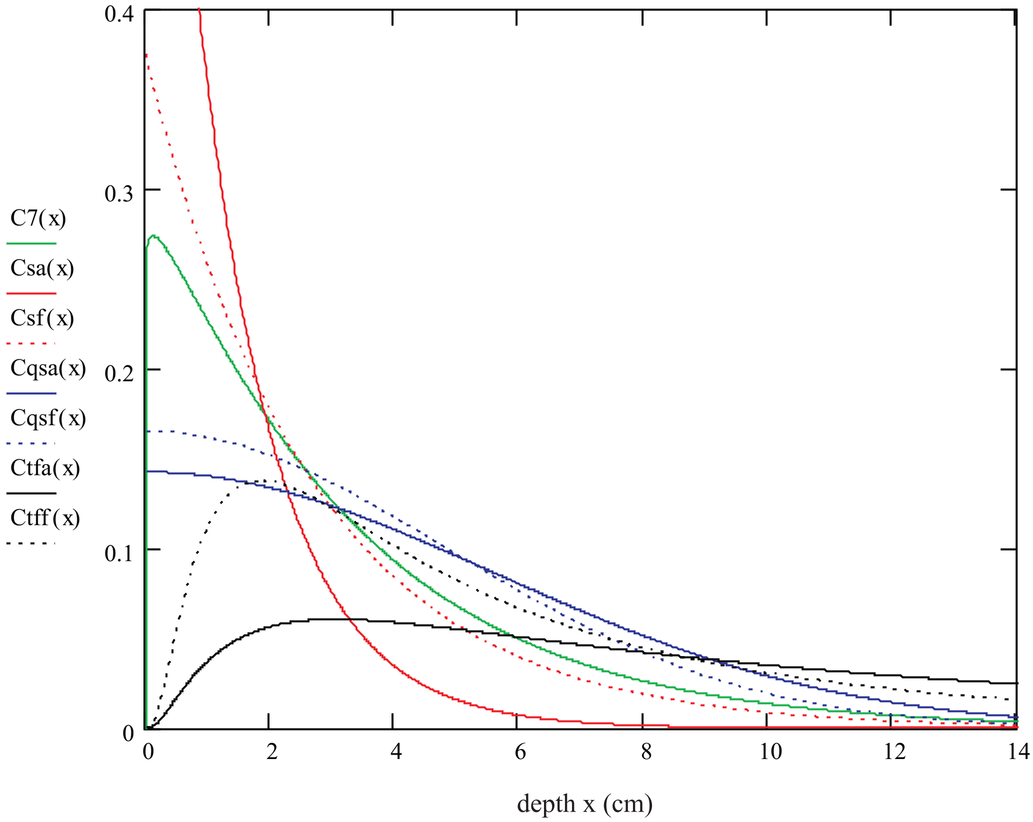

Fig. 6.6-8: Relative concentrations after 8 (a), resulting from different models (time series 2, Ru-106)

legend:

ordinate axis: relative concentration (cm^{-1})

C7(x) : relative concentration after 8 (a), based on 2-dimensional nest of intervals

Csa(x) : relative concentration after 8 (a), based on Eq. (2-2), a-profile

Csf(x) : relative concentration after 8 (a), based on Eq. (2-2), f-profile

Cqsa(x): relative concentration after 8 (a), based on Eq. (2-3), a-profile

Cqsf(x): relative concentration after 8 (a), based on Eq. (2-3), f-profile

Ctfa(x) : relative concentration after 8 (a), based on Eq. (2-4), a-profile

Ctff(x) : relative concentration after 8 (a), based on Eq. (2-4), f-profile

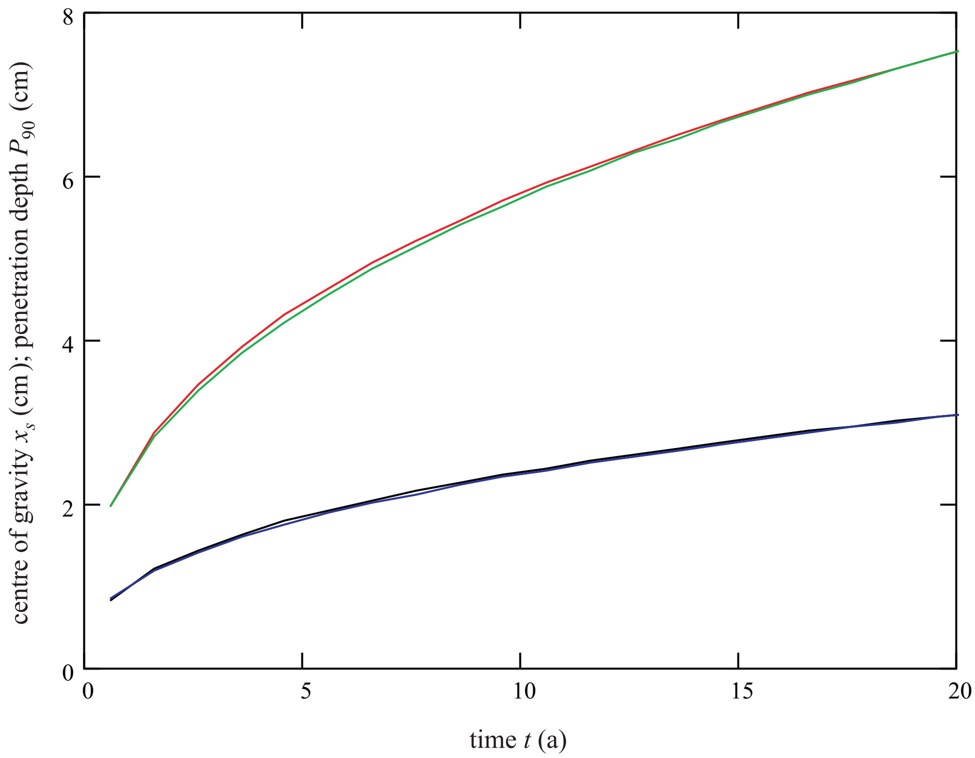

Fig. 6.6-9: Matching of the centres of gravity and of the penetration depths (time series 3, Cs-134)

legend:

black: x_s-fit

blue : matching of the x_s-fit, based on Eq. (2-24)

red : P_{90}-fit

green: matching of the P_{90}-fit; (a(t), n(t) from second fits)

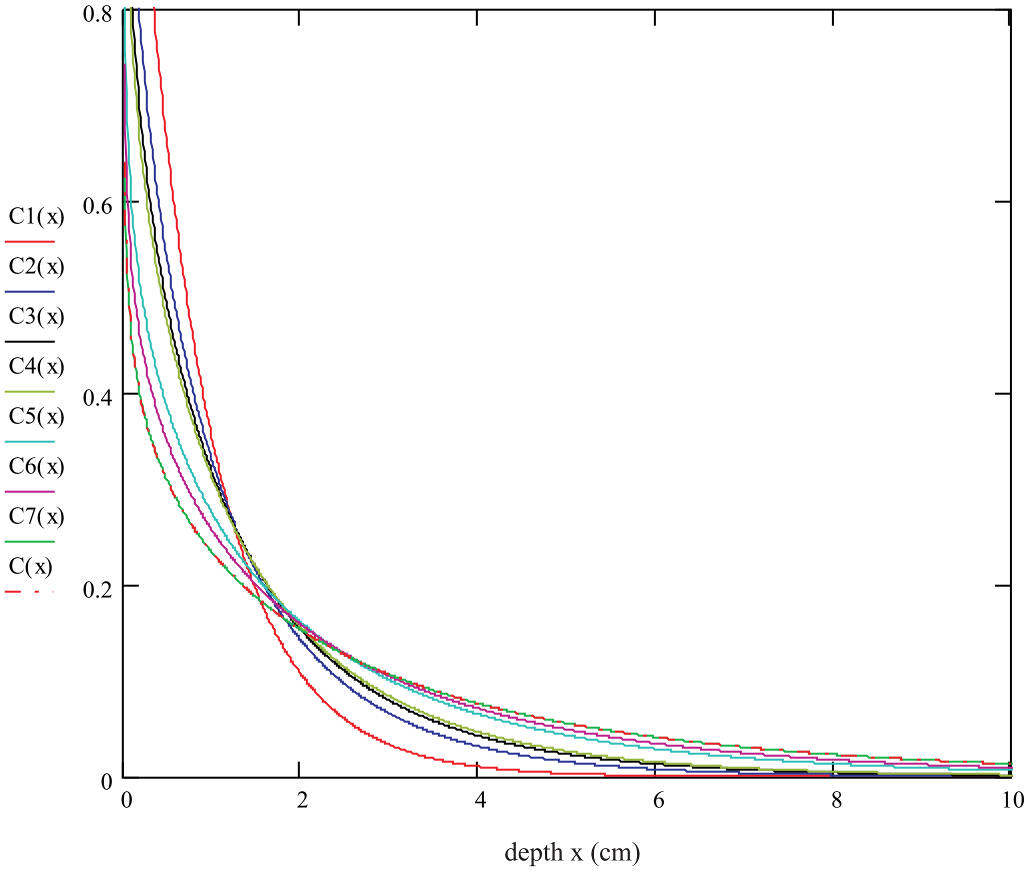

Fig. 6.6-10: Relative concentrations for different points of time (time series 3, Cs-134)
legend:
ordinate axis: relative concentration (cm^{-1})

C1(x): relative concentration after 0.583 (a)
C2(x): relative concentration after 1.583 (a)
C3(x): relative concentration after 2.583 (a)
C4(x): relative concentration after 3.083 (a)
C5(x): relative concentration after 8 (a)
C6(x): relative concentration after 12 (a)
C7(x): relative concentration after 20 (a)

(C1(x)–C7(x): based on 2-dimensional nest of intervals)

C(x) : relative concentration after 20 (a), based on second fits of a(t) and n(t)

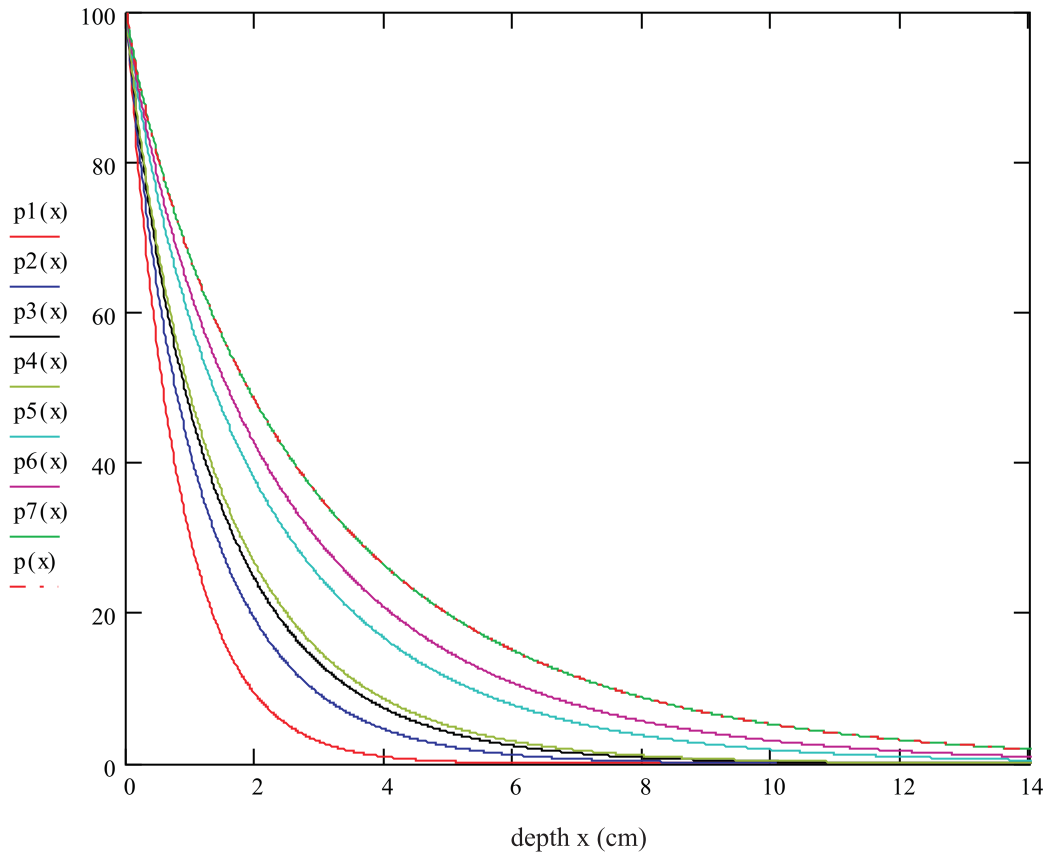

Fig. 6.6-11: Inventories below x in (%) for different points of time (time series 3, Cs-134)
legend:
ordinate axis: inventories below x (%)
p1(x): inventory below x in (%) after 0.583 (a)
p2(x): inventory below x in (%) after 1.583 (a)
p3(x): inventory below x in (%) after 2.583 (a)
p4(x): inventory below x in (%) after 3.083 (a) based on 2-dimensional nest of intervals
p5(x): inventory below x in (%) after 8 (a)
p6(x): inventory below x in (%) after 12 (a)
p7(x): inventory below x in (%) after 20 (a)
p(x) : inventory below x in (%) after 20 (a), based on second fits of a(t) and n(t)

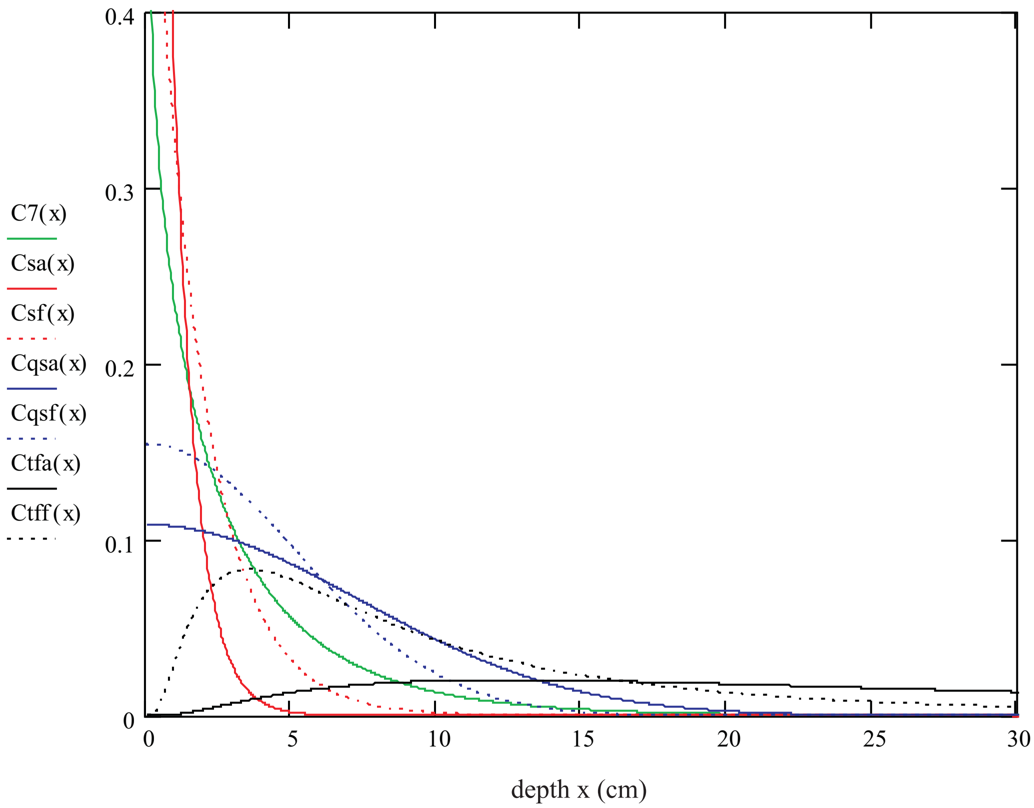

Fig. 6.6-12: Relative concentrations after 20 (a), resulting from different models (time series 3, Cs-134)

legend:

ordinate axis: relative concentration (cm^{-1})

C7(x) : relative concentration after 20 (a), based on 2-dimensional nest of intervals

Csa(x) : relative concentration after 20 (a), based on Eq. (2-2), a-profile

Csf(x) : relative concentration after 20 (a), based on Eq. (2-2), f-profile

Cqsa(x) : relative concentration after 20 (a), based on Eq. (2-3), a-profile

Cqsf(x) : relative concentration after 20 (a), based on Eq. (2-3), f-profile

Ctfa(x) : relative concentration after 20 (a), based on Eq. (2-4), a-profile

Ctff(x) : relative concentration after 20 (a), based on Eq. (2-4), f-profile

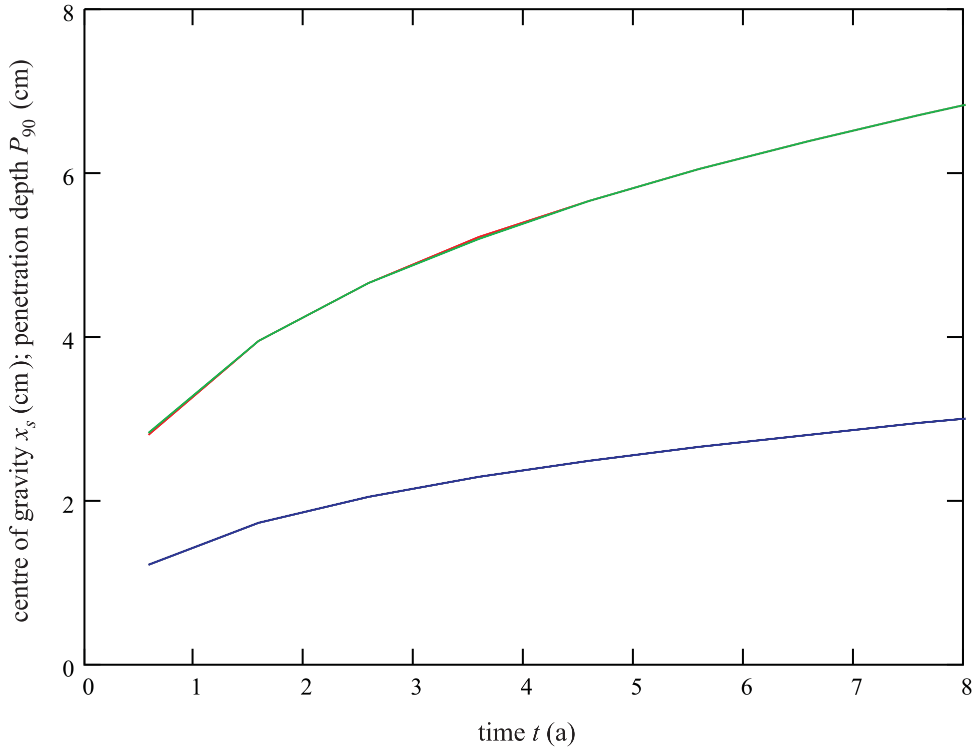

Fig. 6.6-13: Matching of the centres of gravity and of the penetration depths (time series 4, Ru-106)
legend:
black: x_s-fit
blue : matching of the x_s-fit, based on Eq. (2-24)
red : P_{90}-fit
green: matching of the P_{90}-fit; (a(t), n(t) from second fits)

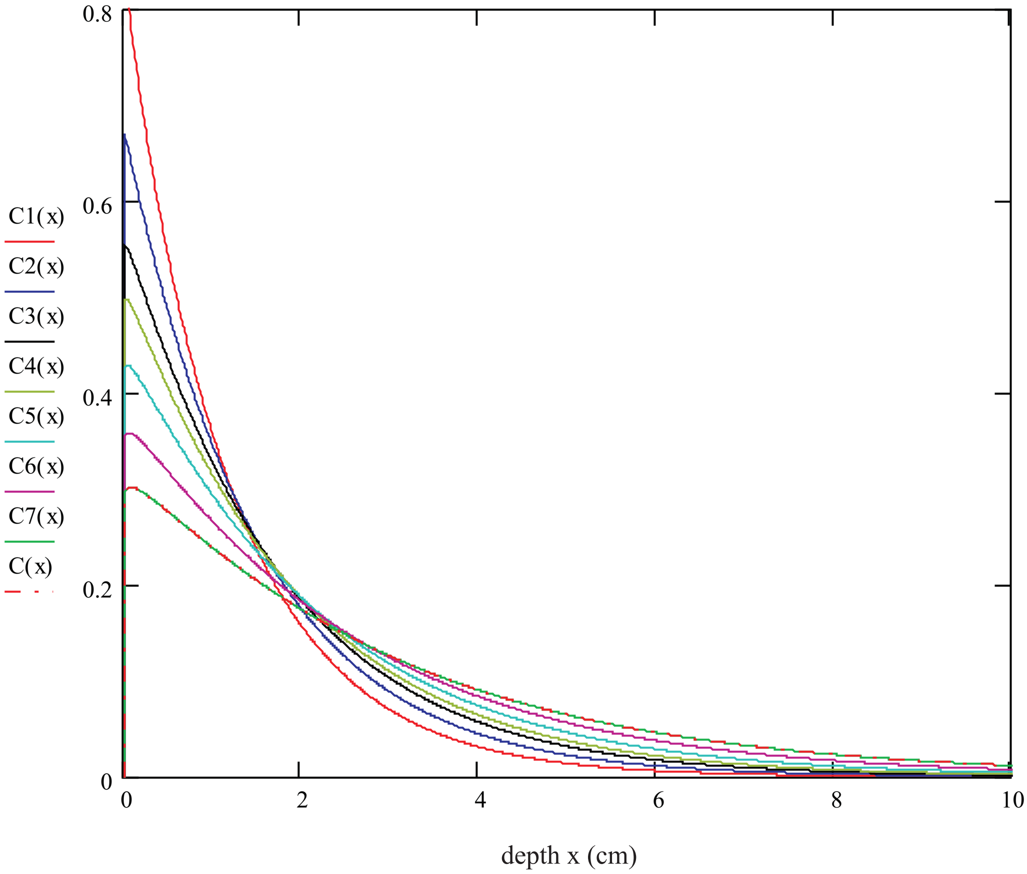

Fig. 6.6-14: Relative concentrations for different points of time (time series 4, Ru-106)
legend:
ordinate axis: relative concentration (cm^{-1})
C1(x): relative concentration after 0.583 (a)
C2(x): relative concentration after 1.0 (a)
C3(x): relative concentration after 1.583 (a)
C4(x): relative concentration after 2.083 (a)
C5(x): relative concentration after 3.083 (a)
C6(x): relative concentration after 5 (a)
C7(x): relative concentration after 8 (a)
} based on 2-dimensional nest of intervals
C(x) : relative concentration after 8 (a), based on second fits of a(t) and n(t)

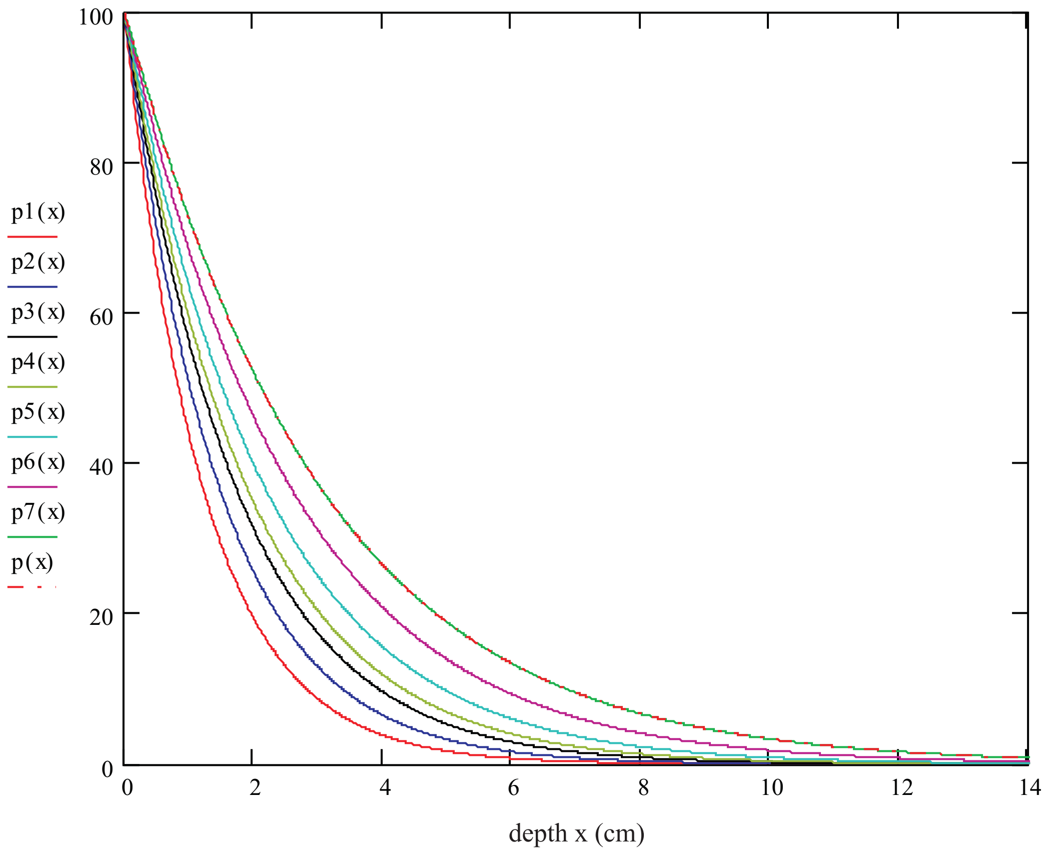

Fig. 6.6-15: Inventories below x in (%) for different points of time (time series 4, Ru-106)
legend:
ordinate axis: inventories below x (%)
p1(x): inventory below x in (%) after 0.583 (a)
p2(x): inventory below x in (%) after 1.0 (a)
p3(x): inventory below x in (%) after 1.583 (a)
p4(x): inventory below x in (%) after 2.083 (a) based on 2-dimensional nest of intervals
p5(x): inventory below x in (%) after 3.083 (a)
p6(x): inventory below x in (%) after 5 (a)
p7(x): inventory below x in (%) after 8 (a)
p(x) : inventory below x in (%) after 8 (a), based on second fits of a(t) and n(t)

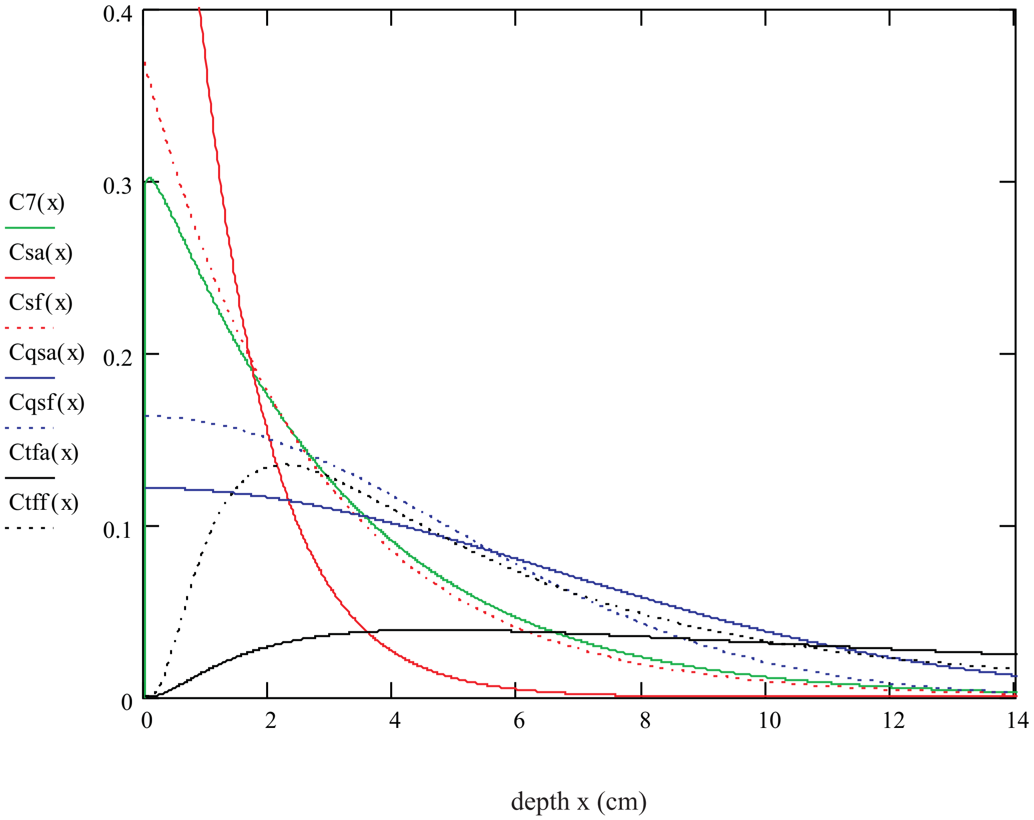

Fig. 6.6-16: Relative concentrations after 8 (a), resulting from different models (time series 4, Ru-106)

legend:

ordinate axis: relative concentration (cm^{-1})

C7(x) : relative concentration after 8 (a), based on 2-dimensional nest of intervals
Csa(x) : relative concentration after 8 (a), based on Eq. (2-2), a-profile
Csf(x) : relative concentration after 8 (a), based on Eq. (2-2), f-profile
Cqsa(x): relative concentration after 8 (a), based on Eq. (2-3), a-profile
Cqsf(x) : relative concentration after 8 (a), based on Eq. (2-3), f-profile
Ctfa(x) : relative concentration after 8 (a), based on Eq. (2-4), a-profile
Ctff(x) : relative concentration after 8 (a), based on Eq. (2-4), f-profile

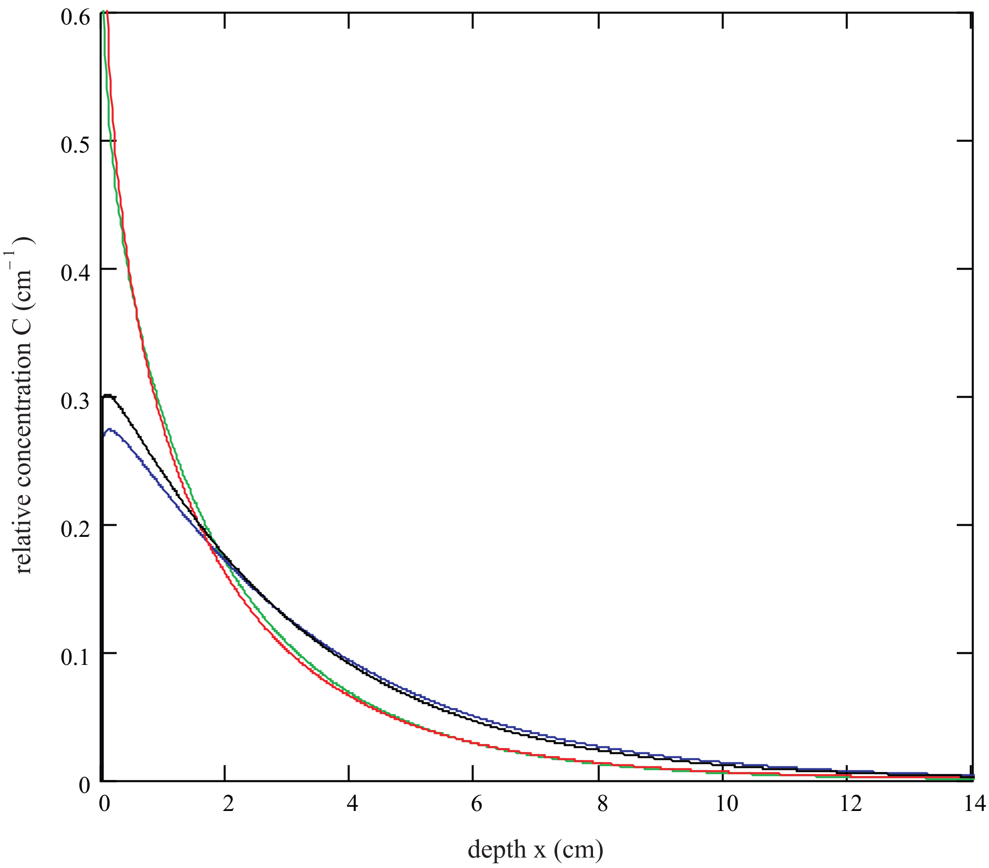

Fig. 6.6-17: Comparison of relative concentrations of Cs-134 and Ru-106, based on 2-dimensional nests of intervals, in different soils after 8 (a)

legend:

green: time series 1 (loamy sand, unused garden, Ivrea (Piemonte, Italy), Cs-134)
red : time series 3 (sandy loam, unused garden, Castagneto Po (Piemonte, Italy), Cs-134)
blue : time series 2 (loamy sand, unused garden, Ivrea (Piemonte, Italy), Ru-106)
black: time series 4 (sandy loam, unused garden, Castagneto Po (Piemonte, Italy), Ru-106)

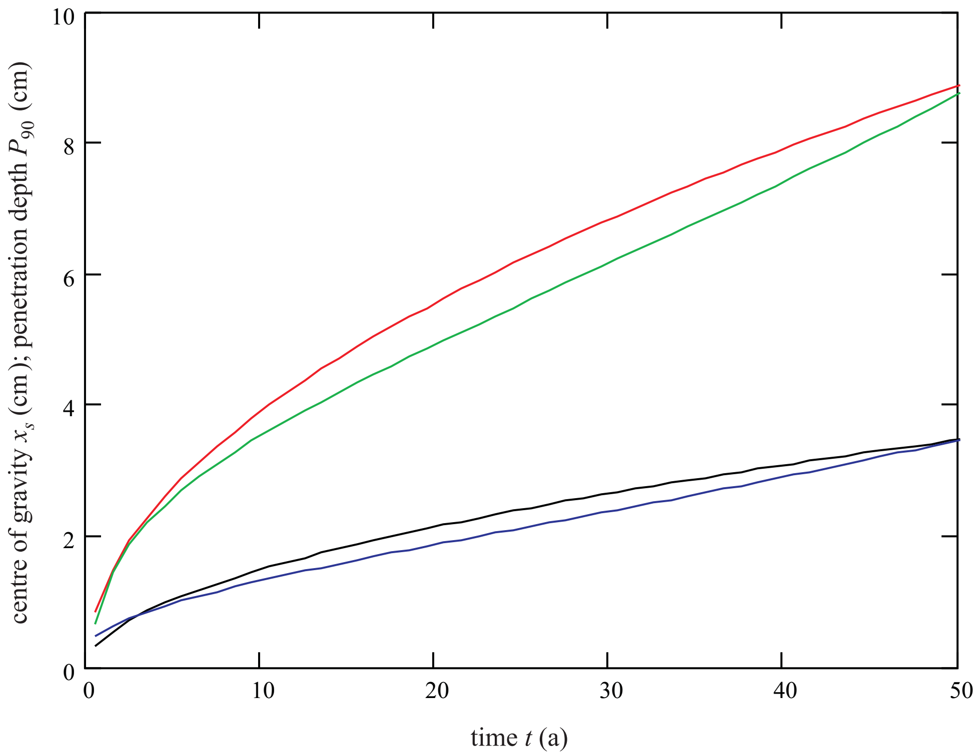

Fig. 6.7-1: Matching of the centres of gravity and of the penetration depths (time series 1, Cs-137)

legend:

black: x_s-fit

blue : matching of the x_s-fit, based on Eq. (2-24)

red : P_{90}-fit

green: matching of the P_{90}-fit; (a(t), n(t) from second fits)

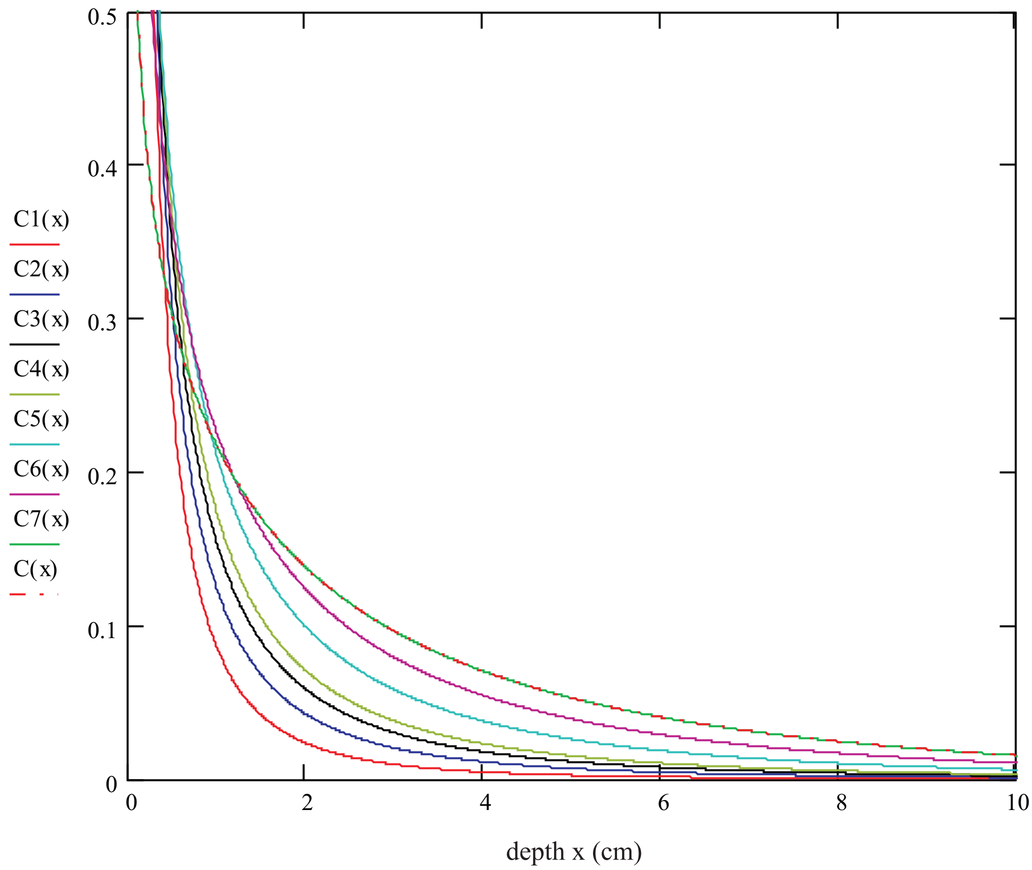

Fig. 6.7-2: Relative concentrations for different points of time (time series 1, Cs-137)
legend:
ordinate axis: relative concentration (cm^{-1})
C1(x): relative concentration after 0.500 (a)
C2(x): relative concentration after 1.750 (a)
C3(x): relative concentration after 3.833 (a)
C4(x): relative concentration after 6.083 (a)
C5(x): relative concentration after 15 (a)
C6(x): relative concentration after 30 (a)
C7(x): relative concentration after 50 (a)
based on 2-dimensional nest of intervals
C(x) : relative concentration after 50 (a), based on second fits of a(t) and n(t)

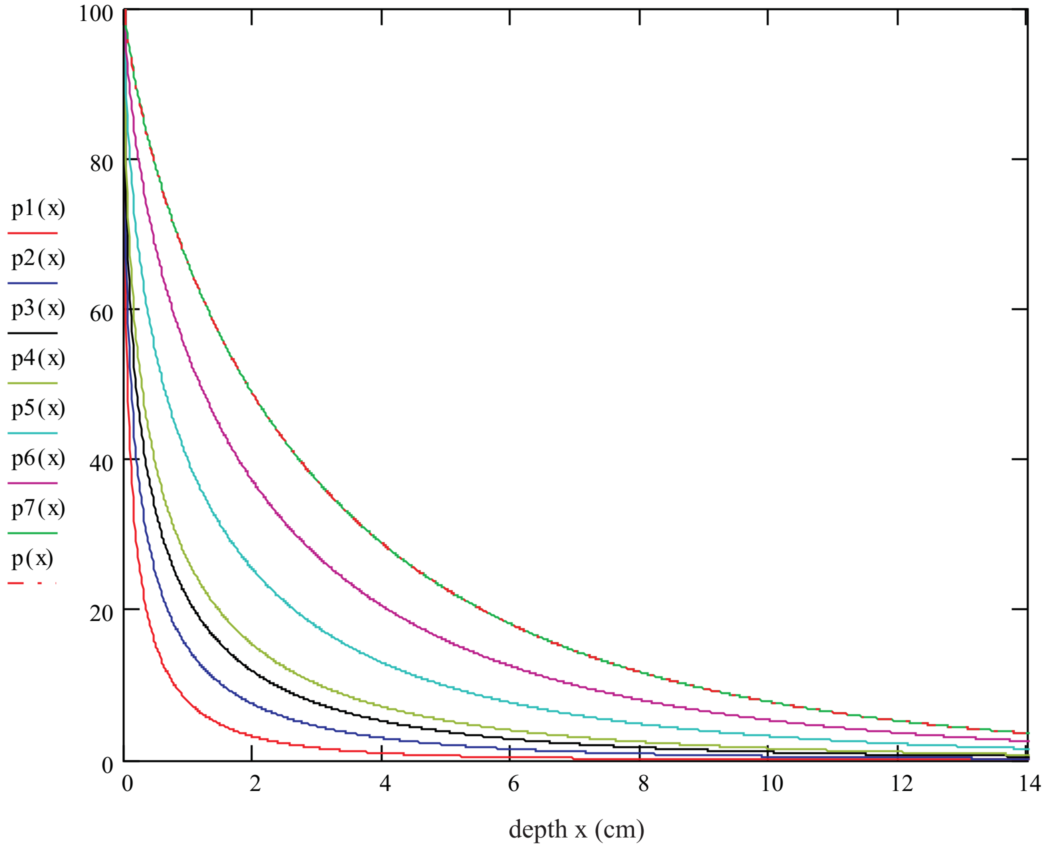

Fig. 6.7-3: Inventories below x in (%) for different points of time (time series 1, Cs-137)
legend:
ordinate axis: inventories below x (%)

p1(x): inventory below x in (%) after 0.500 (a) p2(x): inventory below x in (%) after 1.750 (a) p3(x): inventory below x in (%) after 3.833 (a) p4(x): inventory below x in (%) after 6.083 (a) p5(x): inventory below x in (%) after 15 (a) p6(x): inventory below x in (%) after 30 (a) p7(x): inventory below x in (%) after 50 (a)	} based on 2-dimensional nest of intervals

p(x) : inventory below x in (%) after 50 (a), based on second fits of a(t) and n(t)

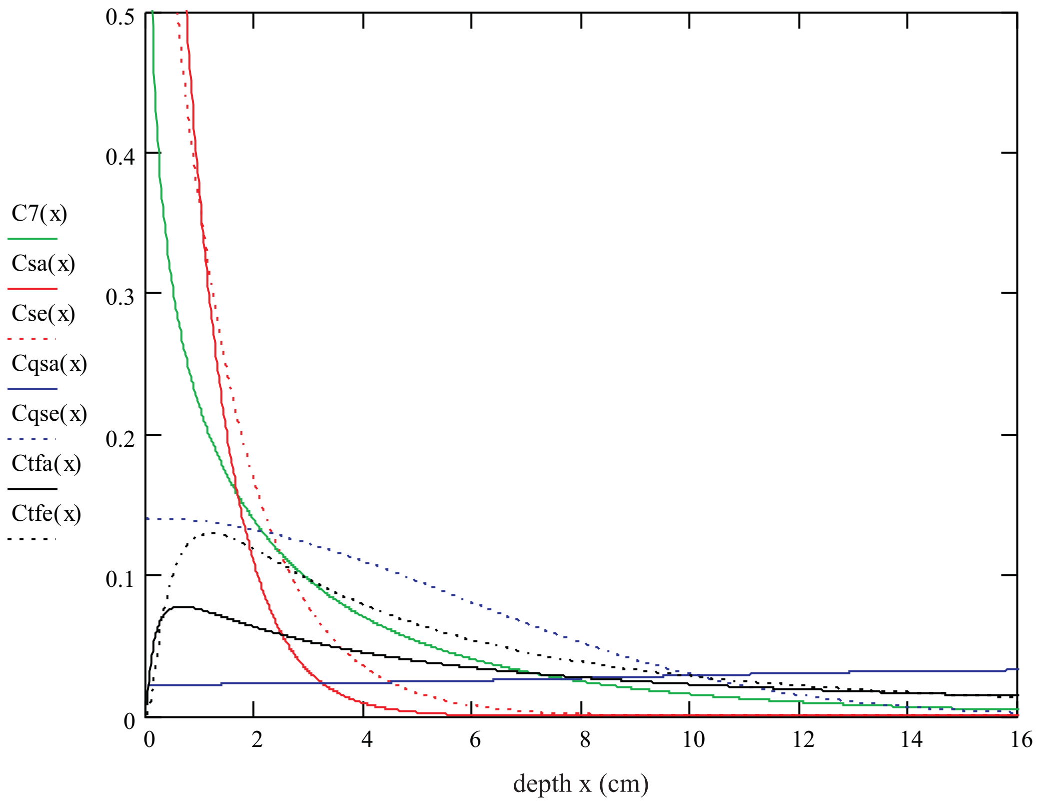

Fig. 6.7-4: Relative concentrations after 50 (a), resulting from different models (time series 1, Cs-137)

legend:

ordinate axis: relative concentration (cm^{-1})

C7(x) : relative concentration after 50 (a), based on 2-dimensional nest of intervals

Csa(x) : relative concentration after 50 (a), based on Eq. (2-2), a-profile

Cse(x) : relative concentration after 50 (a), based on Eq. (2-2), e-profile

Cqsa(x): relative concentration after 50 (a), based on Eq. (2-3), a-profile

Cqse(x): relative concentration after 50 (a), based on Eq. (2-3), e-profile

Ctfa(x) : relative concentration after 50 (a), based on Eq. (2-4), a-profile

Ctfe(x) : relative concentration after 50 (a), based on Eq. (2-4), e-profile

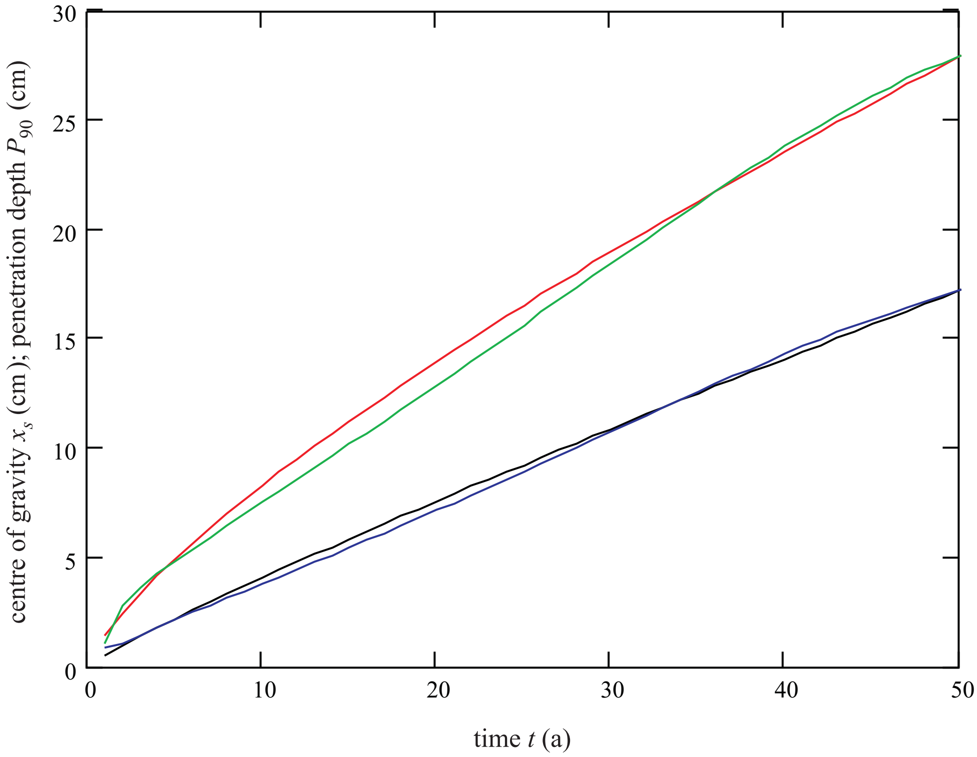

Fig. 6.7-5: Matching of the centres of gravity and of the penetration depths (time series 2, Cs-137)

legend:

black: x_s-fit

blue : matching of the x_s-fit, based on Eq. (2-24)

red : P_{90}-fit

green: matching of the P_{90}-fit; (a(t), n(t) from second fits)

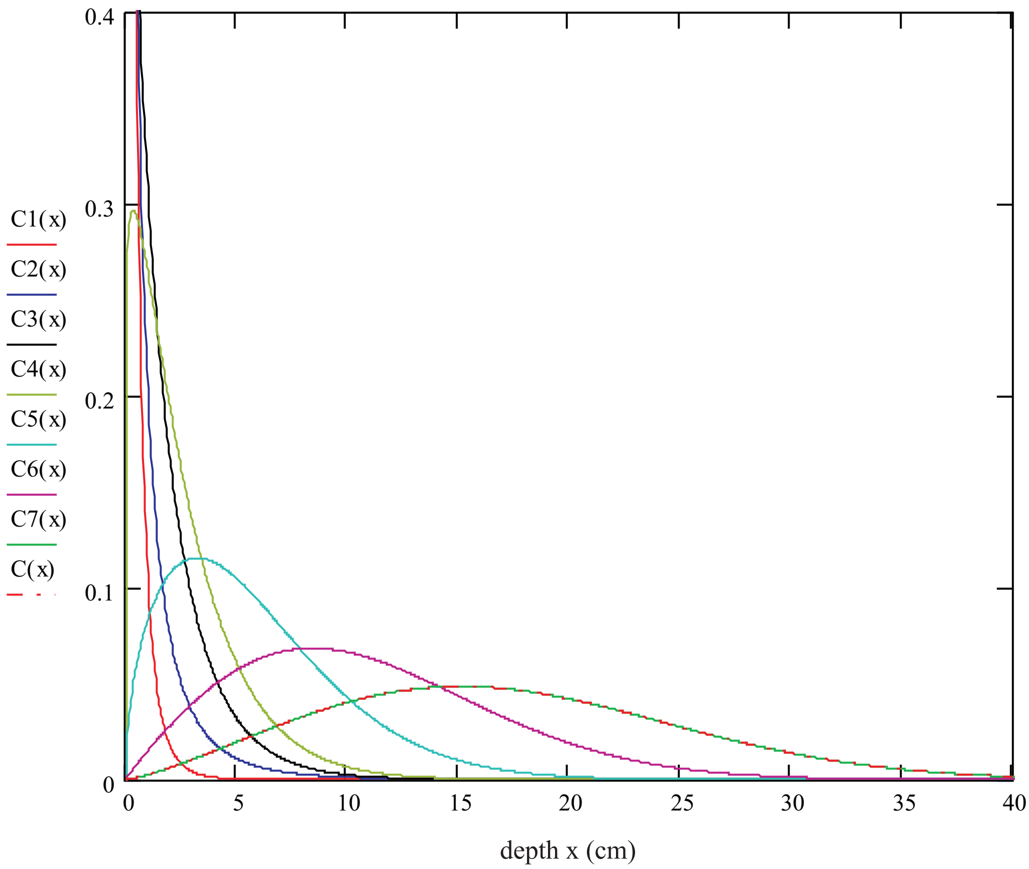

Fig. 6.7-6: Relative concentrations for different points of time (time series 2, Cs-137)
legend:
ordinate axis: relative concentration (cm^{-1})
C1(x): relative concentration after 0.500 (a)
C2(x): relative concentration after 1.750 (a)
C3(x): relative concentration after 3.833 (a)
C4(x): relative concentration after 6.083 (a)
C5(x): relative concentration after 15 (a)
C6(x): relative concentration after 30 (a)
C7(x): relative concentration after 50 (a)
based on 2-dimensional nest of intervals
C(x) : relative concentration after 50 (a), based on second fits of a(t) and n(t)

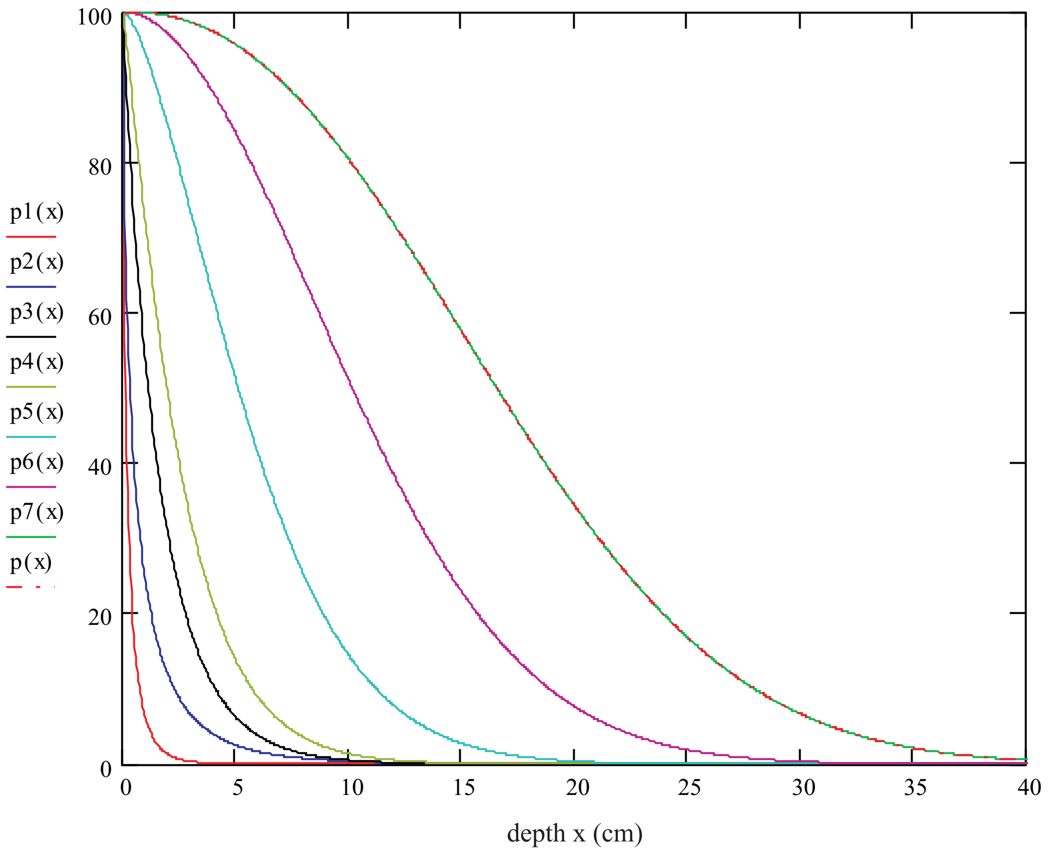

Fig. 6.7-7: Inventories below x in (%) for different points of time (time series 2, Cs-137)
legend:
ordinate axis: inventories below x (%)
p1(x): inventory below x in (%) after 0.500 (a)
p2(x): inventory below x in (%) after 1.750 (a)
p3(x): inventory below x in (%) after 3.833 (a)
p4(x): inventory below x in (%) after 6.083 (a)
p5(x): inventory below x in (%) after 15 (a)
p6(x): inventory below x in (%) after 30 (a)
p7(x): inventory below x in (%) after 50 (a)

based on 2-dimensional nest of intervals (p1(x) to p7(x))

p(x) : inventory below x in (%) after 50 (a), based on second fits of a(t) and n(t)

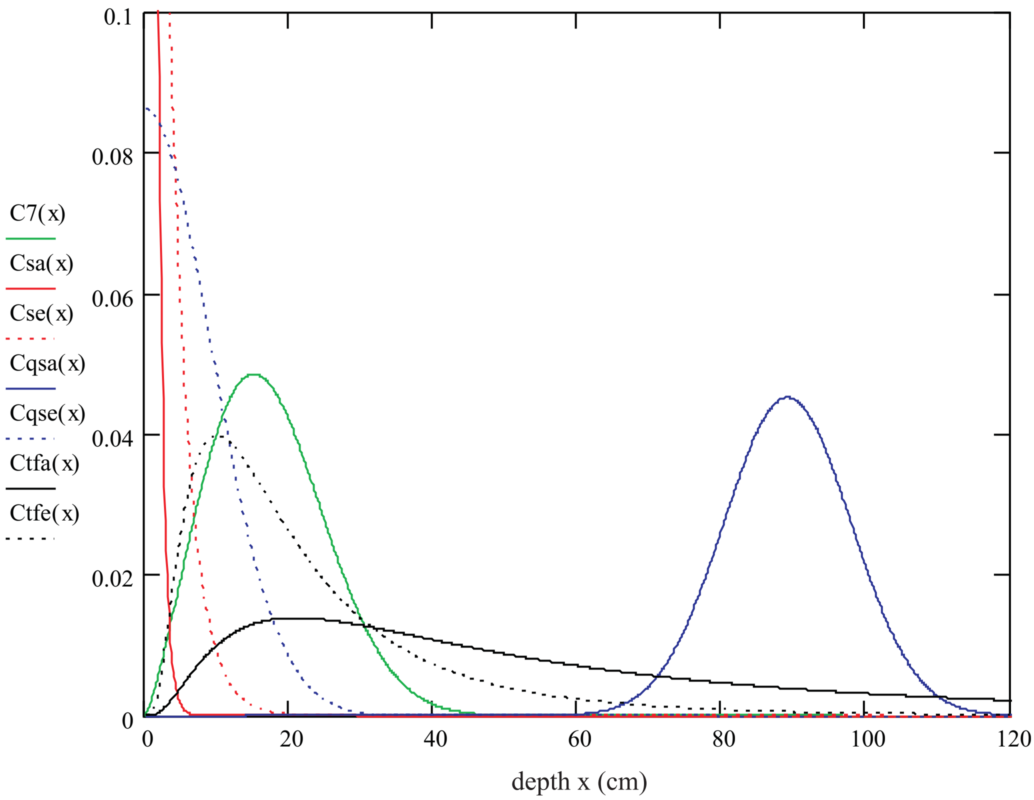

Fig. 6.7-8: Relative concentrations after 50 (a), resulting from different models (time series 2, Cs-137)

legend:

ordinate axis: relative concentration (cm^{-1})

C7(x) : relative concentration after 50 (a), based on 2-dimensional nest of intervals

Csa(x) : relative concentration after 50 (a), based on Eq. (2-2), a-profile

Cse(x) : relative concentration after 50 (a), based on Eq. (2-2), e-profile

Cqsa(x): relative concentration after 50 (a), based on Eq. (2-3), a-profile

Cqse(x): relative concentration after 50 (a), based on Eq. (2-3), e-profile

Ctfa(x) : relative concentration after 50 (a), based on Eq. (2-4), a-profile

Ctfe(x) : relative concentration after 50 (a), based on Eq. (2-4), e-profile

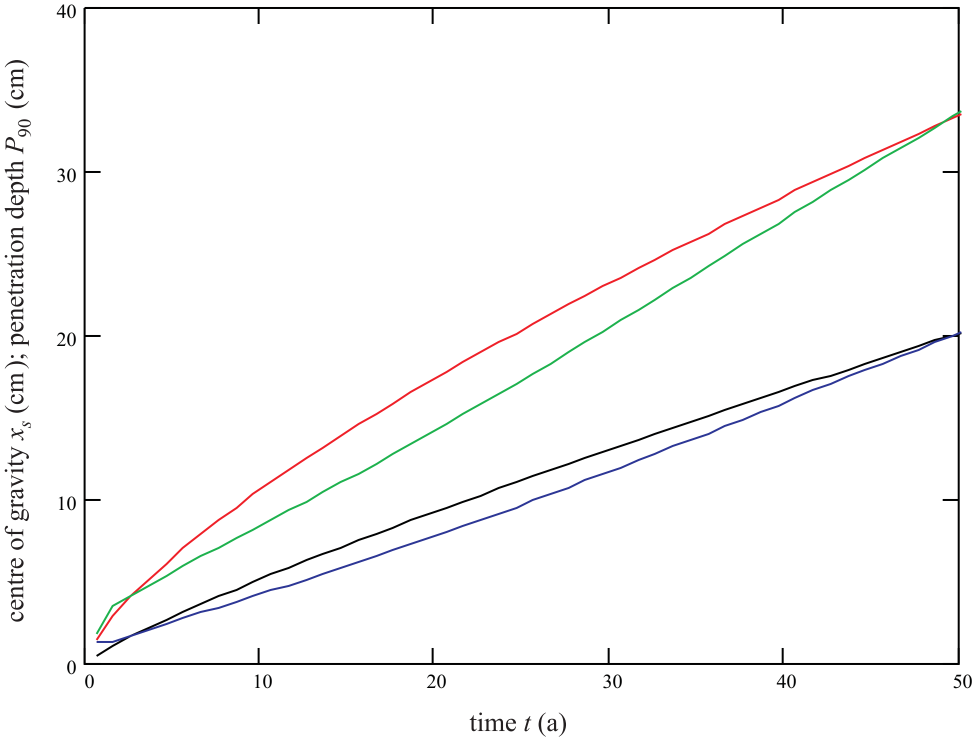

Fig. 6.7-9: Matching of the centres of gravity and of the penetration depths (time series 3, Cs-137)
legend:
black: x_s-fit
blue : matching of the x_s-fit, based on Eq. (2-24)
red : P_{90}-fit
green: matching of the P_{90}-fit; (a(t), n(t) from second fits)

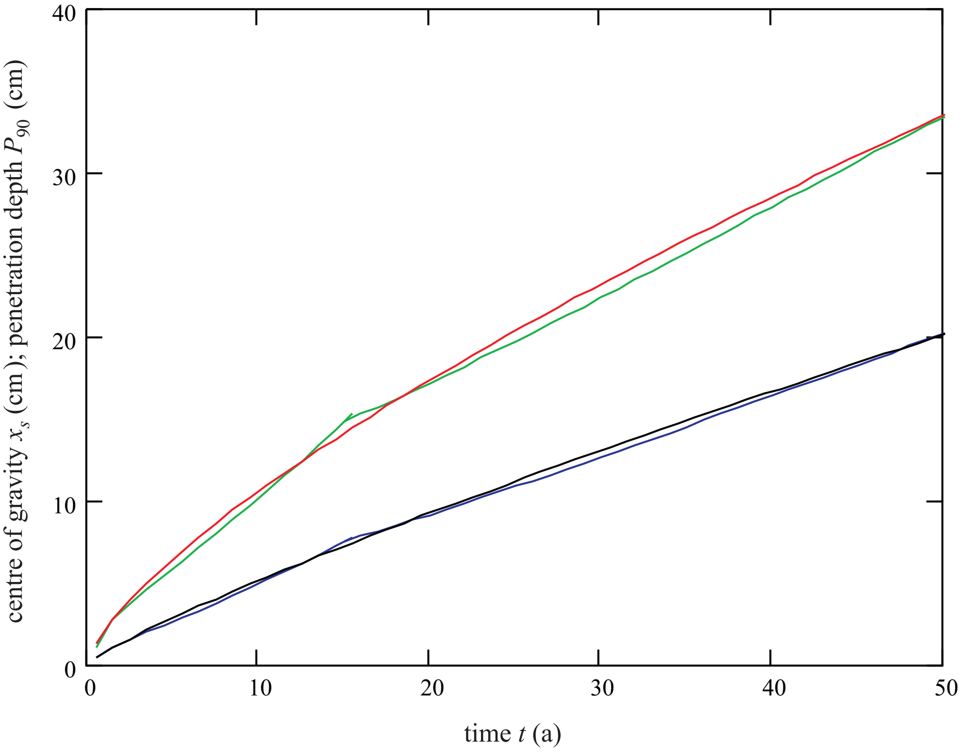

Fig. 6.7-9a: Improved matching of the centres of gravity and of the penetration depths, achieved by fitting of n(t) in 2 pieces (time series 3, Cs-137)
legend:
black: x_s-fit
blue : matching of the x_s-fit, based on Eq. (2-24)
red : P_{90}-fit
green: matching of the P_{90}-fit; (a(t), n(t) from second fits)

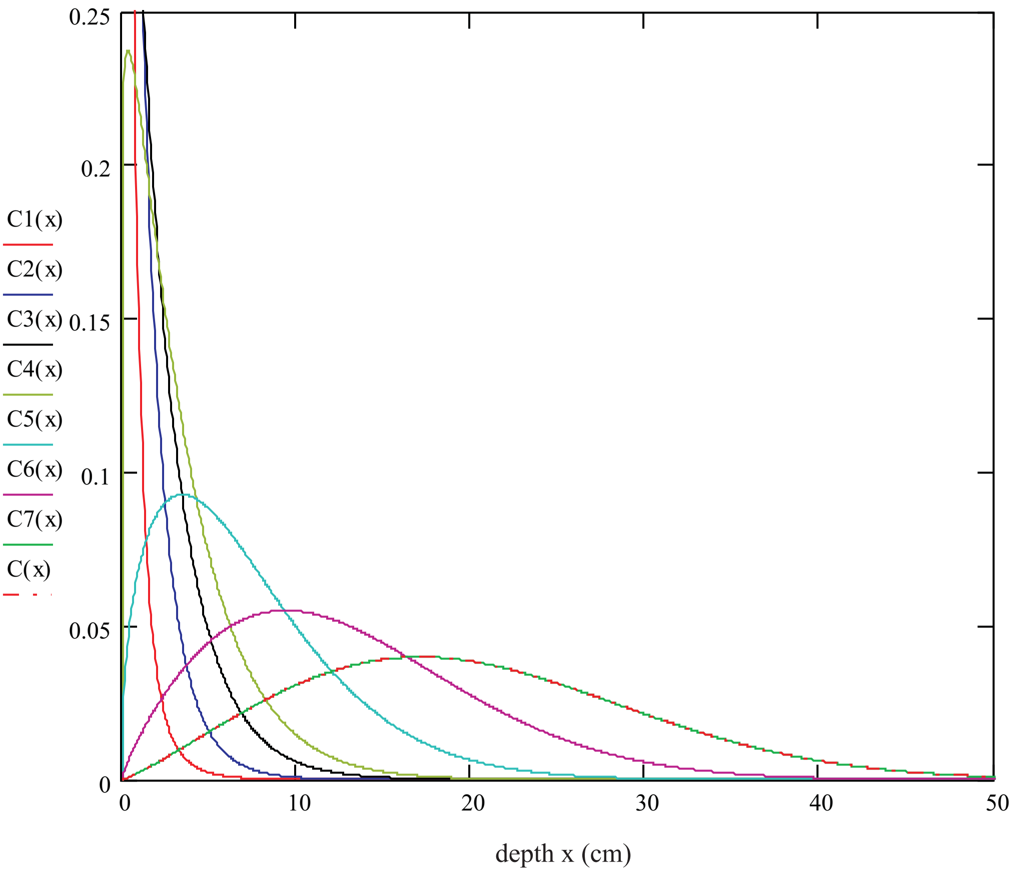

Fig. 6.7-10: Relative concentrations for different points of time (time series 3, Cs-137)
legend:
ordinate axis: relative concentration (cm^{-1})
C1(x): relative concentration after 0.500 (a)
C2(x): relative concentration after 1.750 (a)
C3(x): relative concentration after 3.833 (a)
C4(x): relative concentration after 6.083 (a) based on 2-dimensional nest of intervals
C5(x): relative concentration after 15 (a)
C6(x): relative concentration after 30 (a)
C7(x): relative concentration after 50 (a)
C(x) : relative concentration after 50 (a), based on second fits of a(t) and n(t)

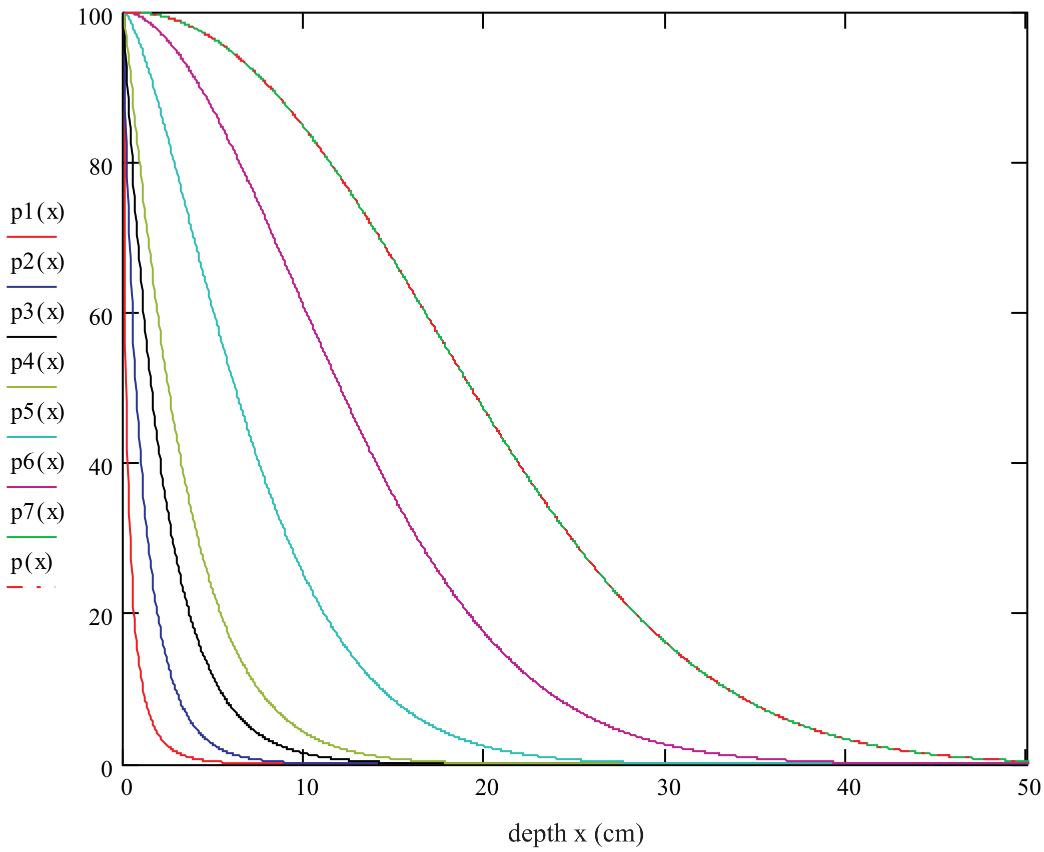

Fig. 6.7-11: Inventories below x in (%) for different points of time (time series 3, Cs-137)
legend:
ordinate axis: inventories below x (%)
p1(x): inventory below x in (%) after 0.500 (a)
p2(x): inventory below x in (%) after 1.750 (a)
p3(x): inventory below x in (%) after 3.833 (a)
p4(x): inventory below x in (%) after 6.083 (a)
p5(x): inventory below x in (%) after 15 (a)
p6(x): inventory below x in (%) after 30 (a)
p7(x): inventory below x in (%) after 50 (a)
based on 2-dimensional nest of intervals
p(x) : inventory below x in (%) after 50 (a), based on second fits of a(t) and n(t)

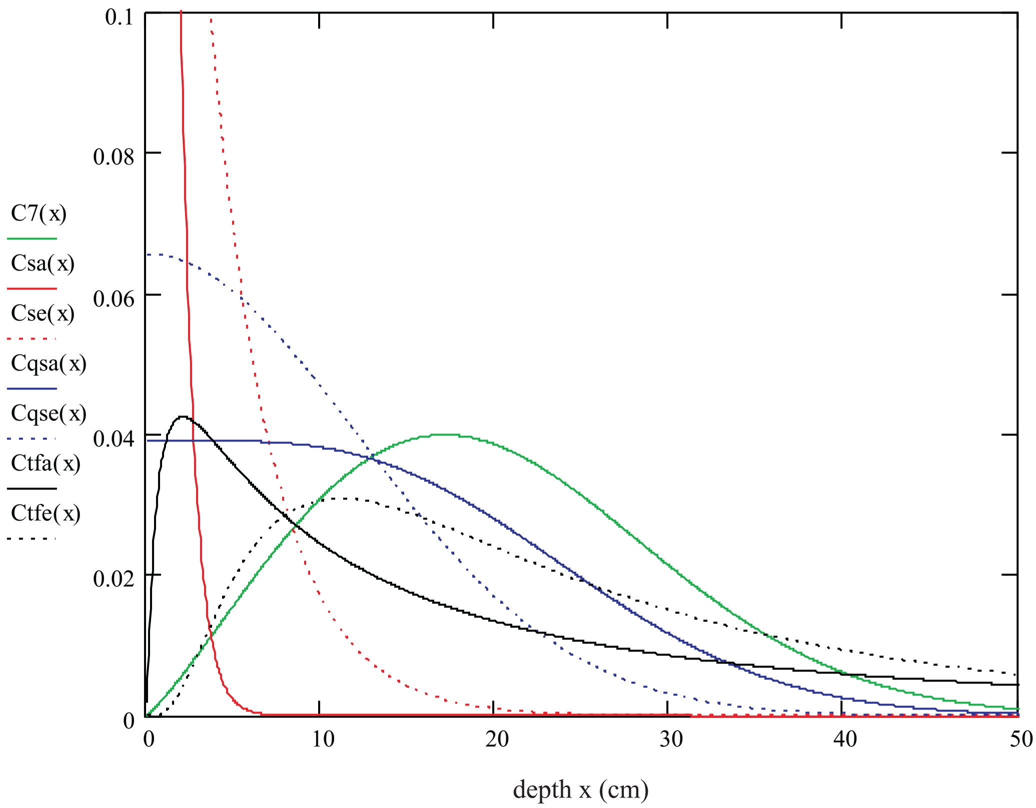

Fig. 6.7-12: Relative concentrations after 50 (a), resulting from different models (time series 3, Cs-137)

legend:

ordinate axis: relative concentration (cm^{-1})

C7(x) : relative concentration after 50 (a), based on 2-dimensional nest of intervals

Csa(x) : relative concentration after 50 (a), based on Eq. (2-2), a-profile

Cse(x) : relative concentration after 50 (a), based on Eq. (2-2), e-profile

Cqsa(x): relative concentration after 50 (a), based on Eq. (2-3), a-profile

Cqse(x): relative concentration after 50 (a), based on Eq. (2-3), e-profile

Ctfa(x) : relative concentration after 50 (a), based on Eq. (2-4), a-profile

Ctfe(x) : relative concentration after 50 (a), based on Eq. (2-4), e-profile

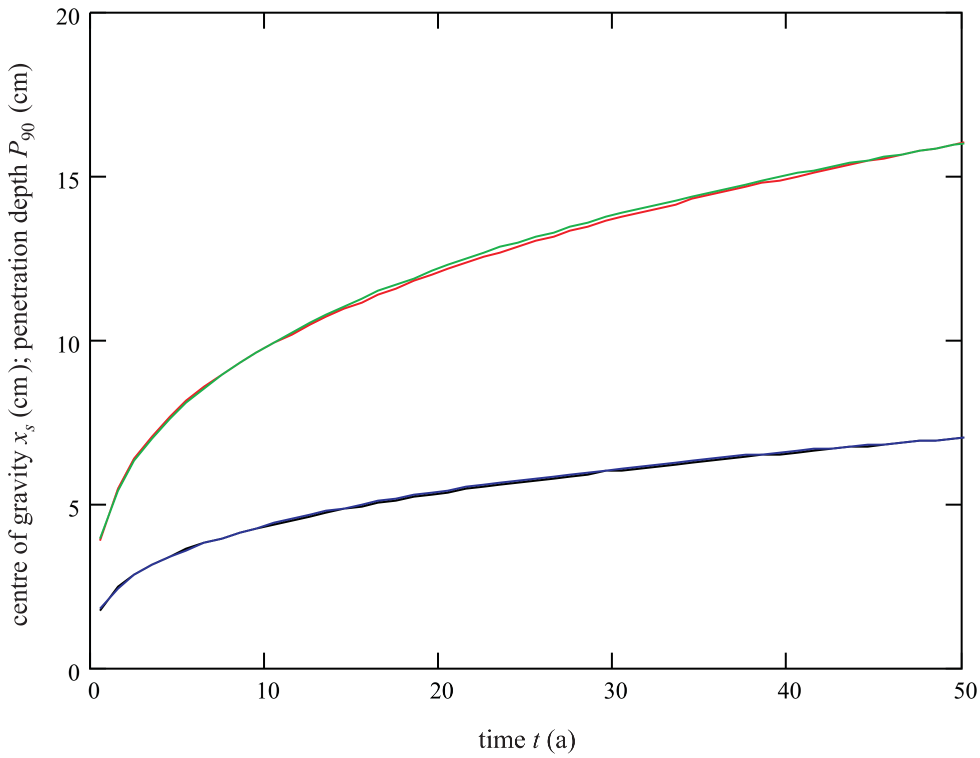

Fig. 6.7-13: Matching of the centres of gravity and of the penetration depths (time series 4, Cs-137)

legend:

black: x_s-fit

blue : matching of the x_s-fit, based on Eq. (2-24)

red : P_{90}-fit

green: matching of the P_{90}-fit; (a(t), n(t) from second fits)

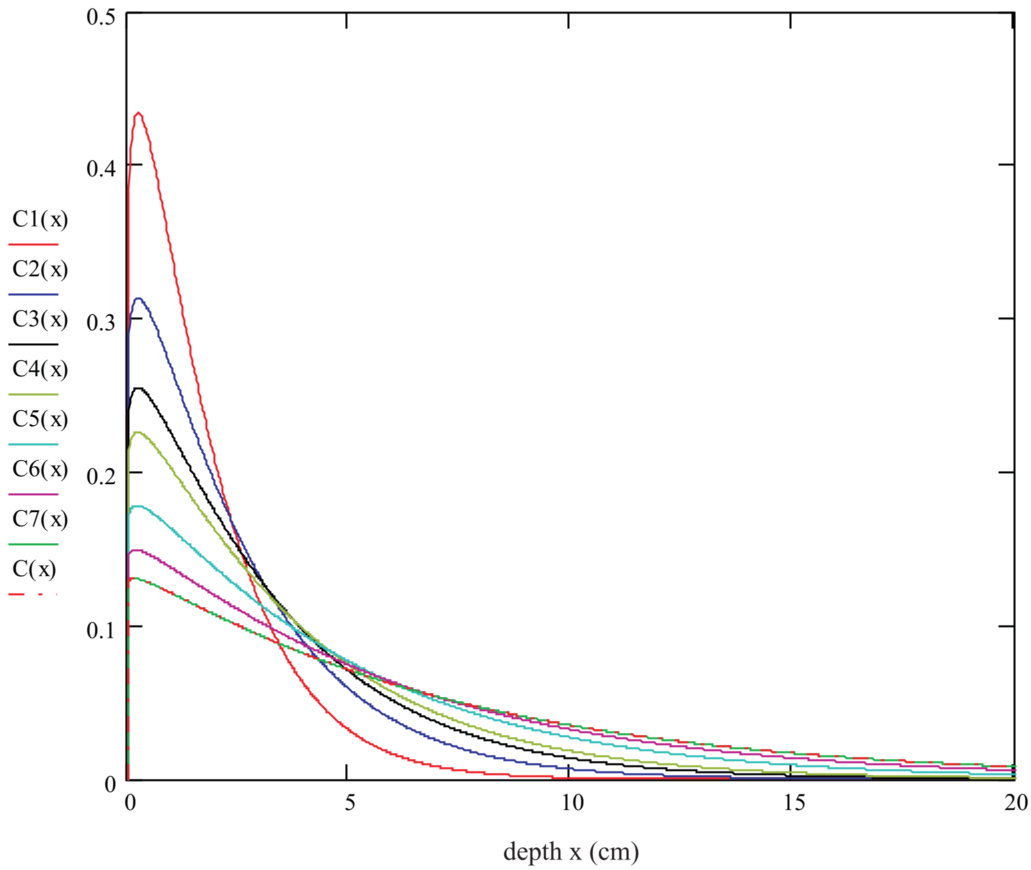

Fig. 6.7-14: Relative concentrations for different points of time (time series 4, Cs-137)
legend:
ordinate axis: relative concentration (cm^{-1})

C1(x): relative concentration after 0.500 (a)	based on 2-dimensional nest of intervals
C2(x): relative concentration after 1.750 (a)	
C3(x): relative concentration after 3.833 (a)	
C4(x): relative concentration after 6.083 (a)	
C5(x): relative concentration after 15 (a)	
C6(x): relative concentration after 30 (a)	
C7(x): relative concentration after 50 (a)	

C(x) : relative concentration after 50 (a), based on second fits of a(t) and n(t)

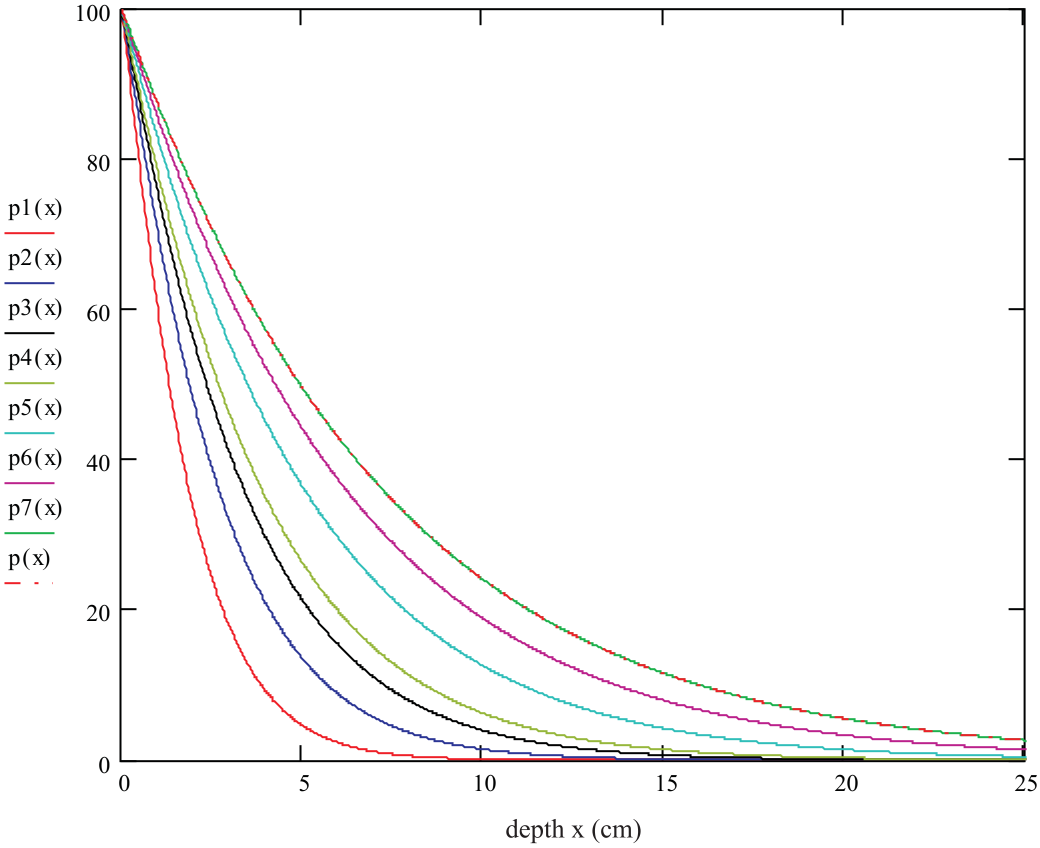

Fig. 6.7-15: Inventories below x in (%) for different points of time (time series 4, Cs-137)
legend:
ordinate axis: inventories below x (%)

p1(x): inventory below x in (%) after 0.500 (a)
p2(x): inventory below x in (%) after 1.750 (a)
p3(x): inventory below x in (%) after 3.833 (a)
p4(x): inventory below x in (%) after 6.083 (a)
p5(x): inventory below x in (%) after 15 (a)
p6(x): inventory below x in (%) after 30 (a)
p7(x): inventory below x in (%) after 50 (a)

based on 2-dimensional nest of intervals

p(x) : inventory below x in (%) after 50 (a), based on second fits of a(t) and n(t)

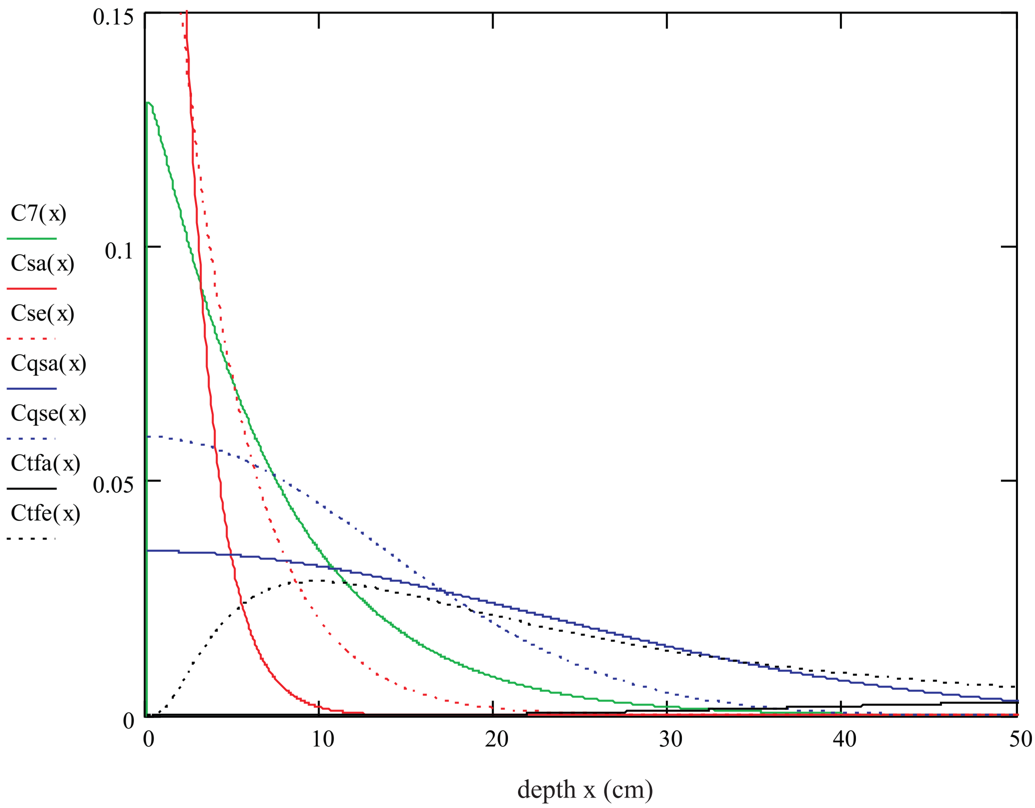

Fig. 6.7-16: Relative concentrations after 50 (a), resulting from different models (time series 4, Cs-137)

legend:

ordinate axis: relative concentration (cm^{-1})

C7(x)   : relative concentration after 50 (a), based on 2-dimensional nest of intervals
Csa(x) : relative concentration after 50 (a), based on Eq. (2-2), a-profile
Cse(x) : relative concentration after 50 (a), based on Eq. (2-2), e-profile
Cqsa(x): relative concentration after 50 (a), based on Eq. (2-3), a-profile
Cqse(x : relative concentration after 50 (a), based on Eq. (2-3), e-profile
Ctfa(x) : relative concentration after 50 (a), based on Eq. (2-4), a-profile
Ctfe(x) : relative concentration after 50 (a), based on Eq. (2-4), e-profile

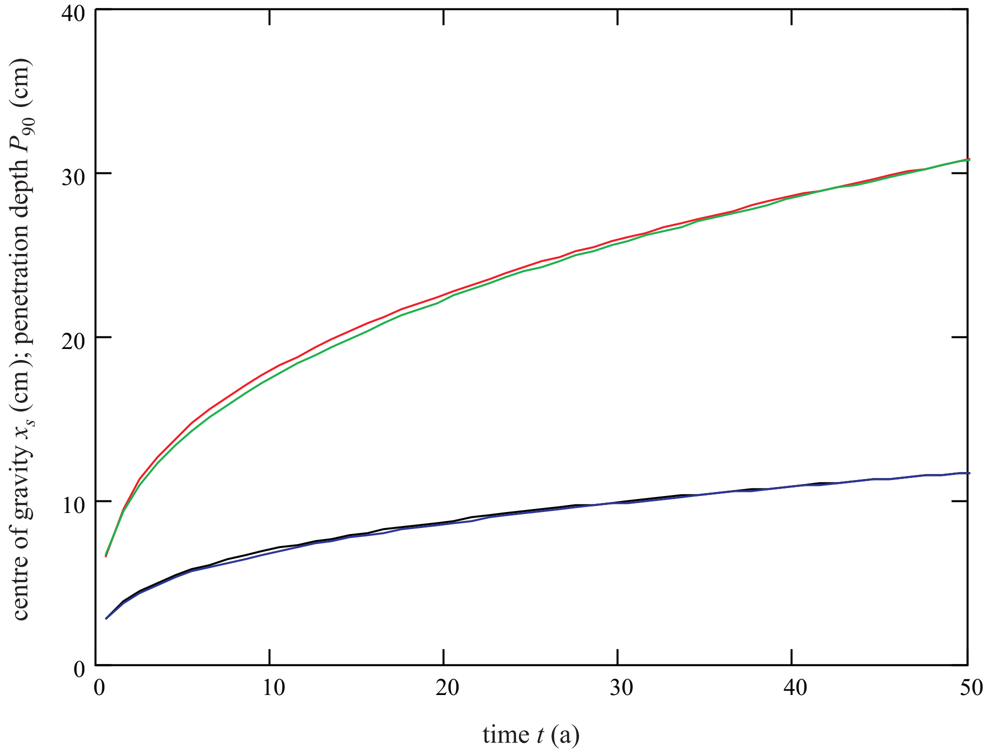

Fig. 6.8-1: Matching of the centres of gravity and of the penetration depths (time series 1, Sr-90)

legend:

black: x_s-fit

blue : matching of the x_s-fit, based on Eq. (2-24)

red : P_{90}-fit

green: matching of the P_{90}-fit; (a(t), n(t) from second fits)

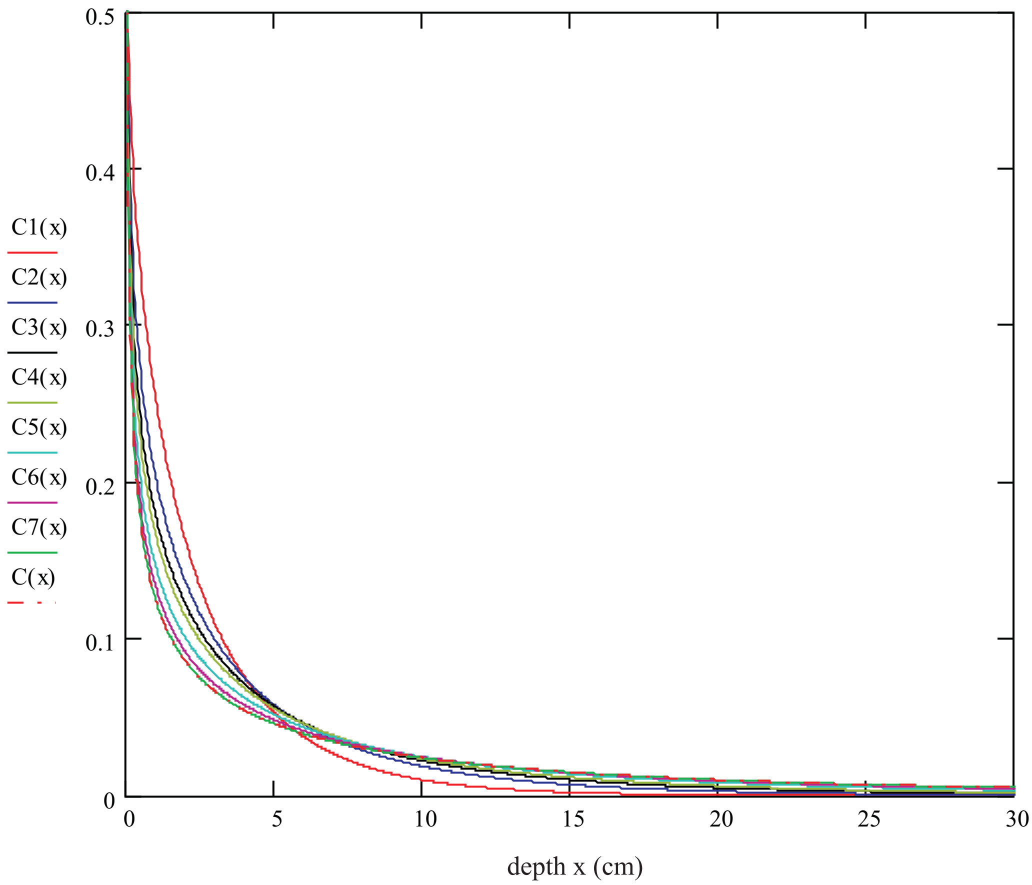

Fig. 6.8-2: Relative concentrations for different points of time (time series 1, Sr-90)
legend:
ordinate axis: relative concentration (cm^{-1})
C1(x): relative concentration after 0.500 (a)
C2(x): relative concentration after 1.750 (a)
C3(x): relative concentration after 3.833 (a)
C4(x): relative concentration after 6.083 (a)
C5(x): relative concentration after 15 (a)
C6(x): relative concentration after 30 (a)
C7(x): relative concentration after 50 (a)
} based on 2-dimensional nest of intervals
C(x) : relative concentration after 50 (a), based on second fits of a(t) and n(t)

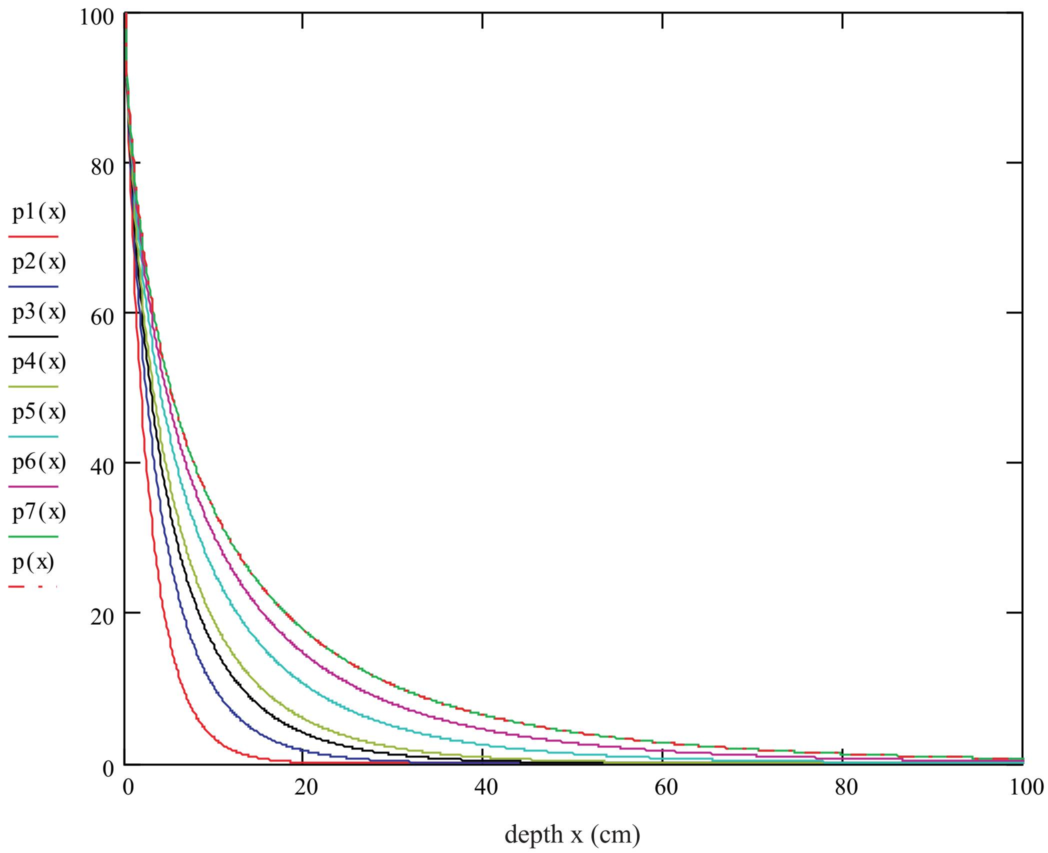

Fig. 6.8-3: Inventories below x in (%) for different points of time (time series 1, Sr-90)
legend:
ordinate axis: inventories below x (%)

p1(x): inventory below x in (%) after 0.500 (a)	based on 2-dimensional nest of intervals
p2(x): inventory below x in (%) after 1.750 (a)	
p3(x): inventory below x in (%) after 3.833 (a)	
p4(x): inventory below x in (%) after 6.083 (a)	
p5(x): inventory below x in (%) after 15 (a)	
p6(x): inventory below x in (%) after 30 (a)	
p7(x): inventory below x in (%) after 50 (a)	

p(x) : inventory below x in (%) after 50 (a), based on second fits of a(t) and n(t)

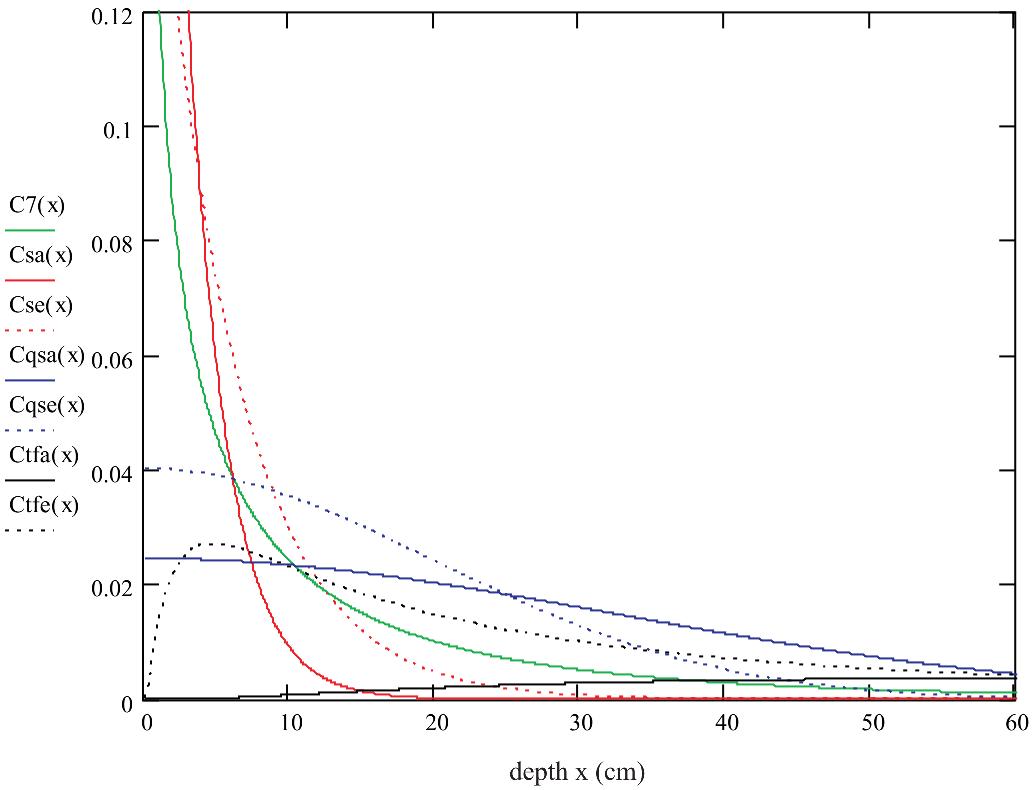

Fig. 6.8-4: Relative concentrations after 50 (a), resulting from different models (time series 1, Sr-90)

legend:

ordinate axis: relative concentration (cm^{-1})

C7(x) : relative concentration after 50 (a), based on 2-dimensional nest of intervals
Csa(x) : relative concentration after 50 (a), based on Eq. (2-2), a-profile
Cse(x) : relative concentration after 50 (a), based on Eq. (2-2), e-profile
Cqsa(x): relative concentration after 50 (a), based on Eq. (2-3), a-profile
Cqse(x): relative concentration after 50 (a), based on Eq. (2-3), e-profile
Ctfa(x) : relative concentration after 50 (a), based on Eq. (2-4), a-profile
Ctfe(x) : relative concentration after 50 (a), based on Eq. (2-4), e-profile

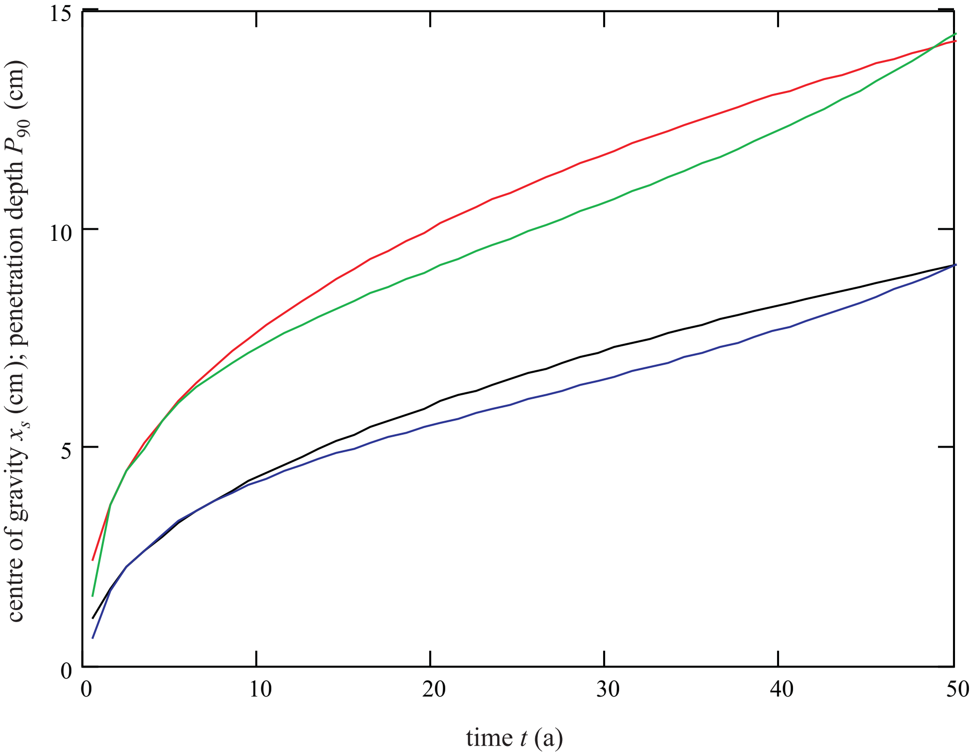

Fig. 6.8-5: Matching of the centres of gravity and of the penetration depths (time series 2, Sr-90)

legend:

black: x_s-fit

blue : matching of the x_s-fit, based on Eq. (2-24)

red : P_{90}-fit

green: matching of the P_{90}-fit; (a(t), n(t) from second fits)

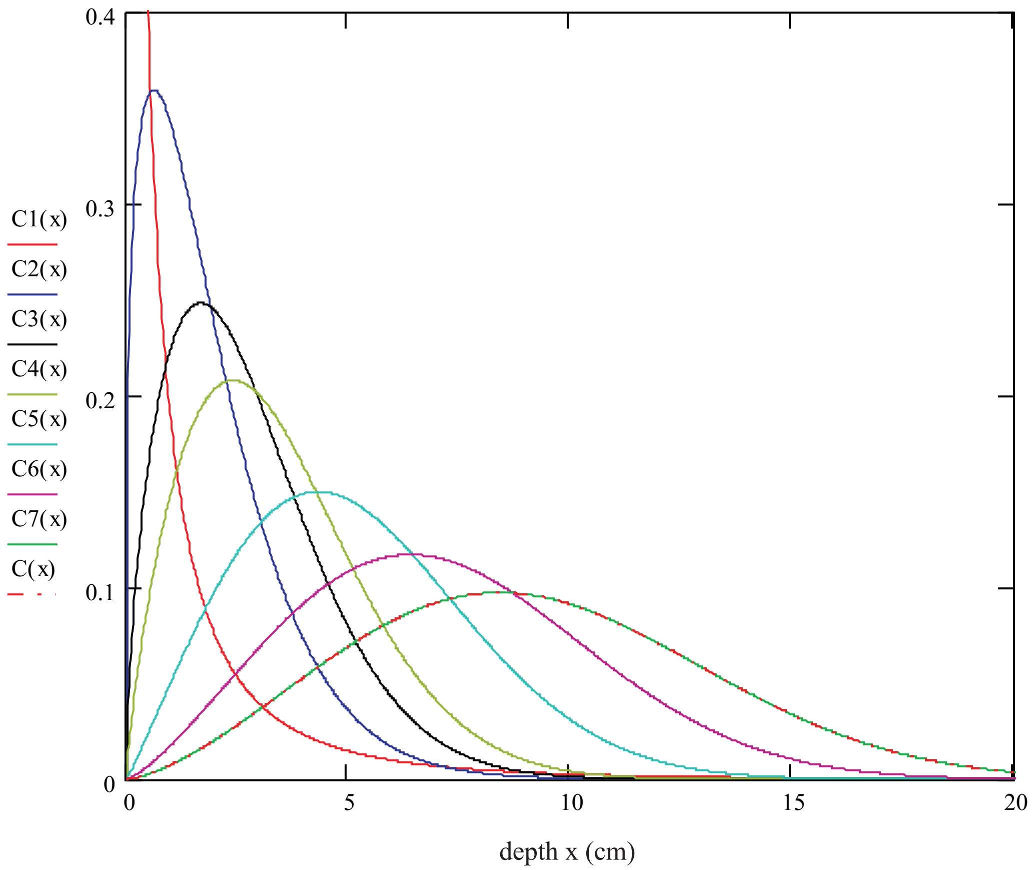

Fig. 6.8-6: Relative concentrations for different points of time (time series 2, Sr-90)
legend:
ordinate axis: relative concentration (cm^{-1})

C1(x): relative concentration after 0.500 (a)
C2(x): relative concentration after 1.750 (a)
C3(x): relative concentration after 3.833 (a)
C4(x): relative concentration after 6.083 (a)
C5(x): relative concentration after 15 (a)
C6(x): relative concentration after 30 (a)
C7(x): relative concentration after 50 (a)
} based on 2-dimensional nest of intervals

C(x) : relative concentration after 50 (a), based on second fits of a(t) and n(t)

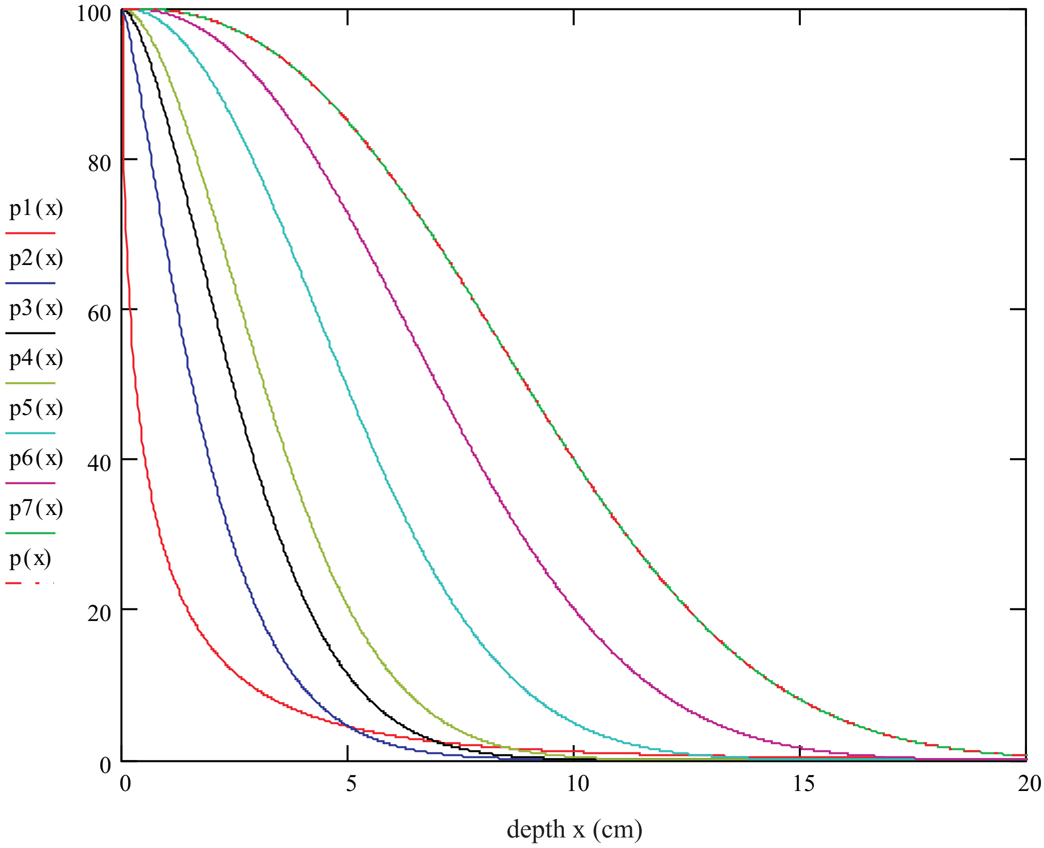

Fig. 6.8-7: Inventories below x in (%) for different points of time (time series 2, Sr-90)
legend:
ordinate axis: inventories below x (%)

$\left.\begin{array}{l}\text{p1(x): inventory below x in (\%) after 0.500 (a)}\\ \text{p2(x): inventory below x in (\%) after 1.750 (a)}\\ \text{p3(x): inventory below x in (\%) after 3.833 (a)}\\ \text{p4(x): inventory below x in (\%) after 6.083 (a)}\\ \text{p5(x): inventory below x in (\%) after 15 (a)}\\ \text{p6(x): inventory below x in (\%) after 30 (a)}\\ \text{p7(x): inventory below x in (\%) after 50 (a)}\end{array}\right\}$ based on 2-dimensional nest of intervals

p(x) : inventory below x in (%) after 50 (a), based on second fits of a(t) and n(t)

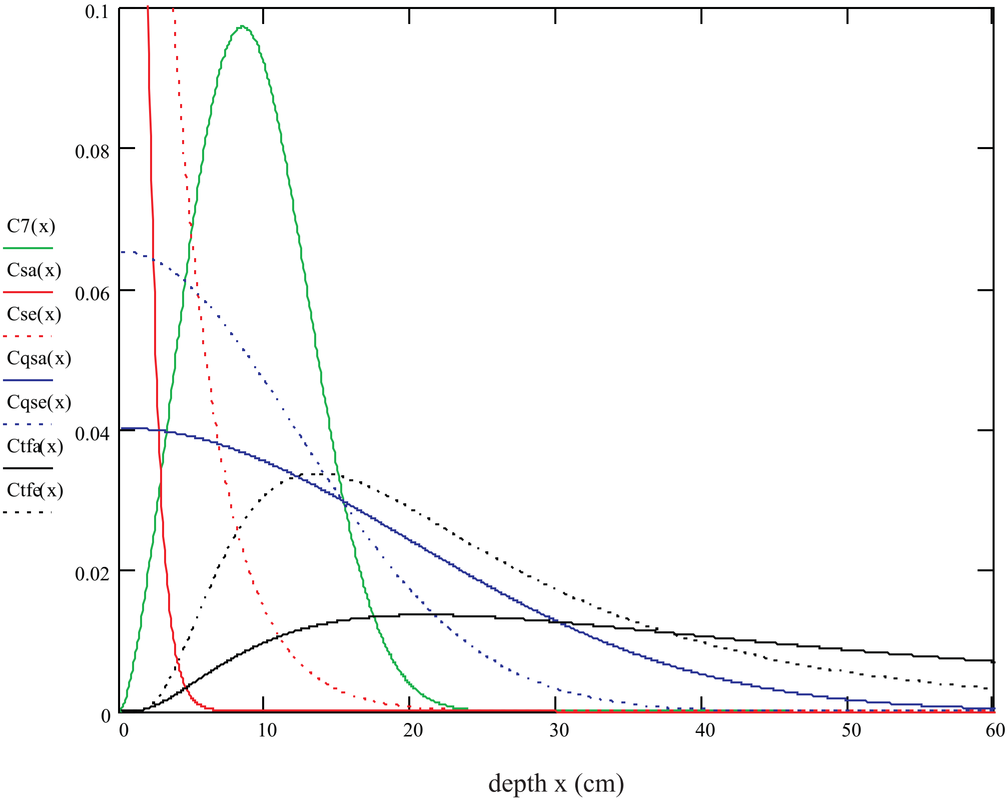

Fig. 6.8-8: Relative concentrations after 50 (a), resulting from different models (time series 2, Sr-90)

legend:

ordinate axis: relative concentration (cm^{-1})

C7(x) : relative concentration after 50 (a), based on 2-dimensional nest of intervals

Csa(x) : relative concentration after 50 (a), based on Eq. (2-2), a-profile

Cse(x) : relative concentration after 50 (a), based on Eq. (2-2), e-profile

Cqsa(x): relative concentration after 50 (a), based on Eq. (2-3), a-profile

Cqse(x): relative concentration after 50 (a), based on Eq. (2-3), e-profile

Ctfa(x) : relative concentration after 50 (a), based on Eq. (2-4), a-profile

Ctfe(x) : relative concentration after 50 (a), based on Eq. (2-4), e-profile

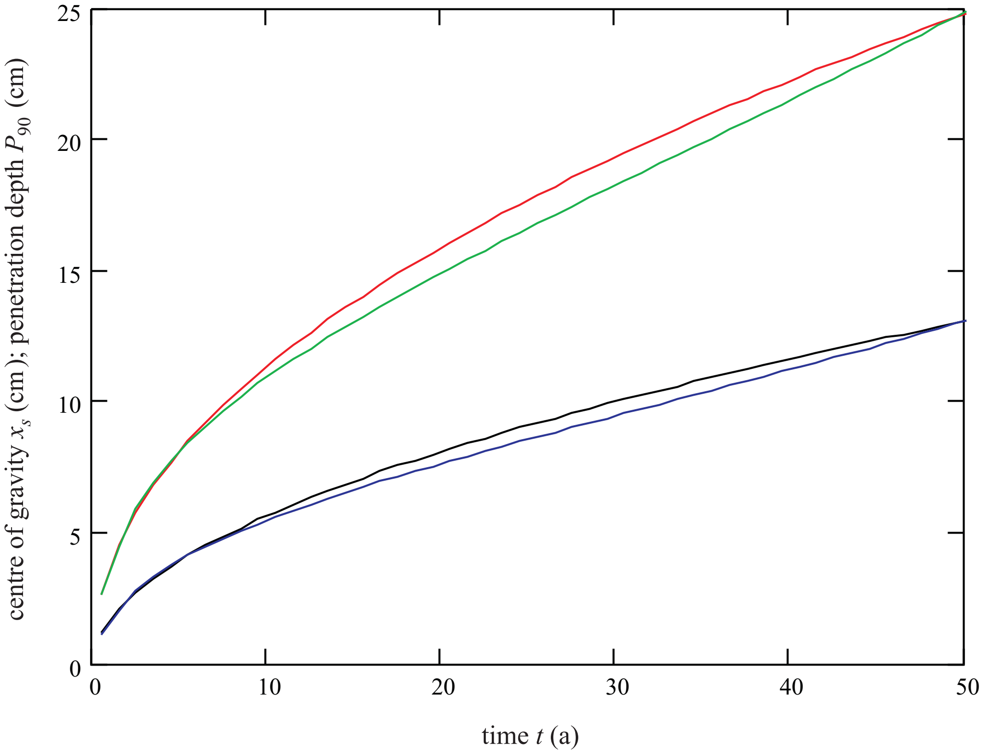

Fig. 6.8-9: Matching of the centres of gravity and of the penetration depths (time series 3, Sr-90)

legend:

black: x_s-fit

blue : matching of the x_s-fit, based on Eq. (2-24)

red : P_{90}-fit

green: matching of the P_{90}-fit; (a(t), n(t) from second fits)

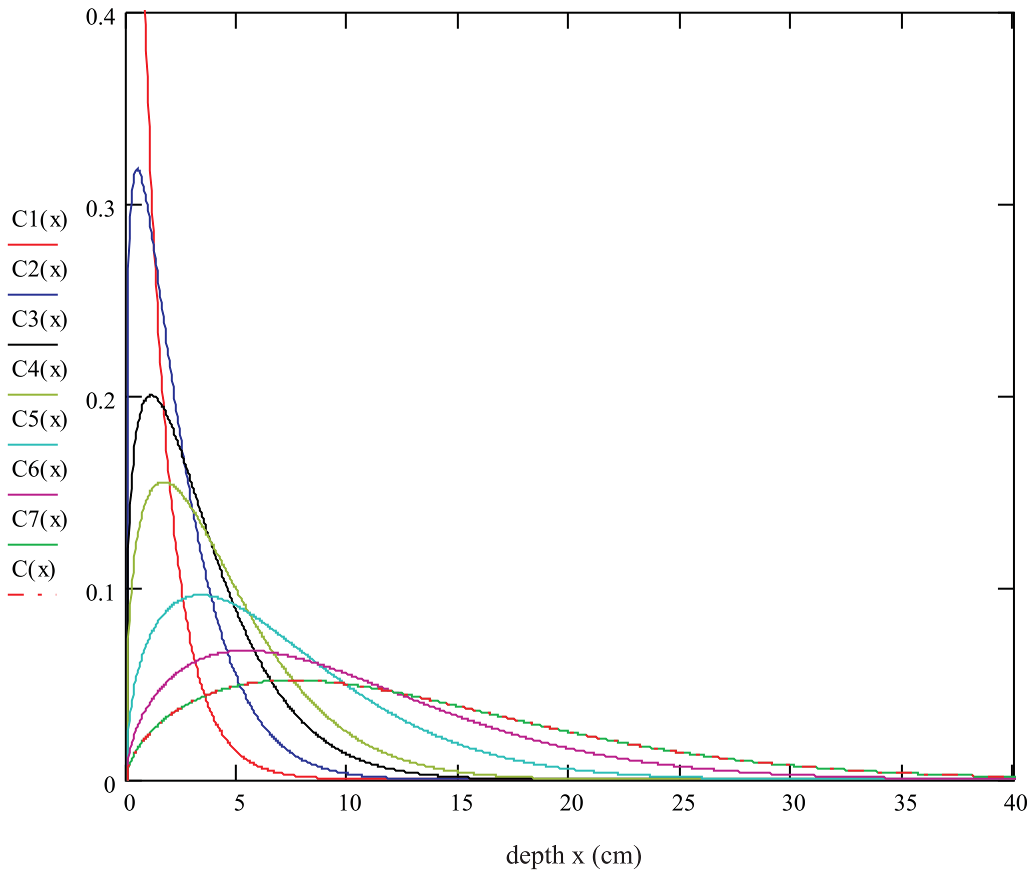

Fig. 6.8-10: Relative concentrations for different points of time (time series 3, Sr-90)
legend:
ordinate axis: relative concentration (cm^{-1})

C1(x): relative concentration after 0.500 (a)
C2(x): relative concentration after 1.750 (a)
C3(x): relative concentration after 3.833 (a)
C4(x): relative concentration after 6.083 (a)
C5(x): relative concentration after 15 (a)
C6(x): relative concentration after 30 (a)
C7(x): relative concentration after 50 (a)

} based on 2-dimensional nest of intervals

C(x) : relative concentration after 50 (a), based on second fits of a(t) and n(t)

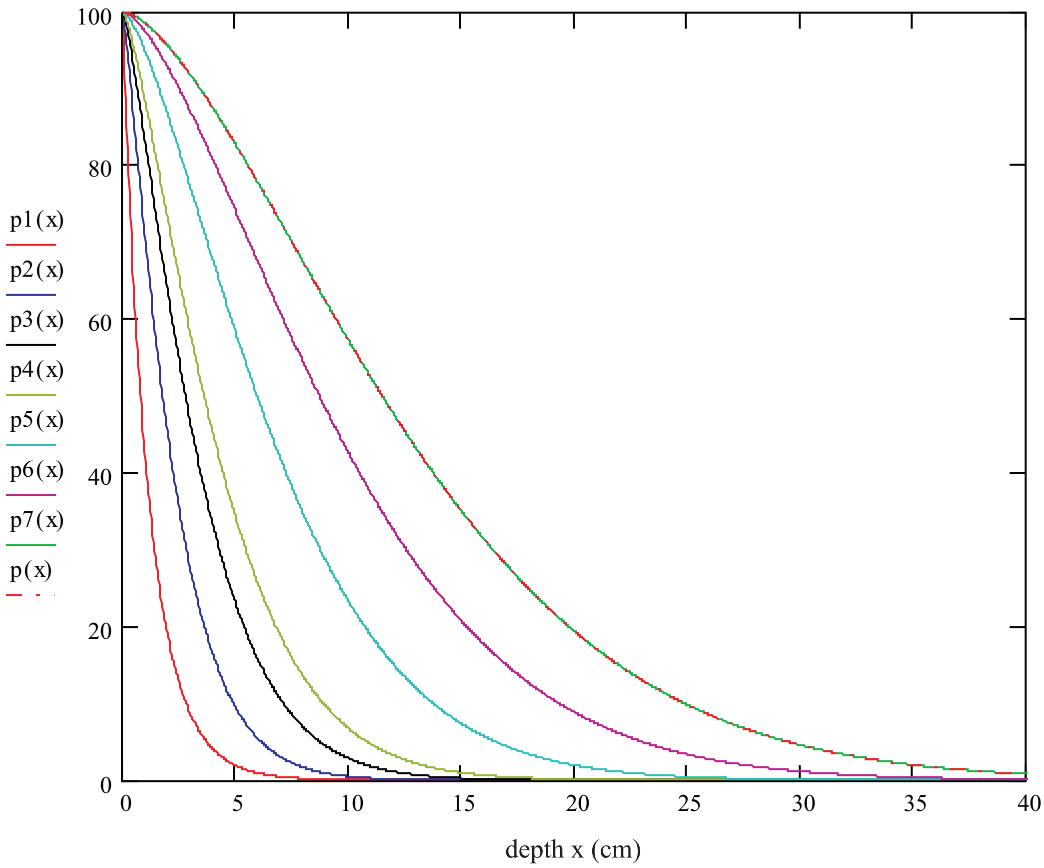

Fig. 6.8-11: Inventories below x in (%) for different points of time (time series 3, Sr-90)
legend:
ordinate axis: inventories below x (%)
p1(x): inventory below x in (%) after 0.500 (a)
p2(x): inventory below x in (%) after 1.750 (a)
p3(x): inventory below x in (%) after 3.833 (a)
p4(x): inventory below x in (%) after 6.083 (a) $\Bigg\}$ based on 2-dimensional nest of intervals
p5(x): inventory below x in (%) after 15 (a)
p6(x): inventory below x in (%) after 30 (a)
p7(x): inventory below x in (%) after 50 (a)
p(x) : inventory below x in (%) after 50 (a), based on second fits of a(t) and n(t)

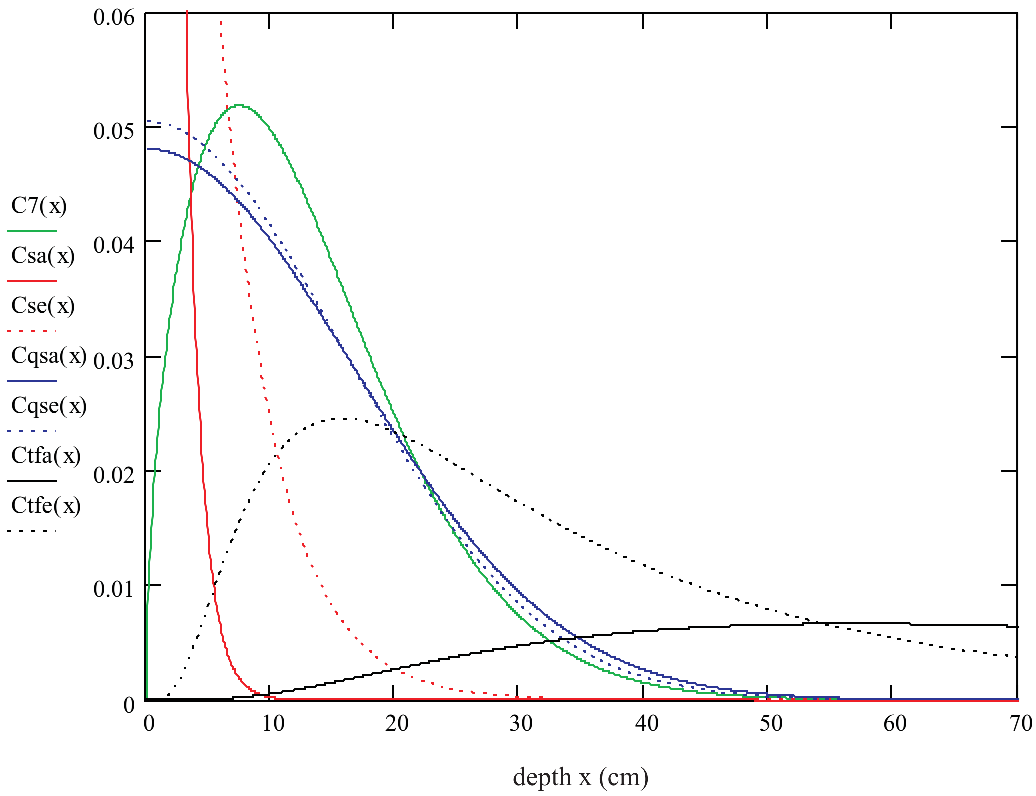

Fig. 6.8-12: Relative concentrations after 50 (a), resulting from different models (time series 3, Sr-90)

legend:

ordinate axis: relative concentration (cm^{-1})

C7(x) : relative concentration after 50 (a), based on 2-dimensional nest of intervals
Csa(x) : relative concentration after 50 (a), based on Eq. (2-2), a-profile
Cse(x) : relative concentration after 50 (a), based on Eq. (2-2), e-profile
Cqsa(x): relative concentration after 50 (a), based on Eq. (2-3), a-profile
Cqse(x): relative concentration after 50 (a), based on Eq. (2-3), e-profile
Ctfa(x) : relative concentration after 50 (a), based on Eq. (2-4), a-profile
Ctfe(x) : relative concentration after 50 (a), based on Eq. (2-4), e-profile

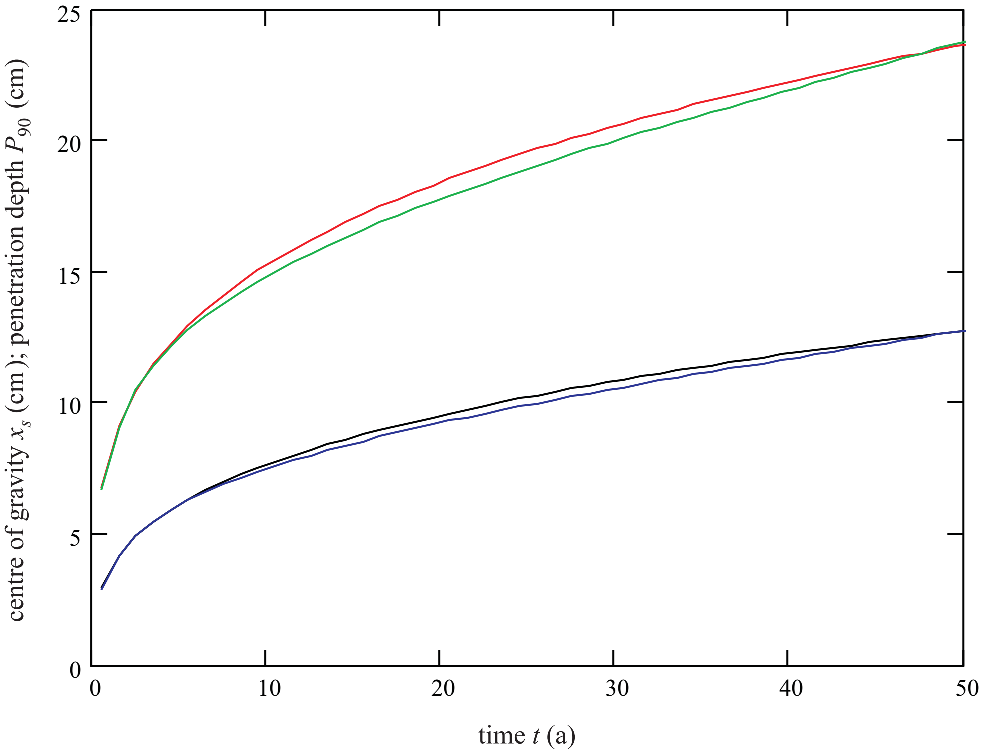

Fig. 6.8-13: Matching of the centres of gravity and of the penetration depths (time series 4, Sr-90)

legend:

black: x_s-fit

blue : matching of the x_s-fit, based on Eq. (2-24)

red : P_{90}-fit

green: matching of the P_{90}-fit; (a(t), n(t) from second fits)

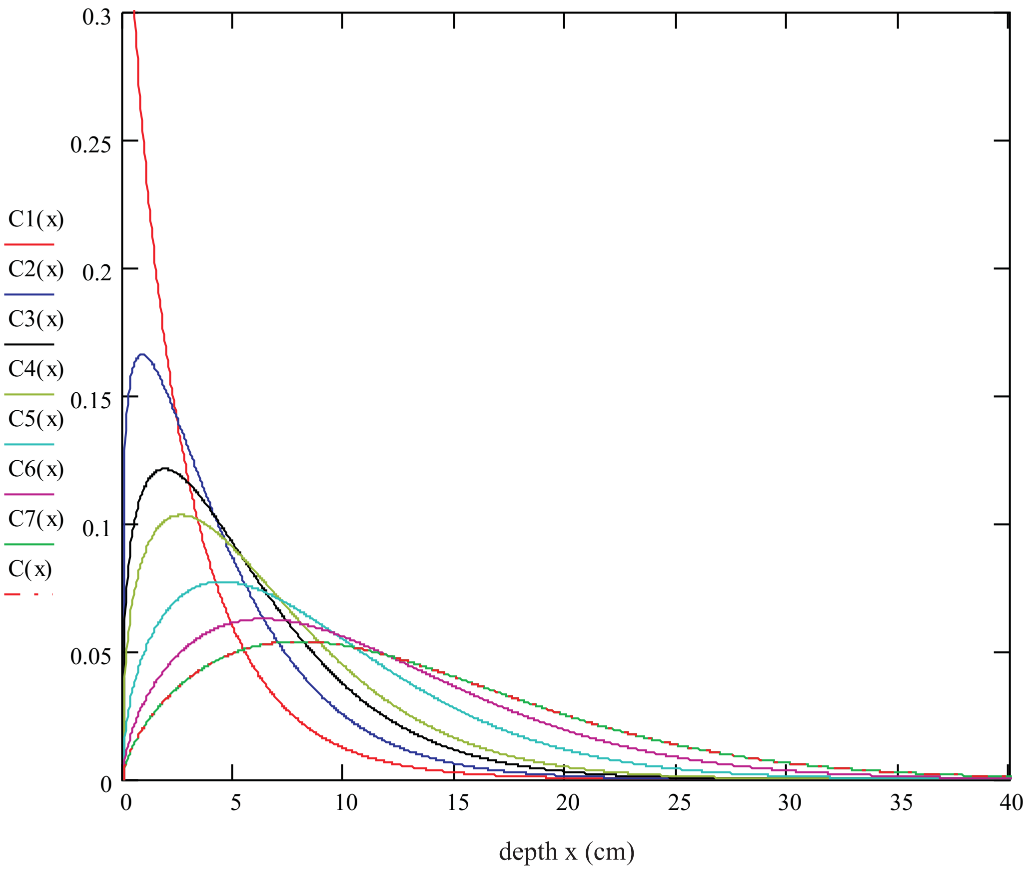

Fig. 6.8-14: Relative concentrations for different points of time (time series 4, Sr-90)
legend:
ordinate axis: relative concentration (cm^{-1})
C1(x): relative concentration after 0.500 (a)
C2(x): relative concentration after 1.750 (a)
C3(x): relative concentration after 3.833 (a)
C4(x): relative concentration after 6.083 (a)
C5(x): relative concentration after 15 (a)
C6(x): relative concentration after 30 (a)
C7(x): relative concentration after 50 (a)
(C1(x) to C7(x): based on 2-dimensional nest of intervals)
C(x) : relative concentration after 50 (a), based on second fits of a(t) and n(t)

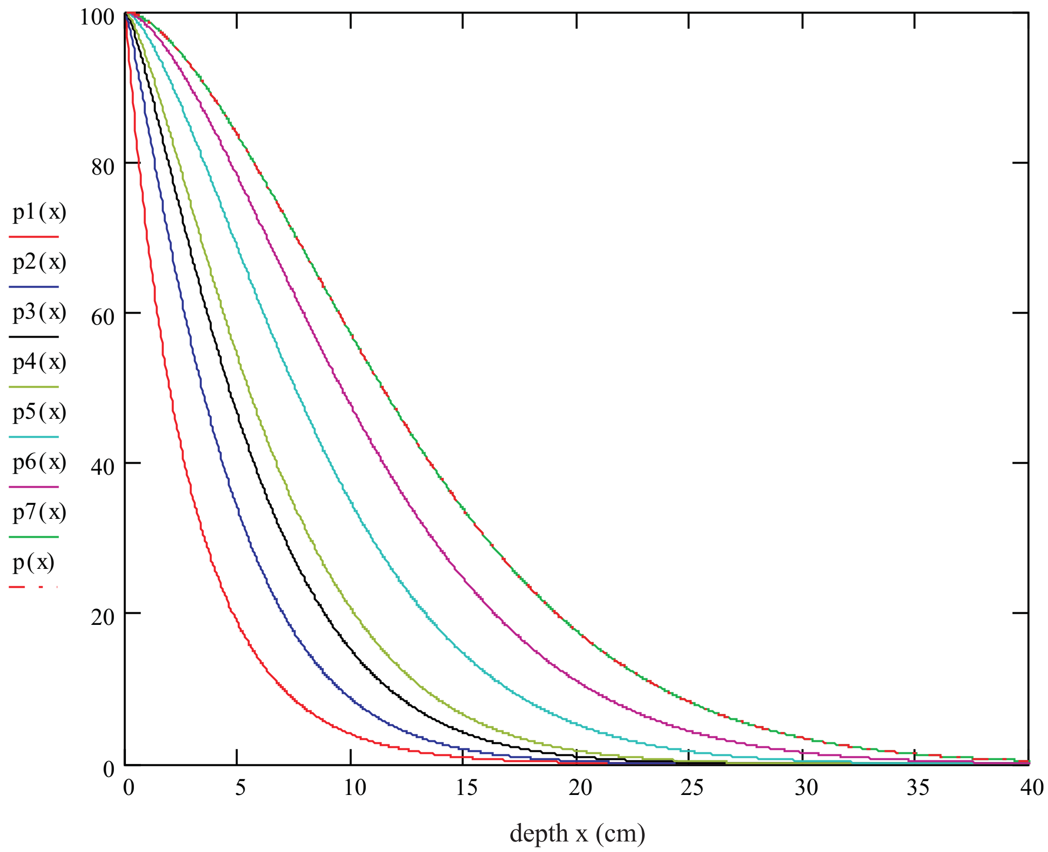

Fig. 6.8-15: Inventories below x in (%) for different points of time (time series 4, Sr-90)
legend:
ordinate axis: inventories below x (%)
p1(x): inventory below x in (%) after 0.500 (a)
p2(x): inventory below x in (%) after 1.750 (a)
p3(x): inventory below x in (%) after 3.833 (a)
p4(x): inventory below x in (%) after 6.083 (a) based on 2-dimensional nest of intervals
p5(x): inventory below x in (%) after 15 (a)
p6(x): inventory below x in (%) after 30 (a)
p7(x): inventory below x in (%) after 50 (a)
p(x) : inventory below x in (%) after 50 (a), based on second fits of a(t) and n(t)

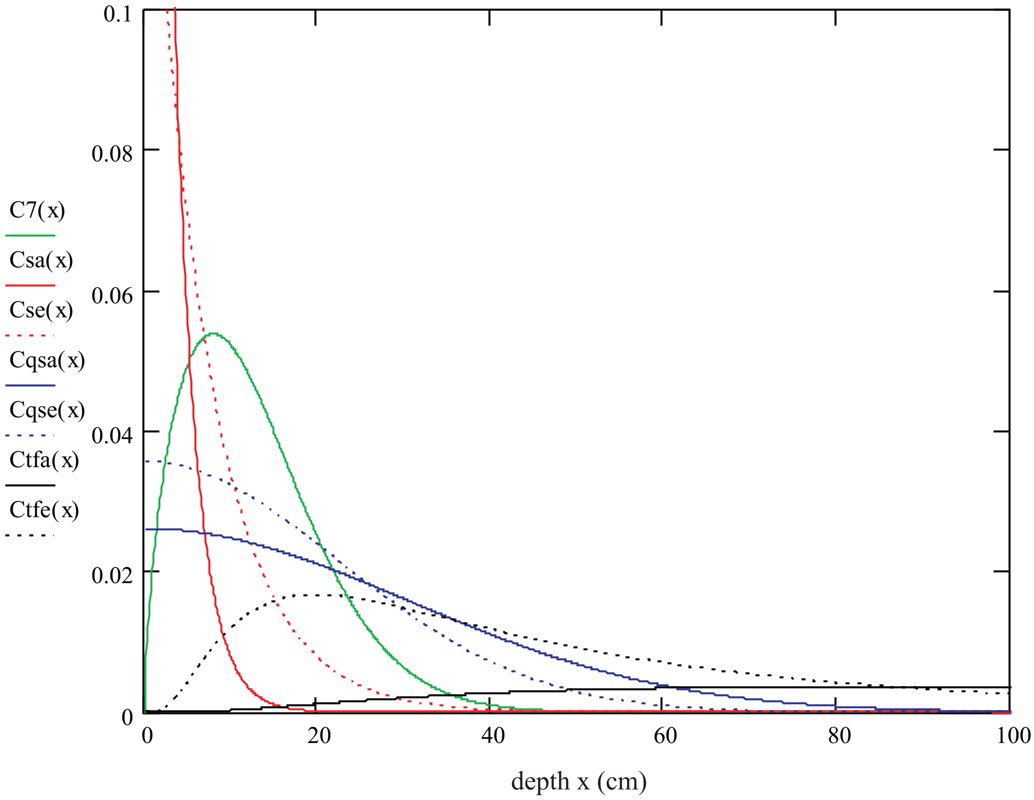

Fig. 6.8-16: Relative concentrations after 50 (a), resulting from different models (time series 4, Sr-90)

legend:

ordinate axis: relative concentration (cm^{-1})

C7(x) : relative concentration after 50 (a), based on 2-dimensional nest of intervals
Csa(x) : relative concentration after 50 (a), based on Eq. (2-2), a-profile
Cse(x) : relative concentration after 50 (a), based on Eq. (2-2), e-profile
Cqsa(x): relative concentration after 50 (a), based on Eq. (2-3), a-profile
Cqse(x): relative concentration after 50 (a), based on Eq. (2-3), e-profile
Ctfa(x) : relative concentration after 50 (a), based on Eq. (2-4), a-profile
Ctfe(x) : relative concentration after 50 (a), based on Eq. (2-4), e-profile

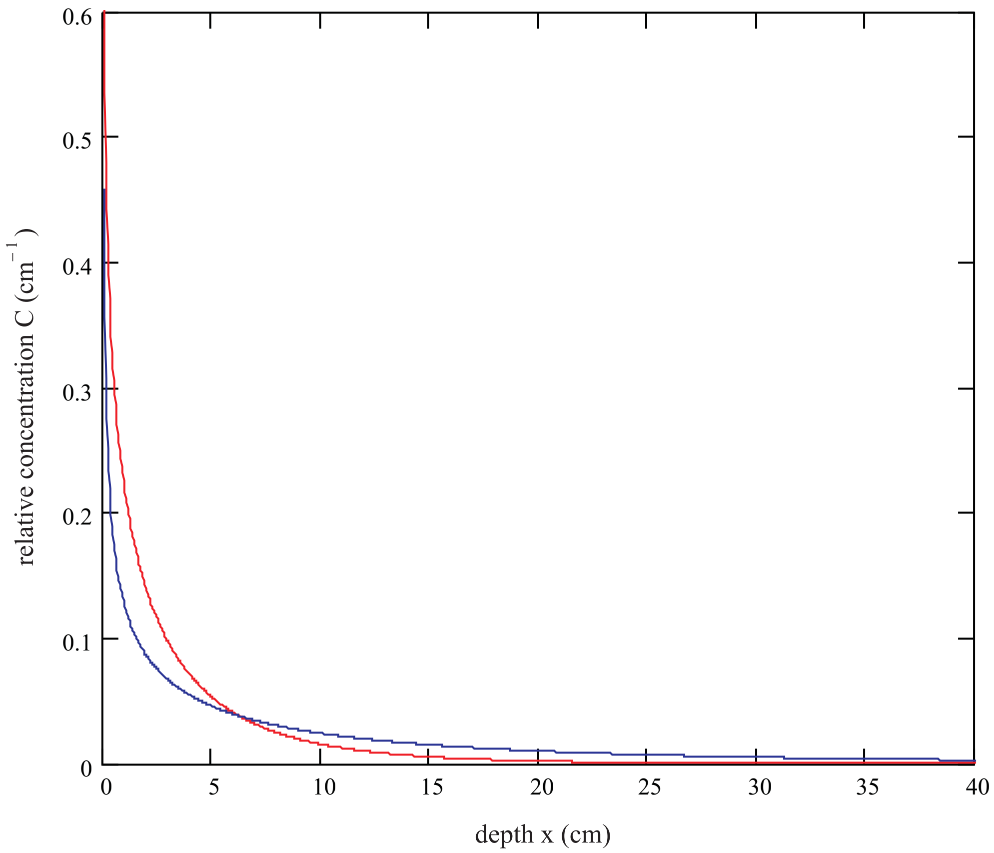

Fig. 6.8-17: Comparison of relative concentrations of Cs-137 and Sr-90 in soil no. 1, based on 2-dimensional nests of intervals, after 50 (a)
legend:
red : Cs-137, case study 7, time series 1
blue : Sr-90, case study 8, time series 1

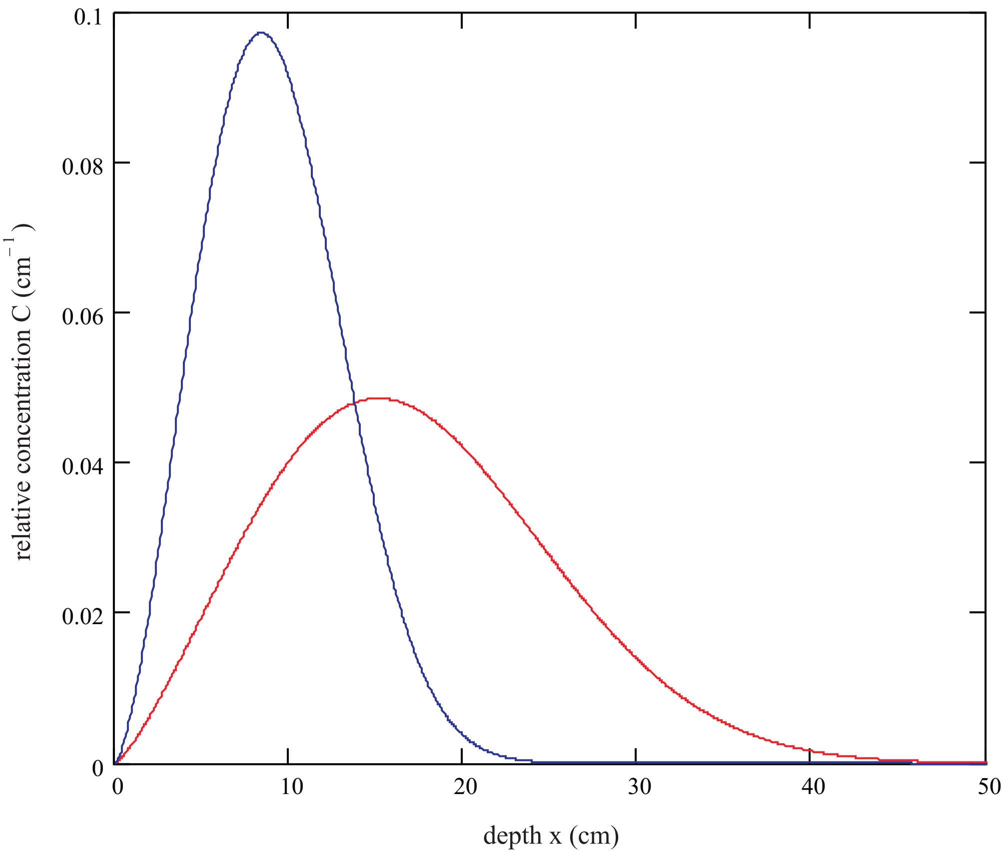

Fig. 6.8-18: Comparison of relative concentrations of Cs-137 and Sr-90 in soil no. 3, based on 2-dimensional nests of intervals, after 50 (a)
legend:
red : Cs-137, case study 7, time series 2
blue : Sr-90, case study 8, time series 2

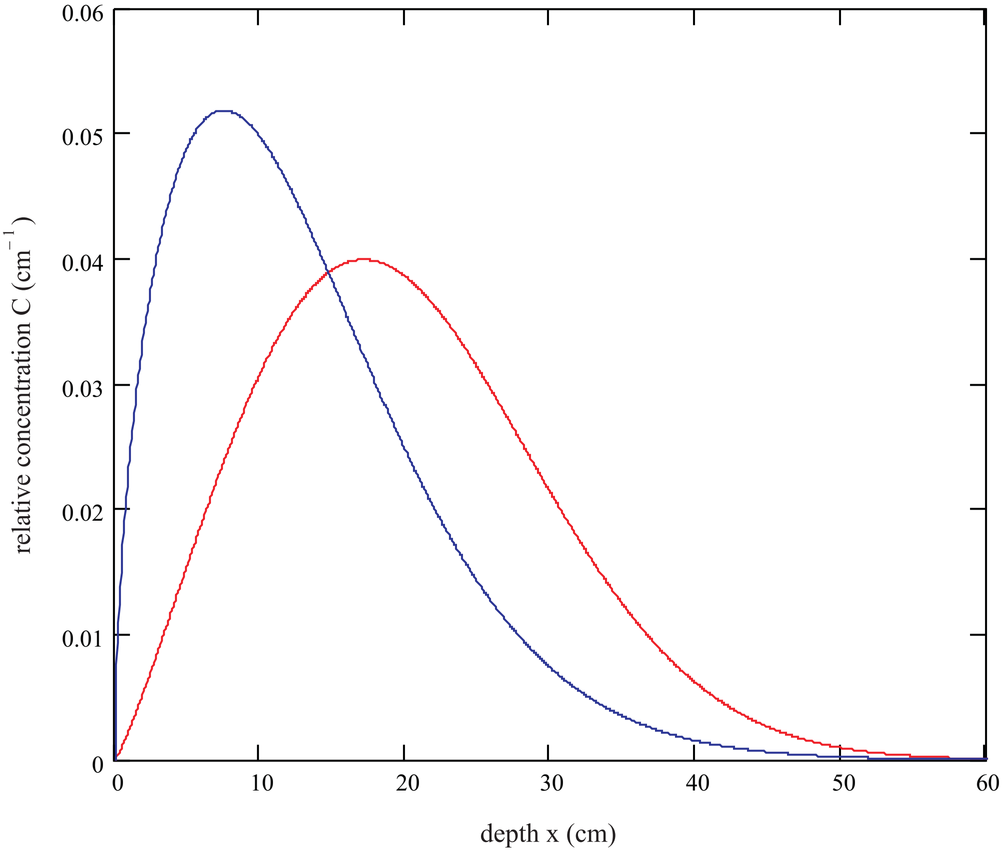

Fig. 6.8-19: Comparison of relative concentrations of Cs-137 and Sr-90 in soil no. 6, based on 2-dimensional nests of intervals, after 50 (a)
legend:
red : Cs-137, case study 7, time series 3
blue : Sr-90, case study 8, time series 3

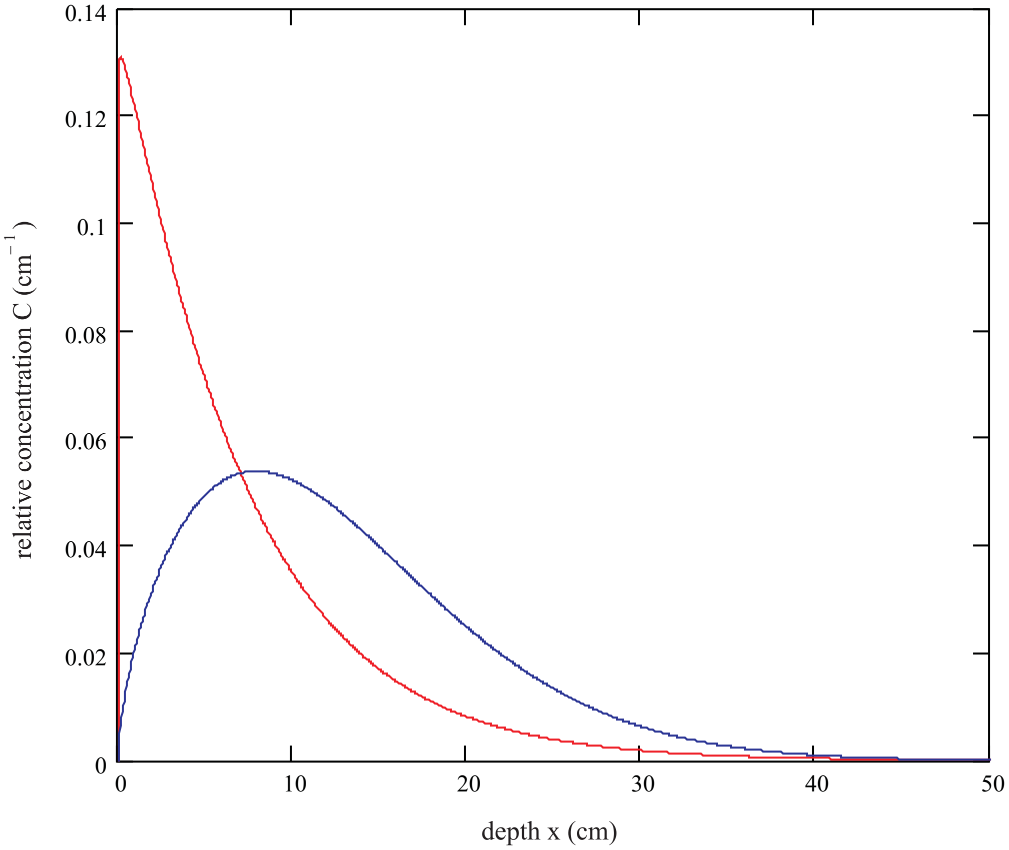

Fig. 6.8-20: Comparison of relative concentrations of Cs-137 and Sr-90 in soil no. 8, based on 2-dimensional nests of intervals, after 50 (a)
legend:
red : Cs-137, case study 7, time series 4
blue : Sr-90, case study 8, time series 4

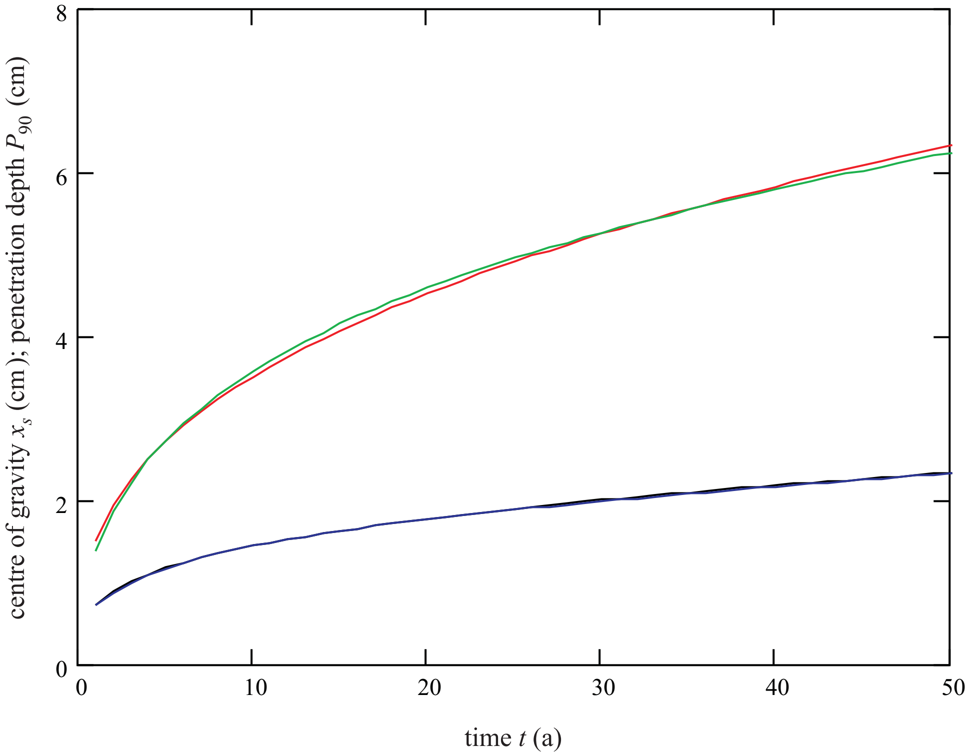

Fig. 6.9-1: Matching of the centres of gravity and of the penetration depths (time series 1, Chernobyl-Cs-137)
legend:
black: x_s-fit
blue : matching of the x_s-fit, based on Eq. (2-24)
red : P_{90}-fit
green: matching of the P_{90}-fit; (a(t), n(t) from second fits)

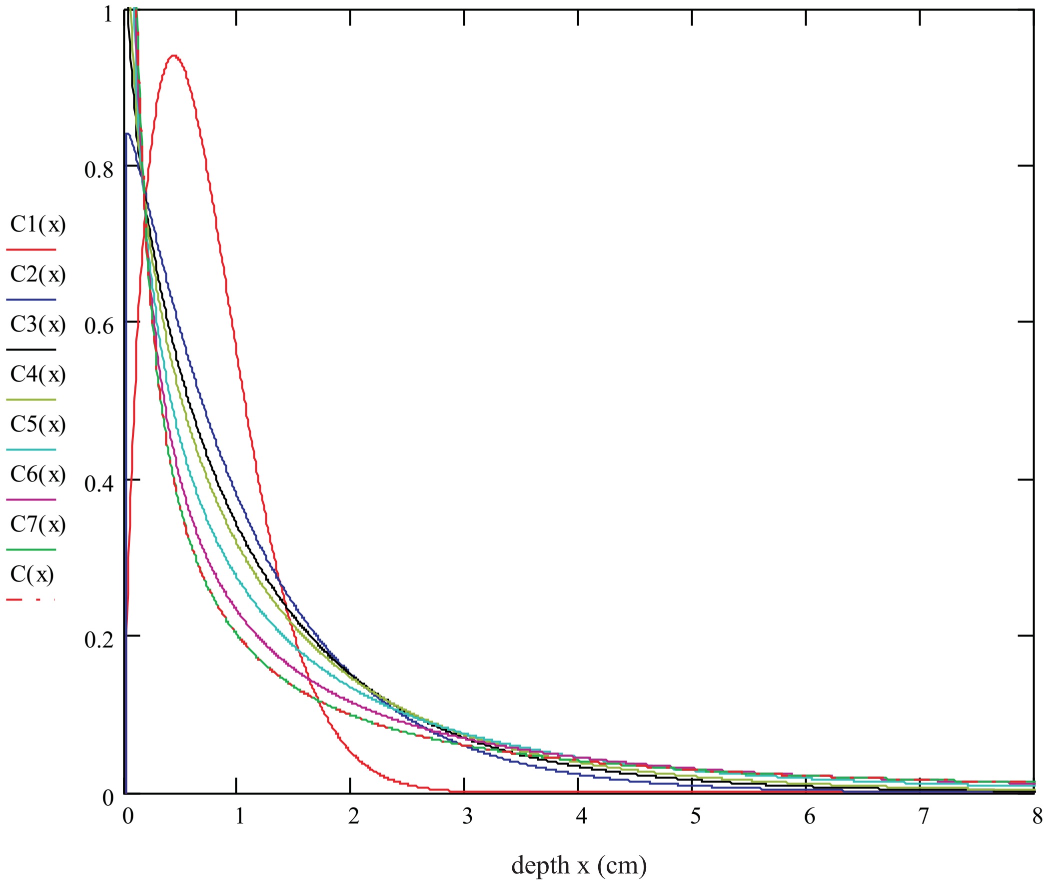

Fig. 6.9-2: Relative concentrations for different points of time (time series 1, Chernobyl-Cs-137)

legend:

ordinate axis: relative concentration (cm^{-1})

C1(x): relative concentration after 1 (a)
C2(x): relative concentration after 4 (a)
C3(x): relative concentration after 6 (a)
C4(x): relative concentration after 8 (a)
C5(x): relative concentration after 15 (a)
C6(x): relative concentration after 30 (a)
C7(x): relative concentration after 50 (a)

(C1(x)–C7(x): based on 2-dimensional nest of intervals)

C(x) : relative concentration after 50 (a), based on second fits of a(t) and n(t)

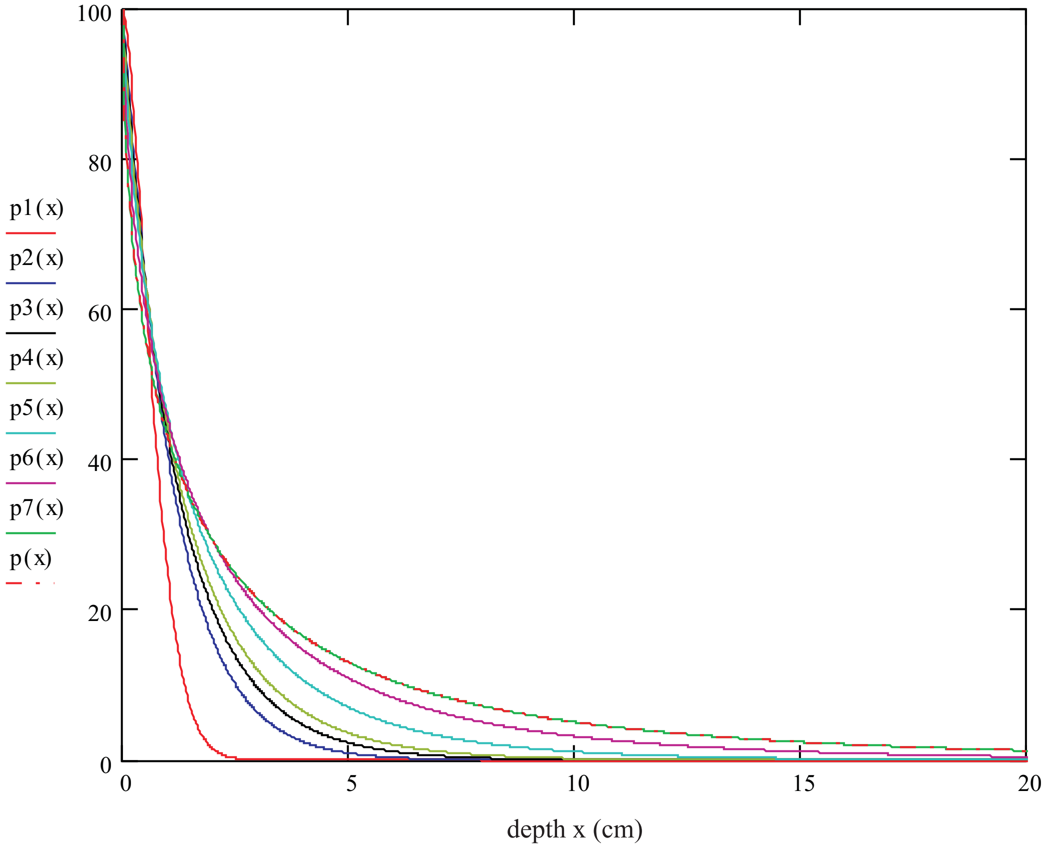

Fig. 6.9-3: Inventories below x in (%) for different points of time (time series 1, Chernobyl-Cs-137)

legend:

ordinate axis: inventories below x (%)

p1(x): inventory below x in (%) after 1 (a)
p2(x): inventory below x in (%) after 4 (a)
p3(x): inventory below x in (%) after 6 (a)
p4(x): inventory below x in (%) after 8 (a)
p5(x): inventory below x in (%) after 15 (a)
p6(x): inventory below x in (%) after 30 (a)
p7(x): inventory below x in (%) after 50 (a)

based on 2-dimensional nest of intervals

p(x) : inventory below x in (%) after 50 (a), based on second fits of a(t) and n(t)

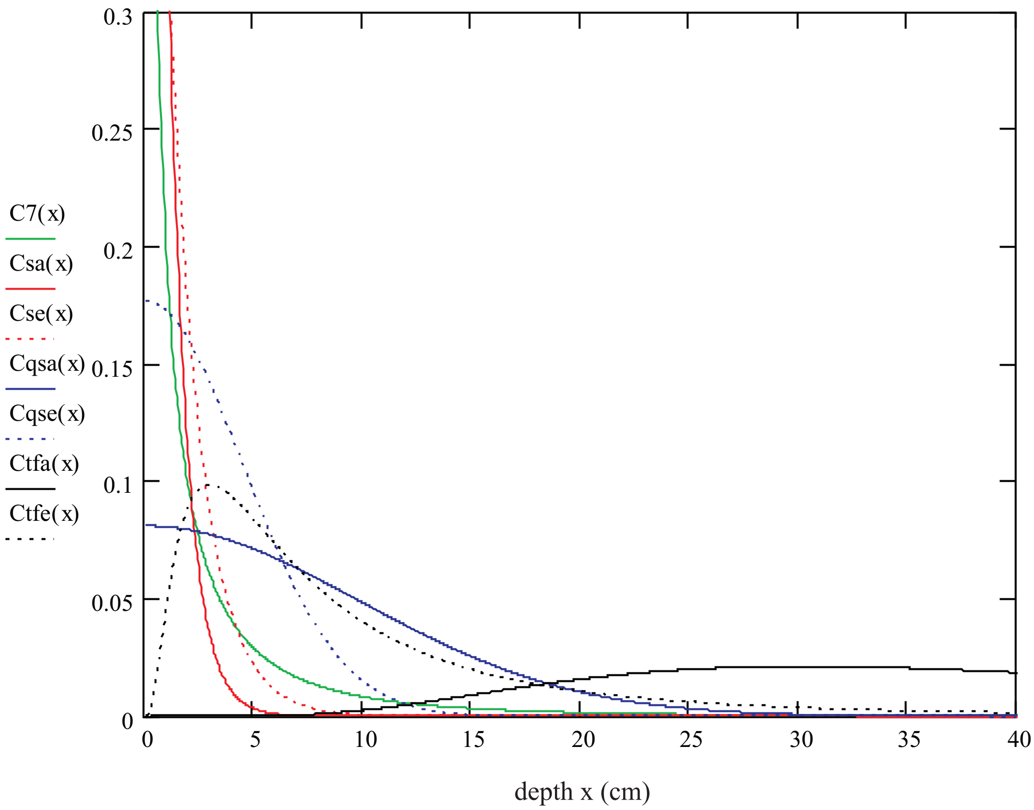

Fig. 6.9-4: Relative concentrations after 50 (a), resulting from different models (time series 1, Chernobyl-Cs-137)

legend:

ordinate axis: relative concentration (cm^{-1})

C7(x) : relative concentration after 50 (a), based on 2-dimensional nest of intervals

Csa(x) : relative concentration after 50 (a), based on Eq. (2-2), a-profile

Cse(x) : relative concentration after 50 (a), based on Eq. (2-2), e-profile

Cqsa(x): relative concentration after 50 (a), based on Eq. (2-3), a-profile

Cqse(x): relative concentration after 50 (a), based on Eq. (2-3), e-profile

Ctfa(x) : relative concentration after 50 (a), based on Eq. (2-4), a-profile

Ctfe(x) : relative concentration after 50 (a), based on Eq. (2-4), e-profile

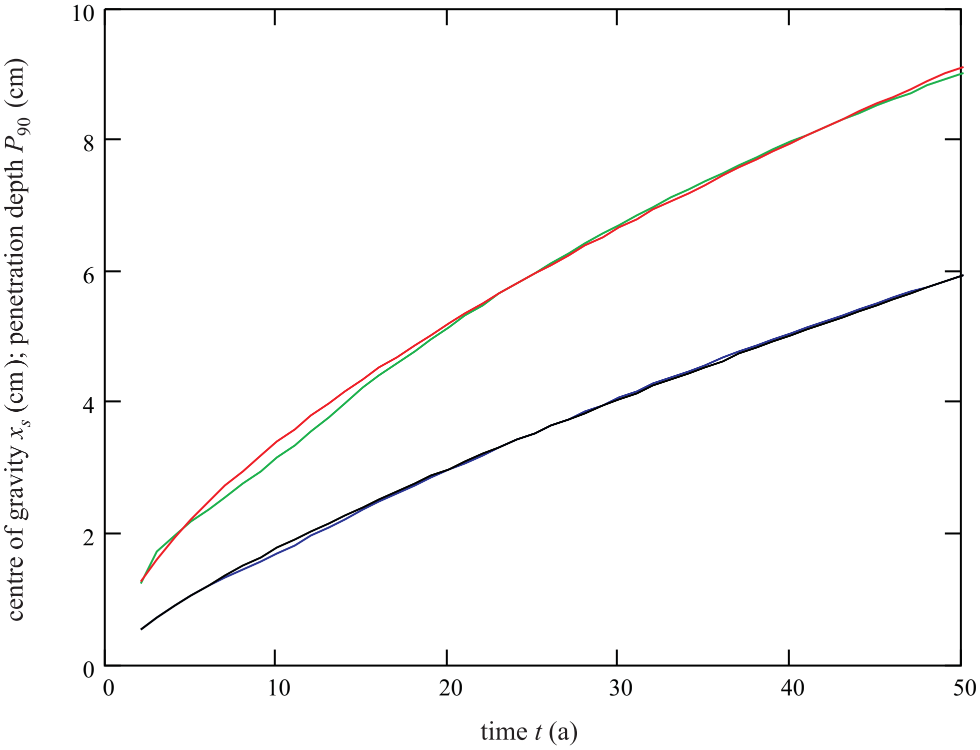

Fig. 6.9-5: Improved matching of the centres of gravity and of the penetration depths, achieved by fitting of n(t) in 2 pieces (time series 2, Chernobyl-Cs-137)

legend:

black: x_s-fit

blue : matching of the x_s-fit, based on Eq. (2-24)

red : P_{90}-fit

green: matching of the P_{90}-fit; (a(t), n(t) from second fits)

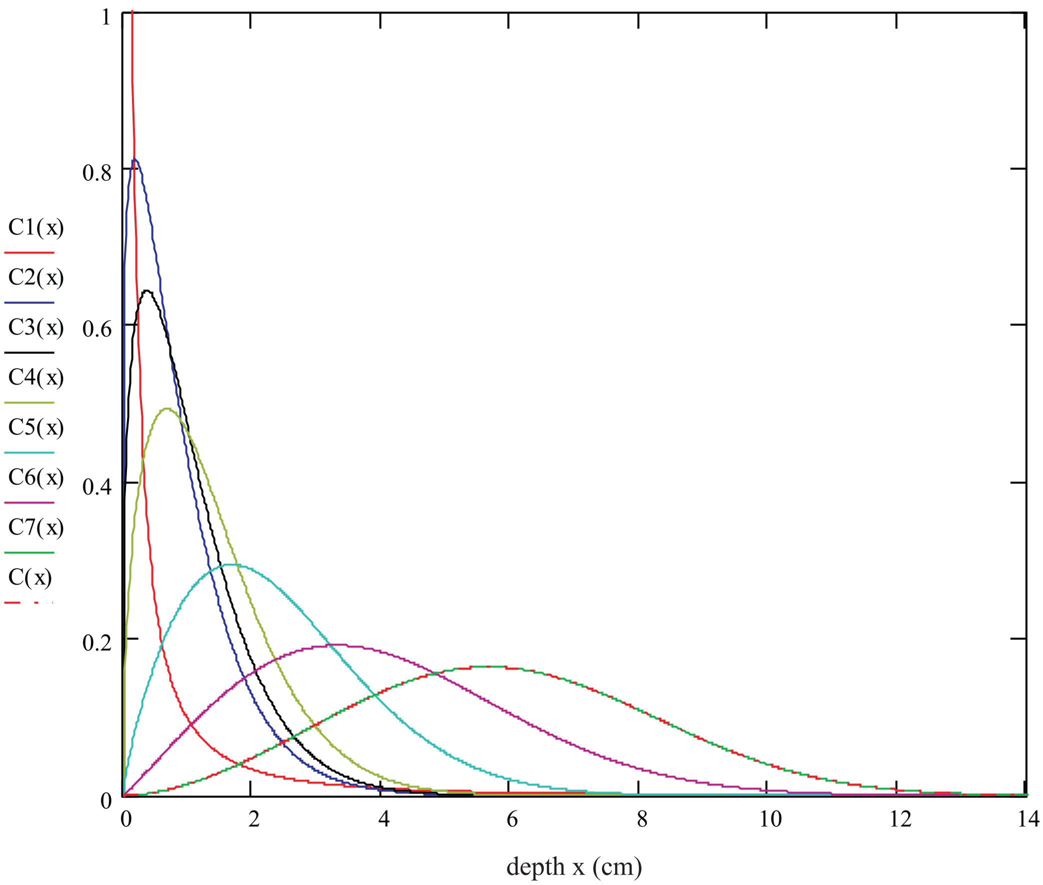

Fig. 6.9-6: Relative concentrations for different points of time (time series 2, Chernobyl-Cs-137)

legend:

ordinate axis: relative concentration (cm^{-1})

C1(x): relative concentration after 2 (a)
C2(x): relative concentration after 4 (a)
C3(x): relative concentration after 5 (a)
C4(x): relative concentration after 7 (a)
C5(x): relative concentration after 15 (a)
C6(x): relative concentration after 30 (a)
C7(x): relative concentration after 50 (a)

(C1(x)–C7(x): based on 2-dimensional nest of intervals)

C(x) : relative concentration after 50 (a), based on second fits of a(t) and n(t)

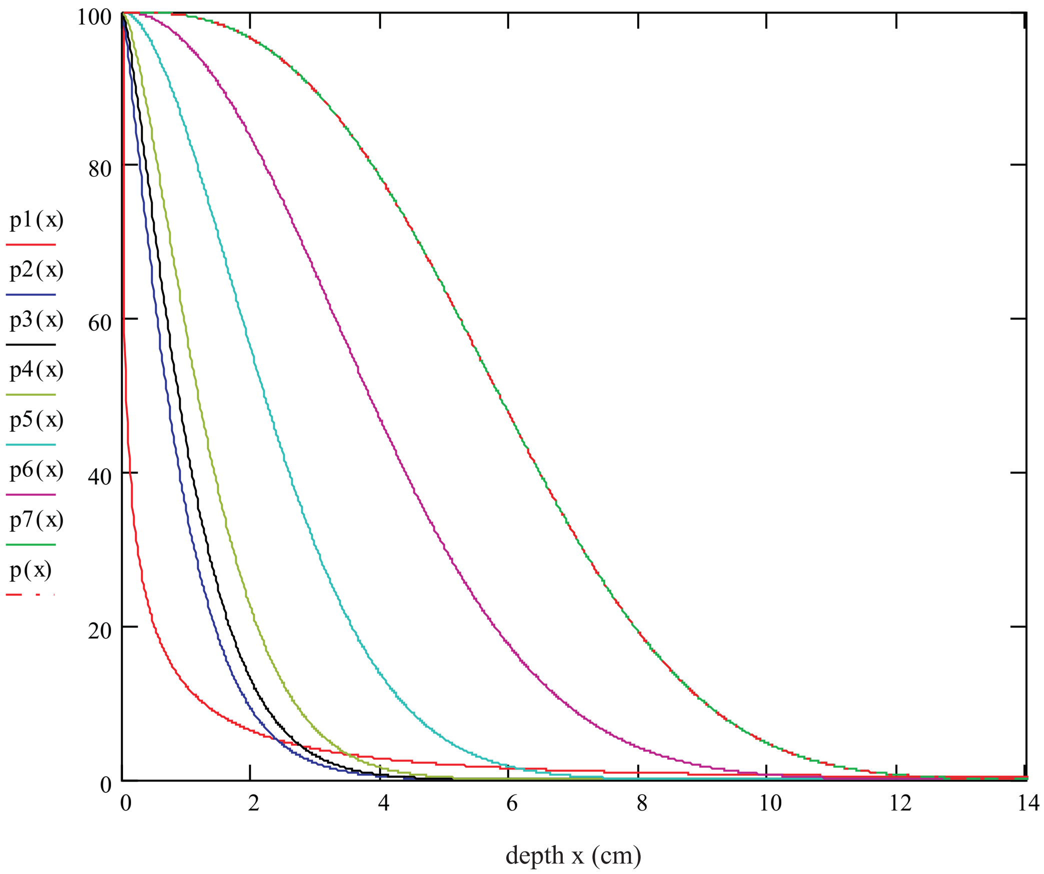

Fig. 6.9-7: Inventories below x in (%) for different points of time (time series 2, Chernobyl-Cs-137)

legend:

ordinate axis: inventories below x (%)

p1(x): inventory below x in (%) after 2 (a)
p2(x): inventory below x in (%) after 4 (a)
p3(x): inventory below x in (%) after 5 (a)
p4(x): inventory below x in (%) after 7 (a)
p5(x): inventory below x in (%) after 15 (a)
p6(x): inventory below x in (%) after 30 (a)
p7(x): inventory below x in (%) after 50 (a)

} based on 2-dimensional nest of intervals

p(x) : inventory below x in (%) after 50 (a), based on second fits of a(t) and n(t)

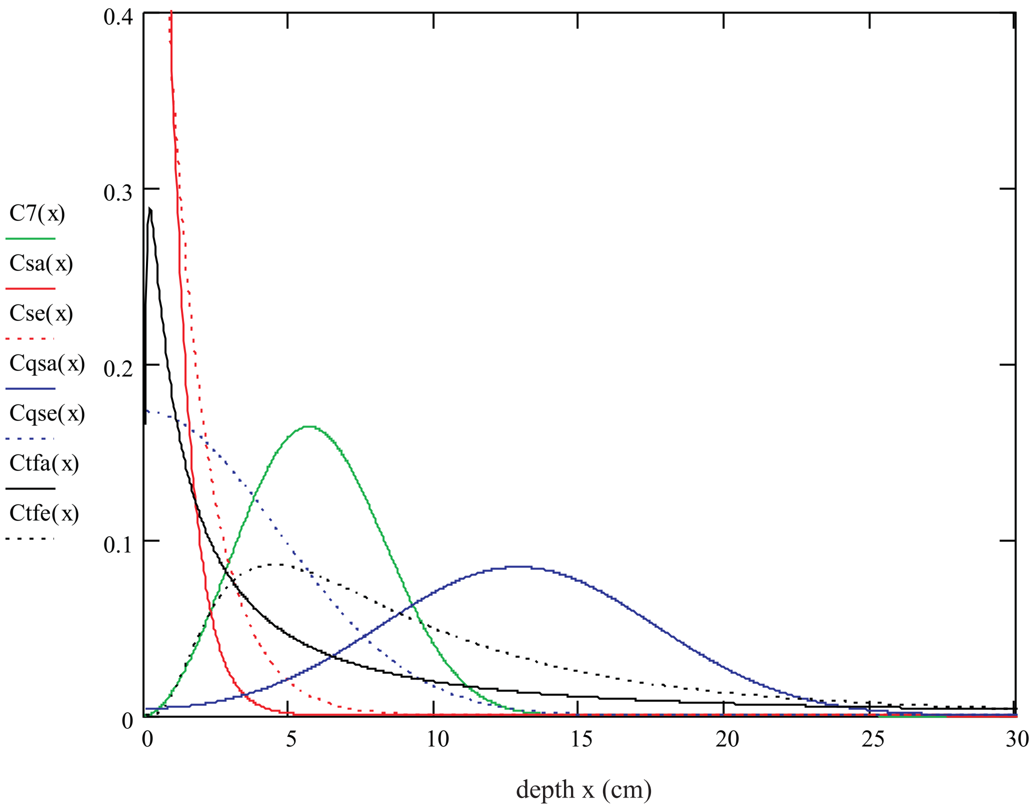

Fig. 6.9-8: Relative concentrations after 50 (a), resulting from different models (time series 2, Chernobyl-Cs-137)

legend:

ordinate axis: relative concentration (cm^{-1})

C7(x) : relative concentration after 50 (a), based on 2-dimensional nest of intervals
Csa(x) : relative concentration after 50 (a), based on Eq. (2-2), a-profile
Cse(x) : relative concentration after 50 (a), based on Eq. (2-2), e-profile
Cqsa(x): relative concentration after 50 (a), based on Eq. (2-3), a-profile
Cqse(x): relative concentration after 50 (a), based on Eq. (2-3), e-profile
Ctfa(x) : relative concentration after 50 (a), based on Eq. (2-4), a-profile
Ctfe(x) : relative concentration after 50 (a), based on Eq. (2-4), e-profile

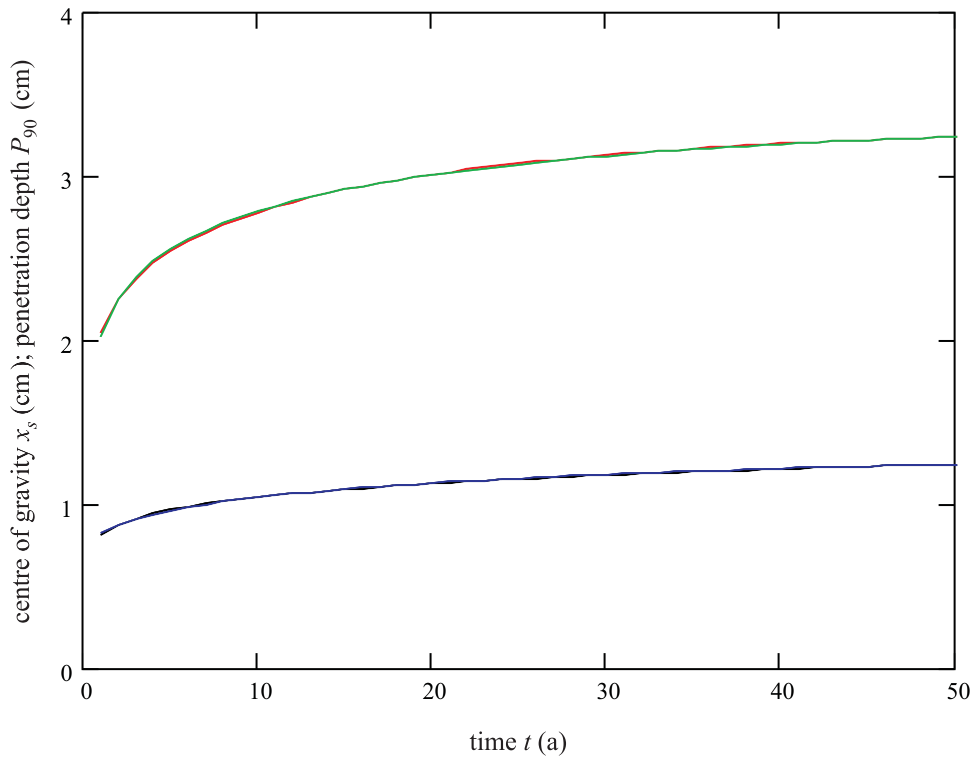

Fig. 6.9-9: Matching of the centres of gravity and of the penetration depths (time series 3, Chernobyl-Cs-137)
legend:
black: x_s-fit
blue : matching of the x_s-fit, based on Eq. (2-24)
red : P_{90}-fit
green: matching of the P_{90}-fit; (a(t), n(t) from second fits)

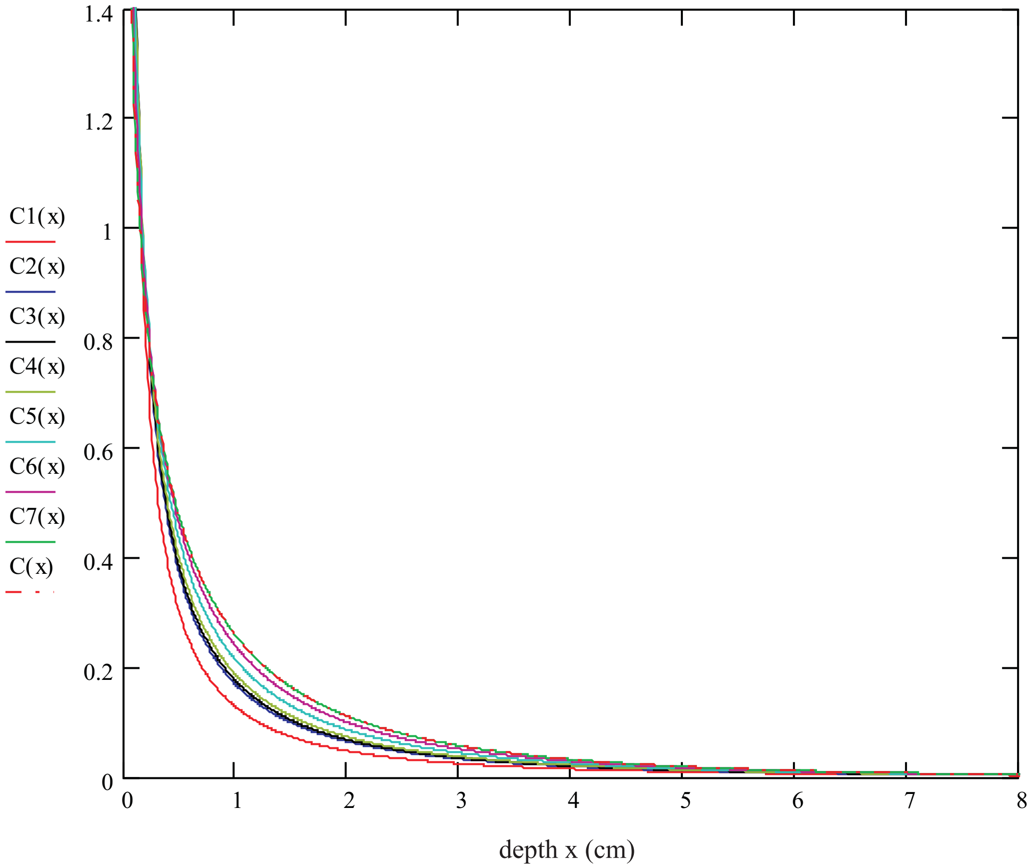

Fig. 6.9-10: Relative concentrations for different points of time (time series 3, Chernobyl-Cs-137)

legend:

ordinate axis: relative concentration (cm^{-1})

C1(x): relative concentration after 1 (a)
C2(x): relative concentration after 4 (a)
C3(x): relative concentration after 5 (a)
C4(x): relative concentration after 7 (a)
C5(x): relative concentration after 15 (a)
C6(x): relative concentration after 30 (a)
C7(x): relative concentration after 50 (a)

} based on 2-dimensional nest of intervals

C(x) : relative concentration after 50 (a), based on second fits of a(t) and n(t)

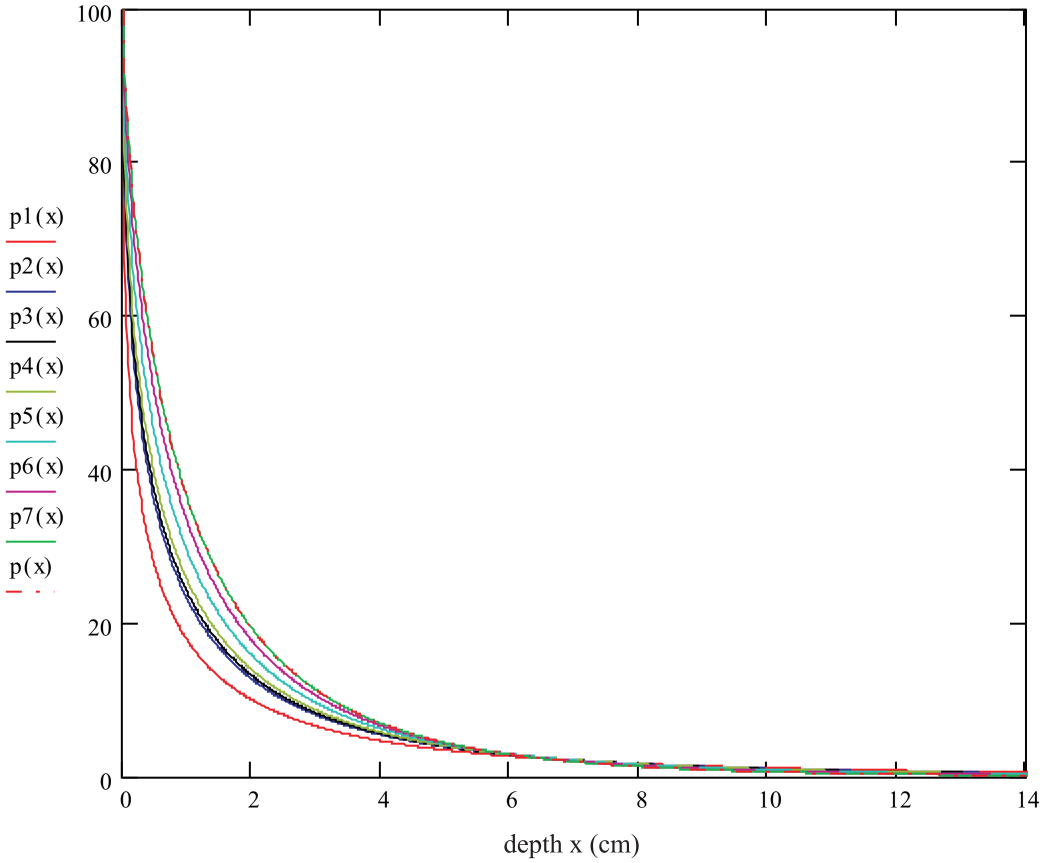

Fig. 6.9-11: Inventories below x in (%) for different points of time (time series 3, Chernobyl-Cs-137)

legend:

ordinate axis: inventories below x (%)

p1(x): inventory below x in (%) after 1 (a)
p2(x): inventory below x in (%) after 4 (a)
p3(x): inventory below x in (%) after 5 (a)
p4(x): inventory below x in (%) after 7 (a)
p5(x): inventory below x in (%) after 15 (a)
p6(x): inventory below x in (%) after 30 (a)
p7(x): inventory below x in (%) after 50 (a)

$\Big\}$ based on 2-dimensional nest of intervals

p(x) : inventory below x in (%) after 50 (a), based on second fits of a(t) and n(t)

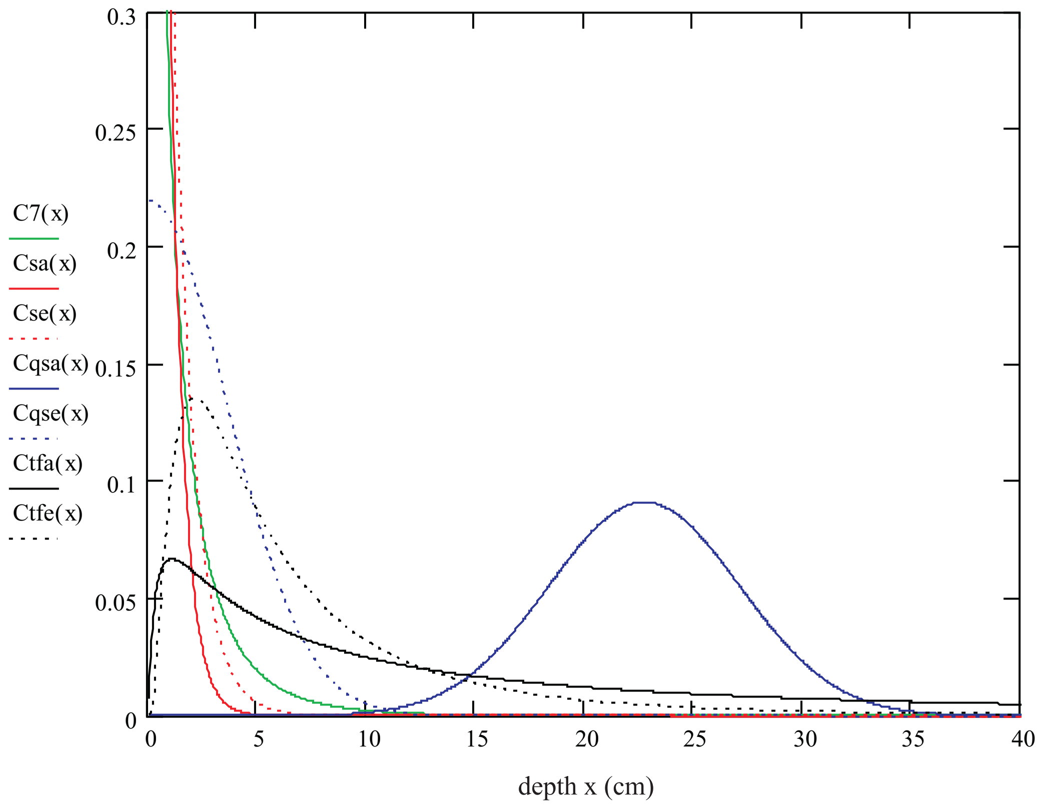

Fig. 6.9-12: Relative concentrations after 50 (a), resulting from different models (time series 3, Chernobyl-Cs-137)

legend:

ordinate axis: relative concentration (cm^{-1})

C7(x)   : relative concentration after 50 (a), based on 2-dimensional nest of intervals
Csa(x) : relative concentration after 50 (a), based on Eq. (2-2), a-profile
Cse(x) : relative concentration after 50 (a), based on Eq. (2-2), e-profile
Cqsa(x): relative concentration after 50 (a), based on Eq. (2-3), a-profile
Cqse(x): relative concentration after 50 (a), based on Eq. (2-3), e-profile
Ctfa(x) : relative concentration after 50 (a), based on Eq. (2-4), a-profile
Ctfe(x) : relative concentration after 50 (a), based on Eq. (2-4), e-profile

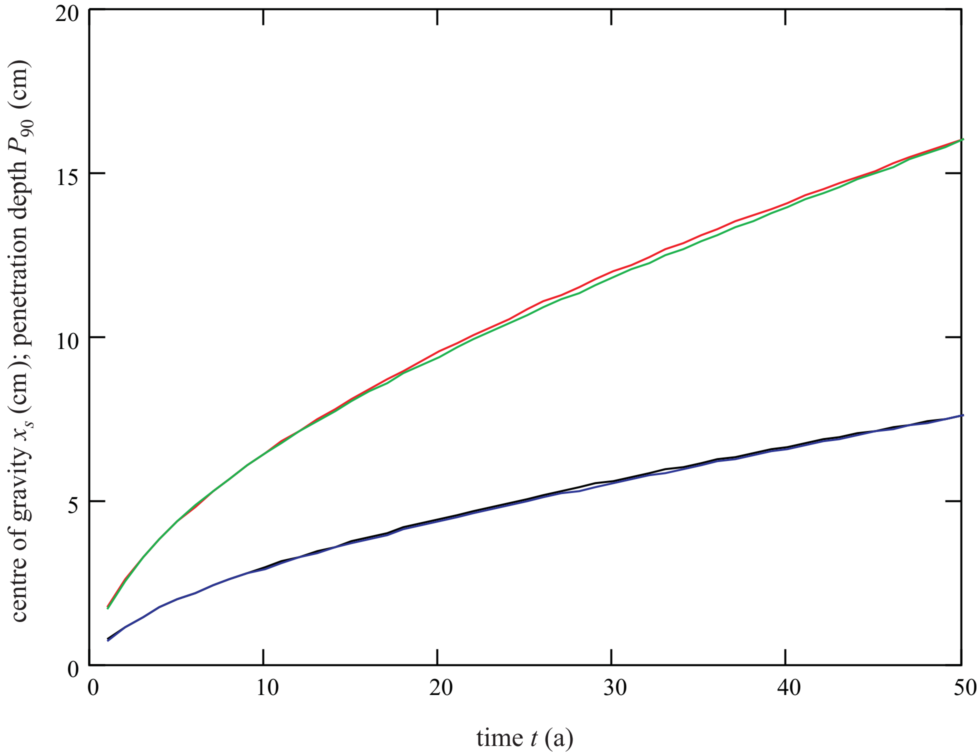

Fig. 6.9-13: Matching of the centres of gravity and of the penetration depths (time series 4, Chernobyl-Cs-137)

legend:

black: x_s-fit

blue : matching of the x_s-fit, based on Eq. (2-24)

red : P_{90}-fit

green: matching of the P_{90}-fit; (a(t), n(t) from second fits)

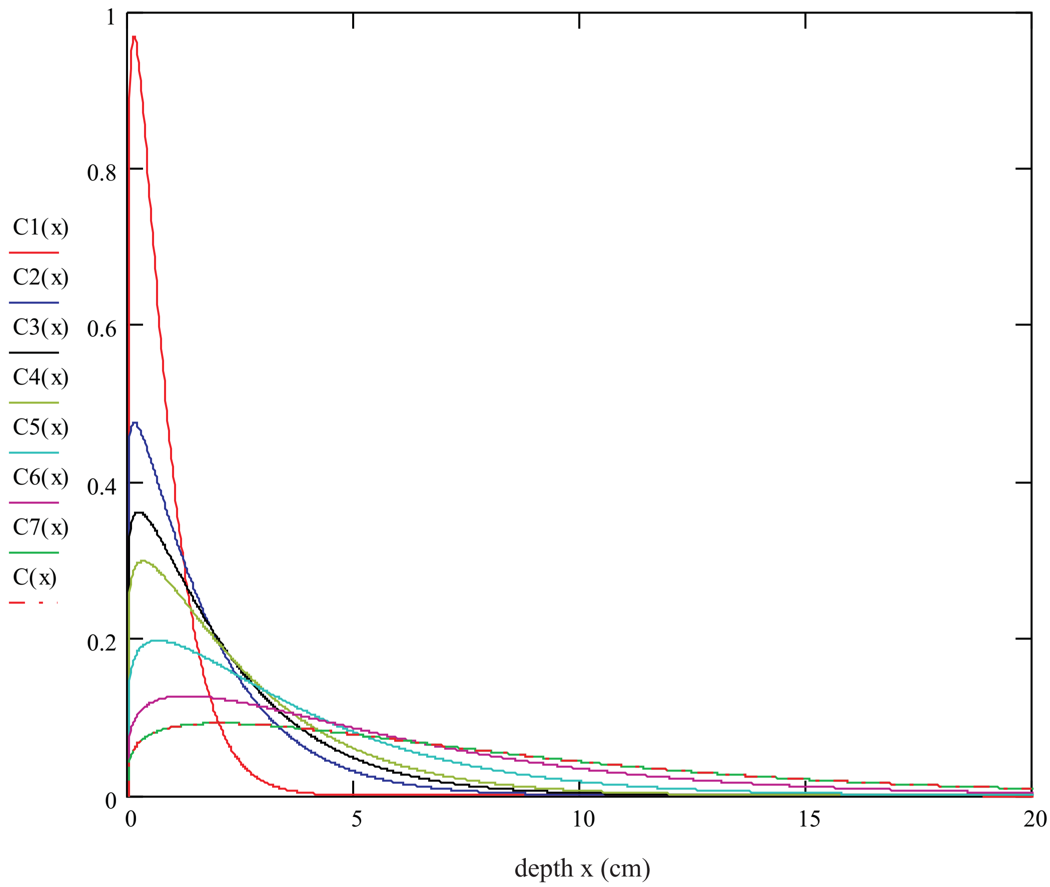

Fig. 6.9-14: Relative concentrations for different points of time (time series 4, Chernobyl-Cs-137)

legend:

ordinate axis: relative concentration (cm^{-1})

C1(x): relative concentration after 1 (a)
C2(x): relative concentration after 4 (a)
C3(x): relative concentration after 6 (a)
C4(x): relative concentration after 8 (a)
C5(x): relative concentration after 15 (a)
C6(x): relative concentration after 30 (a)
C7(x): relative concentration after 50 (a)

(C1(x)–C7(x): based on 2-dimensional nest of intervals)

C(x) : relative concentration after 50 (a), based on second fits of a(t) and n(t)

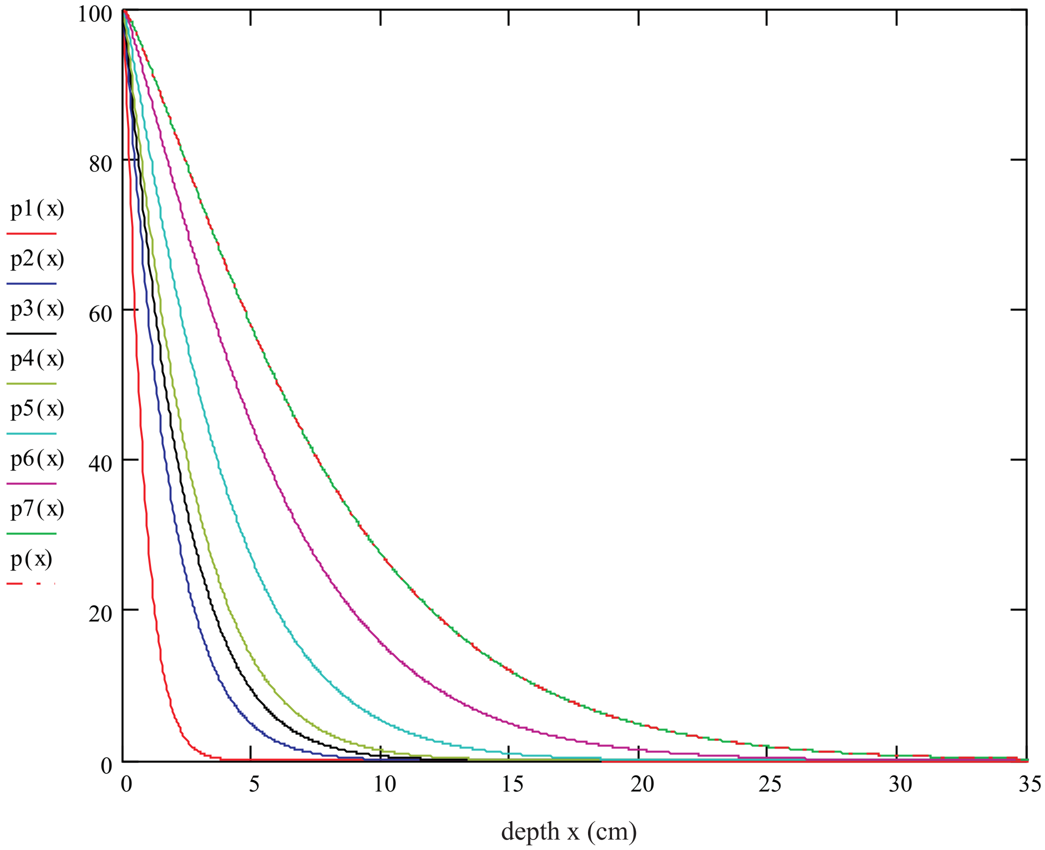

Fig. 6.9-15: Inventories below x in (%) for different points of time (time series 4, Chernobyl-Cs-137)

legend:

ordinate axis: inventories below x (%)

p1(x): inventory below x in (%) after 1 (a)
p2(x): inventory below x in (%) after 4 (a)
p3(x): inventory below x in (%) after 6 (a)
p4(x): inventory below x in (%) after 8 (a)
p5(x): inventory below x in (%) after 15 (a)
p6(x): inventory below x in (%) after 30 (a)
p7(x): inventory below x in (%) after 50 (a)

} based on 2-dimensional nest of intervals

p(x) : inventory below x in (%) after 50 (a), based on second fits of a(t) and n(t)

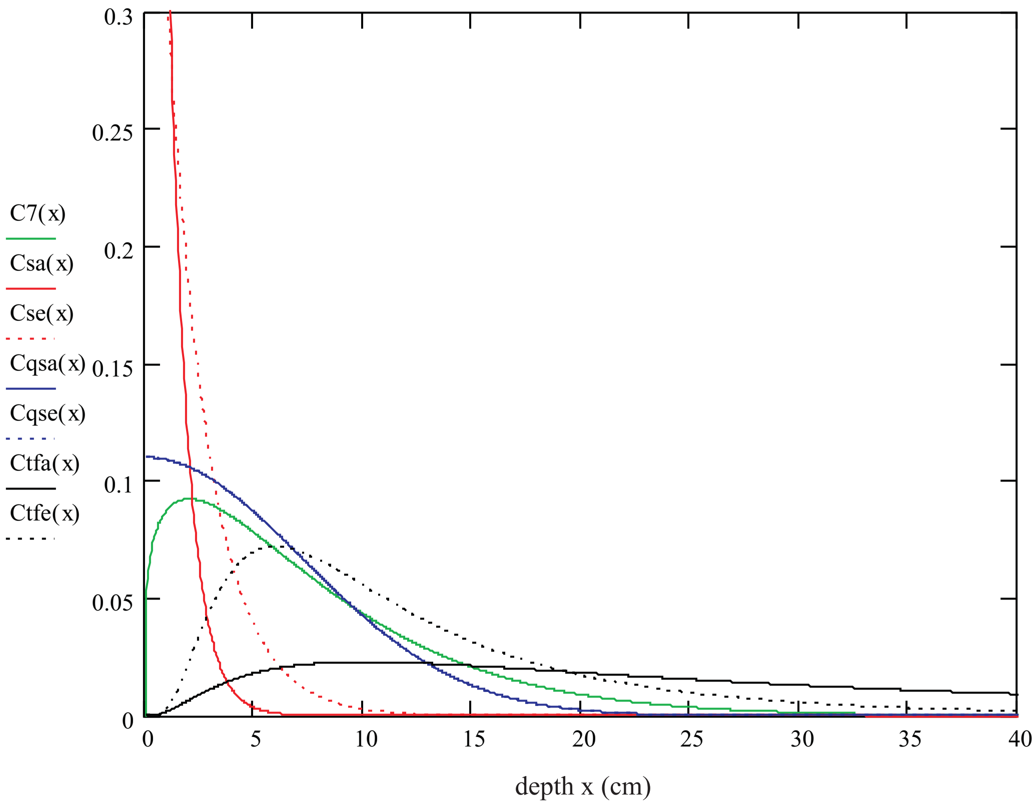

Fig. 6.9-16: Relative concentrations after 50 (a), resulting from different models (time series 4, Chernobyl-Cs-137)

legend:

ordinate axis: relative concentration (cm^{-1})

C7(x) : relative concentration after 50 (a), based on 2-dimensional nest of intervals
Csa(x) : relative concentration after 50 (a), based on Eq. (2-2), a-profile
Cse(x) : relative concentration after 50 (a), based on Eq. (2-2), e-profile
Cqsa(x): relative concentration after 50 (a), based on Eq. (2-3), a-profile
Cqse(x): relative concentration after 50 (a), based on Eq. (2-3), e-profile
Ctfa(x) : relative concentration after 50 (a), based on Eq. (2-4), a-profile
Ctfe(x) : relative concentration after 50 (a), based on Eq. (2-4), e-profile

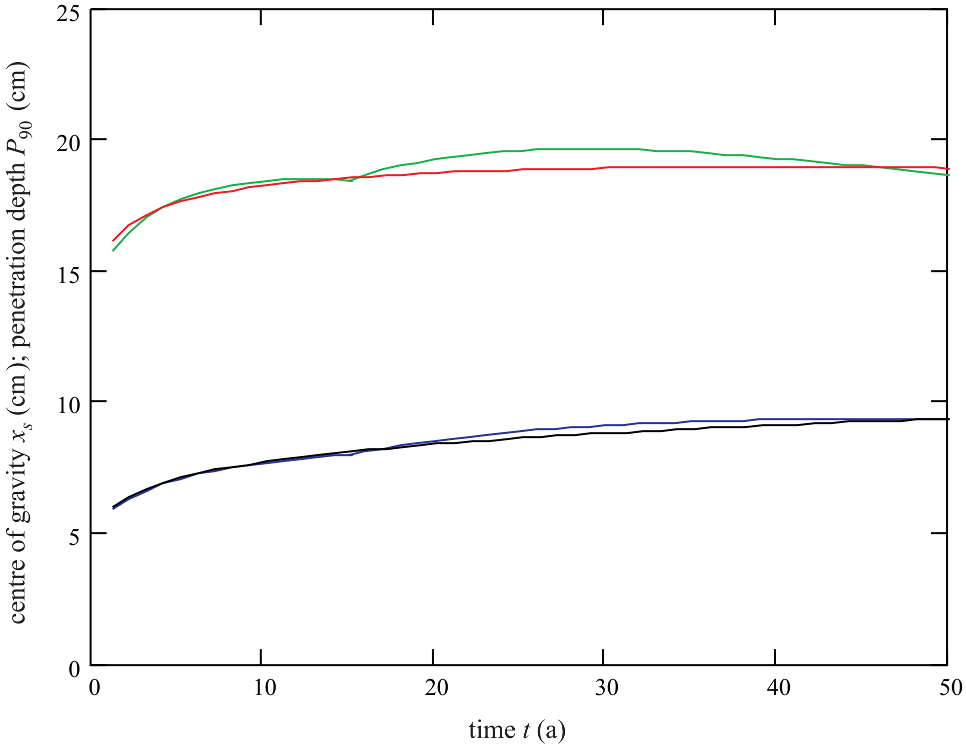

Fig. 6.10-1: Improved matching of the centres of gravity and of the penetration depths, achieved by fitting of n(t) in 2 pieces (time series 1, Chernobyl-Cs-137)
legend:
black: x_s-fit
blue : matching of the x_s-fit, based on Eq. (2-24)
red : P_{90}-fit
green: matching of the P_{90}-fit; (a(t), n(t) from second fits)

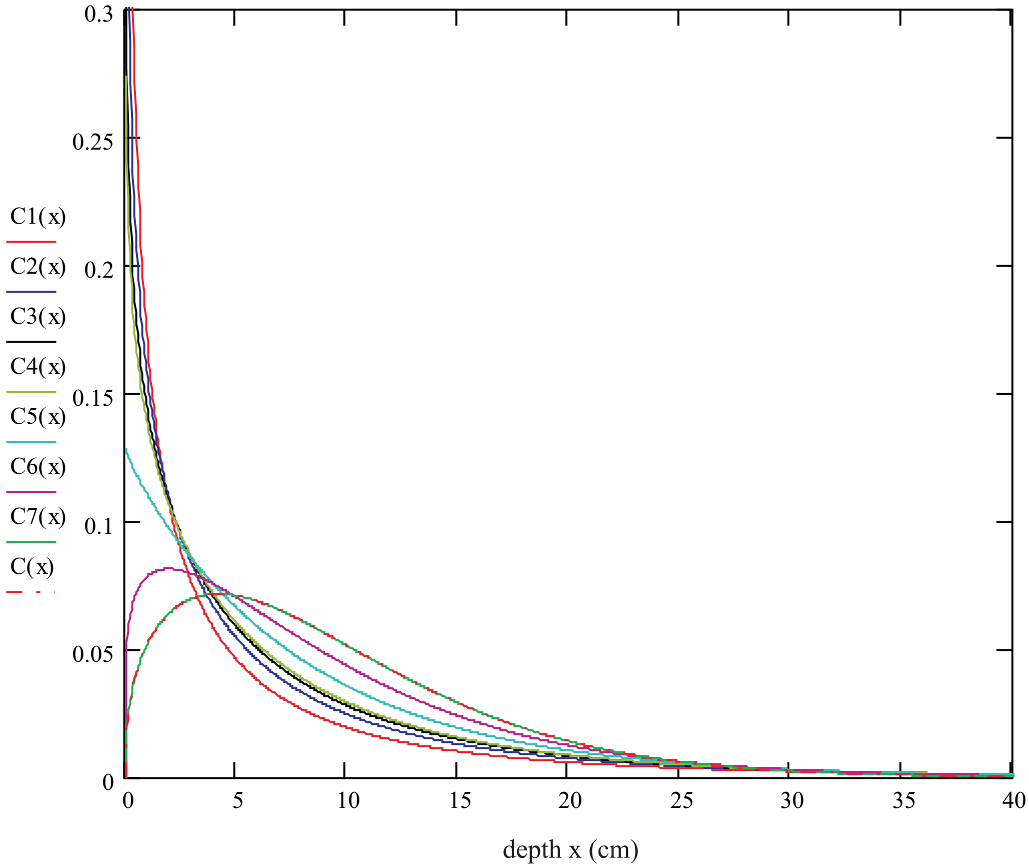

Fig. 6.10-2: Relative concentrations for different points of time (time series 1, Chernobyl-Cs-137)

legend:

ordinate axis: relative concentration (cm^{-1})

C1(x): relative concentration after 1.2 (a)
C2(x): relative concentration after 3.4 (a)
C3(x): relative concentration after 5.8 (a)
C4(x): relative concentration after 7 (a)
C5(x): relative concentration after 15 (a)
C6(x): relative concentration after 30 (a)
C7(x): relative concentration after 50 (a)

(C1(x) – C7(x): based on 2-dimensional nest of intervals)

C(x) : relative concentration after 50 (a), based on second fits of a(t) and n(t)

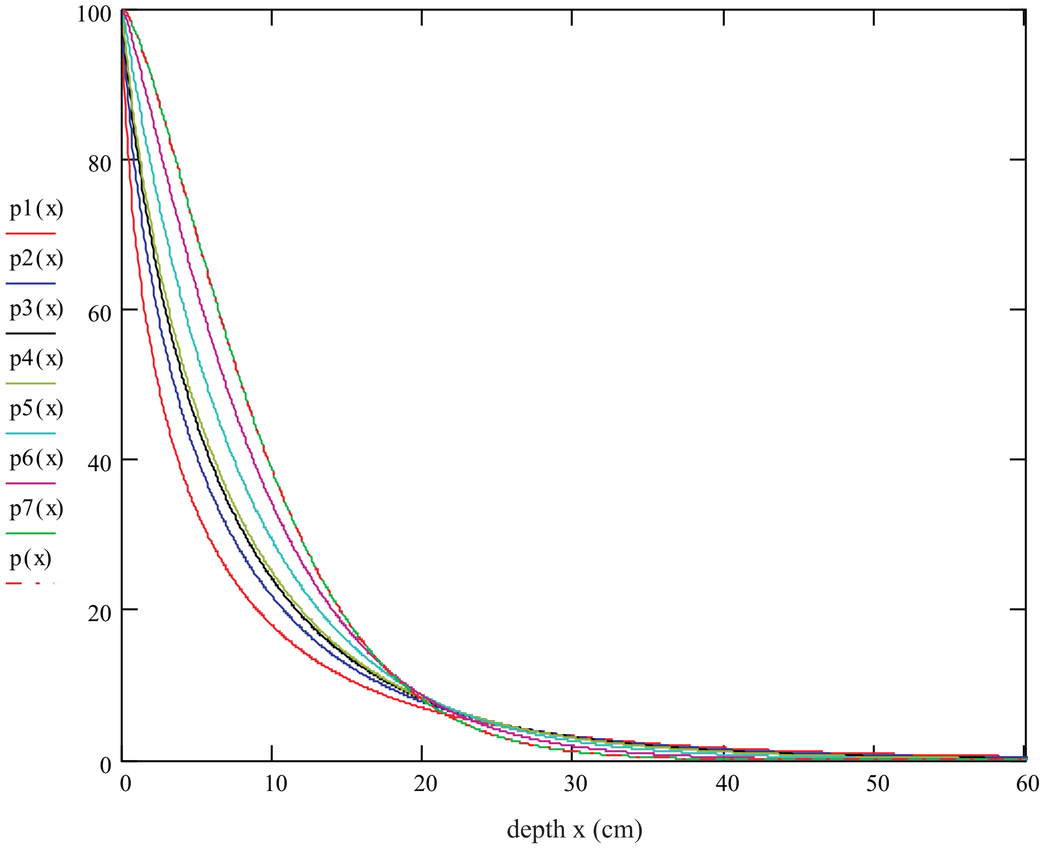

Fig. 6.10-3: Inventories below x in (%) for different points of time (time series 1, Chernobyl-Cs-137)

ordinate axis: inventories below x (%)

p1(x): inventory below x in (%) after 1.2 (a)
p2(x): inventory below x in (%) after 3.4 (a)
p3(x): inventory below x in (%) after 5.8 (a)
p4(x): inventory below x in (%) after 7 (a)
p5(x): inventory below x in (%) after 15 (a)
p6(x): inventory below x in (%) after 30 (a)
p7(x): inventory below x in (%) after 50 (a)

(p1(x) to p7(x): based on 2-dimensional nest of intervals)

p(x) : inventory below x in (%) after 50 (a), based on second fits of a(t) and n(t)

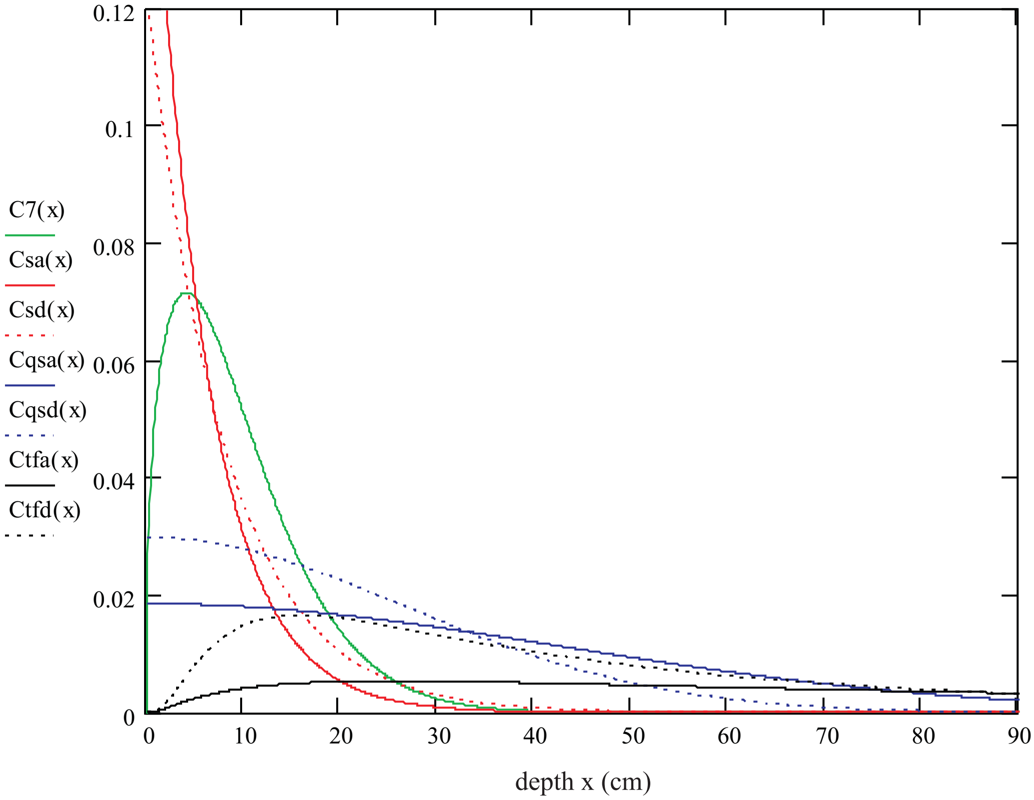

Fig. 6.10-4: Relative concentrations after 50 (a), resulting from different models (time series 1, Chernobyl-Cs-137)

legend:

ordinate axis: relative concentration (cm^{-1})

C7(x) : relative concentration after 50 (a), based on 2-dimensional nest of intervals
Csa(x) : relative concentration after 50 (a), based on Eq. (2-2), a-profile
Csd(x) : relative concentration after 50 (a), based on Eq. (2-2), d-profile
Cqsa(x): relative concentration after 50 (a), based on Eq. (2-3), a-profile
Cqsd(x): relative concentration after 50 (a), based on Eq. (2-3), d-profile
Ctfa(x) : relative concentration after 50 (a), based on Eq. (2-4), a-profile
Ctfd(x) : relative concentration after 50 (a), based on Eq. (2-4), d-profile